Applications and Industry®

May 1959

Transactions Papers

NUMBER 42

Published Bimonthly by

AMERICAN INSTITUTE OF ELECTRICAL ENGINEERS

(See inside back cover)

Applications and Industry. Published bimonthly by the American Institute of Electrical Engineers, from 20th and Northampton Streets, Easton, Pa. AIEE Headquarters: 33 West 39th Street, New York 18, N. Y. Address changes must be received at AIEE Headquarters by the first of the month to be effective with the succeeding issue. Copies undelivered because of incorrect address cannot be replaced without charge. Editorial and Advertising offices: 33 West 39th Street, New York 18, N. Y. Nonmember subscription $8.00 per year (plus 50 cents extra for foreign postage payable in advance in New York exchange). Member subscriptions: one subscription at $2.50 per year (balance of $5.00 subscription price to be paid by application of annual dues) to any one of three divisional publications: Communication and Electronics, Applications and Industry, or Power Apparatus and Systems: additional annual subscriptions $5.00 each. Single copies when available $1.50 each. Second-class mail privileges authorized at Easton, Pa. This publication is authorized to be mailed at the special rates of postage prescribed by Section 132.122.

Printed in United States of America

Number of copies of this issue 5,500

Relay-Type Feedback Control Systems with Dead Time and Sampling

KEISUKE IZAWA
NONMEMBER AIEE

LYNN E. WEAVER
ASSOCIATE MEMBER AIEE

HIS investigation is a time domain study of relay-type feedback control tems with dead time and sampling. It oduces a new approach to the analysis design of relay-type control systems loying sampling. Because of the pler, clamper, and relay, the system onlinear, and discontinuous in time. tems of this general nature have been lyzed in the past by Chow[1] and sell[2] using the sinusoidal response hod introduced by Goldfarb[3] and henburger.[4]

he investigation herein approaches the blem of analysis and design of relay- feedback control systems with dead and sampling in the time domain ugh the use of the phase plane hod. By means of the phase plane, y-type control action coupled with pling and holding action can be con- red as a varying dead time in the time ain. In the phase plane there exists nit band within which all possible limit es lie. The exact boundaries of the t band can be predicted. Control of band makes possible control of the imum and minimum amplitude and period of oscillation of the output var- . The investigation brings out the t of minor loop feedback on the limit l. It will become evident that minor feedback permits tight control of the band. The phase plane approach ides an intuitive insight upon the t on system performance of varying one or a combination of the system meters.

cription of System

ne block diagram of the system under ideration in this investigation is n in Fig. 1. Both system input $r(t)$ and output $c(t)$ are continuous functions of time. The sampler, designated by the switch, consists of a constant rate-sampling device plus holding circuit of such a nature that its output is a stair step, or so-called jump function. The power amplifier, or relay, has the characteristic shown in Fig. 1, where $\varepsilon^*(t)$, the sampler output, is the relay input, and $\pm k$ the relay output. The symbol Δ is termed the relay hysteresis or differential gap. The output of the relay is a series of rectangular pulses of constant amplitude and varying period. T_d in Fig. 1 represents a fixed value of dead time.

With reference to Fig. 1, the following equations are written:

$$\varepsilon(t)=r(t)-[\alpha m(t)+c(t)] \tag{1}$$

$$T\dot{c}(t)+c(t)=K_2 m(t) \tag{2}$$

where $\dot{c}(t)$ denotes the time derivative of $c(t)$.

$$\dot{m}(t)=\begin{cases} kK_1 \text{ if } \varepsilon^*(t-T_d)>\Delta \\ \pm kK_1 \text{ if } \Delta>\varepsilon^*(t-T_d)>-\Delta \\ -kK_1 \text{ if } \varepsilon^*(t-T_d)<-\Delta \end{cases} \tag{3}$$

From equations 2 and 3

$$T\ddot{c}(t)+\dot{c}(t)=\begin{cases} kK_1K_2 \text{ if } \varepsilon^*(t-T_d)>\Delta \\ \pm kK_1K_2 \text{ if } \Delta>\varepsilon^*(t-T_d)>-\Delta \\ -kK_1K_2 \text{ if } \varepsilon^*(t-T_d)<-\Delta \end{cases} \tag{4}$$

Substituting equation 2 into equation 1 yields

$$\varepsilon(t)=r(t)-\frac{\alpha}{K_2}[T\dot{c}(t)+c(t)]-c(t) \tag{5}$$

Let

$$c(t)=r(t)-\zeta(t) \tag{6}$$

Putting equation 6 into equation 4 yields

$$T\ddot{\zeta}(t)+\dot{\zeta}(t)=T\ddot{r}(t)+\dot{r}(t)+\begin{cases} -kK_1K_2 \text{ if } \varepsilon^*(t-T_d)>\Delta \\ \pm kK_1K_2 \text{ if } \Delta>\varepsilon^*(t-T_d)>-\Delta \\ kK_1K_2 \text{ if } \varepsilon^*(t-T_d)<-\Delta \end{cases} \tag{7}$$

and equation 5 becomes

$$\varepsilon(t)=-\left[\frac{\alpha}{K_2}r(t)+\frac{\alpha}{K_2}T\dot{r}(t)\right]+\left(1+\frac{\alpha}{K_2}\right)\zeta(t)+\frac{\alpha T}{K_2}\dot{\zeta}(t) \tag{8}$$

If it is assumed that $r(t)=0$, equations 7 and 8 become respectively

$$T\ddot{\zeta}(t)+\dot{\zeta}(t)=\begin{cases} -kK_1K_2 \text{ if } \varepsilon^*(t-T_d)>\Delta \\ \pm kK_1K_2 \text{ if } \Delta>\varepsilon^*(t-T_d)>-\Delta \\ kK_1K_2 \text{ if } \varepsilon^*(t-T_d)<-\Delta \end{cases} \tag{9}$$

$$\varepsilon(t)=\left(1+\frac{\alpha}{K_2}\right)\zeta(t)+\frac{\alpha T}{K_2}\dot{\zeta}(t) \tag{10}$$

A similar procedure may be followed for the case when $r(t)$ is constant.

To normalize equations 9 and 10 let

$$\zeta=TkK_1K_2X$$

$$t=T\tau$$

Then equations 9 and 10 become

$$x''(\tau)+x'(\tau)=\begin{cases} -1 \text{ if } \eta^*\left(\tau-\frac{T_d}{T}\right)>a \\ \pm 1 \text{ if } \eta^*\left(\tau-\frac{T_d}{T}\right)>a>-\eta^*\left(\tau-\frac{T_d}{T}\right) \\ 1 \text{ if } \eta^*\left(\tau-\frac{T_d}{T}\right)<-a \end{cases} \tag{11}$$

$$\eta^*(\tau)=\overline{\lfloor}[x(\tau)+hx'(\tau)] \tag{12}$$

where the symbol $\overline{\lfloor}$ is used to denote the stair-step-type function.

$$h=\frac{\alpha}{\alpha+K_2}$$

and

$$a=\frac{\Delta}{(\alpha+K_2)TkK_1}$$

Considering the relationship between on-off control and sampling action, equations 11 and 12 are rewritten as

$$x''(\tau)+x'(\tau)=\begin{cases} -1 \text{ if } \eta(\tau-\lambda)>a \\ \pm 1 \text{ if } |\eta(\tau-\lambda)|<a \\ 1 \text{ if } \eta(\tau-\lambda)<-a \end{cases} \tag{13}$$

$$\eta(\tau)=x(\tau)+hx'(\tau) \tag{14}$$

where λ is a stochastic parameter varying between T_d/T and $(T_d+L)/T$. L is the sampling period.

Phase Plane Analysis

The phase plane is a plot of the system error x as a function of error rate x'. Because of the on-off action of the relay, the system under investigation will have two modes of operation, one when the relay

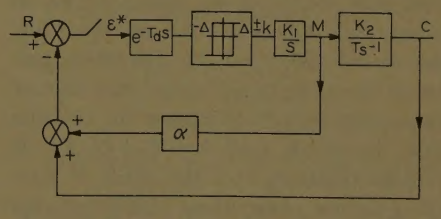

Fig. 1. System diagram

58-1026, recommended by the AIEE Feed- Control Systems Committee and approved e AIEE Technical Operations Department for itation at the AIEE Pacific General Meeting, mento, Calif., August 19–22, 1958, and re- ited at the Winter General Meeting, New N. Y., February 1–6, 1959. Manuscript sub- l May 7, 1958; made available for printing er 22, 1958.

KE IZAWA is with Purdue University, ette, Ind., and LYNN E. WEAVER is with the rsity of Arizona, Tucson, Ariz.

vork was done under the sponsorship of the ne National Laboratory.

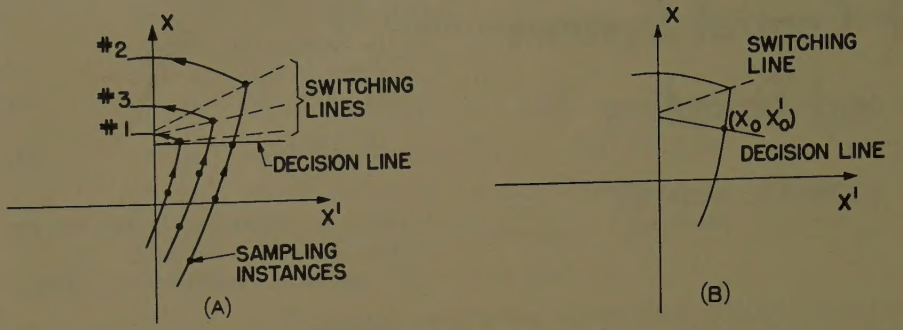

Fig. 2. A—Phase plane trajectories showing effects of sampling. B—Portion of phase plane trajectory showing switching and decision lines

output is $+1$ and the other when it is -1. The phase plane will thus be divided into two parts with relay operations occurring on the dividing line between the two regions.

For relay-type control systems without sampling, the dividing line is fixed. Introduction of the sampler and clamper causes this line to vary, the variation being caused by the varying dead time λ introduced by the sampler and clamper in conjunction with on-off control action. To clarify this, consider Fig. 2(A) showing a portion of the phase plane trajectories, where the dots on the trajectories represent sampling instances. The solid line, termed the decision line, is the division between the on and off control modes in the absence of sampling corresponding to $\eta(\tau)=\pm a$ of equation 14. The dashed line, called the switching line, corresponds to the dividing line between on and off control modes in the presence of sampling corresponding to $\eta(\tau-\lambda)=\pm a$ of equation 14. To illustrate the varying dead time concept, first consider trajectory 1. This is indicative of the case when the the sampler samples at the instant the phase trajectory is slightly past the decision line. At that instant, relay action occurs and the system switches to the other mode of operation. Trajectory 2 corresponds to the occurrence of sampling when the trajectory is slightly below the decision line. Since the sampling point falls below the decision line, relay action does not occur and the system must wait one sample period before switching modes of operation. Trajectory 3 is an example of any arbitrary switching. The switching line has two extreme limits, one limit when sampling occurs on the decision line, in which case it becomes the switching line associated with $\lambda=T_d/T$, the other limit when sampling takes place the instant before the trajectory crosses the decision line, in which case $\lambda=(T_d+L)/T$. It follows therefore that the effect of sampling on the phase plane plot is to cause the switching line to vary. The location of the varying switching line in the phase plane may be derived as follows.

Considering equation 13

$$x''+x'=\pm 1$$

Solving equation 13 for x, where x_0 and x_0' are the initial conditions, gives x_0 and x_0'.

$$x=x_0+(1-\epsilon^{-\tau})x_0'\pm(\epsilon^{-\tau}+\tau-1) \qquad (15)$$

Differentiating equation 15 and solving for x_0' yields

$$x_0'=\epsilon^{\tau}x'\pm(\epsilon^{\tau}-1) \qquad (16)$$

Substituting equation 16 into equation 15 yields

$$x_0=x-(\epsilon^{\tau}-1)x'\pm(\epsilon^{\tau}-1-\tau) \qquad (17)$$

Since the relay will trip the moment the error signal η becomes greater than $+a$ or less than $-a$, the decision lines are expressed by

$$\eta=x+hx'=\pm a \qquad (18)$$

Now, x_0 and x_0', the initial values of x and x', lie on the decision line; see Fig. 2(B). Therefore the equation of the switching line is given by substituting x_0 and x_0' of equations 16 and 17 for x and x' in equation 18, and is obtained as

$$x=(\epsilon^{\lambda}-1-h\epsilon^{\lambda})x'\pm a\pm(\epsilon^{\lambda}-1)(h-1)\pm\lambda \qquad (19)$$

where λ is the varying dead time.

The two switching line equations are for on-off

$$x=(\epsilon^{\lambda}-1-h\epsilon^{\lambda})x'+a+(\epsilon^{\lambda}-1)(h-1)+\lambda \qquad (20)$$

and for off-on

$$x=(\epsilon^{\lambda}-1-h\epsilon^{\lambda})x'-a-(\epsilon^{\lambda}-1)(h-1)-\lambda \qquad (21)$$

From equations 20 and 21, it is obvious that varying λ will cause the slope and the x-axis intercept of the switching line to vary.

Limit Band

Observing the switching line equations 20 and 21, it is evident that there exist two extreme locations for the on-to-off and off-to-on switching lines, corresponding to the two extreme values of λ, i.e., $\lambda=T_d/T$ and $(T_d+L)/T$.

Fig. 3(A) illustrates the two extreme limit cycles corresponding to the two extreme values of λ. Since λ varies in a stochastic manner between T_d/T and $(T_d+L)/T$, all steady-state trajectories will lie between the two limit cycles of Fig. 3(A). The band formed by the two limit cycles is called the limit band. Once any trajectory enters the limit band it cannot escape from this band. The inner boundary of the limit band gives the minimum possible amplitude and period of the steady-state trajectories. In like manner the outer boundary of the limit band gives the maximum possible amplitude and period of the steady-state trajectories.

Considering the system equation corresponding to the off cycle

$$x''+x'=-1 \qquad (22)$$

equation 23 is obtained with the initial values x_0 and x_0'

$$-x=x'-x_0'-x_0+\ln(x_0'+1)-\ln(x'+1) \qquad (23)$$

Equation 23 describes the path of th

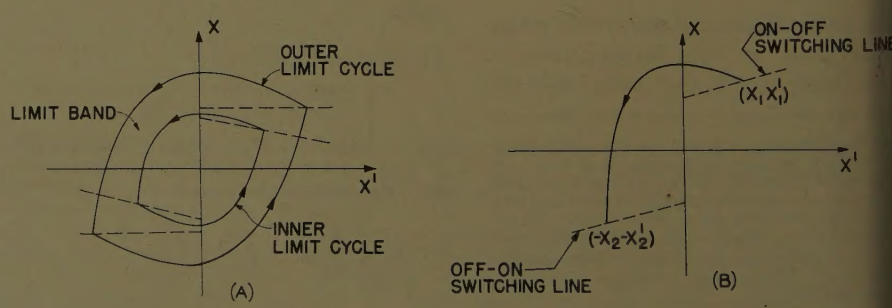

Fig. 3. Phase plane plot

A—Showing limit band
B—Off-trajectory for outer or inner limit cycle

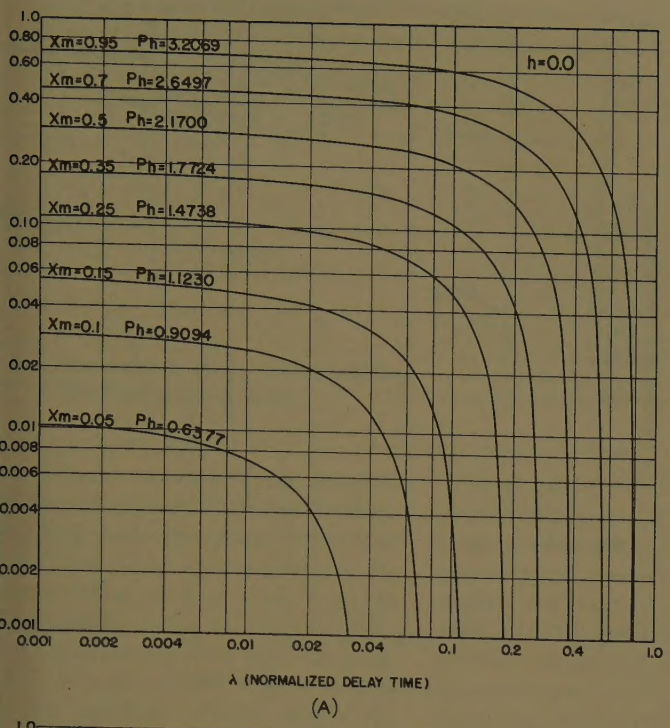

(A)

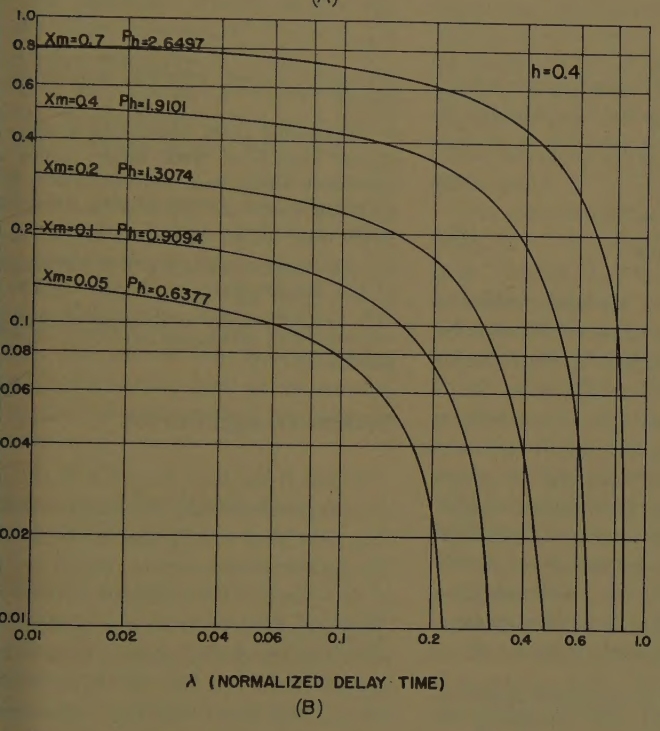

(B)

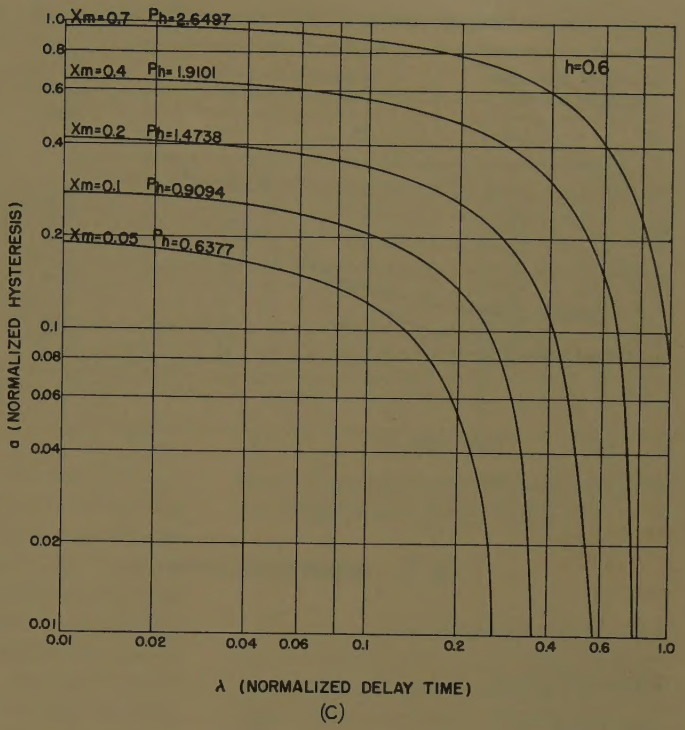

(C)

Fig. 4. System characteristic curves

A—For h = 0
B—For h = 0.4
C—For h = 0.6

se plane trajectory corresponding to off cycle of the relay. Consider the se plane trajectory in Fig. 3(B) cribed by equation 23. Let this trajec- be representative of the two extreme ectories corresponding to the bound- s of the limit band. Then (x_1, x_1') point on the on-off switching line, and $-x_2, -x_2')$ a point on the off-on switch- line corresponding to the inner or r limit cycle; (see Fig. 3(A). Fig.) represents a portion of the outer or r limit cycle, and the following two ations are formed:

$$x_2 = -x_2' - x_0' - x_0 - \ln(-x_2'+1) + \ln(x_0'+1) \quad (24)$$

$$-x_1 = x_1' - x_0' - x_0 - \ln(x_1'+1) + \ln(x_0'+1) \quad (25)$$

Subtracting equation 24 from equation 25 yields

$$x_2 + x_1 = -x_1' - x_2' + \ln(x_1'+1) - \ln(x_2'-1) \quad (26)$$

Because of symmetricity of the two pairs of extreme switching lines, $x_1 = x_2$ and $x_1' = x_2'$ in Fig. 3(B).

Replacing x_1 and x_2 by x, and x_1' and x_2' by x' in equation 26, equation 27 follows:

$$x = -x' + \frac{1}{2}\ln\left(\frac{1+x'}{1-x'}\right) \quad (27)$$

From equation 27 x and x' correspond to the values given by the switching line equations 20 and 21 for the two extreme values of λ. Substitute for x in equation 27 its value as given by equation 20. This substitution results in

$$a = (\epsilon^{\lambda}-1)(1-h) - \lambda - \epsilon^{\lambda}(1-h)x' + \frac{1}{2}\ln\left(\frac{1+x'}{1-x'}\right) \quad (28)$$

where $\lambda = T_d/T$ or $(T_d+L)/T$.

To find x' in terms of x_m, the possible maximum and minimum values of x corresponding to the outer and inner limit cycle, set $x'=0$ in equation 23.

$$x_m = x' + x - \ln(x'+1) \quad (29)$$

Since, from the switching line equation

$$x = (\epsilon^{\lambda}-1-h\epsilon^{\lambda})x' + a + (\epsilon^{\lambda}-1)(h-1) + \lambda \quad (30)$$

combining equations 29 and 30 yields

$$x_m = \epsilon^{\lambda}(1-h)x' - \ln(x'+1) + a + (\epsilon^{\lambda}-1)(h-1) + \lambda \quad (31)$$

From equations 27 and 30

$$\frac{1}{2}\ln\left(\frac{1+x'}{1-x'}\right) = \epsilon^{\lambda}(1-h)x' - (\epsilon^{\lambda}-1)(1-h) + \lambda + a \quad (32)$$

Combining equations 31 and 32 yields

$$x_m = \frac{1}{2}\ln\left(\frac{1+x'}{1-x'}\right) - \ln(1+x') \quad (33)$$

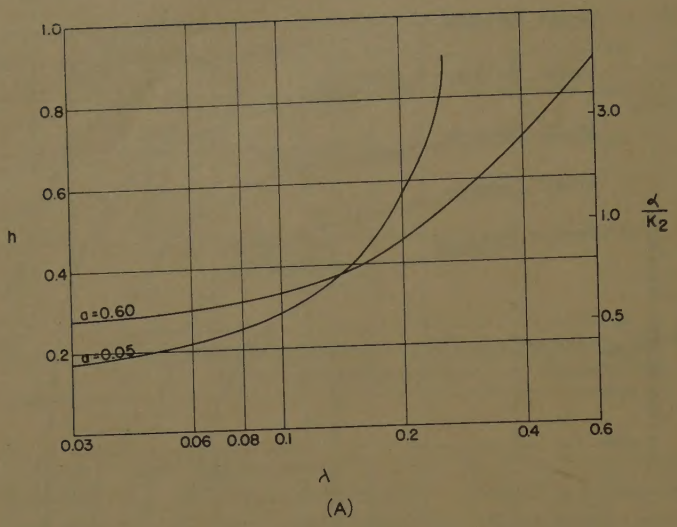

(A)

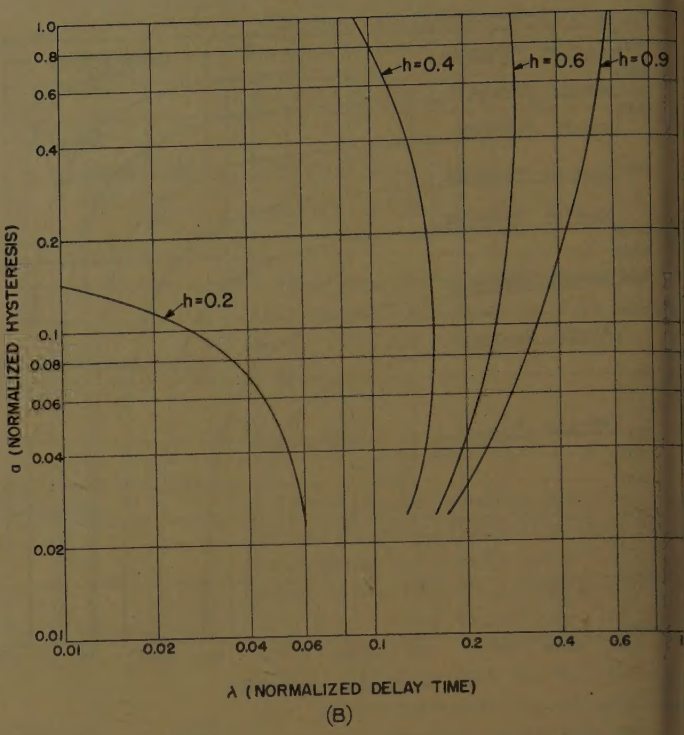

(B)

Fig. 5. System design curves

which reduces to

$$x' = \sqrt{1-\epsilon^{-2x_m}} \tag{34}$$

Equation 34 is substituted in equation 28, and the following expression is obtained:

$$a = (\epsilon^{\lambda}-1)(1-h)-\lambda-\epsilon^{\lambda}(1-h)\times \sqrt{1-\epsilon^{-2x_m}}+\frac{1}{2}\ln\frac{1+\sqrt{1-\epsilon^{-2x_m}}}{1-\sqrt{1-\epsilon^{-2x_m}}} \tag{35}$$

where $\lambda = T_d/T$ or $(T_d+L)/T$.

Equation 31 shows the relationship between the possible maximum and minimum value of the normalized output variable and the normalized system parameters. When the value of the system parameters are known, the maximum value of the output variable can be predicted. To evaluate equation 35, a digital computer was used. For a fixed value of h, incremental values of x_m were chosen. Values of a, corresponding to a series of values of λ, were calculated for each x_m; h was then changed and another set of calculations made. From the computer evaluation, a set of tables were constructed for values of $h=0$, $h=0.2$, $h=0.4$, $h=0.6$, $h=0.8$, and $h=0.9$. To visualize better the relations between system parameters and the output variables, a family of curves was plotted for the various values of h see Fig. 4. From these curves, the possible maximum and minimum values of the amplitude of the steady-state oscillations of the output variable can be predicted. The half-period of any symmetrical limit cycle is uniquely expressed by

$$P_h = \ln\left(\frac{1+x'}{1-x'}\right) \tag{36}$$

where x' and $-x'$ are the abscissas of the two symmetrical switching points.

If equation 34 is substituted into equation 36, the half-period corresponding to the outer or inner limit cycle of the limit band is given by

$$P_h = \ln\left[\frac{1+\sqrt{1-\epsilon^{-2x_m}}}{1-\sqrt{1-\epsilon^{-2x_m}}}\right] \tag{37}$$

With equation 37, for each value of x_m a corresponding value of P_h can be calculated and included in the system characteristic curves; see Fig. 4.

Several examples of characteristic curves are shown in Fig. 4. It becomes evident, upon examination of the characteristic curves, that an intuitive insight on the effect of parameter variation of the system steady-state performance can be obtained from the curves. Following are six conclusions drawn from observations of the system characteristic curves.

1. For a fixed value of the sampling period, delay and differential gap, increasing the minor loop feedback gain decreases the amplitude and increases the frequency of the steady state oscillations of the output variable.

2. For a fixed value of feedback gain, differential gap, and delay, increasing the sampling rate decreases the amplitude and increases the frequency of the steady-state oscillations.

3. For a fixed value of feedback gain, delay, and sampling period, increasing the differential gap of the relay will cause an increase in the amplitude and period of the steady-state oscillations.

4. There is a region associated with small values of λ for which the amplitude and period of the steady-state oscillations remains essentially constant. This implies that for certain sampling rates the output will have almost constant amplitude an period.

5. Following from conclusion 4 there is region associated with large values of for which there is a wide variation in t amplitude and period of the steady-st oscillations of the output variable.

6. For each maximum and minimum valu of the steady-state oscillations of the ou put variable, there corresponds a uniq value for the maximum period of oscillati possible.

System Design Curves

So far, it has been shown how the cha acteristic curves can be used in analysi The next step will be the introduction the system design curves, which are plo of h versus λ for constant values of They are derived from the system cha acteristic curves by picking points on t characteristic curves for each h whe $a=x_m$, and recording the correspondi value of λ. Through the use of syste design curves, shown in Fig. 5(A) t feedback gain, or the varying dead tim can be selected so that the oscillations the output variable will lie within a regi bounded by $\pm a$. In other words, a fe back gain, sampling rate, or fixed de time can be chosen so that the amplitu of oscillation of the output variable always be less than a. To illustrate use of the design curves, suppose following specifications were placed on system shown in Fig. 1:

Fixed dead time = 0.1
Sampling period = 0.05
Hysteresis = 0.1
$x_m \leq a = 0.1$

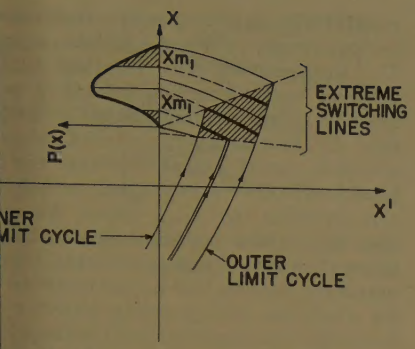

6. Approximate shape of probability distribution curve for x_m

Table I. Comparison of Computer and Theoretical Results

Runs	Normalized Parameter Values h	a	Measured Maximum Values of x_m, P_h x_m	P_h	Expected Maximum Values of x_m, P_h x_m	P_h
1	0	0.03	0.34	2.0	0.34	2.0
2	0	0.3	0.79	3.0	0.80	3.0
3	0.2	0.1	0.36	1.9	0.36	1.9
4	0.2	0.3	0.62	2.6	0.62	2.6
5	0.4	0.2	0.36	2.0	0.35	1.8
6	0.4	0.6	0.79	3.0	0.80	3.0
7	0.6	0.2	0.23	1.5	0.24	1.5
8	0.6	0.4	0.43	2.2	0.43	2.0
9	0.8	0.3	0.28	1.7	0.28	1.6
10	0.8	0.6	0.55	2.5	0.55	2.3

For all runs $\lambda_{max} = 0.075$, and $\lambda_{min} = 0.325$.

he amount of minor loop feedback
n required to meet these specifications
obtained from the design curves as
ows: Draw a line corresponding to the
ximum value of dead time λ_{max}. In
example, $\lambda_{max} = 0.1 + 0.05 = 0.15$.
d its intersection point with the speci-
a curve and read the value of $h = 0.38$
n the ordinate. Points above the
stant *a* curve correspond to $x_m < a$, and
its below the curve to $x_m > a$.
nother set of design curves constructed
n the characteristic curves is shown in
5(B). These curves are a plot of *a*
us λ for values of $x_m = a$ and constant
This set of curves is used to select λ_{max}
hat $x_m < a$ when the minor loop feed-
k gain is fixed. For example, if the (*a*,
) point falls above the constant *h*
e, then $x_m < a$ if it falls below $x_m > a$.
ough the use of the system design
es, the maximum limit of the steady-
e oscillation of the output variable can
reset.

nparison of Predicted and omputer Results

mulating the system shown in Fig. 1,
analog computer runs were made for
value of $h = 0$, $h = 0.2$, $h = 0.6$, $h = 0.8$.
system output and output rate were
rded on a Sanborn recorder. To
rate the limit band concept, the
dy-state phase trajectories were dis-
ed on a cathode-ray oscilloscope and a
re taken for several of the runs made.
e clearly indicate the limit band and
ing limit cycles. The maximum
e of the output variable was obtained
these recordings and normalized.
maximum half-period was also taken
the recordings and normalized.
e normalized values were then com-
d with the predicted values of x_m
P_h obtained from the system char-
istic tables and curves. Table I
ares the analog computer results
those obtained from the character-
curves.

In comparing the theoretical and computer results, it was noticed that the maximum possible value of the output variable checks very closely with the computer result. However, in comparing the minimum possible value with that obtained from the computer, a considerable discrepancy was noticed. The minimum possible value was always considerably less than the computer value. This difference may be resolved in the following manner: Consider a portion of the phase plane plot shown in Fig. 6. At steady state the phase plane trajectory is always within the limit band.

Since the switching from on-state to off-state may occur only within the shaded area between the extreme switching lines and the boundary of the limit band, it must be at least proper to assume that switching in the shaded area occurs with equal probability. Now, when x_m, the maximum value of the each trajectory crossing *x*-axis, is considered, the crossing between maximum and minimum possible value of x_m will no longer occur with equal probability. The probability $P(x)dx$ with which x_m occurs between x_m and $x_m + dx$ is proportional to the area of the strip segment cut from the shaded area by two parallel trajectories which cross the *x*-axis at x_m and $x_m + dx$. A rough sketch of the probability density $P(x)$ is shown in Fig. 6. For the cases tested by the analog computer, the width of the limit band is relatively larger than the distance between the two extreme switching lines. It is found that the peak value of $P(x)$ occurs at a value of *x* closer to the maximum possible x_m.

The same discussion may be applied to the other switching region. Therefore, the succeeding switching point in the shaded area no longer occurs with equal probability, but will have zero probability along the outer and inner limit cycle and a maximum probability in between. This indicates that the maximum and minimum of x_m always lie within the maximum and minimum possible value of x_m, which can be predicted from the characteristic curves in Fig. 4.

Conclusions

The phase plane technique may be used for the analysis of relay type, second-order feedback control systems with dead time. The sampling function in conjunction with the type of system considered here may be treated as a stochastically varying dead time.

For systems of the type considered in this investigation, there exists in the phase plane a limit band within which all steady-state trajectories must lie. The limits of this band can be predicted from the phase plane analysis.

References

1. Contactor Servomechanisms Employing Sampled Data, C. K. Chow. *AIEE Transactions*, vol. 73, pt. II, March 1954, pp. 51–64.

2. Design Criterion for Stability of Sampled-Data On-Off Servomechanisms, Frederick A. Russell. *Thesis*, Columbia University, New York, N. Y., June 1953.

3. On Some Non-Linear Phenomena in Regulatory Systems (in Russian), L. C. Goldfarb. *Automatika i Telemechanika*, Moscow, U.S.S.R., vol. 8, no. 5, Sept.-Oct. 1947, pp. 349–83. (English Translation: *Report 1691*, United States National Bureau of Standards, Washington, D. C., May 29, 1952.)

4. A Frequency Response Method for Analyzing and Synthesizing Contactor Servomechanisms, Ralph J. Kochenburger. *AIEE Transactions*, vol. 69, pt. I, 1950, pp. 270–84.

Discussion

J. E. Gibson (Purdue University, Lafayette, Ind.): The introduction of stochastic parameters into the analysis of a sampled data system with a relay is one of the most interesting points of this paper. The use of the stochastic parameter λ and the establishment of the boundaries within which a limit cycle must exist appears to be a very useful approach. Apparently the authors have established the necessary conditions for the existence of this limit band to their own satisfaction and indeed it is not difficult to

demonstrate the upper and lower bounds by the use of the describing function analysis. However, this discusser feels that this proof should be demonstrated rather than merely mentioning in the simple statement preceding equation 22 that the limit band exists.

In the authors' comparison of predicted and computer results, the heuristic presentation of the shape of the probability density of the x-axis crossings shown in Fig. 6 seems reasonable but certainly the conclusions would be strengthed if this probability density were derived rigorously and then found to agree with the actual simulator runs. This discusser also feels that a plot of the data in Table I would simplify the task of comparing the predicted and simulator results.

The block diagram shown in Fig. 2(A) may be rearranged into a single loop diagram consisting of a sampler plus hold, the relay, and a linear transfer,

$$H=\frac{\alpha K_1(hTS+1)}{hS(TS+1)}$$

This fact will allow the system design curves shown in Figs. 4 and 5 to be employed for a single-loop system with an integration and with or without a lag or a lead.

Finally, this discusser wishes to raise the question of the system response to various inputs, other than the step function mentioned following equation 10. He realizes that this is an easy question to ask and an extremely difficult one to answer in any generality. However, any data the authors might have obtained previously or since their paper was written would make a welcome addition to their already quite useful work.

Keisuke Izawa and Lynn E. Weaver: The authors thank Prof. Gibson for his comments. To verify the existence of the limit band, consider equations 20, 21, and 27. Actual switching between two trajectories in the phase plane, i.e., the on and off trajectories, occurs λ after the corresponding decision is made (on-off at $x=a$ and off-on at $x=-a$). This switching will take place along straight lines given by equations 20 and 21. If the switching point, which is indicated by equations 20 and 21, satisfies equation 27, then a periodic limit cycle exists. Since λ varies between $\lambda_{min}=T_d/T$ and $\lambda_{max}=(T_d+L/T)$, two possible corresponding symmetrical limit cycles exist, and form the boundaries of the limit band shown in Fig. 3(A). These two closed trajectories are the extreme cases in the steady state and may or may not actually occur, depending on whether the switching point correspondi to the extreme values of λ satisfies equati 27. Furthermore, since the time durati between two succeeding switching poi must be an integral multiple of the sampli time L, the existing trajectories, after t transient, would always be within the li band. In other words, if half period P_h corresponding to λ_{max}, given by eq tions 28 and 36 is smaller than $(N+1)L$ a larger than NL, N being an integer, then t maximum possible half-period would be N for which the corresponding trajectory l inside the outer boundary of the limit ba The same discussion follows for the mi mum possible trajectory. A quantitat verification of the existence of the li band and varying limit cycle is given in F 7, which shows the cathode-ray oscillosc display of the steady-state phase plane p trait corresponding to analog computer ru 3 and 4 as listed in Table I. Run 3 cor sponds to the upper portrait and run 4 to lower portrait.

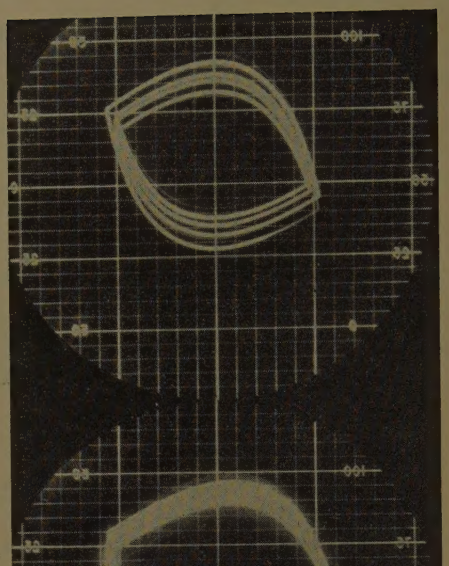

Fig. 7. Limit band and varying limit cycle; see Table I

The authors used the heuristic presen tion of the shape of the probability dens curve of the x-axis crossings to explain discrepancy between the predicted stea state minimum value of the output varia and that actually obtained with the ana computer. The predicted maximum va agreed closely with the values actu obtained. In either case the steady-st value of the output variable fell with limits set by the limit band. Since, practice, interest will mainly be in predict the maximum possible steady-state am tude of the output variable, no furt effort has been made to derive rigorou the probability density curve. Such derivation however, would certai strengthen our conclusions.

Prof. Gibson's rearrangement of Fig. 2 to a single-loop system with a lead t helps to extend further the technique sented in the paper. In answer to final comment, work is currently being d to apply the techniques developed in paper to other types of nonlinearities as as various inputs.

Control of Infrared Radiation

IRA J. BARBER
MEMBER AIEE

THE CHARACTERISTICS of commonly used infrared sources have been rather well delineated in the past,[1,2] so that the quantity and quality of their radiant outputs need not be covered in this paper. Generally speaking, these sources have one or two dimensions, represented by point sources, line sources, and area sources. All are basically omnidirectional, and their utilization is dependent on some form of optical control, both individually and when combined to form an oven.

It is with the type of control, its optics, and the geometry of utilization of these units in multiple that this paper is chiefly concerned. Except for the specific reflectivity of the material involved, the spectral characteristics of the source are not of importance in consideration of these points. The immediate directional control of an infrared generator is important where operating expense must be considered, in practically all line production ovens. It is desirable to transform the largest possible share of the initially developed radiant ene into useful radiation (i.e., absorbed the product) and the efficiency of individual reflector is shown by the r of forward useful radiation to initi generated radiation. Prime factors fluencing this amount are optical de of the reflector, and reflectivity of terials used.

In initiating a study of the m effective methods of distributional con of radiation, it is first necessary

Paper 59-31, recommended by the AIEE El Heating Committee and approved by the A Technical Operations Department for present at the AIEE Winter General Meeting, New N. Y., February 1–6, 1959. Manuscript subm October 31, 1958; made available for pri November 19, 1958.

IRA J. BARBER is with The Fostoria Pressed Corporation, Fostoria, Ohio.

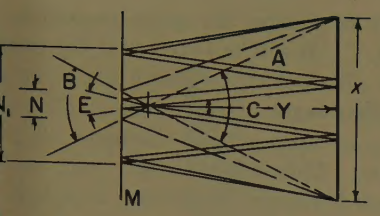

1. Energy reaching target from bare source

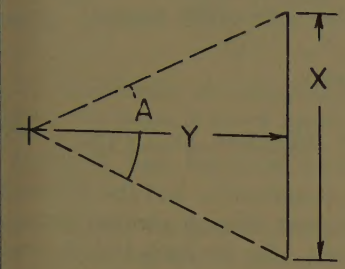

2. Energy control through flat reflector

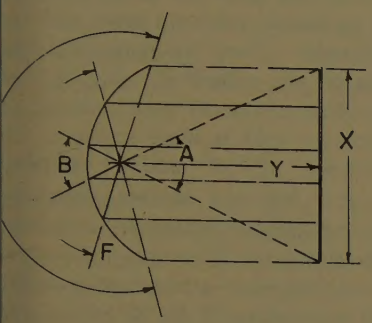

3. Properly contoured reflector, which greatly increase energy reaching target

lish the desired end result. Pur- for directed radiation will vary y, and the solution for one problem not be the most suitable for another. nost usual requirement is to provide iform field of radiant flux at some ed distance. To a lesser extent, are requirements for concentrated and concentrated spots. This paper eal with the development of specific urations for each.

s of Individual Reflector

nsidering initially, then, the point es, represented principally by the lar tungsten filament lamp, the m usually is to start with a con- ated source of radiation and through ction and redirection of its rays le a heating area of substantial nity at a given distance from the . In addition, in industrial ap- ions this uniform field should be ced by these units in multiple the use for a single unit is very Reference to Fig. 1 will show the effect of the use of a flat reflector back of the source. Graphical appraisal of the relative intensities thus obtained will illustrate that the energy resulting on a plane at a distance y from the source will be about double the amount which will result from direct radiation with no reflector at all; see Fig. 2. If, however, a properly contoured reflector is provided for the source (Fig. 3), it is possible to increase this amount to four or five times that of the bare source. Thus, from the same unit input of energy, it is possible to provide effectively several times the original amount of radiation at a useful location at no increase in power consumption.

To examine this statement more closely, consider the condition of a bare source. Assume a product of x dimension of zero reflectivity at a distance of y from this source. Under these circumstances, only a percentage of the developed energy equal to angle $A/360$ (considered in a plane) will initially reach the product; see Fig. 2. Since none will be rereflected, it is obvious that this is the total amount of energy which can be expected to develop useful work.

Now, if a flat reflective surface m be placed at some point back of the source with the other conditions of distance and dimension held equal, it is apparent that the amount of energy reaching the surface x has been increased by the amount of the angle $B/360$ times the reflectivity of m; see Fig. 1. The total energy reaching x would then become $A/360+BR_m/360$. For constant values of x and y, it is apparent the angle B decreases as the distance back of the source is increased. This can be of importance where x and y are small; it is of little or no value as these dimensions approach infinity. The small dimension n is all that is necessary where the reflectivity of x is zero. If the reflectivity of x (R_x) is greater than zero, the larger value of n_1 becomes involved. As the dimension x increases, with $R_x > 0$ and with multiple sources, the need for a continuous flat reflector becomes apparent. If, however, $R_x=0$, no reflector beyond n is required. A rule may be stated, then:

The importance of net oven reflectivity increases with the reflectivity of the product.

Returning to Fig. 1, if $R_x>0$, the total energy absorbed by x would be, roughly

$$a_x/360[(A-C)+(B-\mathrm{E})R_m+Ca_xR_m+Ea_xR_m{}^2]$$

If a parabolic shape p is introduced in such a fashion that its total face width

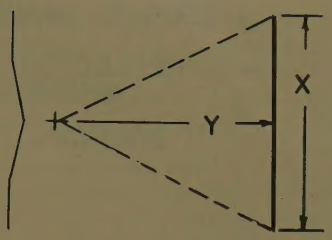

Fig. 4. Improperly contoured reflector, which may add nothing to energy on product

is equal to x and the source is in its focal point, the amount of energy reaching x in addition to that represented by $A/360$ would be $DR_p/360$. If $R_x>0$, this flux represented by $D/360$ would be reflected and rereflected between the parabolic surface p and the surface x until it divides itself so that the energy from the reflector is

$$a_x/360\{(D-2F-B)R_p+(B+2F)/[(1-R_p)+a_x]\}$$

and the total energy resulting in x equals

$$a_x/360\{A+(D-2F-B)R_p+(B+2F)/[(1-R_p)+a_x]\}$$

both equations approximate.

If specific values are assigned to the foregoing symbols (angle $A=60$ degrees, $a_x=100\%$), the following rough comparison would exist. In the case of no reflector, 60/360, or 16.7% of the radiant energy developed by the source would reach x. If a flat surface m of high reflectivity were used at a distance of $0.1x$ in back of the source where $R_x=0$, the resultant reflected angle B would approximately equal A and the additional amount of energy reaching x would be 16.7% times the assumed 95% value of R_m, or 15.8%. Thus, the efficiency of transfer would have been increased from 16.7 to 32.5%, or nearly doubled.

In the event of the third case in which a contoured reflector is employed, the initial direct radiation again=16.7%. The value of the reflected energy provided through the large angle D, however, is now nearly 54% and the total percentage of initially developed energy in forward useful radiation over 70%, or something more than four times that achieved where no reflector is involved and over double that which exists from a flat oven wall of equally reflective material and optically unadapted to the source location. It should be noted in passing that it is possible (Fig. 4) to illustrate a condition in which a reflector adds nothing to energy in a given area. In this case, the forward useful radiation remains 16.7%. While this would rarely be done deliberately, it is obvious that

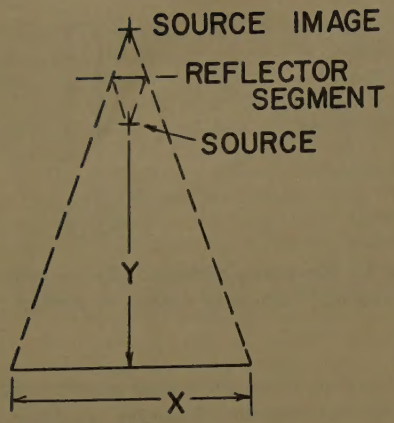

Fig. 5. Line from source image to limits of work area, which marks dimension of reflector segment

the use of a corrugated backing sheet with indiscriminate source locations would inevitably lead to some degree of this condition.

If the dimension x is made infinite, the percentage of impinged energy with no reflector reaches a maximum just under 50%. In the case of the flat reflecting surface, the same reasoning holds since the angle of lost energy approaches zero and the utilization is just less than theoretical maximum of 97% which is, however, double that of no reflector. Where contoured reflector p is used with x infinite, the theoretical maximum is $97^1/_2$% where the reflectivity of m and p is 95%. To the extent that the flat oven walls are not continuously reflective but are composed partly of areas of no reflectivity (zero per cent) or poorly reflective materials, the net oven radiant efficiency will vary between 50% and 100% of that which could be achieved with continuous flat reflective walls. Similarly, to the extent that a material of lesser reflectivity than 95% is introduced as a reflector material, the maximum net reflectivity of the infinitely large oven will vary from about 50% to 100% of the ultimate.

In the mention of a reflector optically contoured to fit a job, reference was made to a parabolic form. While this is frequently a satisfactory solution, where the source is located properly with respect to its focal point, for various reasons it is frequently desirable to provide an equal control through the use of reflectors composed of properly angled flat surfaces rather than continuous curves. In this latter instance, the development of the desired surface geometry through the use of source images is illustrated in Figs. 5 and 6.

Control for area sources is practically restricted to flat reflectors. In the case of no reflectors, the percentage of radiation forward and backward from a heated plate will be a function of the relative emissivities of the two surfaces. Where these are equal, it is obvious that 50% in one direction will be a maximum. The per cent of radiation in one direction may be determined by dividing the emissivity of that side by the sum of the two emissivities. In determining actual figures, where a flat backing-up reflective surface, is employed, and if the plate is transparent or translucent, the relative surface temperatures must be known as well as the opacity of the coating.

If concentration into a spot or line of heat is desired, it is necessary only to define the area desired to be covered, and to pursue the same procedure se Fig. 7. It will be noted that the smalle the ultimate spot desired, the more an smaller segments there are in the reflec tor, to approach an ultimate elliptica form. This cross section can be ex tended linearly to develop a trough fo a linear source, or rotated to form round reflector for a point source. I will be seen that the same basic rule would apply to development of reflector for either point or line sources.

Materials

The reflectance of various materia has been cataloged and described b different authorities and this informatio was derived through various methods appraisal. On the basis that the matte should be re-explored with the use the total radiation theory dealt wit later in this paper, a stable system wa set up based on known areas and know materials. There are more authoritativ data on the reflectivity of gold than any other commonly used material. Fu thermore, gold is more stable in its r flectivity at all usable temperatu ranges,[3] has less surface deteriorati than comparable materials,[4] and has hi reflectivity for all source temperature It was therefore selected as a standar and a test area 22 by 22 inches was s up for the comparison. Holding t voltage constant and with the roo ambient constant, sample specime 22 by 22 inches of various materials we interchanged in the test area and th relative temperature rise noted. The temperature rises were assigned intensi valuations based on the curve in Fig.

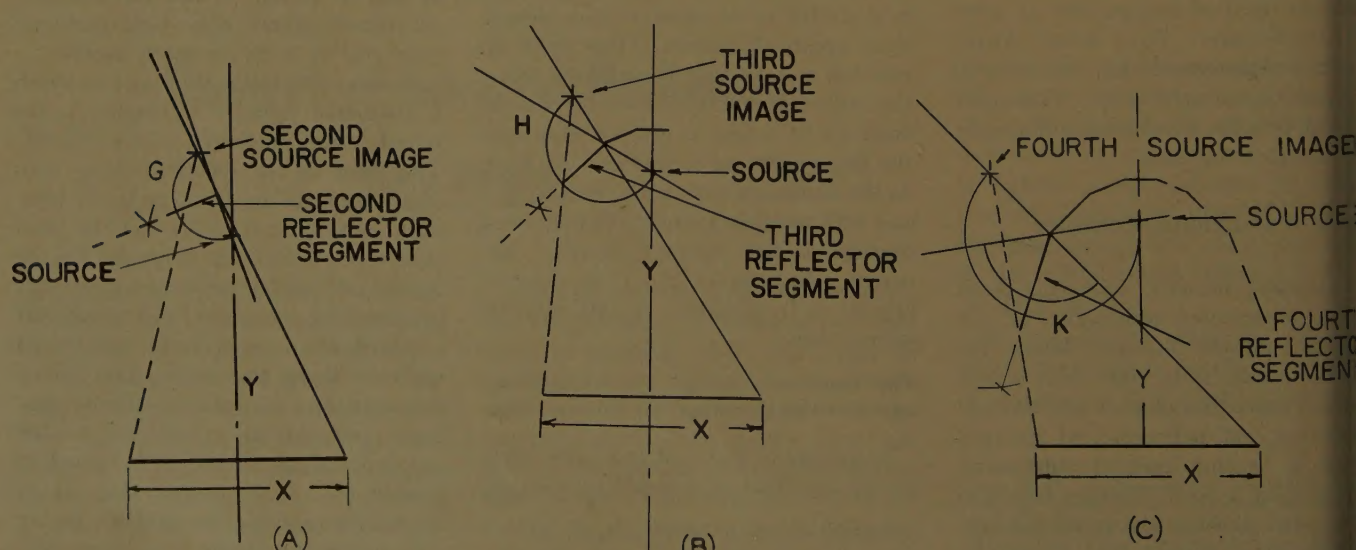

Fig. 6. Slopes fixed by bisecting lines G, H, and K; lines from source images to limits of work areas mark dimensions of reflector segm

A—Second image and segment B—Third image and segment C—Fourth image and segment

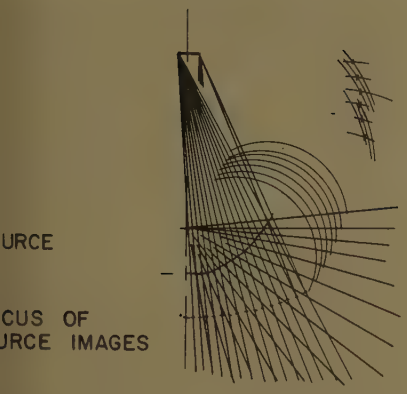

7. Construction of concentrating type eflector by means of source images which require many small segments

ch has been fairly well certified over rs of checking and application. The centage of subject area was checked substituting metals in the primary ecting areas of the same materials as se being tested. This permitted ac-ate determination of the factors in total radiation formula, so that it omes:

$$a_p)/(K_2+K_3+K_4+K_5)=H$$

uivalent heat units, Fig. 8), or $Ka_p=H$ re the constants K_1, K_2, K_3, K_4, and represent fixed products of area and orptivity of the various parts of the system. On this basis, the following ues for specific reflectivity of the erials tested based on radiation from 500 degree K source, were as follows:

Material	Per Cent
ular gold plate	98
k	78
rolytically brightened anodized minum	75
ightened anodized aluminum	59
inized steel	55

ata published by Hottel[6] indicate metal reflectivities as high as 96% highly polished aluminum with some to 89% for the oxides. Gold is n at 98.2% with nickel 89%. These es, however, are for the reciprocal he emissivities over the entire infra-range, and do not reflect the pre-lerance of energy in specific bands ying to commercial sources. industrial application, the relative ctances used should be related to the acteristics of the source. These es are considered the specific re-ances of the materials within the ning of this paper. High values are assigned silver and copper but it t be considered that commercially king these are not practical figures use of the transience of pure metal surfaces which is due to their tendency almost immediately to develop a thin oxide film. This is especially true of aluminum.[7] Of all of these, gold continues to present a relatively pure metal face for reflectivity and commercial comparisons must be based to a degree on the relative value of metallic gold compared with the oxides or other salts of alternate metals. Alzak and anodized aluminum are deliberately formed oxides, which accounts for their relative low reflectivities in the infrared range.

Specularity in a reflective surface is important in that it redirects a larger portion of the impinging beam in a situation in which the proportion of the beam which is diffused laterally or along the plane of the reflecting surface is largely lost through lateral "spill" in average installations.

Oven Geometry

The net radiant efficiency of an oven enclosure can be approximated by the following method. The absorptivity of the materials involved being known and their areas being calculable, it is possible through the theory of total radiation[8] to predict the approximate absorption of the product x as follows:

A_r = surface area of oven wall
A_p = surface area of product
A_e = area of no wall, oven ends, gaps, etc.
A_f = area of floor, all poorly reflective surfaces
a_r = absorptivity of oven wall material
a_p = absorptivity of product
$a_e = 100\%$
a_f = absorptivity of floor, poor surfaces
E = total developed radiation
$A_pa_p/(A_ra_r+A_pa_p+A_ea_f)$ = per cent E in product

The percentage of this amount absorbed by the product will represent the net oven radiant utilization. This, therefore, provides a simple method for predicting relative results by various types of oven construction and material. Further, where a standard test oven is so constructed that the constants are all known figures other than the product, it is possible to determine the product absorptivity quickly. Similarly, by using sources of definite radiating characteristics on a selected subject, it is possible to determine accurately the surface characteristics of the subject. By working continuously with known factors and introducing one variable at a time, it is possible to determine correct values of specific absorptivity for various metals and materials. (See preceding section on materials.)

It will be apparent that color sensi-

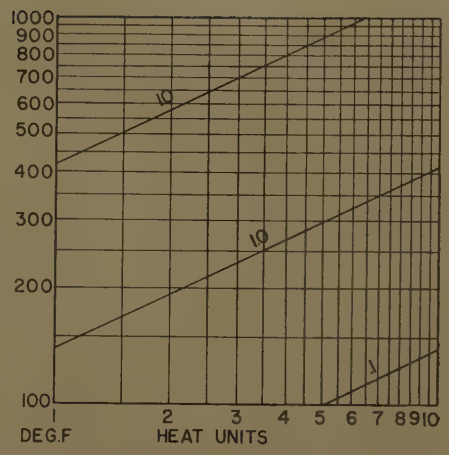

Fig. 8. Relationship between absorbed radiant energy and ultimate product temperature

tivities can be accurately determined by this method. Failure to consider total relationship between radiator and product has led to some incorrect data in published color absorptance tables. What has been tabulated has largely been the relative temperature rises in systems of low net radiant efficiency, and the poorer the net radiant efficiency, the wider the color disparity.[1] The foregoing method provides a means of accurately expanding pilot or laboratory test installations into final recommendations. It crystallizes the "size factor" to permit a more logical approach to layout problems.

To consider an example: A typical automotive oven is 10 feet wide by 10 feet high by 100 feet long. It has a total inside surface of 3,000 sq ft (square feet). It could contain, in operation, approximately five finished automobiles with a total exposed surface area of approximately 2,400 sq ft with an assumed absorptivity of 50%. There are approximately 1,000 sq ft of floor to this oven, estimated at 80% absorptivity, and there are 200 sq ft of ends. Assuming the oven walls to be highly reflective (5% absorption), the division of energy introduced in this oven would theoretically be: 3,000 by 0.5=150; 2,400 by 0.50=1,200; 1,000 by 0.80=800; 200 by 1.00=200. Thus, of a total of 2,350, only 1,200, or 51% of the input energy would be reflected in useful work. If, by contrast, the oven walls are painted black and the other factors remain the same, the calculation becomes: 3,000 by 1.00=3,000; 2,400 by 0.50 remains 1,200; 1,000 by 0.80 remains 800; 200 by 1.00 remains 200. Now, however, only 1,200/5,200, or 23% of the input energy, will be found in the product. Thus the reflectivity of the oven walls can account for more than doubling the

efficiency of the oven measured in terms of kilowatt-hours per car. (As a corollary, it should be noted that absence of oven wall is equal to oven walls of 100% absorptivity with resultant low net efficiency.) If plain oxidized aluminum or aluminized steel were used, the same method of calculation would show that roughly 34% of the input energy would reach the product, which would mean that approximately 51% more developed radiation would be required in the source to produce an equal temperature rise in the product. This is reasonably close to data derived in actual practice and serves to add validity to the theory. In the highly reflective oven first considered, operated without product, the radiated energy would theoretically divide itself as follows: 3,000 by 0.05=150; 1,000 by 0.80=800; 200 by 1.00=200; for a total of 1,150. The oven walls would thus receive 150/1,150, or 13% of the radiated energy instead of the 6.4% initially absorbed. If the oven walls had reached 150 degrees Fahrenheit in the first instance, they could now be expected to attain slightly over 200 degrees Fahrenheit. (The higher air temperature prevailing in a filled oven, however, tends to offset this effect, and in practice, little change can be measured.)

The foregoing material may be used to advantage in an examination of the relative efficacy of types of solution to an oven problem. For example, if it is desired to heat a panel of an assumed 2 ft by 2 ft with radiant energy, it is obvious that several oven selections can be made. It is possible to accomplish this result with one-sided radiation emanating from a radiating panel of the same size as the product. Assuming that this course is followed, the total radiation theory would indicate a reflector area of 4 sq ft with absorptivity of 5% (assuming reflectors to be gold), and a product area of 4 sq ft with an assumed absorptivity of 50%. If the distance between target and radiating panel is 6 inches, the area of total absorptivity (no reflecting walls) represented by ends, top and bottom, is 4 sq ft plus an equal area of total absorptivity of radiation from the back of the target. A total of 19.6% of the developed radiation would result in the product. If, however, two-sided radiation is employed, the radiating panels are increased to 3 feet by 3 feet, the unit is enclosed on two sides with reflective panels (as would be possible in a conveyorized oven) and, by means of a reflective silhouette, the end areas are reduced by providing an aperture for entry and departure with a 2-inch clearance in all directions, the flux can be recomputed as follows: 18 sq ft of reflecting area at (5%); 8 sq ft (at 50%) product area; an additional 10.44 sq ft (at 5%) (reflective baffling) with an area of total loss amounting to 1.56 sq ft of 100% absorptivity. On this basis 57.2% of the developed radiation (4 divided by 6.982) would end up in the product. Comparatively the total radiant energy required would be only one third that involved in the first solution; the amount of equipment required would be approximately five times as great and the rating of individual sources would be only 1/14 that initially considered. In practical terms, if the original solution had required four 1,400-watt sources, the latter solution would require 18 100-watt sources to perform exactly the same heating task. This illustrates a basic rule of oven geometry:

Oven-radiant efficiency varies directly with the percentage of surrounding area occupied by reflective material.

It is interesting to rework the foregoing example on the basis of a material such as aluminized steel with relatively low specific reflectivity. Here the figures will become 16.4% instead of the earlier 19.6% where the 2-ft by 2-ft radiant panel is employed and where the fully surrounded oven of the second example is constructed of the same low reflectivity material, the oven-radiant efficiency is increased only to 18.9%.

It should also be noted that if the total oven wall area is made up partly of highly reflective areas and partly of areas where the reflector is omitted, or of material of low reflectance, the resultant net oven efficiency is lowered in the same manner as if the reflecting areas were all of low reflectivity. This emphasizes the inherent error of oven constructions wherein blank or missing areas in oven walls are involved, or where consideration is given only to the reflectivity of individual reflectors, either separate or, as with reflector lamps, built into the source structure.

An oven of high radiant efficiency cannot be constructed of materials of low specific reflectivity.

A corollary rule may be derived from the foregoing: In ovens of low basic efficiency due to low percentage of enclosure area, selection of reflecting materials becomes of lesser importance. It should be remembered at this point that these conclusions deal with radiation only and do not take into consideration the effect that changes in physical oven structure might have on air movemen and convection loss. Other observatio relating to the foregoing example migh be that it is better engineering to provi a larger number of small sources (1 versus 4) on the basis that failure of o source would drop the total flux on 5½% as compared to 25%; the fa that a uniform radiant field is mo easily secured with a larger number sources; and the fact that a larg radiating area provides better angul direction of radiation in so far as irreg larities of product are concerned. O setting factors are the higher initi equipment costs as well as somewh higher maintenance problems incident increased equipment areas, and (perhap decreased accessibility. Oven geomet in the use of control equipments f point, line, or area sources is basical the same since all may be reduced to equ heated panels for this consideratio There is no critical angle of impingeme in the application of radiant energ Angular effects are subject wholly to t cosine aw. The proper engineering a proach in all applications is, of course, evaluate all factors specifically as a gui to final determination. There may be i stances where intermittent use of equi ment, mobility, or low ratio of operati cost to end value may dictate the deli erate sacrifice of operating efficiency favor of low initial cost. It is, howeve important that operating cost be proper weighed in full consideration of the pro lem. Many examples of economic co parison could be worked out to illustra this point. A basic 10-year amortizati working figure, which may surprise man is:

One per cent saved in operating cost w usually justify 3% additional in first cost.

There are then three factors which c importantly affect the utilization of e ergy developed by any source applied an oven structure. These may be rec pitulated as follows: 1. Per-cent surroun or percentage of product surrounded oven walls in terms of total enclosu 2. Average specific reflectively of all in rior oven materials. 3. Optical efficien of the system both in individual reflect and total oven. One striking conclusi appears in connection with the foregoi In an average-sized oven with medi "fill," say 50%, where all the forego factors of design are omitted, it appe as though the total energy initially rea ing the product could be as low as 1 of that developed by the source. T product absorptivity would permit utili tion of no more than 80% of that amo

n perhaps 8% of the originally de-ped radiant energy thus ending in use-work. Where careful attention is paid ll of the foregoing factors and practical imums are achieved, it appears likely an ultimate of 70% to 75% might be ized. Thus, in oven design alone, n the same product, it would appear over-all radiant efficiency might from 8% to 75%. Where the radi- efficiencies of various sources are en into consideration (ranging from ally 45% to 87%), it will be seen that not difficult to visualize one infrared n which is as much as 15 times as ient with respect to radiant energy another. While these extremes of iation are not commonly encountered, observation has been made that the erence between a good infrared oven a bad one may be much greater than is ally possible in the case of convection ns.

nmary

o recapitulate, the fundamental rules lying to the control and utilization of ant heat sources, in single and in multiple housings which are in radiant-oven use may be stated as follows:

1. The radiant efficiency of an individual reflector is measured by the accuracy of its optical design and the specific reflectivity of its surface. It may attain a little more than 90%.

   Corollary A: A correctly contoured reflector may provide several times as much forward useful radiation as a flat reflecting surface, and many times as much as no reflector at all.

   Corollary B: An incorrectly designed reflector may contribute little or nothing to a specific heating problem.

   Corollary C: Any departure from specularity or "gloss" in a reflector surface detracts from its control efficiency, rather than its total reflectance.

2. The net reflective control of a radiant oven is measured by:
   - A. The radiant efficiency of the individual reflectors involved.
   - B. The per cent of total enclosure achieved.
   - C. The net specific reflectivity of the materials making up the total oven interior.

3. The net thermal efficiency of a radiant oven is determined by:
   - A. The radiant efficiency of the source.
   - B. Its net reflective control.
   - C. The absorptivity, effective area, and physical disposition of the product.
   - D. The amount of convective loss involved.

References

1. Radiant Heating Using Lamps and Quartz Tubes, **Ira J. Barber.** *Proceedings*, National Industrial Electric Heating Conference, Cincinnati, Ohio, vol. 3, Feb. 4, 1958.

2. Industrial Application of Infrared, **Ira J. Barber.** *Electrical Engineering*, vol. 72, no. 9, Sept. 1953, pp. 764–69.

3. *WADC-TR 57-159*, Wright Air Development Center, Dayton, Ohio, 1957, p. 36.

4. Gold and Gold Alloys, **E. M. Wise.** "Corrosion Handbook," Electrochemical Society, Inc., John Wiley & Sons, Inc., New York, N. Y., 1948, p. 112.

5. Infrared Reflector Surfaces, **J. D. Hall.** "Industrial Applications of Infrared" (book), McGraw-Hill Book Company, Inc., New York, N. Y., 1947, p. 37.

6. Applied Heat Transmission (book), **Herman J. Stoever.** McGraw-Hill Book Company, Inc., 1941, p. 213, Table IV, **H. C. Hottel.**

7. Aluminum for Reflectors, **Junius D. Edwards.** *Transactions*, The Illuminating Engineering Society, New York, N. Y., vol. XXIX, no. 5, May 1934, pp. 351–57.

8. General Theory of Enclosure, **H. H. Higbie.** "Lighting Calculations" (book), John Wiley & Sons, Inc., 1934, pp. 249–51.

The Use of Frequency-Response Tests the Analysis of a Foil Mill Automatic Gage Control

S. J. JONES MEMBER AIEE

R. M. SILLS MEMBER AIEE

REQUENCY-response measurements are often made in the laboratory to rmine performance of components or ems. Such tests are far more rare on plete processes. To the authors' wledge, the tests described here were first to vary sinusoidally, while rolling, speed of a metal rolling mill to determine how strip thickness was affected by the frequency of oscillation.

The results obtained indicate that such tests can be useful for substantiating simplified theoretical analysis, determining quantitative relationships for complex transfer functions, and improving system performance.

r 59-78, recommended by the AIEE Metal stry Committee and approved by the AIEE nical Operations Department for presentation e AIEE Winter General Meeting, New York, ., February 1–6, 1959. Manuscript submitted mber 3, 1958; made available for printing mber 3, 1958.

Jones is with the Aluminum Company of rica, Pittsburgh, Pa.; and R. M. Sills is the General Electric Company, Schenectady, .

uthors are indebted to Messrs. R. G. Beadle R. A. Phillips of the General Electric Company he physical and mathematical concepts used e Appendix.

Controlling Gage on a Foil Mill

Any strip less than 0.006 inch thick is classed as "foil," although aluminum strip rolled for containers of various sorts may be as heavy as 0.0105 inch but rolled on a "foil" mill. Although foil may be made of many metals, this paper is confined to aluminum foil, which will simply be referred to as "foil."

The process of cold rolling foil is quite different in many respects from those usually used for other products. Since this is not a treatise on foil rolling, only those characteristics that affect gage control will be mentioned.

Perhaps the most notable aspect is the fact that the rolls are always jammed together, or set "below face," such that roll pressure may be 100 tons or more per screw with no metal in the mill. This is also characteristic of tinplate steel mills on the last pass or two. This results in considerable roll flattening; so much so, in fact, that small changes in screwdown settings change only the deformation of the rolls and the cross-sectional shape of the foil, but not the thickness. This condition will be reached on any rolling mill when the ratio of roll diameter to metal thickness is made high enough.[1]

Another factor is the effect of mill speed on thickness. The "speed effect" occurring in all strip mills is well known, and is attributed largely to a decrease in the coefficient of friction between work rolls and strip as speed is increased.[1] On a foil mill, this effect is more pronounced than on mills rolling heavier thicknesses. In fact, it is so pronounced at all speeds at which foil is rolled that it is the means most often used by the operators to man-

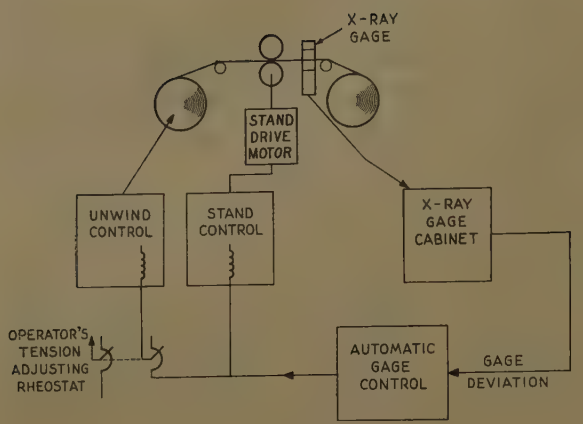

Fig. 1. Simplified schematic block diagram of original gage control system

ually adjust gage. It is also the method used in the gage control discussed in this paper.

Description of Gage Control

Fig. 1 is a schematic block diagram of the foil mill gage regulator, as originally designed, but with certain details omitted. An X-ray gage, mounted close to the work rolls, provides a thickness deviation signal. This is amplified by three stages of magnetic amplifiers, and the resultant voltage is applied to a control field on the mill voltage or speed regulator, to vary the speed in proportion to thickness deviation. The original design included the circuit shown to adjust unwind reel current (and hence tension) in proportion to deviation but this was later disconnected because it did not appear to be necessary. Other circuits included, but not shown, were forcing, which will be discussed later, and an integrating reset circuit to readjust the mill motor-operated rheostat to keep the regulator within range. This circuit does not enter into the analysis which is described here so it need not be considered further.

When the regulator was installed, it was found to be difficult to stabilize. Although the loop gain was not high, the system had to be made quite slow to obtain stability. Indications were that the gain increased in the middle frequency range. To learn how to improve its performance, it was decided to make frequency-response measurements on the complete system.

Preliminary Analysis

Prior to making the frequency-response tests, a preliminary block diagram analysis was made. Fig. 2 shows a somewhat abbreviated block diagram of the system. The Appendix gives the derivation of the $\Delta S_1/\Delta v_m$ block. In order to reduce the diagram to more manageable form it is necessary to make some simplifying assumptions.

As a start, it was assumed that $\Delta I/\Delta v_m = 0$. This states that the reel current regulators are fast compared with mil speed changes, and have a high gain, bot of which seemed like good assumption This makes $\Delta\tau_d = 0$, and eliminates th reel voltage regulators, reel current regula tors, and reel counter electromotive forc regulators all at once, leaving only th tension loop ($\Delta S_1/\Delta v_m$) to be reduced a far as the reels are concerned.

The transfer function required is $\Delta S_1/\Delta v_m$. From the block diagram, usin $C/R = G/1+GH$, the following is writte

$$\frac{\Delta S_1}{\Delta v_m} = \frac{\dfrac{E_1' A_1}{v_1(1+pT_{t1})}}{1+\dfrac{E_1' A_1}{v_1(1+pT_{t1})}\dfrac{r_1^2}{pJ_1G_1^2}} = \frac{pT_{r1}E_1' A_1/v_1}{1+pT_{r1}+p^2T_{r1}T_{t1}} \quad (1$$

where $T_{r1} = J_1G_1^2v_1/E_1' A_1 r_1^2$, one of th time constants between torque and ten sion.

The system block diagram now can b redrawn as shown in Fig. 3.

It will be recalled that experience wit the gage control indicated a rising gain i the middle frequencies. Since all el ments of the control except the mill-strip reels block were known, it could b assumed that any peculiar behavio originated in this area. It was the obje tive of the preliminary analysis, there fore, to determine a transfer function fo the mill. This had to be simple enoug to have physical significance and to b verified by tests.

With no further justification, ther other than that subsequent tests seeme to prove the assumptions reasonable, th block diagram of Fig. 3 was further sim plified.

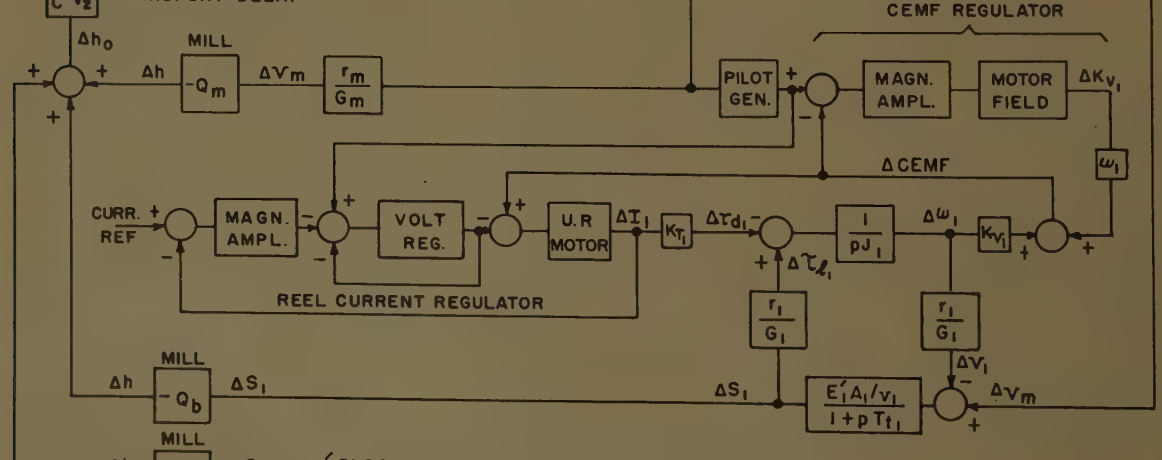

Fig. 2. Syste block diagram i cluding mill stan reels, strip, and ga control

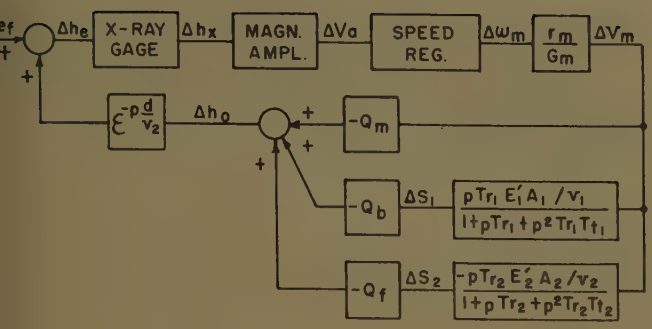

Fig. 3. Simplified block diagram of gage-control system

The three parallel paths making up $\Delta h_0/\Delta v_m$ could have been combined at is point, but the result would be a ther complex expression without much ysical significance. Therefore another nplification was made by assuming at $T_r >> T_r T_t$. This says that the feedck around the mill (see Appendix) is ong, making E' small, which was beved to be true, and will presently be own to be true. Now the three blocks n be added, yielding

$$\frac{\Delta h_0}{\Delta v_m} = -Q_m \times \left[1+p\left\{T_{r1}\left(1+\frac{Q_b}{Q_m}\frac{E_1'A_1}{v_1}\right)+T_{r2}\left(1-\frac{Q_f}{Q_m}\frac{E_2'A_2}{v_2}\right)\right\}+p^2T_{r1}T_{r2}\left(1+\frac{Q_b}{Q_m}\frac{E_1'A_1}{v_1}-\frac{Q_f}{Q_m}\frac{E_2'A_2}{v_2}\right)\right] \Big/ (1+pT_{r1})(1+pT_{r2}) \qquad (2)$$

This is still not as simple an expression desired although its connection with ality will become apparent.

The final simplifying assumption to be ade was that front tension had negligible ect on gage compared with back tension. ery operator knows that back tension several times as effective as front nsion, so this assumption is not entirely e of convenience. By making $Q_f = 0$ equation 2 the following is obtained

$$\frac{\Delta h_0}{\Delta v_m} = -Q_m \frac{1+pT_{r1}\left(1+\frac{Q_b}{Q_m}\frac{E_1'A_1}{v_1}\right)}{1+pT_{r1}} \qquad (3)$$

Since the p term in the numerator is larger than in the denominator, the mill has the characteristics of a lead circuit. That is, between the frequencies

$$1/T_{r1}\left(1+\frac{Q_b}{Q_m}\frac{E_1'A_1}{v_1}\right)$$

and $1/T_{r1}$ the gain will increase in proportion to frequency (20 decibels/decade) over what it would be without the lead effect. This effect can be explained physically as follows.

If the mill speed is varied sinusoidally at low frequencies the reel, being tied to the mill by the strip, will follow, so that unwind tension remains constant. As the frequency is increased, the reel, due to the combined effects of its inertia and the elasticity of the strip, will be unable to follow, so tension will oscillate. Since tension will tend to increase while the mill is increasing in speed, and vice versa, the net effect will be to cause a greater change in thickness than would be caused by mill speed alone. That is, the gain increases.

As frequency is further increased, the reel will eventually not change in speed at all. Above this frequency, gain will be constant again, at least insofar as the effect of the unwind reel goes. The more nearly correct equation 2 indicates that there is another down-break and another up-break, so that possibly as frequency is further increased the gain will drop down to a lower level, due to the effect of the rewind reel.

Effect of Unwind Coil Diameter

Remembering that $T_{r1} = J_1 G_1^2 v_1 / E_1' A_1 r_1$, equation 3 can be rewritten:

$$\frac{\Delta h_0}{\Delta v_m} = -Q_m \frac{1+p\frac{J_1G_1^2}{r_1^2}\left(\frac{v_1}{E_1'A_1}+\frac{Q_b}{Q_m}\right)}{1+p\frac{J_1G_1^2}{r_1^2}\frac{v_1}{E_1'A_1}} \qquad (4)$$

Equation 4 shows that as the diameter of the coil on the unwind reel decreases, both the up-break and the down-break will decrease in frequency (because r_1^2 decreases faster than J_1), maintaining the same ratio. Thus, the frequency-response tests should be made at as nearly constant coil diameter as possible (that is, they should be completed quickly), and the coil diameter should be measured during the test.

Equation 4 also indicates that the time constants will change with speed, increasing as speed increases. This would imply that maximum speed would be the least stable condition, especially since Q_b/Q_m probably increases with speed.

Frequency-Response Tests

With this preliminary analysis completed, the next step was to run frequency-response tests. It was hoped that these would confirm the analysis and provide a number for T_{r1} and hence for E_1'.

Although several more sophisticated methods are available for determining frequency response, and these are commonly used in the laboratory, it was decided that for tests on the mill a Brush recorder would be used. This was, in part, because unlimited time would not be available since the mill would be rolling foil, and in part because considerable distortion was expected, due to inherent thickness variations and X-ray gage noise. Accordingly a Kronhite model *400-A* signal

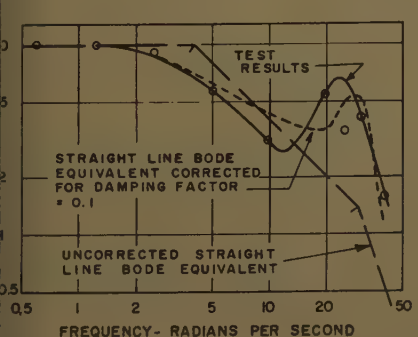

Fig. 4 (left). Gain versus frequency curves for X-ray gage

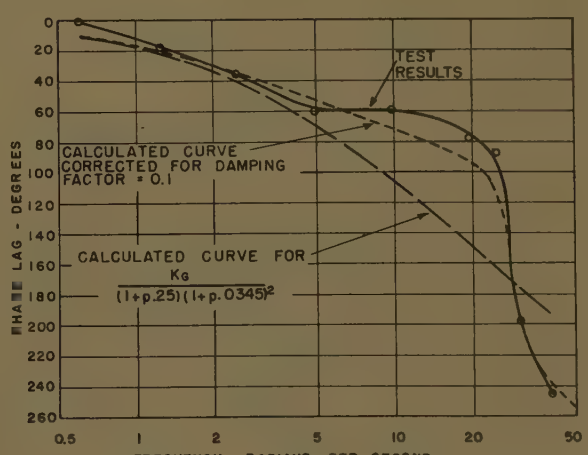

Fig. 5 (right). Phase lag versus frequency curves for X-ray gage

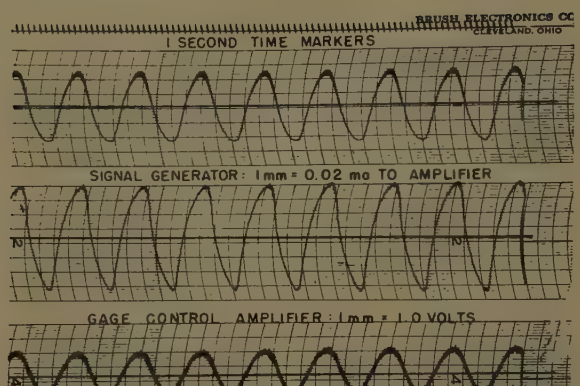

Fig. 6 Typical recording taken during frequency-response test. The approximate zero line is drawn in to aid in determining average amplitude and phase shift

generator and a 6-channel Brush oscillograph were used for the tests.

Mill Description

The mill on which the frequency-response tests were run was a 10-inch and 24- by 48-inch single-stand nonreversing foil mill. The mill stand is driven by a 1,000-hp (horsepower) 575/1,150-rpm d-c motor through a pinion stand. The unwind reel is powered by two 50-hp 200/800-rpm motors, and the rewind reel is driven by two 50-hp 400/1,600-rpm machines, both through reduction gears. Each reel and the mill stand has its own generator.

X-Ray Gage Response

The first step was to measure the frequency response of the X-ray gage, since it is most important to know this to determine the response of the mill. It was discovered after the tests were run on the mill that the amplifier used with the recorder was disturbing the operation of the gage. Although this did not invalidate the mill tests it did not give accurate information on the gage, so the interaction was eliminated by using an isolating transformer and another test run on the gage.

Fig. 4 shows the resulting gain curve, and Fig. 5 the phase lag. From previous tests on the same design gage it was known normally to have a resonant peak at about 25 rad/sec (radians per second). Hence, additional data were taken near this frequency, although the other points were all approximately an octave apart. It will be noted that all points seem to fall on a plausible curve except the one at 25 rad/sec. The gage output at this frequency was quite irregular, indicating that something unorthodox was happening.

Although not at all necessary to the solution of the problem, an attempt was made to justify the shape of the measured gain curve. It is known that when a transfer function has imaginary roots both gain and phase shift will be greater than calculated from the approximate transfer function (or measured with a Bode ruler from the straight-line approximation, as was done here).[2] Using the curves given in reference 2 the corrected gain- and phase-lag curves shown in Figs. 4 and 5 were obtained, using a damping factor of 0.1.

While the correlation with test data is still not very good this at least makes the data seem more plausible. In connection with correlation it should be recognized that because of the size of the recorder charts used and width of traces, amplitudes could be read only to an accuracy of about 5 or 6% and phase angles to about 9 degrees at best. Added to these errors are those due to nonlinearities of system components.

Tests on Mill

After getting the first-mentioned gage-response data the signal generator and recorder were set up for the big test. Referring to Fig. 3, the circuit was opened between the X-ray gage and the magnetic amplifier and the signal generator was connected to the input of the amplifier. The quantities recorded were, in addition to the signal generator output, ΔV_a, Δv_m, and Δh_x. The lowest frequency used

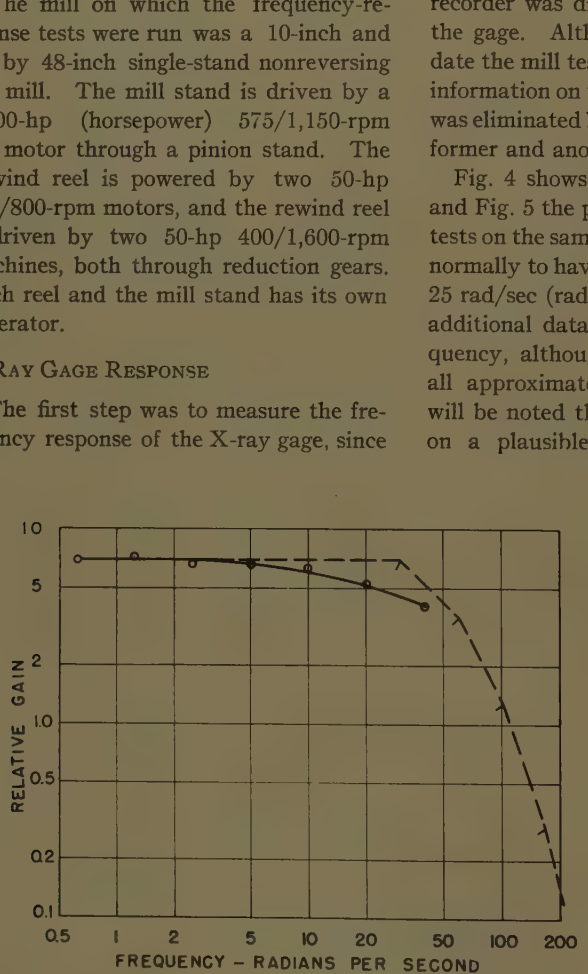

Fig. 7 (above). Gain versus frequency for magnetic amplifier

0 = test points
- - - = straight-line Bode approximation

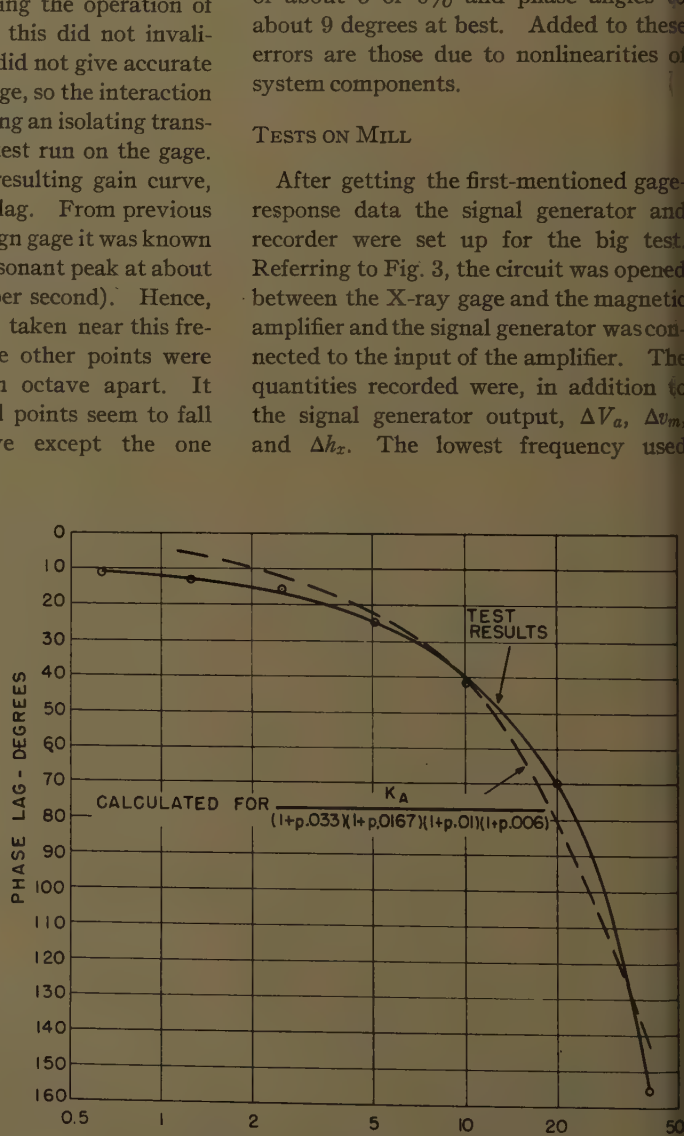

Fig. 8 (right). Phase lag versus frequency for magnetic amplifier

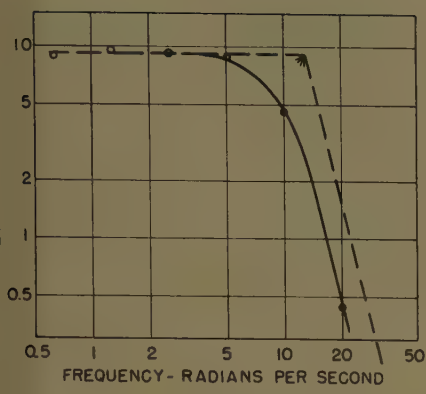

ig. 9. Gain versus frequency for mill motor and control

0 = test points
- - - = straight-line Bode approximation

as 0.1 cps (cycle per second), as any ower frequencies would take too much ime, and it was desirable to cover a omplete range of frequencies with as early as possible the same coil diameter. bove 1 or 2 cps the attenuation increased ery rapidly, putting an upper limit on he frequency range. Fig. 6 shows a ypical recording for one frequency, and ives some idea of the difficulty of obtain- ng precise data from the gage. At lower requencies the wandering and gage noise eriously distort the supposedly sinusoidal utput, and at higher frequencies the mplitude becomes so small as to make ccurate measurements impossible. Nevertheless, one of the purposes of this aper is to show that even under such ircumstances it can be feasible to secure ntelligible results.

From the charts thus obtained amplitude nd phase shift versus frequency were lotted for $\Delta V_a/\Delta V_s$, $\Delta v_m/\Delta V_a$, and $\Delta h_x/\Delta v_m$. From the first two, approxi- nate transfer functions were obtained by cut-and-try methods. That is, based on the gain curve a straight-line Bode approximation was drawn. Its phase shift was then measured with a Bode ruler and plotted on the phase-shift curve. By successive trials a compromise was reached that represented the best fit of both curves. The results are shown in Figs. 7–10.

Alternate Methods

These transfer functions could have been obtained by calculation accurately enough for designing stabilizing circuits, although the frequency-response test method was used since the test was being run anyway. However, as the analysis showed, obtaining the transfer function of the mill by calculation would be very difficult if not impossible with the knowledge available.

It should also be pointed out that it is not absolutely necessary to measure phase shift to obtain usable results. That is, a transfer function accurate enough for designing stabilizing circuits can often be deduced from the gain versus frequency curves. This is a great timesaver, as determining phase shift from oscillograph charts is a tedious job.

Mill Transfer Function

To obtain the mill transfer function, $\Delta h_x/\Delta v_m$ was first plotted. However, what was required was $\Delta h_0/v_m$. This was obtained by dividing $\Delta h_x/\Delta v_m$ by the X-ray gage gain, $\Delta h_x/\Delta h_0$, previously determined. Fig. 11 shows the results.

To obtain phase shift it was necessary to subtract the phase shift contributed by the gage, by the noise filter used for recording purposes, and by the transport time between roll bite and gage. Since this required the subtraction of two large numbers, individual points were not subtracted, but smooth curves were drawn through each set of data. These are shown in Fig. 12. Fig. 13 was then drawn by subtracting the two curves. Again, the best fitting straight line approximation was determined by trial, and it and its phase shift are plotted on Figs. 11 and 13 respectively.

It is interesting to note that while the measured gain has the shape predicted by equation 3 over the frequency range it was possible to use, the best fit for the phase-shift curve was a transfer function more nearly resembling equation 2. However, in the frequency range of importance to the regulator the simpler expression is probably adequate, and was used. This made it possible to take into account the change in coil diameter.

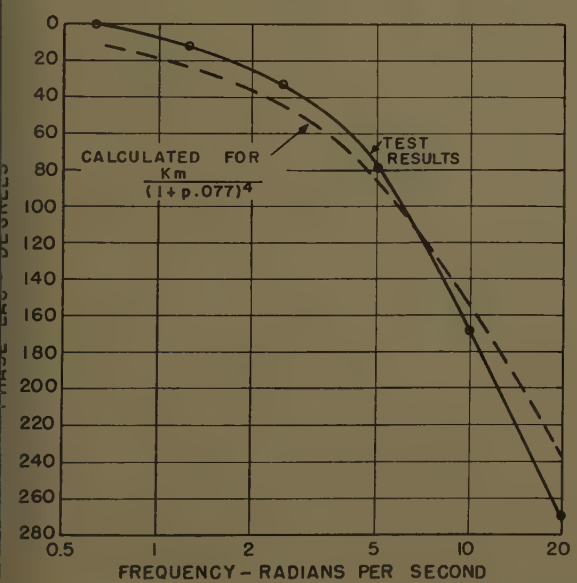

Fig. 10. Phase lag versus frequency for mill motor and control

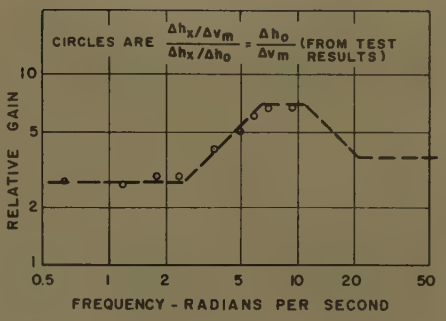

Fig. 11. Gain versus frequency for mill
- - - = straight-line Bode approximation

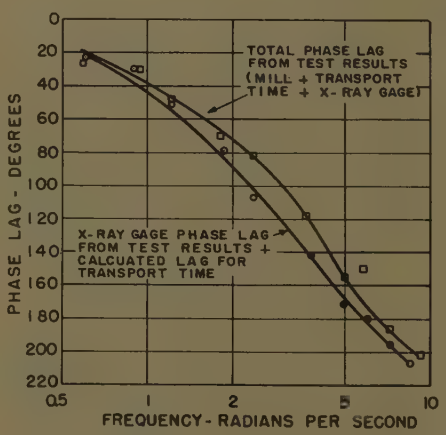

Fig. 12. Phase lag versus frequency from tests on mill and X-ray gage

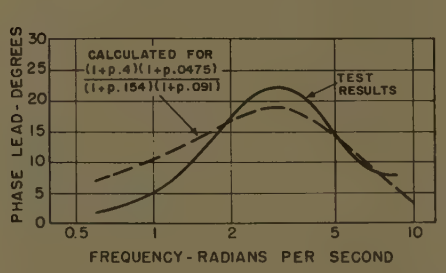

Fig. 13. Phase lead versus frequency for mill

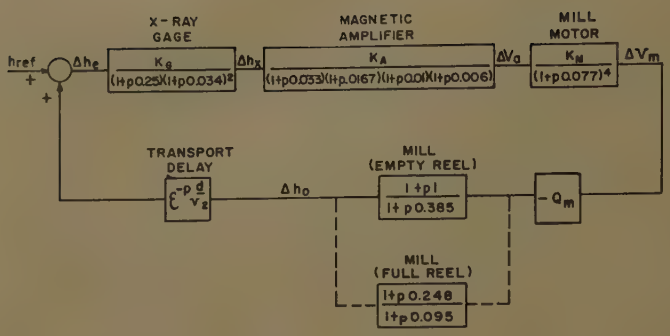

Fig. 14 (left). Final block diagram of system, not including stabilizing circuits

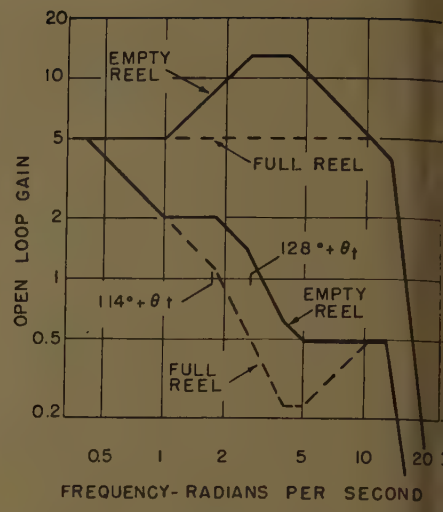

Fig. 15. Bode diagrams for the gage control. Upper curves are without stabilizing circuits. Note that at full reel the up-break of the mill is cancelled by the gage time constant. Lower curves include effect of notch network and rate feedback

As has been pointed out, the mill transfer function varies with coil diameter, whereas the tests were made at approximately a constant diameter. Thus it is necessary to calculate the time constants at full and empty unwind reel. The results are given in Table I.

Discussion of Reel Time Constant, T_{r1}

As shown in Fig. 11, the time constant T_{r1} was seen to be about 0.154 second. Since all numbers in the expression for T_{r1} are known except E_1', we can use this result of the frequency-response tests to determine a value of E_1', the "apparent" modulus of elasticity.

Thus, $E_1' = J_1 G_1^2 v_1 / T_{r1} A_1 r_1^2$. For the conditions under which the frequency-response tests were taken the following numbers apply:

$J_1 = 14.5$ slug ft (feet)^2
$T_{r1} = 0.154$ sec
$G_1^2 = 7.76$
$A_1 = 0.1$ in. (inch)^2
$v_1 = 7.7$ ft/sec
$r_1^2 = 0.69$ ft^2 (average measured during test)

From these calculate $E_1' = 81{,}000$ psi (pounds per square inch). Since aluminum has an E of 10^7 psi, this is an apparent reduction of over 120 to 1 in the modulus of elasticity. In other words, the strip acts more as if it were made of rubber than of aluminum. This is a direct result of the feedback discussed in the Appendix. Phillips has calculated the amount of this apparent reduction in modulus for steel strip in a tandem cold mill and found it to be about 35 to 1 between the last stand and the reel, and between 240 to 1 and 335 to 1 between stands.[3]

Obviously, it is because E_1' is so low that the reels affect the gage control at frequencies in the vicinity of crossover. There are other consequences of what might be called this basic fact of rolling. For example, it is probably what makes a tandem mill possible, for without it, it would be difficult to keep interstand tensions within reasonable bounds.

It is partly because E_1' is so low, and hence T_{r1} is so long, that controlling gage on a foil mill by adjusting back tension does not appear to be as satisfactory as using mill speed. It can be shown that, when back tension is used, the block diagram will be very similar to that existing when mill speed is used except that the inertia time constant of the mill motor is replaced by T_{r1}, the time constant between reel torque and back tension. If the latter is larger, as will frequently be the case, the system response will be poorer. In addition, the lead effect of the unwind reel, which frequently improves response, will not be present.

The time constant T_r, and the phenomenon of reduced apparent modulus of elasticity, is also an important factor in tension regulators. It can adversely affect both stability and gain if not understood and taken into account.

Table I

Diameter	38 in. (full)	20 in. (test)	12 in. (empty)
J_1/r_1^2	13	21	52.5
Up-break	0.248	0.4	1.0 sec
Down-break, T_{r1}	0.095	0.154	0.385

Measuring E′

The use of frequency-response tests is not the easiest or most direct method of measuring E′. A more direct method is to make tension changes and measure the resulting change in v_r. If mill speed is held constant, then from equation 18 in the Appendix,

$$E_1' = \frac{-\Delta S_1}{A_1} \frac{v_1}{\Delta v_1} \qquad (5)$$

for the unwind reel. One might expect that Δv_1 would be too small to measure with simple equipment, but such is not the case. On several rough tests on both aluminum and steel mills the authors have measured reel speed changes of as much as 20% with tension changes that still permitted rolling. Although no very accurate tests have been made, the results have at least confirmed the order of magnitude expected for E_1'.

Gage-Control Performance

Stabilizing the Regulator

In addition to increasing our understanding of the system, the real reason for this work has been to improve the performance of the gage control and learn how to design such controls for best performance.

The first step in stabilizing the system was to draw the final block diagram, using the transfer functions determined from the frequency-response tests. This is shown in Fig. 14. The d-c gain figures are not shown, since the individual gains are not important. In practice, the amplifier gain is made sufficiently large to give the desired open-loop gain.

From the block diagram, the straight-line Bode diagrams for both empty and full reel were drawn, as shown in Fig. 15. The d-c gain was somewhat arbitrarily set at 5, based on experience with other gage controls. Any loop gain above about 3 is usually sufficient if the response is fast enough.

The first step taken to stabilize the system was to design a lag-lead or notch network. Because of the multitude of time constants in most gage-control systems we have generally found the notch network rather than a simple lag circuit to be worth the additional complication. After some experimenting (on paper) a notch was selected having a down-break at 0.4 rad/sec, and up-breaks at the gage time constant (4 rad/sec) and at 5 rad/sec.

If the notch were loaded by pure resistance it would have one more down-break at 75 rad/sec for the values chosen. For

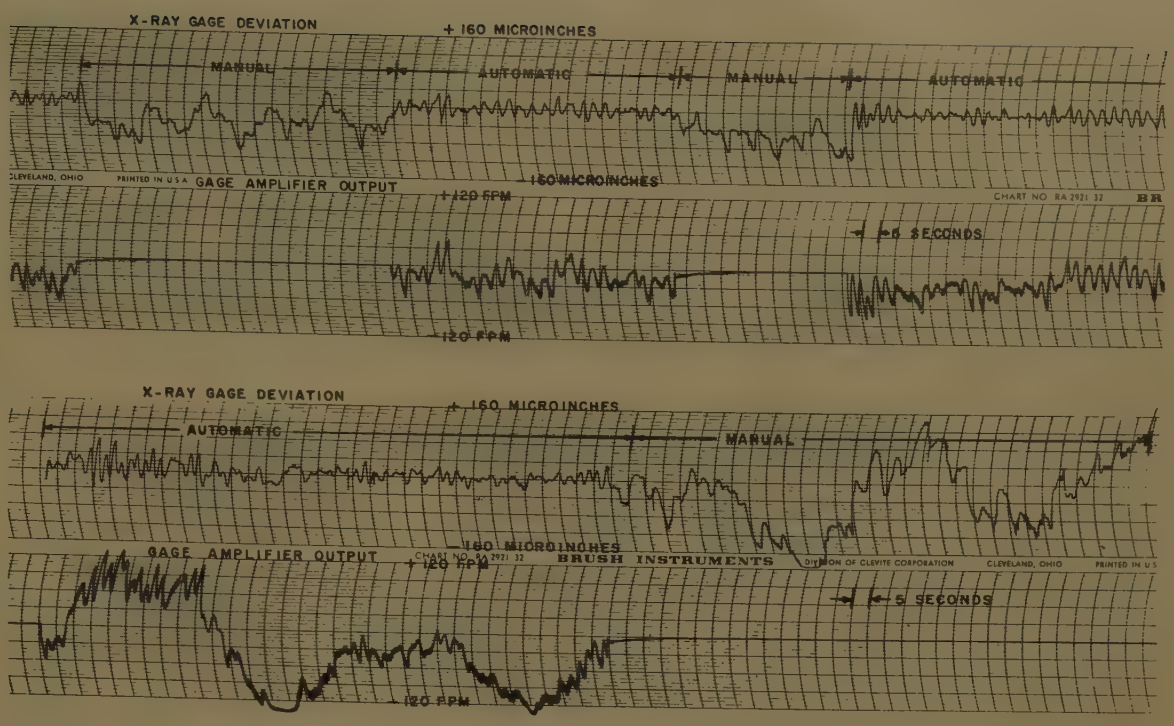

g. 16. Recordings thickness and plifier output owing effective- ss of gage control

ominal thickness = 0.002 in.
ominal mill speed = 450 ft/minute

cuit reasons, it was necessary to put e notch network in series with a rela- ely low resistance and a relatively gh inductance of a magnetic-amplifier ntrol winding. This causes an addi- nal down-break, so the final notch has wn-breaks at 30 and at 62.5 rad/ . The extra down-break is helpful in s instance in attenuating the 120-cycle ple from the first stage magnetic plifier.

A rate feedback, producing a lag, was ded around one stage of magnetic plifier partially to cancel the lead used by the unwind reel, although the de diagram shows that stability can be ieved without this on this mill. e resulting stabilized Bode diagram is shown on Fig. 15.

Similar frequency-response tests were de on another mill, which had a higher l inertia and a higher reel-gear ratio. least partially because of this the e constant T_{r1}, was considerably longer, change from full to empty reel was ch greater, and the total gain increase about 6 to 1. The gage control was alled first on this mill, and it is the one in which the rising gain was suspected, prompting this study. On it, both the Bode diagram and field experience confirm that the rate feedback is necessary to obtain stability with reasonably fast response. Incidentally, the same notch network is used for this and a number of other mills, leaving only the rate feedback and over-all gain to be adjusted in this field.

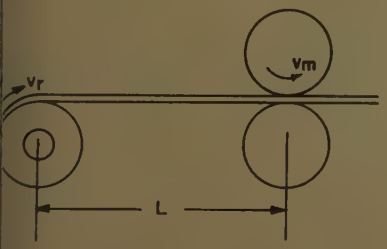

17. Unwind reel and mill stand with no reduction

Performance

None of the gage controls have been operating for enough time to have accumulated very complete data on the overall improvement contributed by the gage control. Fig. 16 shows part of two recordings made at the time the stabilizing circuits were being adjusted. This is the mill on which the frequency-response tests described here were made. The upper chart seemed to represent average quality foil of this thickness, while the lower chart is an example of unusually poor foil. In both instances, it will be noted that the gage control makes an appreciable improvement over manual control.

Later checks, while not yet conclusive, indicate that the automatic control limits gage variation to approximately one-half that experienced when using manual control.

Side benefits, which have occurred, are fewer breaks in the strip and consequently increased mill production.

Conclusions

On the basis of the work done on two foil-mill gage controls it is concluded that frequency-response tests on a complete system can be a very useful tool to supplement frequency-response analysis.

In summary, the tests described here accomplished at least the following three objectives:

1. They confirmed the simplified analysis of the system, thus adding to the understanding of the gage control.

2. They provided experimental verification for the theoretically predicted apparent reduction in modulus of elasticity thus increasing knowledge and understanding of all metal-rolling processes.

3. They made it possible to design new stabilizing circuits for the foil-mill gage control and thus improve its performance appreciably.

Appendix

Derivation of Tension Transfer Function

The following is not a rigorous proof. It is a simplified explanation intended primarily to provide a clear physical picture of relationships that actually exist.

Consider first an unwind reel feeding a mill stand, which for the moment is not taking any reduction. This is illustrated in Fig. 17.

By definition

$$E = \frac{\text{Stress}}{\text{Strain}} = \frac{S/A}{e/l}$$

from which

$$e = \frac{Sl}{AE} \qquad (6)$$

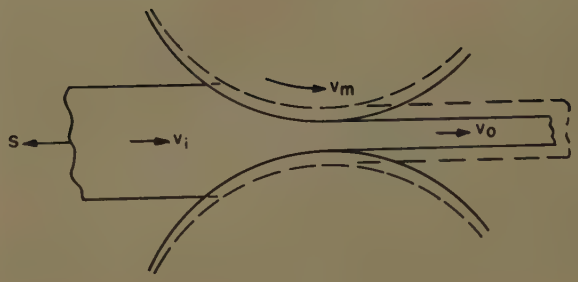

Fig. 18 (left). Cross section of mill-roll gap showing two different reductions

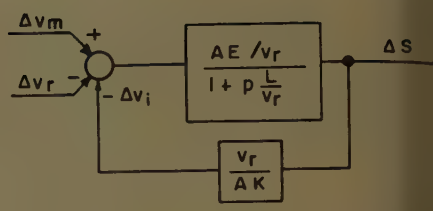

Fig. 19 (right). Block diagram of mill

where

E = modulus of elasticity, lb (pounds)/in.^{2}
S = tension, lb
A = strip cross section, in.^{2}
e = elongation, ft
l = unstressed length, ft

From Fig. 17, L is the stressed length. From the above definitions we can write

$$l+e=L \tag{7}$$

Substituting equation 6 into equation 7

$$l+\frac{Sl}{AE}=L$$

and

$$l=\frac{L}{1+S/AE} \tag{8}$$

Differentiating both sides of equation 8

$$dl=\frac{-L/AE}{(1+S/AE)^2}\,dS \tag{9}$$

Typically, $S/A=5{,}000$ lb/in.^{2} and $E=10^7$ lb/in.^{2}, so that $(1+S/AE)^2=(1+0.0005)^2=1+0.00000025$.

Thus little error is introduced by neglecting the term in parentheses and writing

$$dl=\frac{-L}{AE}\,dS \tag{10}$$

When the mill is rolling, strip, which for this analysis can be considered to be unstressed, is continually being unwound from the reel and stressed. The equivalent length of stressed strip unwound in time dt is

$$dl_t=v_r dt(1+S/AE) \tag{11}$$

Also, strip is continually leaving the mill after being stressed and elongated. The length leaving the mill in time dt is

$$dl_0=v_m dt \tag{12}$$

The change in length $dl=dl_t-dl_0$. Subtracting equation 12 from equation 11 yields

$$dl=dl_t-dl_0=(v_r+v_r S/AE-v_m)dt \tag{13}$$

Substituting equation 10 in equation 13

$$-\frac{L}{AE}\,dS=(v_r+v_r S/AE-v_m)dt \tag{14}$$

Substituting $p=d/dt$ produces

$$-LpS/AE=v_r+v_r S/AE-v_m \tag{15}$$

Rearranging equation 15 and solving for S yields

$$S=\frac{\frac{AE}{v_r}(v_m-v_r)}{1+pL/v_r} \tag{16}$$

For small changes we can write

$$\Delta S=\frac{\frac{AE}{v_r}(\Delta v_m-\Delta v_r)}{1+pL/v_r} \tag{17}$$

Equation 17 is true if the mill is taking no reduction. Now imagine that the rolls are brought closer together, so that some reduction is taken, as represented by the dashed lines in Fig. 18.

For this explanation, the neutral point, or point of no slip, will be assumed to be at the exit of the roll gap, so that $v_0=v_m$. In actuality the neutral point can be anywhere in the roll gap, depending on reduction, tensions and other factors, but this does not change the result qualitatively.

Now, let us start with a well known fact that requires no proof; i.e., that if back tension is increased the reduction will increase. The condition with increased back tension is represented in Fig. 18 by solid lines.

By inspection of Fig. 17, as well as by equation 17, to increase tension v_r must be reduced. As soon as this is done, and the reduction increases, v_t must also become smaller, if $v_0=v_m=$ constant. This partially relieves the tension that was established. To re-establish it v_r must be reduced further. Thus, in the practical case where tension affects reduction the tension obtained is no longer correctly determined by equation 17. The change in v_t is in effect a negative feedback from ΔS to $\Sigma\Delta v$, which can be represented in block diagram form as shown in Fig. 19.

Without the feedback this is a block diagram representation of equation 17. In order to give the feedback the correct dimensions, so that the loop gain is dimensionless, we can make the feedback block v_r/AK. The feedback factor K, which Phillips has called the "Modulus of Plasticity,"[4] has the same units as E. Closing this loop results in

$$\frac{\Delta S}{\Delta v_m-\Delta v_r}=\frac{\frac{\frac{AE}{v_r}}{1+p\frac{L}{v_r}}}{1+\frac{\frac{E}{K}}{1+p\frac{L}{v_r}}}=\frac{\frac{\frac{AE}{v_r}}{1+\frac{E}{K}}}{1+p\frac{\frac{L}{v_r}}{1+\frac{E}{K}}}=\frac{\frac{AE'}{v_r}}{1+pT_t} \tag{18}$$

where

E' = "apparent" modulus of elasticity

$$=\frac{E}{1+\frac{E}{K}}$$

and T_t = transport time constant

$$=\frac{\frac{L}{v_r}}{1+\frac{E}{K}}=\frac{L}{v_r}\frac{E}{E}$$

Equation 18 is represented in block diagram form in Fig. 2. It has been derived for the unwind side of the mill, but by the same method a similar expression can be derived for the rewind side.

Nomenclature

A = strip cross-sectional area, in.^{2}
d = distance from mill to x-ray gage, ft
E' = "apparent" modulus of elasticity lb/in.^{2}; see Appendix
G = gear ratio between reel motor and reel
G_m = gear ratio between mill motor and mill
h_{ref} = X-ray gage thickness reference
h_0 = strip thickness leaving mill
h_e = thickness error $=h_{ref}-h_0$
h_x = X-ray gage output (deviation)
I = reel motor current
J = total reel inertia referred to motor slug ft^2
K_A = magnetic amplifier-gain factor
K_G = X-ray gage-gain factor
K_M = mill-motor gain factor
K_V = reel-motor voltage constant, volt/revolution/sec
K_T = reel-motor torque constant, lb-ft/ampere
L = reel-to-mill distance, ft
p = heaviside operator $=d/dt$
$Q_m=\Delta h_0/\Delta v_m$
$Q_b=\Delta h_0/\Delta S_1$
$Q_f=\Delta h_0/\Delta S_2$
r = radius of reel (including coil), ft
r_m = radius of driven mill roll, ft
S = tension, lbs
T_r = tension time constant $=JG^2v/E'Ar^2$
T_t = transport time constant; see Appendix
τ_d = developed motor torque, lb-ft
τ_t = tension torque, lb-ft
v, v_r = peripheral speed of reel, ft/sec
v_m = mill roll peripheral speed, ft/sec
V_a = magnetic amplifier output voltage
V_s = signal generator, output voltage
ω = reel-motor speed, revolutions/sec
ω_m = mill motor speed, revolutions/sec
θ_t = phase shift due to transport time between mill and X-ray gage

$$=\frac{180^\circ}{\pi}\frac{d}{v_2}\text{ per rad/sec}$$

Subscripts 1 and 2 refer to unwind and rewind reel respectively. Where they are omitted from reel quantities the expression can be applied to either reel by using the appropriate subscript.

References

Rolling of Thin Strip, M. D. Stone. *Pro-ings*, Association of Iron and Steel Engineers, sburgh, Pa., 1953, pp. 116–28.

2. Servomechanisms and Regulating System Design, Vol. I (book), H. Chestnut, R. W. Mayer. John Wiley & Sons, Inc., New York, N. Y., 1951, pp. 310–14.

3. Analysis of Tandem Cold Reduction Mill with Automatic Gage Control, R. A. Phillips. *AIEE Transactions*, vol. 73, pt. II, 1956 (Jan. 1957 section), pp. 355–63.

4. Process Analysis Plus Analog Simulation Yields Better Mill Controls, R. A. Phillips, *Control Engineering*, New York, N. Y., May 1958, pp. 113–18.

The Optimum Control of Multiactuator Systems

IAN McCAUSLAND
ASSOCIATE MEMBER AIEE

MUCH of the theory of control systems deals with the problem of reing to the lowest possible value the amic error in single-variable control tems. In the study of that problem it enerally assumed that any conceivable hod of compensation is justified, pro-ed that it allows the error, as meas-d in accordance with some criterion, e reduced; in other words, the pur-e of the controller is to reduce the r at all costs.

here are, however, many systems in ch other considerations may become e important than reduction of error. h a system might be a process involv-the use of large amounts of power, in ch considerable effort must be exerted rder to achieve a change in the con-led or output variable. In such a cess there may often occur a system e such that the benefit derived from a ll change in the output variable re-es more effort than it is worth. In a like this it is better to be satisfied the existing system state than to at-pt to reduce the error between the ac-value of the output variable and the red value.

Many industrial processes which re-e the use of effort to obtain a desired lt are characterized also by the fact the output variable can be altered he adjustment of any of several input ntities. It is as if there were more ators than one, and it is clear that in ocess of this type a desired change in output can be accomplished in many rent ways, depending on how the l change in output is shared among separate actuators. In general some ese methods of sharing will be better others, so that the control problem he problem of choosing a suitable sion of the load. It is obvious that e is no problem of choice if all the ac-ors which are available are identical, for in such a system the correct decision would be to treat all the actuators alike. If the change in the output variable can be achieved without effort, by any one actuator, there is no problem of choice because the actuator which can accomplish the result without effort can be used exclusively.

The criteria by which the best division of effort is chosen may involve many considerations. In some cases it may be a question of sharing a given power load in the best way; in others it may be a question of minimizing wear and tear on equipment, while in still other cases the effects of changes in the input quantities on certain secondary output variables may be significant. The common feature about all such processes is that it is not sufficient to concentrate on keeping only one variable at its desired value, but it is necessary also to recognize the importance of other variables. That is, instead of seeking a particular value of a particular variable, the controller should seek the most desirable over-all state for the system under its control.

A basic theory of control of multiactuator systems is described in this paper, with a brief outline of a portion of economic theory which deals with a similar type of problem. Methods of automatically realizing the optimum system state are described, and some brief suggestions concerning practical applications are included.

Division of Effort Among Actuators

The problem of control in a multiactuator system is the problem of using actuators of limited capabilities in the best over-all way. This problem is remarkably similar to one of the fundamental problems of economics, i.e., the administration of scarce resources in such a way as to achieve the best possible result. In economics, as in the control system, the problem becomes meaningless if the resources are available in unlimited quantity.

The theory of consumer demand deals with the problem in economics which corresponds to the multiactuator control problem. In this theory it is assumed that a consumer derives a certain amount of utility from the goods he purchases, the amount of utility being a function of the quantities of the goods acquired. The consumer's problem is to spend his income on the commodities available, in such proportions as to derive the maximum possible amount of utility. The theory involved in this maximization will be outlined shortly; before doing this some ideas on the optimum state of a multiactuator system will be considered. The most important idea is that of a "penalty function," which will now be described.

Penalty Function

Just as in economics the consumer wishes to maximize the utility, so in the control system it is desired to use the available actuators in such a way as to maximize or minimize some quantity which represents the performance of the system. Perfect control in the single-variable system is represented by the condition that the error is zero at all times, and the quality of performance is assessed by some function of the error, which represents the amount by which the system falls short of the ideal. Similarly, in the multiactuator system, perfect control is represented by the condition that all inputs and outputs remain at their desired values at all times. Therefore, instead of trying to maximize the utility, it is more convenient to think in terms of minimizing the amount by which

Paper 59-198, recommended by the AIEE Feedback Control Systems Committee and approved by the AIEE Technical Operations Department for presentation at the AIEE Winter General Meeting, New York, N. Y., February 1–6, 1959. Manuscript submitted June 3, 1958; made available for printing December 5, 1958.

Ian McCausland is with the University of Toronto, Toronto, Ontario, Canada.

The author gratefully acknowledges the advice and encouragement of Prof. J. M. Ham of the University of Toronto, under whose guidance this investigation was carried out. The author's gratitude is also extended to the Canadian Westinghouse Company for financial assistance during the period in which the work was performed.

Fig. 1. Utility of commodity x

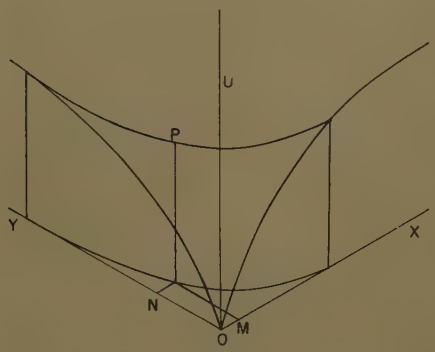

Fig. 2. Utility surface for two commodities x and y

the system falls short of the ideal. The magnitude of this shortcoming is a negative "score" in the system's game against nature, so it is proposed that this quantity be denoted by the term "penalty." That is to say, the purpose of the controller is to minimize the operating penalty. The penalty will usually be a function of the instantaneous system state, and two similar controllers would be compared by comparing the average penalty for the two cases, in the presence of input signals and disturbances of particular types. The nature of the penalty function will be discussed later.

Theory of Consumer Demand

As has already been pointed out, the controller which has several actuators available to obey its commands is in a somewhat similar position to the consumer who has several commodities available to supply his wants. Therefore it is possible to learn something about the situation by studying the consumer who spends his income in such a way as to maximize the utility which he derives from these commodities. This subject has been thoroughly studied,[1] and part of the theory is outlined here because it forms a useful basis for the study of multiactuator systems.

The amount of utility which is derived from one commodity x can be plotted as a function of the quantity of the commodity, as shown in Fig. 1. The shape of the curve is explained by the fact that the incremental utility generally decreases as the quantity of the commodity is increased. In the same way, when dealing with two commodities x and y, a utility surface can be drawn, as shown in Fig. 2; the utility is measured on the vertical axis and is denoted by the symbol u. The vertical height of any point P on the surface therefore represents the amount of utility obtained by the contributions of amounts OM of x and ON of y.

Indifference Curves

The contour lines of the utility surface, when projected onto the xy plane, form a family of curves as shown in Fig. 3. These curves are called "indifference curves." The magnitude of the slope of the indifference curve at any point is the amount of y which is needed by the consumer to compensate him for the loss of a small unit of x. The amount of utility lost, due to the loss of a small unit of x, is the amount of x lost multiplied by the incremental utility of x. A similar relationship holds for y, and these lead to the following equation:

$$\frac{dy}{dx} = -\frac{\partial u}{\partial x} \Big/ \frac{\partial u}{\partial y} \qquad (1)$$

That is, the magnitude of the slope is equal to the incremental utility of x divided by the incremental utility of y. As one moves along the indifference curve in the direction of increasing x (and hence of decreasing y) $\partial u/\partial x$ decreases and $\partial u/\partial y$ increases, so that the magnitude of the slope decreases, i.e., the indifference curve is everywhere convex to the origin.

The condition of maximum utility for a given income may be found from the indifference map. This is illustrated by the graph in Fig. 4. On the diagram, OL is the quantity of x which would be purchased if the whole income were spent on x, and similarly OM is the corresponding quantity of y. Any point on the straight line LM therefore represents a quantity of x and a quantity of y which together would cost the whole income. Starting at the point P, if one moves along the straight line LM in the direction of increasing x, one leaves the indifference curve shown and moves to one of higher utility. Hence P cannot represent the condition of maximum utility. However, starting at the point Q, at which the straight line is tangential to an indifference curve, a movement along the line in either direction causes the utility to decrease; hence Q represents the condition of maximum utility for that particular income. It is easy to show that, at the condition

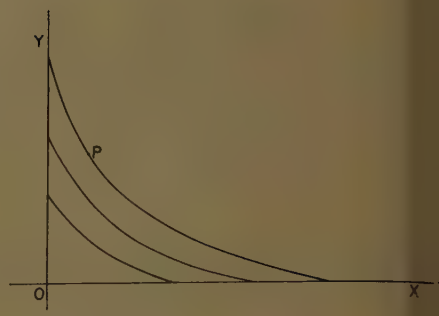

Fig. 3. Indifference curves for x and y

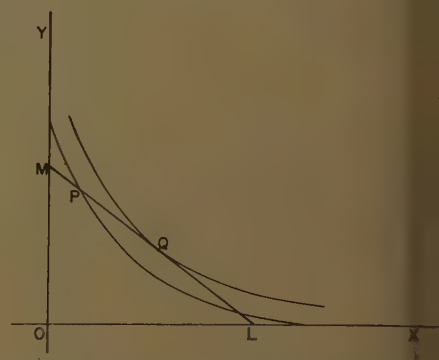

Fig. 4. Indifference curves, illustrating the condition of maximum utility

of maximum utility, the incremental utilities of the two commodities are directly proportional to their prices.

It is interesting to note that it is not necessary to know the actual value of utility which corresponds to a particular indifference curve; it is sufficient to know which direction represents an increase in utility and which represents a decrease. That is, it is only necessary to have a scale of preference, rather than a quantitative knowledge of the utility.

Application to Control Systems

The 2-actuator control problem is similar to the problem of the consumer to whom two commodities are available. The basic 2-actuator system is shown in Fig. 5; it is desired to control the output variable c by one or both of the actuators G_1 and G_2. In general the variables inside the dotted rectangle are unobservable, i.e., it is not possible by observation of the output side to determine how much of c has been contributed by which actuator. However, each transfer function can be determined directly by varying one input and keeping the other fixed at zero, so that it is possible to observe the input under steady-state conditions and thereby, if the system is linear, to know the contributions made by the respective actuators to the output quantity.

In this preliminary exposition of the theory of control of multiactuator systems it is assumed that all reference inputs

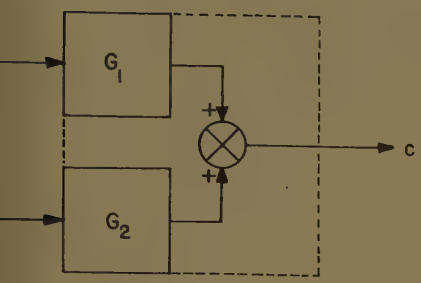

g. 5. The basic 2-actuator control system

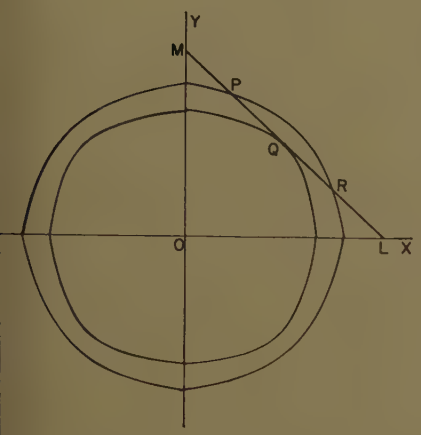

g. 6. Indifference map for 2-actuator system

d disturbance inputs to the system are very low frequency, so that it is ssible to consider the function of the ntroller as being to alter the steady-ate operating point of the system to the ndition of minimum penalty whenever departs from that condition. Every ansfer function which appears in an uation in this paper will therefore be ken to mean the value of the transfer nction at zero frequency. Thus the tput c of the system shown in Fig. 5 given by

$$= G_1.x + G_2.y \qquad (2)$$

In the case of a control system a set indifference curves of penalty can be awn, which are similar to the indifference curves of utility in the economic ample except that the penalty curves e normally concave to the origin. The rves are concave to the origin because most practical cases large errors are atively more costly than small errors, , the penalty contributed by a particular riable usually increases more rapidly the value of the variable departs further m the desired value. Another difence between the indifference curves the economic system and those of the ntrol system is that those for the control stem can be drawn in all four quadrants the xy plane, instead of in the first quadrant only as in the economic example.

Fig. 6 shows a hypothetical indifference map for a 2-actuator control system. Here, similarly to the economic case, OL represents the amount of input x which would be required to give output c if y were set at zero; similarly OM is the corresponding quantity for y, i.e., $OL = c/G_1$ and $OM = c/G_2$. Any point on the line LM therefore represents a pair of inputs x and y which if acting together would give an output c. As before, it may be seen that the point P in Fig. 6 is not a point of minimum penalty, but that Q represents the desired condition. It is required to design a controller which will adjust the inputs x and y in such a way that the point of minimum penalty is reached.

That the control system should be able to seek the point of minimum penalty, it is necessary that information about the relationship between the penalty and the system variables should be available to the controller. Therefore an essential feature of such a controller is a function generator whose inputs are the significant variables of the system and whose output is the penalty. Such a function generator is shown in Fig. 7. It is assumed that the state of the system is such that the output is at the desired value c, but that the inputs x and y require adjustment so as to minimize the penalty. The purpose of the function generator is the following: the inputs to the function generator are altered by an auxiliary signal source, as shown in Fig. 7, in such a way that the apparent operating point, as seen by the function generator, moves alternately to one side and to the other of the actual operating point. This can be achieved by adding small sinusoidal signals $aG_2 \sin \omega t$ and $-aG_1 \sin \omega t$ to the signals x and y respectively, and using the two sums as

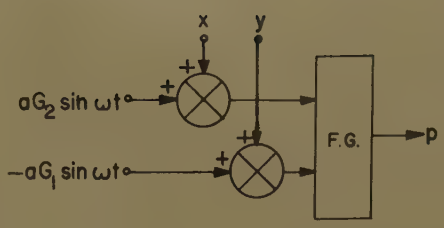

Fig. 7. The penalty function generator

the inputs to the function generator as shown in Fig. 7. The path of the apparent operating point is along the line LM in Fig. 6, as shown by the following equation:

$$(x + aG_2 \sin \omega t)G_1 + (y - aG_1 \sin \omega t)G_2 = x.G_1 + y.G_2 = c \qquad (3)$$

Therefore, with the sinusoidal inputs shown, the apparent operating point oscillates about the actual operating point, along the line LM, with simple harmonic motion of small amplitude. The output of the function generator therefore varies in a way which depends on the position of the actual operating point. For example, at point P (see Fig. 6) when the apparent operating point is moving in the direction of increasing x, the penalty is decreasing; therefore the incremental output of the function generator is opposite in phase to the incremental x input. The total output of the function generator is a steady value plus an alternating component. At the point R the incremental output is in phase with the incremental x input, while at Q the incremental output is negligible.

If the output of the system is to be kept at a fixed value c, there is only one degree of freedom for the inputs, represented by the line LM in Fig. 6. Therefore the relative adjustment of the inputs can be made by a single-variable actuator. If a voltage supply $b.\sin(\omega t - \pi/2)$ is used to energize the reference phase of a 2-phase

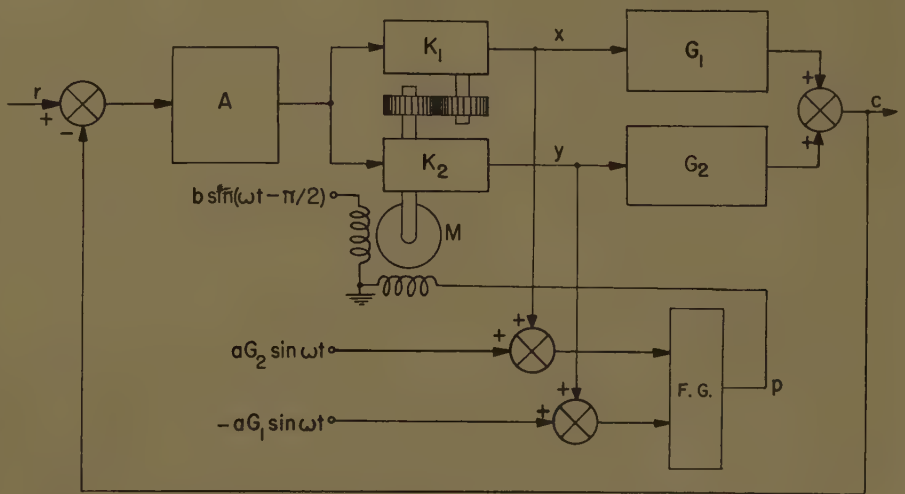

Fig. 8. Block diagram of complete 2-actuator servomechanism

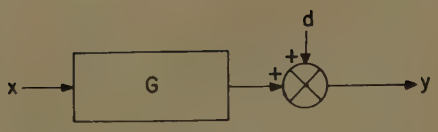

Fig. 9. The single-variable regulator

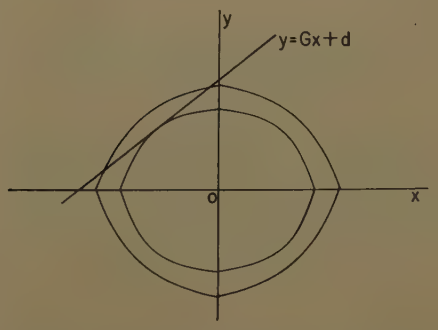

Fig. 10. Indifference map for single-variable regulator

servomotor, and if the control phase is energized by a voltage proportional to the incremental output of the function generator, the motor will run in one direction when the operating point is on one side of the minimum-penalty point, and in the opposite direction when it is on the other side. At the point of minimum penalty the motor will develop no torque. A block diagram showing a complete servomechanism operating on this principle is shown in Fig. 8. The high-gain amplifier A ensures a low steady-state error, while the servomotor M adjusts the two series gains K_1 and K_2 in opposite directions to each other in order to provide the inputs x and y in the correct proportions for minimum penalty.

It is conceivable that a control system of this type might be used to control the temperature of a furnace, the controlled variable being temperature, and the inputs being the amounts of heat supplied by two fuels. Open-hearth and soaking-pit furnaces in the steel industry can be operated in a multiple-fuel fashion, the fuels used being in many cases by-products of other processes and therefore varying widely in cost and availability. The penalty would be a function of the fuel costs, and of the burner efficiencies which would vary because of the large variations in the rates of fuel flow. It is possible that certain problems of similar type might be amenable to linear programming methods of solution, but the variation of burner efficiencies with rates of fuel flow makes such methods unsuitable in this case because of the nonlinear relationships involved.

Single-Variable Regulator

In certain physical processes the single-variable regulator problem may be similar to the 2-actuator problem. For example, in processes where the input is at a high power level, the cost of altering the input in order to neutralize a small disturbance in the output variable may be comparable to the cost of allowing the disturbance to remain uncorrected. One way of controlling such a process would be to use an on-off controller with a dead zone of suitable size. An on-off controller has the effect of separating all disturbances into two categories, the significant and the insignificant, and it controls the system in such a way that a disturbance whose magnitude is many times the dead zone is corrected to the same value as one which is just greater than the dead zone, even though the demands on the costly input may be vastly different in the two cases. On the other hand, a human operator of such a system, if he had a thorough knowledge of all the factors involved, could use his knowledge and judgment to decide at what point a small improvement was not worth the extra effort involved.

In other words, it is not always sufficient to control the output of a system to its best possible value; the input must also be considered. It is not possible to adjust every variable in the system to the desired value, because the process will operate only when there is a certain functional relationship linking certain variables together. The system state can, however, be altered from its present condition to the state which is the best of

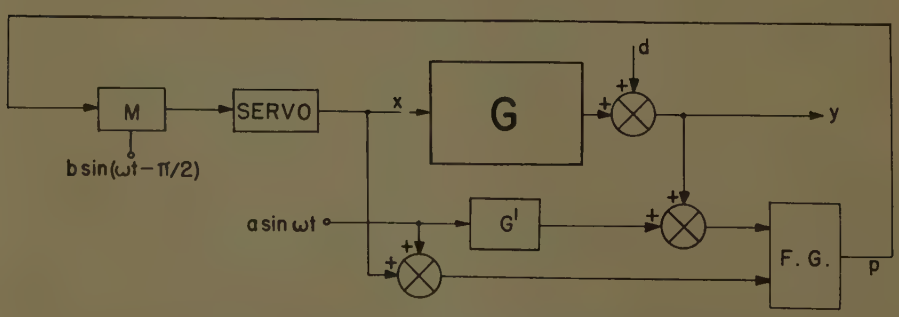

Fig. 11. Block diagram of complete single-variable regulator

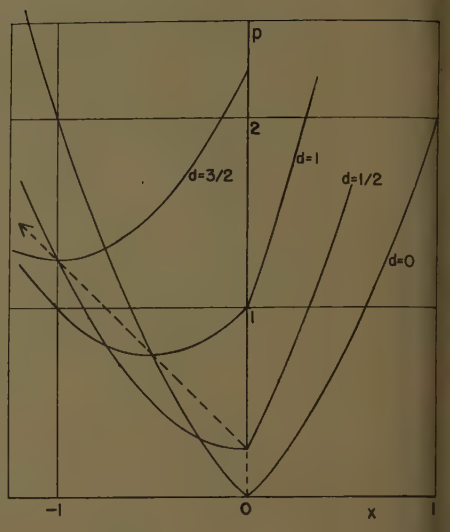

Fig. 12. Typical penalty function of single-variable regulator for various values of d

those available under the existing circumstances. The finding of the best available system state is one of the fundamental problems of control, and it is this problem which the regulators described here are intended to solve.

Consider the single-variable regulator shown in Fig. 9. The variables x and y are taken to represent the incremental values of the input and output respectively; i.e., the nominal system state is $x=0$, $y=0$. It is desired to control the system state in the presence of disturbances represented by d.

Fig. 10 shows the indifference map for the system, i.e., the contour lines of the penalty function $p(x,y)$. For a particular disturbance d, the available system states are represented by the straight line $y=G.x+d$. Therefore the point of minimum penalty is found as before.. An automatic method of adjusting the system to the optimum operating point is shown in Fig. 11. The block G' is a low-power steady-state model of the block G, in the sense that the transfer function of G' is at all frequencies equal to the value of the transfer function of G at zero frequency. The model is used in conjunction with a function generator and a small sinusoidal signal to compute the penalty as the apparent operating point oscillates about the actual operating point. The 2-phase servomotor M is energized by a reference voltage in quadrature with the input to G', and its control phase is energized by the output of the function generator. The block marked "servo" is a conventional servomechanism which is used to convert the low-power variations in the angle of the servomotor shaft to the high-power variations in the input to the process.

In the 3-dimensional xyp space, the

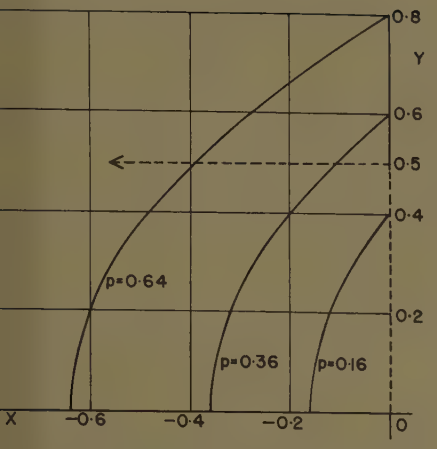

ig. 13. Indifference curves corresponding the same penalty function as in Fig. 12

lane $y=G.x+d$ intersects the surface (x,y) in a curve which gives the penalty s a function of x alone, for that particular alue of d. Fig. 12 shows a typical set f such curves, with d as a parameter, hen $G=1$ and $p(x,y)=|x|+y^2$. Fig. 13 hows the indifference map for the same ystem, for the same penalty function. he path of the minimum-penalty point as increases is shown on each diagram by a ashed line. It can be seen in both iagrams that, as d increases from zero, ie value of x remains at zero until $d=$ /2, and then increases linearly with fur- ier increase in d. If the penalty func- ion is different the path of the operating oint will, of course, be different.

wo-Input Two-Output Regulator

The block diagram of the 2-input 2- utput regulator is shown in Fig. 14. As the single-variable case, the values of ie inputs and outputs are the incre- ental values. The equation for the gulator is

$$Y=HX+D \qquad (4)$$

here Y, X, and D are vectors with two mponents each, and H is a matrix ansformation. The penalty is now a nction of the four variables x_1, x_2, y_1, and $_2$. For a given pair of disturbances d_1 nd d_2, the penalty is a unique function f x_1 and x_2, i.e., the intersection of the yperplane $Y=HX+D$ and the hyper- rface $p(x_1,x_2,y_1,y_2)$ is a surface in the x_2p space. It is convenient to think of is surface as an elastic membrane whose ape is distorted by variations in the alues of the disturbances, thus shifting ie co-ordinates, in the x_1x_2 plane, of the oint of minimum penalty. Since there re two degrees of freedom in the system, is necessary to adjust x_1 and x_2 to chieve the minimum value of penalty. mall-signal excursions of the apparent operating point can in this case be achieved by applying a 2-phase input (two signals in quadrature) to a low-power steady-state model of the basic system (H'), as shown in Fig. 15. This causes the apparent operating point to rotate around the actual operating point in the x_1x_2 plane, and once again the phase of the output of the function generator shows which direction the inputs should be altered. Two 2-phase servomotors M_1 and M_2 are used, the control phases of both being energized by the output of the function generator and each reference phase being energized by a voltage of the appropriate phase. This system will therefore adjust the inputs until the condition of minimum penalty is reached.

The remarks in the previous section, on the subject of the cost of altering the input in a single-variable regulator, may be applied with even greater significance to the 2-variable system. If the output side only is considered, the state of the system may be represented by a point on the y_1y_2 plane. It is possible to manipulate the two inputs in such a way as to move the output state from any point on this plane to any other point, provided that the transforms of the two unit vectors of the input are linearly independent. However, if these two vectors in the y_1y_2 plane are almost parallel, it may be necessary to use excessively large inputs in order to achieve a relatively small variation in the output state.

Tandem Cold-Rolling Mill

An excellent example of a multiactuator control system is the tandem rolling mill used in the manufacture of steel strip. The control of such a mill has already been described in considerable detail.[2,3] There are two independent variables associated with each stand in such a mill, namely, the nominal roll separation and the torque of the driving motor, so that the best scheme of control is by no means obvious. However, it may be assumed that satis-

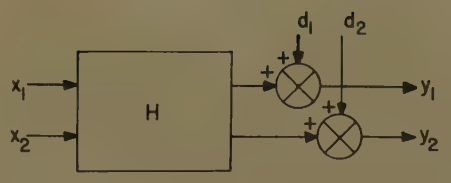

Fig. 14. The 2-input 2-output regulator

factory control of a 5-stand mill can be achieved by adjusting the roll separation of stand 1 (coarse control of output thickness) and the torque of the driving motor of stand 5 (fine control of output thickness).[2] Since both these adjustments have a significant effect on the tension between stands 4 and 5,[3] the system must be controlled in such a way that this tension stays within certain limits. In other words, the four variables on which the system penalty depends are: roll setting of stand 1, torque of stand 5, tension between stands 4 and 5, and thickness of output strip. It should therefore be possible to control the system in an optimum way with respect to these four variables, using the methods described here, if a suitable penalty function is used.

Penalty Function in Rolling Mill

Obviously, the penalty function must be related in some way to the increase in the cost of operation of the process when the system departs from its nominal state of operation. Therefore each of the significant variables will be examined in turn to find out what the nature of the penalty should be; the penalty functions given here are merely the suggestions of the author and are not intended to represent the best possible functions for such a situation.

Roll Setting of Stand 1

Because of the very large forces involved, alteration of the roll setting of stand 1 causes slight deformation of the rolls and therefore the transverse profile of the strip is slightly distorted. The deformation is probably directly pro-

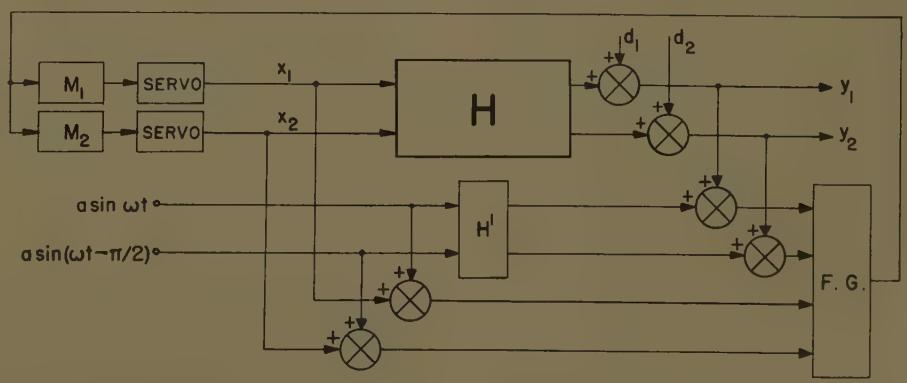

Fig. 15. Block diagram of 2-input 2-output regulator

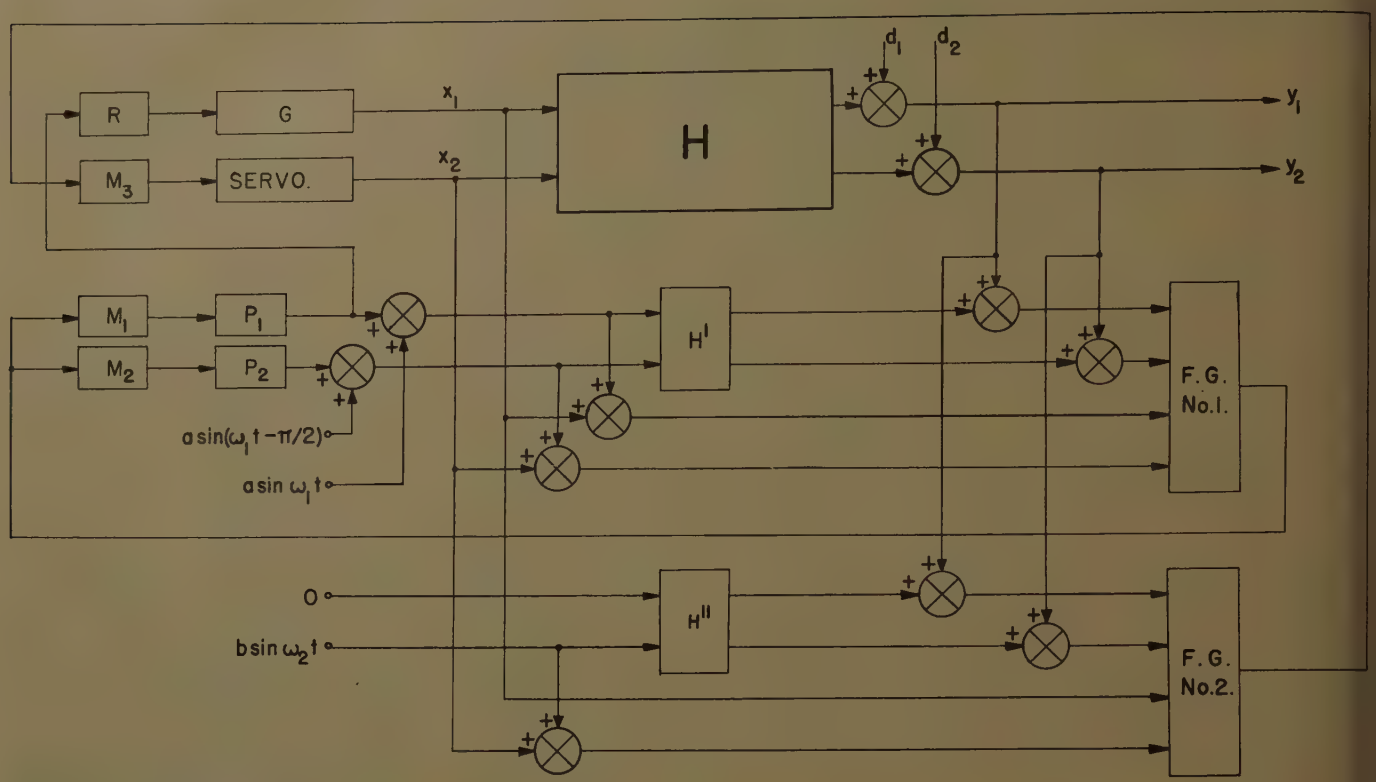

Fig. 16. Block diagram of 2-input 2-output regulator for tandem rolling mill, with on-off control on roll setting (x_1)

portional to the change in roll force, so that the penalty might be proportional to the absolute value of the change in roll setting, i.e.,

$$p(x_1)=a_1|x_1| \tag{5}$$

where x_1 is the incremental roll setting of stand 1 and a_1 is a constant.

Torque of Stand 5

For most efficient use of the mill, high rolling speeds are used and the motors develop almost their total rated power. Small variations in torque incur little or no penalty but larger variations are undesirable. Assume that the penalty associated with this variable is

$$p(x_2)\Big|_{|x_2|\leq b_2}=0,\ p(x_2)\Big|_{|x_2|>b_2}=a_2(|x_2|-b_2) \tag{6}$$

where x_2 is the incremental torque of stand 5, and a_2 and b_2 are constants.

Tension Between Stands 4 and 5

The danger of strip breakage is negligible until the tension between stands 4 and 5 has increased by a considerable amount. Beyond that point the probability of breakage may increase very rapidly, and the penalty should also vary in this way. It is therefore assumed that the penalty varies according to the following equation:

$$p(y_1)\Big|_{|y_1|\leq b_3}=0,\ p(y_1)\Big|_{|y_1|>b_3}=a_3(|y_1|-b_3)^2 \tag{7}$$

where y_1 is the incremental tension between stands 4 and 5, and a_3 and b_3 are constants.

Thickness of Output Strip

In practice the one thing which matters is that the strip should be within the commercial tolerance. This would imply that a suitable penalty function would be a step function at the appropriate thickness, but such a penalty would give no indication of how closely the thickness was approaching the boundary. Therefore it is better to choose a penalty function which places small emphasis on small errors but much larger emphasis on larger errors. A square-law penalty would probably be suitable, so the following penalty is proposed:

$$p(y_2)=a_4y_2^2 \tag{8}$$

where y_2 is the incremental output thickness and a_4 is a constant.

The total penalty function for the mill might therefore be a function of the following form:

$$p=a_1|x_1|+a_2(|x_2|-b_2)\Big|_{|x_2|>b_2}+a_3(|y_1|-b_3)^2\Big|_{|y_1|>b_3}+a_4y_2^2 \tag{9}$$

If the penalty function has been judiciously chosen, the total incremental cost incurred in a given period of time is proportional to the integral of the penalty function over that time. However, there are certain factors which may have to be considered, in which the method of finding the total incremental cost is not so obvious. One example of this will now be considered. It is realized that the example studied here, namely, the problem of wear in the screwdown mechanism, may not be so important in practice as is implied in this paper. However, the example serves to illustrate a principle which is likely to be valid in many practical situations, and therefore it is considered worth while to discuss it here.

Effects of Wear in the Screwdown Mechanism

In most rolling mills the roll setting of any stand is altered by means of a screwdown mechanism. If this mechanism is operated very frequently the wear of the nuts and screws may be excessive, due to the large forces involved. The mill should therefore be operated in such a way as to take account of this fact. It seems reasonable to assign a penalty to the movements of the screwdown mechanism, in such a way that the penalty integrated over a given period is proportional to the total distance traveled by the screws. This would mean that the instantaneous penalty should be proportional to the absolute value of the velocity. Then, since screwdown position and velocity would both be independent variables from the point of view of the penalty function, the finding of the

timum control condition can no longer considered a steady-state problem but ll depend on the frequency components the disturbances as well as on their agnitudes. Also, it is usual to use an -off control on the screwdown motors d drive the screws at a constant speed, that the method of exploring the neighrhood of the operating point by small usoidal signals would not be valid beuse only certain discrete values of eady-state velocity are permitted, and nce the steady-state operating point is t capable of continuous change in the rection of the velocity axis. If a prortional control were used, with conuously variable velocity, it seems likely at other difficulties would be enuntered. For example, the presence of iction would have a detrimental effect the smoothness of control, and it is ely that stiction would also become a gnificant factor in the wear of the screws us necessitating a further penalty based the number of times the screws start move.

The amount of screw operation can be duced by retaining the on-off control and corporating a suitable dead zone so at the screwdown mechanism does not erate unless a definite minimum amount adjustment to the roll setting is reired. This is also difficult to achieve the use of small sinusoidal signals exoring the neighbourhood of the operating int, because it is not possible to find the -ordinates of the minimum point from servations in a small region around the erating point. It is possible to overme this difficulty by using a more aborate system as shown in Fig. 16. his system uses two low-power steadyate models of the system, H' and H'', d two identical penalty function generars. The models H' and H'' are identical th each other, and each has the same ansfer characteristics at all frequencies the basic system has at zero frency. The model H'', with an oscillatg input in the x_2 direction only, operates conjunction with function generator 2 d the 2-phase servomotor M_3 to maintain x_2 (the incremental torque of stand 5) the value corresponding to minimum nalty, where minimum penalty in this se means the lowest value of penalty hich can be achieved by altering x_2 if is fixed at its existing value. At the me time the model H', with a 2-phase put, operates in conjunction with funcon generator 1 and the two 2-phase rvomotors M_1 and M_2 in such a way at the shaft positions of M_1 and M_2 rrespond respectively to the discrepcies between the actual values of x_1 and x_2 and the values corresponding to the absolute minimum penalty (i.e., the lowest value of penalty which can be achieved by varying both x_1 and x_2). The potentiometers P_1 and P_2 are used to convert the shaft positions of the servomotors to corresponding voltages. The relay R and the screwdown motor G act like the forward loop of a servomechanism whose error quantity is the output voltage of P_1. The relay will operate when the discrepancy between the actual value and the desired value of x_1 is above a certain value. It can easily be arranged that the relay remains closed until the error voltage is zero, so that the screwdown mechanism will be driven until the optimum value is reached. In the meantime H'' and the associated control circuit maintain x_2 at the optimum value at all times, regardless of the value of x_1. It is obvious that this method of control will be effective in reducing the amount of screwdown movement, but of course the integral of the instantaneous penalty over a period will in general be greater than if the roll setting changed to correct each little variation. The best value of relay dead zone could be found by simulating the system and submitting it to external disturbances of magnitude and duration similar to those expected in practice, assuming that the total screw motion in a given period contributes to the integrated penalty over that period.

Practical Feasibility

The physical construction of control systems like those described in this paper would not be difficult. Referring to Figs. 15 and 16, it may be seen that most of the controller, including the 2-phase supplies, could be obtained by suitable interconnection of analog computer components. Almost any commercial analogue computer could be used for this purpose. Also, it would be possible to use digital equipment and sampled-data techniques to compute values of the penalty function at selected points in the neighborhood of the operating point, and to make logical decisions as to the best course to take. The cost of operation and the value of the product in industrial processes such as the rolling of steel are so high that the use of such equipment, although it is expensive, would be fully justified.

There are, of course, other methods of altering the system inputs than by 2-phase servomotors. For example, if the incremental output of the function generator is multiplied by the sinusoidal test signal, the product is a unidirectional signal which will reverse in polarity whenever the minimum-penalty point is passed. Such a signal could therefore be used (after suitable filtering) to control the system input variables. Other methods will be found in the literature describing optimizing or optimalizing control systems.

Although the methods outlined in this paper are valid only in the linear region of operation, it is possible to control a nonlinear system in a similar manner if the controller is made more elaborate. Such a controller would include a different kind of model of the physical process, a model which would copy the dynamic behavior and the nonlinearities of the actual process, rather than a steady-state model as in the controllers which are described in the paper.

Conclusions

1. This paper has attempted to show that one of the basic problems of system engineering is the same as one of the basic problems of economics, namely, the economic use of limited resources. Some of the relevant portions of economic theory have been outlined, and the application to control systems has been illustrated by considering the 2-actuator problem. The solution of the problem involves the use of a penalty function, the criterion for the choice of operating point being the minimization of penalty. To allow the problem to be solved automatically, information about the penalty is provided in the controller by a function generator.

2. Proceeding from the 2-actuator problem, the paper has given a method of controlling a 2-dimensional multivariable process such as a tandem rolling mill. The nature of a possible penalty function for such a mill has been considered, the penalty being based on both the input variable and the output variable.

3. The higher the standard of performance required from a process, the greater are the demands made on the total system in terms of power input, wear and tear on equipment, and the like. It is suggested that more thought should be given to the system as a whole, rather than concentrating on reaching the ultimate minimum error according to some criterion without reckoning the incremental cost of removing the last unit of error. This cost may be the cost of the input power or fuel or some other substance, or the cost of wear and tear on equipment, or it may be something quite different such as the increase in complexity as the perform

ance is improved. In the case of increasing system complexity, as in the other cases, there is usually a point beyond which it is uneconomical to go.

4. The problem of sharing the effort among several actuators or several processes is one which occurs in many fields, one of the most obvious to the electrical engineer being the division of load among several generators or among several power stations.[4] That particular problem is also amenable to automatic methods of solution.[5]

References

1. Value and Capital (book), J. R. Hicks. Oxford University Press, London, England, 1946, chaps. I, II.

2. Analysis of Tandem Cold Reduction Mill with Automatic Gauge Control, R. A. Phillips. *AIEE Transactions*, vol. 75, pt. II, 1956 (Jan. 1957 section), pp. 355–63.

3. Incremental Control Equations for Tandem Rolling Mills, J. H. Courcoulas, J. M. Ham. *Ibid.*, pp. 363–74.

4. Economy Loading of Power Plants and Electric Systems (book), M. J. Steinberg, T. H. Smith. John Wiley & Sons, Inc., New York, N. Y., 1943.

5. An Optimalizing Computer Controller for the Electric Utility Industry, L. K. Kirchmayer. *ASME Paper no. 58-IRD-2*, American Society of Mechanical Engineers, New York, N. Y., 1958.

Application of Continuous System Design Concepts to the Design of Sampled Data Systems

STANLEY F. SCHMIDT
ASSOCIATE MEMBER AIEE

THE THEORY associated with the design of sampled data systems[1] has progressed to the point where it is possible to design a digital controller pulse transfer function so as to obtain an overall system pulse transfer function which will meet certain specifications such as being stable, and physically realizable; having a minimum settling time in response to a given input; having ripple-free operation after a short transient, etc.

A survey of the literature, however, indicates a scarcity of information on the sensitivity of a system to parameter variations and on how to control, in the design process, the abruptness of the response. Barker[2] and Bertram[3] touch upon this subject and show that one method of smoothing the response is to design the characteristic equation so that some of the poles of the closed loop transfer function are located at points in the z-plane other than the origin. It is the purpose of this paper to show: first, that considerations of the sensitivity of the response to parameter variations and abruptness of the response to transient inputs preclude the use of finite settling time design (i.e., one in which the error is reduced to zero in a specified number of sampling instants); and second, to show that continuous system design concepts can be used to select the dominant poles of the closed loop pulse transfer function so as to achieve a desired transient response.

To obtain some indication of the practical limitations imposed on the response of the system, the "plant" is taken to be an aircraft and the system to be one which controls the aircraft's altitude. The abruptness and the sensitivity of the response to a transient maneuver will be judged in this application by the magnitude of the maximum load factor and the change in the stability of the system with parameter variations respectively.

System Description and Design Specifications

A block diagram of the altitude control system is shown in Fig. 1, where $r(t)$ and $c(t)$ are respectively the commanded and true altitude of the aircraft. The samplers are indicated by the symbol T. The transfer function used for the hold circuit and the aircraft autopilot, in Laplace transform notation is

$$G(s)=\left[\frac{1-\epsilon^{-sT}}{s}\right]\left[\frac{83.7(s+9.4)(s-8.8)}{s^2(s^2+4.2s+8.9)}\right] \tag{1}$$

The term within the first bracket in equation 1 is the mathematical expression for a zero-order hold circuit. The second term represents the aircraft-autopilot combination having a natural frequency of approximately 0.5 cycle per second and a damping ratio of 0.7. The s^2 term in the denominator arises from the double integration between normal acceleration and vertical distance or altitude.

The design problem, of course, is to select the least complicated digital controller, $D(z)$, to provide stability and other desired characteristics to the complete system. For this application these "other desired characteristics" are chosen to be:

1. A 50-foot step in altitude should not require a normal acceleration response exceeding the assumed 3 g maximum maneuvering capability of the aircraft.

2. The acceleration and altitude response should be insensitive to variations in the aerodynamic characteristics due to large changes in air density (differences in preset altitude); they should be relatively smooth (the sampling rate should be high); and they should be little affected by reasonable limits on control surface rates.

Unlike more conventional requirements of sampled data systems such as zero ripple or finite settling time, these specifications cannot be formulated into an equation for $D(z)$. One can, however, use conventional design methods and investigate the performance of the resulting system with regard to all the desired characteristics, and decide the extent to which the methods lead to a $D(z)$ design which will meet the specifications.

Finite Settling Time Designs

In general, the design equation for the digital controller pulse transfer function is

$$D(z)=\left(\frac{K(z)}{1-K(z)}\right)\left(\frac{1}{G(z)}\right) \tag{2}$$

To insure the the designed system to be stable, have zero ripple, zero steady-state error to some input transient, etc., specifications in mathematical terms are placed on $K(z)$, the closed loop pulse transfer function $C(z)/R(z)$, and 1-$K(z)$, the transfer function relating $E(z)/R(z)$.

Paper 58-1083, recommended by the AIEE Feedback Control Systems Committee and approved by the AIEE Technical Operations Department for presentation at the AIEE Winter General Meeting, New York, N. Y., February 1–6, 1959. Manuscript submitted September 2, 1958; made available for printing December 3, 1958.

Stanley F. Schmidt is with the National Aeronautics and Space Administration, Moffett Field, Calif.

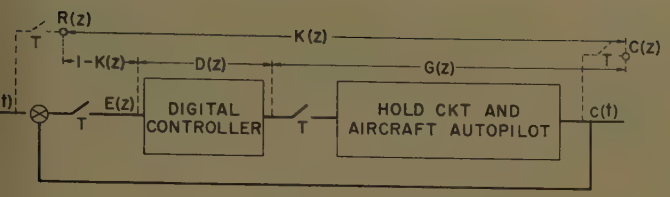

Fig. 1. Block diagram of an aircraft altitude control system

ow, it seems reasonable to assume that a nite settling time system would not be esigned without imposing the zero ripple onstraint, and of course, the system ust be stable. Equations 3 and 4 indicate the mathematical form of the specication to meet only the zero ripple and tability criteria.

$$\text{(}z\text{)=(numerator } G(z)\text{)(polynomial with undetermined coefficients)}$$

$$=\left(\sum_0^J \alpha_k z^{-k}\right)\left(\sum_0^L a_l z^{-l}\right) \qquad (3)$$

$$-K(z)=\text{(poles of } G(z) \text{ on or outside of the unit circle)(undetermined coefficients)}$$

$$=\left(\sum_0^M \beta_k z^{-k}\right)\left(\sum_0^N b_n z^{-n}\right) \qquad (4)$$

Subtracting equation 3 from unity and quating coefficients of equal powers of /z with those of equation 4 allows the nique determination of the a_l's and the $_n$'s. There is a minimum L and N which vill satisfy equation 3 and 4; if more are ised then the additional a_l's and b_n's are ot uniquely determined but may be hosen arbitrarily. If, however, more onstraints are added, such as specifying he time response for several sampling nstants, then a larger L and N will be equired. Substitution of equations 3 nd 4 into equation 2 gives the digital ontroller pulse transfer function as

$$D(z)=\frac{\left(\sum_0^L a_l z^{-l}\right)[\text{stable poles of } G(z)]}{\sum_0^N b_n z^{-n}} \qquad (5)$$

One item to note from this equation is that any stable poles of $G(z)$ will occur as zeros of $D(z)$. Thus, this design process will always involve cancellation if $G(s)$ has some poles in the left half-plane. The design of $K(z)$ on the basis indicated in equations 3 and 4 results in a system with finite settling time, since $K(z)$ will always be a finite polynomial with a last term of $z^{-(J+L)}$ ($J+L$ is equal to the number of sampling instants necessary to correct a transient). Now, it is obvious that the sampling period T has not entered the design process except in the determination of $G(z)$. Thus, whether the system is operated at a sampling frequency of 10 cycles per second or of one cycle per second, the same number of sampling instants will be required to correct an input transient.

To illustrate the effects of sampling period on the altitude autopilot, a finite settling time design was made at two sampling periods, $T=0.25$ second and $T=1.0$ second. The pulse transfer functions for $G(z)$, $K(z)$, 1-$K(z)$, and $D(z)$ for these two periods are given in the following equations 6 through 13.

For $T=0.25$ second:

$$G(z)=\frac{1.02z^{-1}-10.21z^{-2}-7.53z^{-3}+0.730z^{-4}}{(1-z^{-1})^2(1-1.02z^{-1}+0.349z^{-2})} \qquad (6)$$

$$K(z)=(1.02z^{-1}-10.21z^{-2}-7.53z^{-3}+0.730z^{-4})(-0.215+0.153z^{-1}) \qquad (7)$$

$$1-K(z)=(1-z^{-1})^2(1+2.22z^{-1}+1.085z^{-2}-0.112z^{-3}) \qquad (8)$$

$$D(z)=\frac{-0.215(1-0.710z^{-1})(1-1.02z^{-1}+0.349z^{-2})}{1+2.22z^{-1}+1.085z^{-2}-0.112z^{-3}} \qquad (9)$$

For $T=1.0$ second:

$$G(z)=\frac{-110.3z^{-1}-572.1z^{-2}-200.6z^{-3}-7.469z^{-4}}{(1-z^{-1})^2(1+0.125z^{-1}+0.0149z^{-2})} \qquad (10)$$

$$K(z)=(-110.3z^{-1}-572.1z^{-2}-200.6z^{-3}-7.469z^{-4})(-0.0035+0.00238z^{-1}) \qquad (11)$$

$$1-K(z)=(1-z^{-1})^2(1+1.614z^{-1}+0.487z^{-2}+0.0178z^{-3}) \qquad (12)$$

$$D(z)=\frac{(-0.0035)(1-0.679z^{-1})\times(1+0.125z^{-1}+0.0149z^{-2})}{(1+1.614z^{-1}+0.487z^{-2}+0.0178z^{-3})} \qquad (13)$$

The digital controller for both systems was simulated on an analog computer with the use of the method described in reference 4. The transient time responses of both altitude and normal acceleration for the two systems are shown in Fig. 2(A). Of particular note is the large overshoot of the altitude response for both sampling periods, which is a characteristic of a finite settling time design. Of greater importance, however, is the

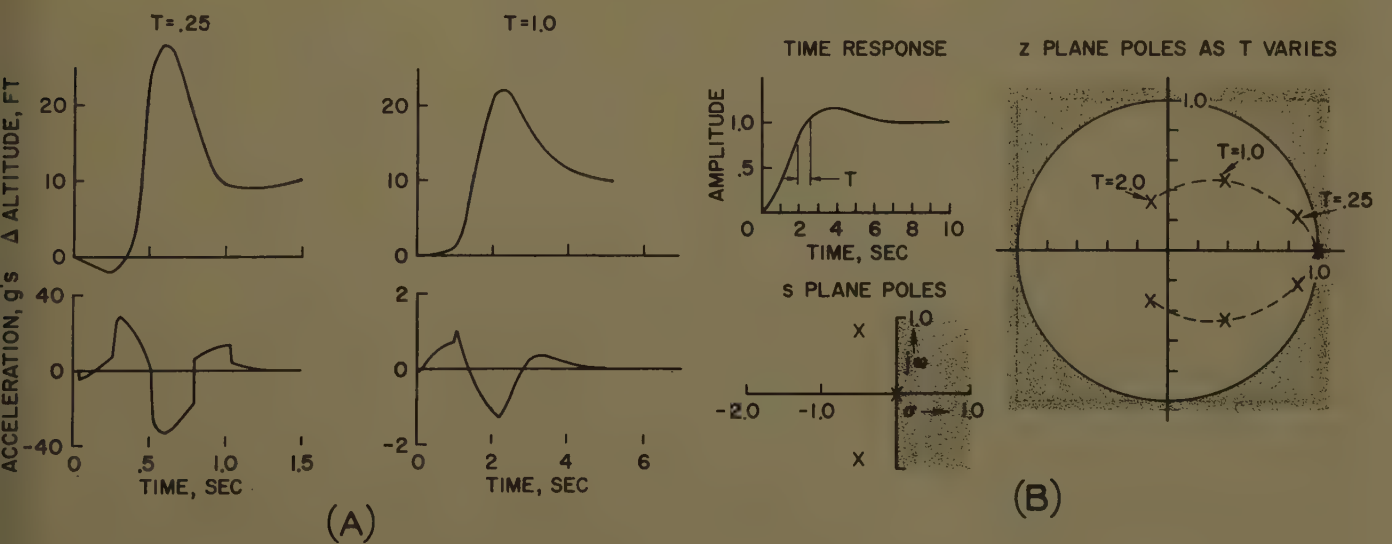

Fig. 2. Effects of sampling period T

A—On transient response

B—On pole positions

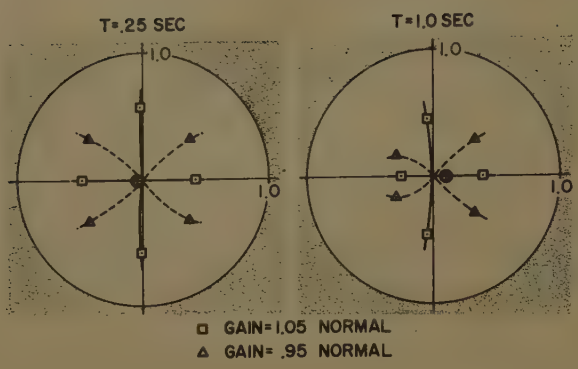

Fig. 3 (left). Root locus plot in z-plane illustrating sensitivity of finite settling time designs

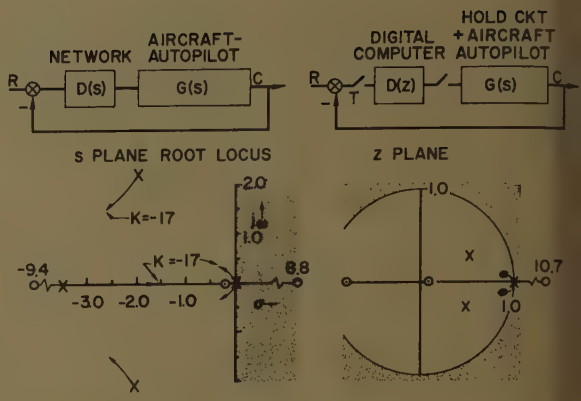

Fig. 4 (right). Design of altitude control system in s plane and corresponding z-plane problem

fact that the peak magnitudes of the normal acceleration differ by a factor of approximately 30. The peak of 32 g's for the $T=0.25$ case obviously could not be achieved by a conventional aircraft and is only a consequence of the linear analysis. For the $T=1.0$ second example the maximum acceleration is slightly higher than is listed in the specification (3 g's for a 50-foot step). These data, however, illustrate that if the sampling period were a variable and could be made somewhat larger than one second, this design could satisfy the abruptness specification.

Another question of importance is the sensitivity of the finite settling time design system to parameter variations. Unpublished simulation studies have indicated that such systems are very sensitive to variations of the aerodynamic parameters. Some appreciation of the sensitivity can be gained with reference to the root locus plot for the two systems shown in Fig. 3 where it can be noted that both systems are very sensitive to small ($\pm 5\%$) open-loop gain changes around the design value of gain (which places all the poles, except those cancelled, at the origin). The root locus plot illustrates the origin to be a position of extreme sensitivity since an additional $\pm 5\%$ change in gain causes the poles to move the short distance from the indicated symbols to the terminating points of the loci shown in the figure.

As was previously mentioned, if it is desired to specify the output time response (for a given input) at chosen sampling instants, additional constraints on the system must be taken into account in the design process of finite settling time designs. This will result in a more complicated $D(z)$. For each sampling instant of the response which is specified, an additional pole at the origin is added to the characteristic equation. From the results presented in Fig. 3 one could conclude that adding more poles will increase sensitivity. Thus, although the abruptness of the response can be controlled by adding more constraints if the sampling period is short, or by increasing the sampling period if it is a variable, the sensitivity of the finite settling time designs to parameter variations will remain large.

System Design Using Continuous System Design Concepts

As has been shown, finite settling time designs are extremely sensitive to parameter changes, due principally to placing the uncancelled poles at the origin in the z-plane. This would be true also if the characteristic equation is of the form $(1-cz^{-1})^n$ as had been proposed by Barker.[2] What appears to be needed, then, is some way of selecting pole locations in the z-plane not all at the same point and which correspond to some known time response that will meet the specifications.

Fig. 2(B) indicates one of the difficulties associated with designing in the z-plane and how it may be overcome by working in the s-plane. Consider the time response shown and presuppose that this response will neet the set specifications in terms of speed and abruptness. Note that it is not too fast, and has adequate stability (actually, corresponding to a second-order system with $\omega_n=1$ and $\zeta=0.5$). Now, in the s-plane, the pole (and zero) correspondence to the time response is fixed. However, note that this is not the case in the z-plane. Here it is shown that the sampling period has a large effect on the pole positions. For each pole location, then (and the corresponding zeros which are not given for convenience), there is an infinite number of time responses if the sampling period is not specified. Thus, locating poles in the z-plane, which will give a satisfactory time response without specifying the sampling period, is not possible.

One possibility of overcoming this difficulty is suggested from a study of Fig. 2(B); i.e., to design, first, a system in the s-plane, transfer the dominant s-plane poles at the system operating sampling period to the z-plane, and then proceed with the design of the digital controller in the z-domain. The merit of this approach is given some support by noting that a sampled data system gives exactly the same response as the continuous system from which it is derived if the sampling period T approaches zero. This may be seen by considering the series expansion of z.

$$z=\epsilon^{sT}=1+sT+(sT)^2+\dots \qquad (14)$$

A mapping in the s-plane in the vicinity of the origin corresponds to a mapping in the z-plane around $z=1$, except for the scale factor T. As T approaches infinity, all stable poles in the s-plane move toward the origin of the z-plane and thus a system designed by fixing the poles in the s-plane approaches a finite settling time design. In between these two extremes there is a large range of sampling periods where the response of the sampled data system is, for all practical purposes, identical with the continuous system.

The proposed procedure, then, for designing a sampled data system is as follows: First, design the system in the s-plane using continuous system methods. Second,* choose the sampling period so that the sampling frequency is high compared to the dominant natural frequencies or break points of the closed loop continuous system. Third, transfer dominant poles to the z-domain and design the digital controller with z-transforms. This procedure will be illustrated with the aircraft-autopilot as the example.

Fig. 4 shows the root locus of the aircraft-autopilot example for a continuous

* There appears, at this time, to be no method of specifying numerically the lowest possible sampling frequency. Sampling, of course, gives rise to error. Unpublished data for the aircraft altitude control system designed for sampling frequencies, approximately 12 and 48 times the dominant continuous system second-order mode frequency, show approximately the same response to the same input.

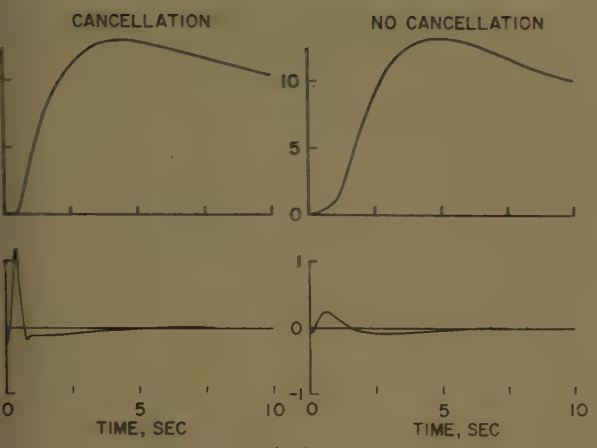

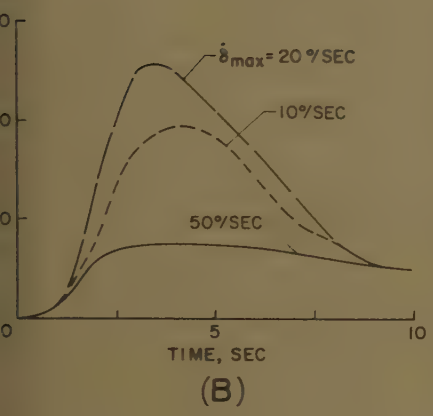

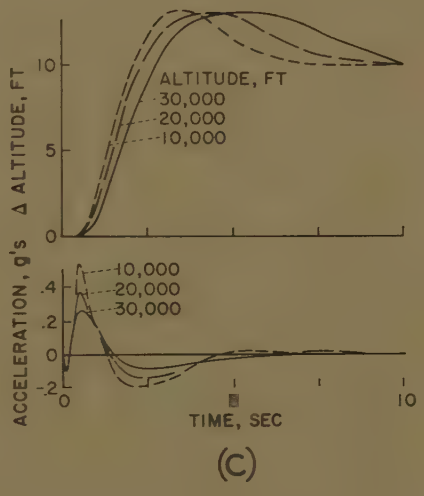

Fig. 5. Step response showing various effects

A—Effects of pole cancellation
B—Effect of control surface rate limits; pole cancellation permitted
C—Effect of change in basic or preset altitude; no pole cancellation permitted

em with a particular choice of lead work

$$=-\left(\frac{s+0.25}{s+3.5}\right)\times\text{constant}$$

should be noted that the simplest sible stabilizing network for this nple is a lead network and that the raft-autopilot zero in the right half- e forces the system gain to be nega- for stability. The design in the s- e is deliberately made sluggish (the inant poles are kept close to the origin pared to the variable poles due to raft dynamics) to reduce the sensi- y of the system to changes in the air- t parameters. For the design gain of 7, the dominant poles (poles nearest origin) are at $\omega_n=0.5$ and $\zeta=0.7$. open-loop z-plane poles and zeros are n also in Fig. 4 for a sampling period .25 second. The dots in the z-plane v the desired location of the dominant ed loop poles mapped from the s-plane the dotted lines indicate the approxi- e loci these poles will take when the of the closed loop system is varied n zero to the desired operating point. e that, as was true for the continuous em, the zero at $z=10.7$ requires that the gain for the sampled data system must be negative for stability.

Once the desired dominant mode poles and zeros are specified in the z-plane (for the system-sampling rate) one can use a trial-and-error procedure with the root locus method to find the digital controller pulse transfer function and gain which will place the open-loop poles at these positions. However, an analytical method for accomplishing the same purpose may be derived in a manner similar to that used by others in obtaining equations 3, 4, and 5 for the finite settling time design. The details of the derivation will not be given here, but the necessary equations and the philosophy for two possible approaches to the design of the digital controller pulse transfer function, $D(z)$ follow. For example, if desired, one can design $D(z)$ to have two complex zeros to cancel the two complex poles of $G(z)$ and place other poles and zeros of $D(z)$ at points in the z-plane in such a way that all poles of the closed loop pulse transfer function $K(z)$ are at the origin, except those cancelled and those of the desired dominant mode. A second method is to design $D(z)$ so that no pole cancellation is permitted. If pole cancellation technique is used, equations 15 and 16 indicate the manner in which the desired constraints are placed on $K(z)$ and $1\text{-}K(z)$

$$K(z)=\frac{\text{[Numerator of } G(z)\text{](undetermined coefficients)}}{\text{desired dominant mode}}$$

$$=\frac{\left(\sum_0^J \alpha_k z^{-k}\right)\left(\sum_0^L a_l z^{-l}\right)}{1-1.825z^{-1}+0.84z^{-2}} \qquad (15)$$

$$1-K(z)=\frac{(G(z)\text{ poles on or outside the unit circle})(\text{undetermined coefficients})}{\text{desired dominant mode}}$$

$$\frac{\left(\sum_0^M \beta_m z^{-m}\right)\left(\sum_0^N b_n z^{-n}\right)}{1-1.825z^{-1}+0.84z^{-2}} \qquad (16)$$

The desired dominant mode given in the foregoing equations (a second-order transfer function with $\omega_n=0.5$ and $\zeta=0.7$ that has been transferred to the z-domain for $T=0.25$) is indicated by the two dots on the z-plane plot of Fig. 4. If pole cancellation is not permitted, equations 17 and 18 replace equations 15 and 16 respectively.

$$K(z)=\frac{\text{[Numerator of } G(z)\text{]}\times\text{(undetermined coefficients)}}{\text{(desired dominant mode)}\times\text{(undetermined coefficients)}}$$

$$=\frac{\left(\sum_0^J \alpha_k z^{-k}\right)(a_0+a_1z^{-1})}{1-1.825z^{-1}+0.84z^{-2})\times(1+c_1z^{-1}+c_2z^{-2})} \qquad (17)$$

$$1-K(z)=\frac{\text{[Denominator of } G(z)\text{]}\times\text{(undetermined coefficients)}}{\text{(desired dominant mode)}\times\text{(undetermined coefficients)}}$$

$$=\frac{\left(\sum_0^P \beta_p z^{-p}\right)(b_0+b_1z^{-1})}{(1-1.825z^{-1}+0.84z^{-2})(1+c_1z^{-1}+c_2z^{-2})} \qquad (18)$$

For this example the substitution of equations 17 and 18 into equation 2 shows that

$$D(z)=\frac{a_0+a_1z^{-1}}{b_0+b_1z^{-1}} \qquad (19)$$

An even simpler $D(z)$ can be obtained if a third undetermined coefficient is added to the denominator of equations 17 and 18. In this case it will be found that b_1 can be chosen to be zero and $K(z)$ will have no poles at the origin. $D(z)$ then, will be of the form

$$D(z)=a_0+a_1z^{-1} \qquad (20)$$

It is interesting to note that in both $D(z)$ designs in which pole cancellation is not permitted (equations 19 and 20) the digital computer pulse transfer function

has been simplified by adding a denominator to $K(z)$. Along this line the first work by Bertram[3] showed only that $D(z)$ need not be more complex if a denominator is added in terms of the delay line synthesis of the digital controller he was considering.

Equations 21 through 26 give the numerical values of the aircraft-autopilot example at a sampling period of 0.25 second for the two design methods indicated by equations 15 through 18.

With cancellation permitted

$$K(z)=\frac{(1.02z^{-1}-10.21z^{-2}-7.53z^{-3}+0.730z^{-4})(-0.0122+0.0113z^{-1})}{1-1.825z^{-1}+0.84z^{-2}} \quad (21)$$

$$1-K(z)=\frac{(1-z^{-1})^2(1+0.187z^{-1}+0.0777z^{-2}-0.0083z^{-3})}{1-1.825z^{-1}+0.84z^{-2}} \quad (22)$$

$$D(z)=\frac{-0.0122(1-0.926z^{-1})\times(1-1.02z^{-1}+0.349z^{-2})}{1+0.187z^{-1}+0.0777z^{-2}-0.0083z^{-3}} \quad (23)$$

With cancellation not permitted

$$K(z)=\frac{(1.02z^{-1}-10.21z^{-2}-7.53z^{-3}+0.730z^{-4})(-0.00276+0.00259z^{-1})}{(1-1.825z^{-1}+0.84z^{-2})\times(1-1.205z^{-1}+0.402z^{-2})} \quad (24)$$

$$1-K(z)=\frac{(1-z^{-1})^2(1-1.02z^{-1}+0.349z^{-2})(1-0.0054z^{-1})}{(1-1.825z^{-1}+0.84z^{-2})\times(1-1.205z^{-1}+0.402z^{-2})} \quad (25)$$

$$D(z)=-0.00276\,\frac{(1-0.936z^{-1})}{1-0.0054z^{-1}} \quad (26)$$

The simplest possible $D(z)$ (equation 20) has been computed but no simulation data are available for this design. However, a comparison of the magnitudes of the coefficients of $D(z)$ indicate that there would be little difference in the response. between that for the simplest possible $D(z)$ and the one given by equation 26.

Fig. 5(A) compares responses for the two systems (equations 23 and 26). Note that there is little difference between the two altitude time responses. However, the acceleration required if pole cancellation is permitted is considerably higher during the initial transient than when pole cancellation is not permitted. This difference in the acceleration response is associated with the fact that the digital computer's output is quite abrupt initially in cancelling the effects of the two poles. From these results it is concluded that little is gained by pole cancellation in terms of response time and one of its poor features is that a more complicated digital controller is required.

Fig. 5(B) illustrates an even more serious drawback to the use of design methods which employ cancellation procedures. These data show, in Fig. 5(B), the effect of having a rate-limited servo driving the aerodynamic control surface. Of particular interest is the large overshoot for a 20 degrees per second rate limit and the large change in the overshoot with the magnitude of rate limiting. The unusual fact that the overshoot is higher for 20 degrees per second than for the 10 degrees per second rate limit is due to the time relationship between the actual control surface motion and the command input during the initial part of the transient. The large overshoots are directly traceable to the fact that true pole cancellation is not possible where a nonlinearity exists between the output of the digital computer and the aircraft's control surface input. These results illustrate that saturation-type nonlinearities cannot be neglected in the design if cancellation is attempted in the design process. Introduction of the same values of control surface limiting in the simulation of the system described by equations 24 through 26 (no pole cancellation) showed no changes in the altitude response with changes in the magnitude of control surface rate.

Fig. 5(C) shows the effect of altitude change on the transient response. Note that in obtaining these data only the aircraft parameters were varied in accordance with the manner in which they were affected by a change in air density. A change from the design altitude, 30,000 feet to 10,000 feet results in a 40% increase in natural frequency of the aircraft and a 90% increase in gain. As may be seen, the response becomes faster as the altitude decreases due to the increase in aerodynamic gain but that no large change occurs in the stability of the system.

Conclusions

The design of a sampled data system in which considerations of the sensitivity of the response to parameter variations and the abruptness of the response are important has been shown to be simplified considerably by first designing a continuous system in the s-plane which will satisfy the requirements. The dominant characteristics of the continuous system are then transformed to the z-domain for final synthesis of the sampled data system. The principal advantage of this method is that the sampling period T has little influence on the transient performance over a very large range of values, provided the sampling frequency is high compared t the dominant closed loop poles of th continuous system design. The prin cipal disadvantage of the method is th fact that system synthesis of the con tinuous system to meet certain specifica tions is somewhat more of an art than science. In any case, the problem ap pears no more difficult for the sample system then for its continuous syste counterpart.

It has been shown that finite settlin time designs are very sensitive to pa rameter changes. One would conclude therefore, that since the performance c such sampled data systems cannot b achieved in actual practice they shoul be avoided.

Designs using pole cancellation shoul be avoided for the following reasons First, the abrupt motion of the digita controller output in attempting to cance the effect of the poles for a transient inpu may lead to saturation of the input t the plant. Saturating type nonlinearitie frequently cause an acceptable design fo linear analysis to become completely un acceptable. Second, if undesirable pole are cancelled by $D(z)$ with respect to th command input, they will not be can celled with respect to distrubance inputs and an undesirable load disturbanc response may result.

References

1. Sampled Data Control Systems, J. R. Ragazzini, G. F. Franklin. McGraw-Hill Book Company, Inc., New York, N. Y., 1958.

2. The Theory of Pulse-Monitored Servos and Their Use for Prediction, R. H. Barker. *Report no. 1046*, Signals Research and Development Establishment, Christchurch, England, Nov. 1950.

3. Factors in the Design of Digital Controllers for Sampled-Data Feedback Systems, John E. Betram. *AIEE Transactions*, vol. 75, pt II, July 1956, pp. 151–59.

4. Network Compensation of Error-Sampled Feedback Control Systems, J. Sklansky. *Technical Report T-7/B*, Columbia University Press New York, N. Y., April 1, 1955.

Discussion

Gene Franklin (Stanford University, Stanford, Calif.): Many of the early papers o sampled data system were concerned wit extending the continuous system desig methods of steady-state frequency-respons shaping to apply to the new area. Late efforts tend to emphasize the difference between continuous and sampled dat design and have developed new time domai design objectives such as finite settling tim designs. This paper represents, in a cer tain sense, a return to the original objectiv of relating sampled data system design t continuous system design. In this paper

ver, the bridge is built from the time
in synthesis methods of the z-trans-
to the pole-zero design methods of
nuous systems. There seems to be
n to expect that both design problems
benefit from the connection.

ie primary purpose of this discussion is
ive an analytical nail in the coffin of
inite settling time design alongside the
or's experimental fastening. Actually,
ite the calculations to follow, the finite
ing time design will remain a useful
ept to illustrate time domain design
ods and will probably remain a
tical design for low-order systems which
operate with very long sampling pe-
.

ie sensitivity of a system may, in gen-
be defined as the percentage change in
performance of the system to a per-
age change in a parameter. That is, if P
e performance index, then the sensitivity
ie system with respect to a parameter k
fined as

$$= \frac{dP/P}{dk/k}$$

the past, in connection with feedback
lifier and, later, in arbitrary feedback
em, the performance P has been taken
ie output/input gain ratio at some fixed
uency, usually zero (direct current).
re is no reason why this should be so.
ently Huang[1] defined the "performance"
ie location of the pole of the output/
t transfer function in the s-plane or in
-plane. Huang's definition and similar
ulations were developed independently
he discusser using the root locus as a
ing point. From this point of view, the
acteristic equation is written in the form

$$G(z)_i = 0 \qquad (26)$$

re k is the parameter of interest. The
s of this equation, $z = z_i$ are the poles of
output/input transfer function of the
em. The shift in a particular pole
tion for a change in the parameter k
be obtained by setting the total deriva-
of equation 26 to zero.

$$dkG(z_i) + kG'(z_i)dz_i = 0$$

$$\frac{dz_i}{dk} = -\frac{G(z_i)}{kG'(z_i)} \qquad (27)$$

where the conventional notation

$$G'(z_i) = \left.\frac{dG}{dz}\right| z = z_i$$

is used. Because of equation 1, it is also possible to write equation 27 in the forms

$$\frac{dz_i}{dk} = \frac{G^2(z_i)}{G'(z_i)} = \frac{1}{k^2 G'(z_i)} \qquad (28)$$

It should be realized that equations 27 and 28 represent the differential change in a root position for a differential change in the parameter k. To obtain percentage changes one needs to normalize the differential changes with respect to the sizes of the quantities involved. In this case, one is led to the definition

$$S_k^{z_i} = \frac{\dfrac{dz_i}{|z_i|}}{\dfrac{dk}{k}} = \frac{G(z_i)}{|z_i|G'(z_i)} = \frac{1}{|z_i|kG'(z_i)} \qquad (29)$$

The sensitivity defined by equation 29 has many implications, only one of which will be considered here, namely that $S_k^{z_i}$ is infinite when $G'(z_i)$ is zero. Points where $G'(z)$ is zero are called saddle points of the complex plane representation of $G(z)$ and they include all poimts of multiple roots of the equation $1 + kG(z_i) = 0$. In other words, the finite settling time design which places all poles at the origin of the z-plane is operating at a point of infinite sensitivity of root position to parameter change! A design which shifts the multiple roots from the origin to a point such as $z = a$ does not change the sensitivity picture. An analysis of equation 29 shows that the speed with which the sensitivity decreases from infinity, as operation shifts from the saddle point, depends upon the order of the saddle point. The larger the number of poles placed at a single operating point, the more sensitive will be the root locations to parameter changes. It is largely for this reason that the low-order systems designed for finite settling time in the past have been relatively successful. The higher order, more practical system described in this paper shows the extreme sensitivity of the design.

REFERENCE

1. THE SENSITIVITY OF THE POLES OF LINEAR, CLOSED-LOOP SYSTEMS, R. Y. Huang. *AIEE Transactions*, vol. 77, pt. II, Sept. 1958, pp. 182–87.

Stanley F. Schmidt: The author appreciates Dr. Franklin's helpful suggestions given during the progress of this investigation. His derivation showing "finite settling time designs" to have infinite sensitivity at their operating conditions, gives further proof as to why they should be avoided and why a design approach such as is presented in the paper should be used.

The definition of sensitivity given by equation 29 has certain implications which should be of use to the control system designer; i.e., it gives a percentage shift in a pole position for a percentage change in some parameter. It is the author's opinion, however, that this does not completely resolve the question of the sensitivity of a closed loop system, since one usually desires to know the magnitude in the pole position shift for a specified incremental change in a parameter. At present, this information can only be obtained by the relatively tedious root locus method. Furthermore, the change in the pole position which is tolerable in a given control system depends on its position in the s-plane (or z-plane) and whether it is a "dominant" pole or one which is significantly far away from the origin in the s-plane (or unity in the z-plane) so that its position has a negligible influence on the desired response of the system.

From these standpoints, further research would be desirable to determine what additional definitions need be added to the sensitivity question as well as how to design control systems which have only a small sensitivity (or change in response) with parameter variations.

---

lectric and Magnetic Conditions Inside an Induction-Heated Workpiece

CHESTER A. TUDBURY
MEMBER AIEE

HE PURPOSE of this paper is to improve the general understanding of ction heating through a familiarity what happens electrically and magally inside a solid bar being heated. E Standard No. 54[1] defines induc- heating as the heating of a nominally luctting material in a varying magnetic due to its internal losses. This r reports the results of a study of how these losses occur, and describes the vector current densities and flux densities inside the material being heated. The AIEE definition is sufficiently general to include not only intentional induction heating as practiced industrially for hardening, forge heating, brazing, and other applications, but also the eddy current and hysteresis heating which appear as core losses in motors and transformers. This paper deals with the case of a long, round, solid bar of homogeneous conducting material located coaxially inside a solenoidal coil carrying sinusoidal alternating current. This is a configuration used frequently in industrial induction heating installations. The same principles apply to more complicated arrangements. The results given here apply over the entire range of sizes and frequencies used in industrial induction heating, as well as to the lower frequencies and smaller dimensions employed to avoid

Paper 59-64, recommended by the AIEE Electric Heating Committee and approved by the AIEE Technical Operations Department for presentation at the AIEE Winter General Meeting, New York, N. Y., February 1–6, 1959. Manuscript submitted November 6, 1958; made available for printing November 25, 1958.

CHESTER A. TUDBURY is with the New Rochelle Tool Corporation, New Rochelle, N. Y.

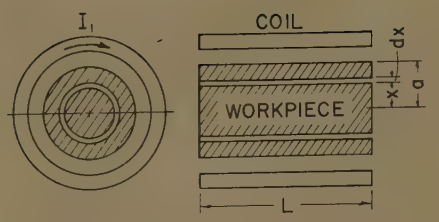

Fig. 1. Coil and workpiece

eddy currents and reduce core losses in electromagnetic equipment.

Accurate methods of designing induction heating coils and of calculating their electrical performance in advance have been available since the 1930's and are still being improved.[2-5] Their emphasis is more on the integrated effect of conditions inside the bar on the electrical characteristics at the coil terminals than on a study of these internal conditions per se.

Conditions

Fig. 1 shows the case under consideration. The bar and the coil are very long, so end effects are neglected. The magnetic field is parallel to the centerline of the bar. The primary current in the coil and the induced currents in the bar follow coaxial paths around the same center line.

Electric resistivity ρ and magnetic relative permeability μ are the two most important properties of the material of the bar. Resistivity depends upon temperature, which in turn depends upon internal power distribution (always greatest at the surface), specific heat, density thermal conductivity, rate of heating, and surface thermal losses. Permeability depends upon degree of magnetic saturation and also upon whether the temperature is below or above the Curie value. In most induction-heating applications for heating steel, the surface flux density is above saturation.

Hysteresis loss is also present when heating magnetic materials. It is insignificant relative to eddy current power in most industrial induction-heating applications.

A complete treatment of the foregoing is beyond the scope of this paper. Resistivity and permeability are assumed to be uniform and hysteresis losses are neglected.

Nomenclature

a = workpiece radius, cm (centimeters)
B = flux density, gausses
ber = Bessel function, real
bei = Bessel function, imaginary
ber′ = d, ber
bei′ = d, bei
c = reference depth, cm
E_2 = voltage induced in workpiece, rms, volts
f = frequency, cycles per second
H = magnetic intensity, oersteds
H_g = magnetic intensity in air gap, oersteds
H_r = real component of H
H_i = imaginary component of H
I_1 = current in coil, rms, amp (amperes)
I_2 = total current in workpiece, rms, amp
I_{2r} = real component of I_2
I_{2i} = imaginary component of I_2
K_R = resistance factor
K_x = reactance factor
L = length of coil and work, cm
N_1 = number of turns in primary coil
P_2 = total power developed in workpiece, watts
S = current density in workpiece, amp/sq cm (amp per square cm)
S_r = real component of S, amp/sq cm
S_i = imaginary component of S, amp/sq cm
Φ_2 = total flux in workpiece, lines
ρ = resistivity, ohm-cm
μ = relative permeability

Qualitative Explanation

Consider the bar to be composed of many thin coaxial sleeves. The magnetic intensity at the surface ($x=a$) is identical with the air gap intensity H_g, where

$$H_g=\frac{4\pi N_1 I_1}{10L}$$

The flux density in the outermost sleeve is H_g. The total flux surrounded by this sleeve induces a voltage in the sleeve. As a consequence, current flows circumferentially in the sleeve. The magnitude of this current is determined by the induced voltage and the resistance of the sleeve. This current, flowing in a substantially opposite instantaneous direction of the primary current, causes the magnetic intensity at the inner surface of the sleeve to be less than at the outer surface. The induced voltage is 90 electrical degrees out of phase with the flux which produces it, but the effect which the resulting current exerts upon that same flux is in phase with the current. The resulting flux density, induced voltage, and current in the second sleeve are thus not only smaller in magnitude but are also more lagging in time phase than in the outer sleeve.

The current in each sleeve is accompanied by an I^2R loss. The total power is the integration of the losses in all the sleeves. This power is densest at the surface of the bar and is zero at the center.

Mathematical Background

Differential equations for magnetic intensity H, and current density S, as functions of distance from the center line x, are obtained by letting the thickness of the sleeves approach zero, equating the induced voltage in a sleeve to its resistance drop, and taking into account the effect of the induced current on the magnetic intensity inside the sleeve.

$$\frac{d^2H}{dx^2}+\frac{1}{x}\frac{dH}{dx}-j\frac{1}{c^2}H=0 \tag{1}$$

where

$$C^2=\frac{10^9\rho}{8\pi^2\mu f}$$

$$S=\frac{10}{4\pi}\frac{dH}{dx} \tag{2}$$

The boundary conditions are

At $x=a$, $H=H_g$.
At $x=0$, H is not infinity.
At $x=0$, $S=0$.

Solving equations 1 and 2, and applying these conditions yields

$$B=\mu H_g(H_r+jH_i) \tag{3}$$

where

$$H_r=\frac{\text{ber } x/c \text{ ber } a/c+\text{bei } x/c \text{ bei } a/c}{\text{ber}^2 a/c+\text{bei}^2 a/c} \tag{4}$$

and

$$H_i=\frac{\text{bei } x/c \text{ ber } a/c-\text{ber } x/c \text{ bei } a/c}{\text{ber}^2 a/c+\text{bei}^2 a/c} \tag{5}$$

$$S=-\frac{N_1 I_1}{CL}(S_r+jS_i) \tag{6}$$

where

$$S_r=\frac{\text{ber } a/c \text{ ber}' x/c+\text{bei } a/c \text{ bei}' x/c}{\text{ber}^2 a/c+\text{bei}^2 a/c} \tag{7}$$

and

$$S_i=\frac{\text{ber } a/c \text{ bei}' x/c-\text{bei } a/c \text{ ber}' x/c}{\text{ber}^2 a/c+\text{bei}^2 a/c} \tag{8}$$

The total flux in the bar is found by integrating equation 3 over the area of the bar:

$$\phi_2=\mu H_g(2\pi ac)\left(\frac{K_x-jK_r}{\sqrt{2}}\right) \tag{9}$$

where

$$K_x=\sqrt{2}\left(\frac{\text{ber } a/c \text{ bei}' a/c-\text{bei } a/c \text{ ber}' a/c}{\text{ber}^2 a/c+\text{bei}^2 a/c}\right) \tag{10}$$

and

$$K_R=\sqrt{2}\left(\frac{\text{ber } a/c \text{ ber}' a/c+\text{bei } a/c \text{ bei}' a/c}{\text{ber}^2 a/c+\text{bei}^2 a/c}\right) \tag{11}$$

This total flux generates a net back electromotive force E_2 in the bar:

$$E_2=-\frac{\rho(2\pi a)}{cL}N_1 I_1\left(\frac{K_R+jK_x}{\sqrt{2}}\right) \tag{12}$$

The total current induced is found by integrating equation 6 from $x=0$ to $x=a$:

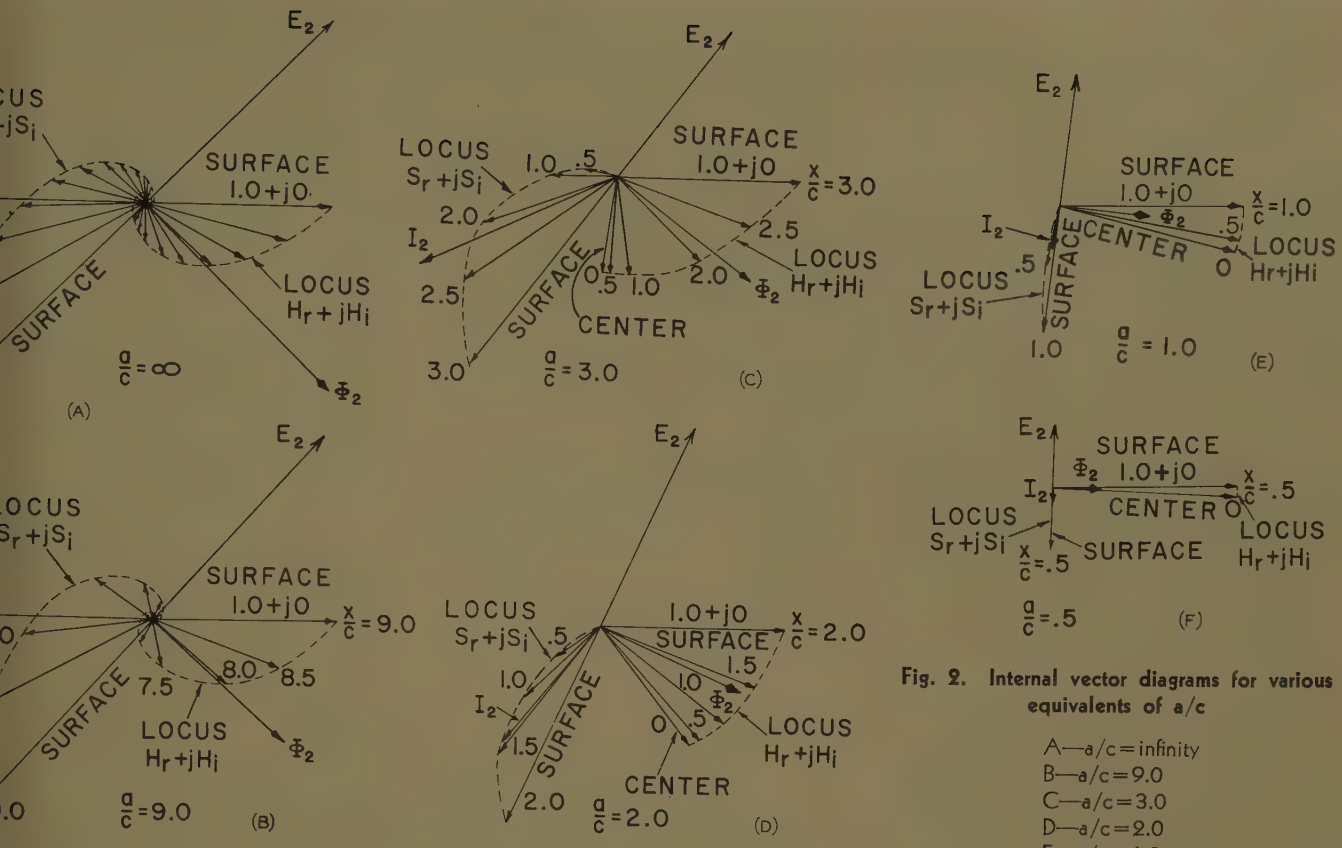

Fig. 2. Internal vector diagrams for various equivalents of a/c

A—a/c=infinity
B—a/c=9.0
C—a/c=3.0
D—a/c=2.0
E—a/c=1.0
F—a/c=0.5

$I_1 I_1(I_{2r}+jI_{2i})$ (13)

e

$$\left(\frac{\text{ber } a/c}{\text{ber}^2 a/c+\text{bei}^2 a/c}-1\right) \quad (14)$$

$$-\left(\frac{\text{bei } a/c}{\text{ber}^2 a/c+\text{bei}^2 a/c}\right) \quad (15)$$

e total power developed by eddy cur- inside the bar is found by integrating ^2R in all the sleeves. It is also equal

os $<\frac{E_2}{I_2}$

$$V_1^2 I^2 \frac{\rho(2\pi a K_r)}{\sqrt{2}cL} \quad (16)$$

rence Depth

e quantity c, which first appeared in sic differential equation 1 is of great cance; c has the dimension of length

$$\sqrt{\frac{10^9\,\rho}{8\pi^2\mu f}}=3{,}560\sqrt{\frac{\rho}{\mu f}}\text{ cm} \quad (17)$$

equation 16 the total power is the as if a uniformly distributed current were flowing circumferentially d a cylinder of average radius $a\,K_r$, thickness of $c\sqrt{2}$, and length L. us terms have been applied to the ity c (also to $\sqrt{2}c$) by different authors: "skin depth," "reference dimension," "reference depth." "Reference depth" is used herein to mean the dimension c.

The key to the choice of frequency is the ratio of radius to reference depth. This ratio is the dimensionless parameter in all the Bessel functions in equations 3 through 15. It increases with frequency and with workpiece size. When $a/c=\infty$, K_R and K_x both equal 1.0. When $a/c=0$, K_R and K_x are zero.

There is nothing in the definition of reference depth which implies smallness. Cases wherein the reference depth approaches or even exceeds the radius of the workpiece are of more than simply academic interest. The presently increasing use of line frequencies for induction heating, and the use of thin laminations in iron cores are examples. This is why the term "reference depth" is preferred over "skin depth." Equation 16 applies even when c exceeds a. However, it is admittedly difficult to visualize a hollow cylinder whose wall thickness exceeds its outer radius!

Infinite Radius: Flat Slab

If the radius of the round bar is increased to infinity the bar becomes a flat slab. The independent variable x, which is the distance from the center, loses its significance, and must be replaced by the distance below the surface. The first derivative in equation 1 disappears and the solution becomes simple exponential functions. The power is the same as if a uniform current $N_1 I_1$ flowed in a surface layer $\sqrt{2}\,c$ deep. This affords an easy way of obtaining approximate results for irregularly shaped workpieces where the cross-sectional dimensions are large com-

Table I. Representative Values

a/c	x/c	Hr	Hi	Sr	Si
9.0	9.0	1.000	0.0	−0.920	−1.000
9.0	8.5	0.679	−0.251	−0.869	−0.450
9.0	8.0	0.398	−0.341	−0.702	−0.088
9.0	7.0	0.042	−0.273	−0.311	0.202
9.0	6.0	−0.078	−0.125	−0.056	0.188
9.0	5.0	−0.076	−0.024	0.040	0.097
9.0	4.0	−0.041	0.022	0.051	0.026
9.0	3.0	−0.005	0.024	0.032	−0.006
9.0	2.0	0.005	0.015	0.014	−0.013
9.0	1.0	0.011	0.007	0.004	−0.008
9.0	0.0	0.012	0.004	0.0	0.0
3.0	3.0	1.000	0.0	−0.764	−1.060
3.0	2.5	0.721	−0.251	−0.797	−0.598
3.0	2.0	0.452	−0.441	−0.701	−0.283
3.0	1.0	0.070	−0.515	−0.365	−0.006
3.0	0.5	−0.026	−0.513	−0.181	0.014
3.0	0.0	−0.058	−0.510	0.0	0.0
2.0	2.0	1.000	0.0	−0.488	−1.095
2.0	1.5	0.830	−0.315	−0.517	−0.705
2.0	1.0	0.655	−0.508	−0.408	−0.408
2.0	0.5	0.538	−0.611	−0.222	−0.184
2.0	0.0	0.498	−0.644	0.0	0.0
1.0	1.0	1.000	0.0	−0.088	−0.698
1.0	0.5	0.978	−0.184	−0.076	−0.335
1.0	0.0	0.964	−0.245	0.0	0.0
0.5	0.5	1.000	0.0	−0.011	−0.353
0.5	0.0	0.996	−0.062	0.0	0.0

Table II. Representative Values

a/c	K_R	K_X
0.0	0.0	0.0
0.5	0.011	0.352
1.0	0.087	0.698
1.5	0.260	0.961
2.0	0.488	1.096
2.5	0.660	1.100
3.0	0.764	1.06
3.5	0.805	1.023
4.0	0.826	1.01
4.5	0.840	1.006
5.0	0.855	1.005
10.0	0.930	1.000
20.0	0.965	1.0
∞	1.000	1.0

Table III. Generality of Ratio a/c

Figure No.	a/c	Radius, Cm: Copper Workpiece at 68 F, 60 Cycles	Copper Workpiece at 68 F, 450 Kc	Steel Workpiece at 2,100 F, 60 Cycles	Steel Workpiece at 2,100 F, 450 Kc
2(B)	9	5.4	0.063	45.0	0.54
2(C)	3	1.8	0.021	15.0	0.18
2(D)	2	1.2	0.014	10.	0.12
2(E)	1	0.6	0.007	5.0	0.06
2(F)	0.5	0.3	0.0035	2.5	0.03

pared to reference depth. This case has been treated in detail in reference 6. A vector diagram for infinite ratio a/c, Fig. 2(A) is included for reference purposes.

Numerical Values of Coefficients

Representative values of H_r, H_t, S_r, S_i, K_x, and K_R have been calculated for various values of the ratio a/c (workpiece size in terms of reference depth) and for various values of the ratio x/c (location inside the work piece). Some of the results are tabulated in Tables I and II. They are illustrated graphically in Figs. 2(B) through (F).

Generality of Vector Diagrams

Table III illustrates the generality with which the ratio a/c describes the electrical size of a workpiece. Fig. 2(B), for example, applies equally to a copper workpiece of 5.4 cm radius at 68 F (Fahrenheit) heated by 60 cycles and to a steel load 0.54 cm in radius at 2,100 F heated by 450 kc. There are many other combinations.

As a numerical example, take the following problem:

Find the total power developed inside a 3.6-cm-diameter copper bar at 68F when it is placed inside a coil which supplies 10,000 ampere-turns per cm at 60 cycles. Find the flux density and current density at one half a reference depth below the surface. Take $\rho = 1.724 \times 10^{-6}$ ohm-cm.

Solution:

From equation 17,

$$c = 3{,}560\sqrt{1.724 \times 10^{-6}/60} = 0.6 \text{ cm}$$

$$a/c = \frac{1.8}{0.6} = 3$$

which means that Fig. 2(C) applies. From equation 16 and Table II, find the power:

$$P_2 = \frac{(10{,}000)^2(1.724) \times 10^{-6}(2\pi)(1.8)(0.764)L}{\sqrt{2}(0.60)}$$

$$= 1{,}760\ L \text{ watts}$$

or 1.76 kw/cm length.

From equation 3, Table I, and Fig. 2(C), at $x/c = 2.5$,

$$B = 4/10\pi\,(10{,}000)\,(0.721 - j0.251)$$
$$= 9{,}060 - j3{,}150 = 9{,}600/\underline{-19.2°} \text{ gauss}$$

From equation 16, Table I, and Fig. 2(C) at $x/c = 2.5$,

$$S = 10{,}000/0.60\ (0.797 + j0.598)$$
$$= 13{,}300 + j9{,}970$$
$$= 16{,}600/\underline{36.8°} \text{ amp/sq cm}$$

Magnetic Intensity

The vector diagrams illustrated in Table I and Fig. 2(A) through (F) are all based on the air-gap magnetic intensity (magnetizing force) as a reference. The diagrams drawn are to scale. The locus of the magnetic-intensity vector has a spiral shape. The magnetic intensity becomes smaller in magnitude and more lagging in time phase with increasing depth below the surface. For large diameters, the magnetic-intensity vector may make several complete revolutions between the surface and the center of a workpiece. For small diameters, the magnetic intensity at the center is hardly different, either in magnitude or phase, from that at the surface. In all cases where the ratio of radius to reference depth is finite, the magnetic intensity at the center of the work piece is larger than zero.

Current Density

In every case, the current density is maximum at the surface and zero at the center. It must be zero at the center, because it changes direction there. With increased depth below the surface, the current density vector also becomes more lagging. In electrically large workpieces, Fig. 2(A) and (B), it describes more than a complete revolution before becoming insignificant. These are the conditions under which induction heating is most efficient.

In electrically small workpieces, the current density falls rapidly to zero at the center with very little change in phase. These are more suitable conditions for transformer laminations than for induction heating.

Total Secondary Current

The optimum conditions for induction heating a round, solid workpiece appear in Fig. 2(A), where $a/c = \infty$. The integrated total induced current I_2 has its maximum value for the applied magnetizing force. The secondary power factor is 70.7% lagging. Fig. 2(B) through (F) illustrate the progressive shrinking of this vector and the change of its phase angle as workpiece size is decreased.

Total Power Developed

The maximum power is developed in Fig. 2(A). Here the projection of the I vector on the E_2 vector is largest. In spite of the fact that the E_2 and I_2 vectors come more into line with each other for smaller workpiece sizes, this is more than offset by the rapid decrease of the magnitudes.

Fig. 2(F) approaches the condition necessary for the ideal transformer lamination. However, it is well to bear in mind that hysteresis losses have been neglected in this analysis. For steel workpieces in the region covered by Fig. 2(F), hysteresis losses are probably not unimportant.

Conclusions

The ratio of workpiece radius to reference depth determines the distribution of magnetic intensity and of current density inside a workpiece being heated by induction. It is also the factor which determines whether or not a workpiece is a good induction heating load. When this ratio is small, while at the same time the workpiece permeability is high, the workpiece would serve better as a transformer lamination.

References

1. Proposed Standard, Test Code, and Recommended Practice for Induction and Dielectric Heating Equipment. *AIEE Standard No.* Oct. 1952.

2. Calculations for Coreless Induction Furnaces, H. B. Dwight, M. M. Bagai. *AIEE Transactions*, vol. 54, March 1935, pp. 312–15.

3. Radio Frequency Heating (book), George Brown, Cyril N. Hoyler, Randolph A. Bierwirth, D. Van Nostrand Company Inc., Princeton, N. J. 1947.

4. Design of Induction-Heating Coils for Cylindrical Nonmagnetic Loads, J. T. Vaughan, J. W. Williamson. *AIEE Transactions*, vol. Aug. 1945, pp. 587–92.

5. Design and Calculation of Induction Heating Coils, R. M. Baker. *Ibid.*, vol. 76, II, March 1957, pp. 31–40.

6. Surface Heating by Induction, Herbert Storm. *Ibid.*, vol. 63, Oct. 1944, pp. 749–54.

Discussion

. Baker (Westinghouse Electric Cor-on Baltimore, Md.): Mr. Tudbury is complimented on the treatment of his t. It is unfortunate that the condi- of flux and current distribution in- n induction-heated workpiece are so lt to visualize in the variety of situa- which arise in practice because it is through such visualization that one now what to expect and plan accord- This situation is undoubtably re- ble for much consternation and fre- disappointment on the part of users of ion heating. The mathematics re- l to treat even a simple case such as the rical shape chosen by Mr. Tudbury te involved. Yet the mathematical ach is the best way to establish itative concepts.

explaining the rudiments of induction g to the uninitiated one usually as- that the frequency used is high enough to make the reference depth much less than the minimum dimension of the workpiece. In this case the reference depth is the effective depth of current penetration, and a simple picture of surface or skin heating results. This simple picture serves for any shape because the skin current flowing around the workpiece follows the surface contour; be it flat, round, fluted, or otherwise. One may even estimate on this basis approximate power input for a given current in the coil and foretell where the workpiece will be relatively hot or cold. It is actually a good starting point even for the expert. It represents the maximum coupling efficiency which can be achieved. Practical considerations however often dictate the use of a lower frequency and in order to anticipate results one must be able to visualize what happens as the reference depth becomes appreciable or when it may even exceed the minimum dimension of the workpiece. For certain regular shapes this can be developed on a purely mathematical basis. For more complicated shapes one may think of the actual work piece in terms of a similar regular shape which can be treated mathematically. This is, in fact, the way one gradually develops an intuitive feeling for what will happen in a particular situation even though the mathematical approach may be replaced or supplemented by the experimental heating of certain typical regular shapes in the laboratory. Everyone sooner or later learns to lean heavily on the concept of reference depth. This very useful concept is a measuring stick incorporating all the variables of the problem except the geometry of the workpiece. It permits one to translate experience from one job to another and suggests the similarity of jobs wherein the materials and frequencies used may be radically different.

All of this points to the need, especially on the part of users, for a better understanding of conditions inside an induction-heated workpiece.

It is to be hoped that Mr. Tudbury's paper will stimulate others to write on the subject.

Transient Voltages in Rectifier Transformers

B. C. BIEGA
MEMBER AIEE

H. W. LORD
FELLOW AIEE

sis: This paper discusses transient- e phenomena which occur in rectifier s involving mercury-vapor hot-cath- bes commonly used as power sources ny electronic equipments such as ast transmitters, high-frequency in- al-heating applications and the like. rticular, reference is made to equip- with power outputs in the range 10– with direct voltages of 3 to 15 kv. ifically it is intended to show the of transformer parameters on these nts, the voltage stresses that may within the transformer windings, and gest means for improving the capa- of withstanding such transients as testing the ability of the transformer hstand transients that may occur in

s of Voltage Transients Rectifier Circuits

Y Operation of Tube

den restriction of current flow. g normal operation, a mercury- filled tube may suddenly cease to ct current in the forward direction as a result of ion starvation, par- ly during severe overload con- , or when the tube is operating normal temperature, or as a of a pinch effect or constriction of c due to electromagnetic forces acting on the plasma. In any of these cases there is an extremely rapid rate of change of current which may be of the order of hundreds of amperes per μsec (microsecond). Consequently, voltages are induced in inductances such as the direct-current windings of the transformer in accordance with the equation

$$e = -L\frac{di}{dt}$$

Tube arc back. This is a spontaneous reversal of conduction in the tube. Some of the causes may be overheating of the tube, too rapid application of reverse voltage after conduction, localized cathode spots forming on the anode, application of reverse voltage of value sufficient to start a glow discharge at the anode.[1]

Frequently an arc back may start but will clear itself. However, if the arc back is sustained, this is equivalent to a short-circuit of the transformer secondary, the short-circuit current being limited only by the impedance of the supply and of the transformer (see Fig. 1). Unless these impedances are large enough to limit the short-circuit current to a safe value and unless circuit-protective devices operate rapidly, severe damage may be inflicted on the tubes, the transformer, and other circuit elements. If the load is a motor the magnitude of the short-circuit current will be substantially increased.[2]

Irrespective of the thermal and mechanical effects of the short-circuit current, damaging overvoltages may occur within the transformer windings as will be discussed later. It should be noted that an arc back may occur as a result of the high induced reverse voltages appearing at the anode following a restriction of current flow described under "Sudden restriction of current flow."

Direct-Current Interruption

In many industrial electronic circuits, particularly in high-frequency heating applications, vacuum switches are used to bias the grid of the oscillator tube in

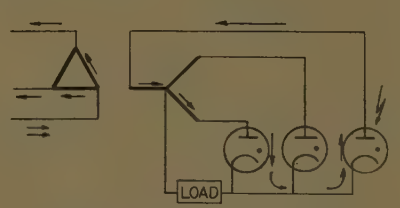

Fig. 1. Flow of arc-back current

Paper 59-149, recommended by the AIEE Electronics Committee of the Communication and Electronics Division and approved by the AIEE Technical Operations Department for presentation at the AIEE Winter General Meeting, New York, N. Y., February 1–6, 1959. Manuscript submitted November 3, 1958; made available for printing December 5, 1958.

B. C. Biega, formerly with the General Electric Company, is now with the Precision Transformer Corporation, Chicago, Ill., and H. W. Lord is with the General Electric Company, Schenectady, N. Y.

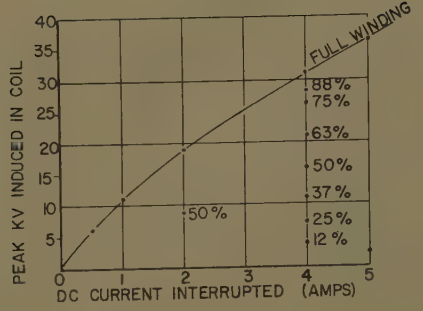

Fig. 2. Induced voltages in coil due to sudden interruption of direct current. Percentages indicate voltages at tap in winding

order to obtain a sharp cutoff to the power tube. Occasionally this may be done as a protective measure, but in other cases this method is used as a means of controlling the heating cycle. The very high rate of change of direct current induces an overvoltage in any inductances in the circuit including the transformer d-c windings.

Fig. 2 illustrates the relationship of peak-induced terminal voltages to the magnitude of the direct current suddenly interrupted in a coil of a 60-kva transformer rated 5,150 volts line-to-neutral. To obtain these data, direct current from a low-voltage external source was circulated through the winding and interrupted with an *RG9* vacuum switch. The voltage rise time was of the order of 100 μsecs.

Alternating-Current Interruption

In many industrial applications involving repetitive cycles of power application, the duration of the cycle is controlled by contactors in the primary lines of the transformer. When the contactor is opened the load current normally continues to flow through the arc which is maintained between the parting contacts until the current passes through zero. Occasionally, and in particular on light loads, the current will extinguish suddenly before current zero is reached.

The electromagnetic energy stored in the magnetic field of the primary winding, $W = {}^1/_2 L_{l,p} i^2$, is transferred to electrostatic energy by charging the capacitance of the transformer primary winding. The maximum value of the induced voltage becomes

$$e = i\sqrt{\frac{L_{l,p}}{C_p}}$$

where

$$\sqrt{\frac{L_{l,p}}{C_p}}$$

is the surge impedance of the transformer. In these equations

i = instantaneous value of the current at the moment of interruption
$L_{l,p}$ = leakage inductance referred to primary
C_p = distributed capacitance of primary winding

Inrush Current

When the primary contactor is closed the initial inrush of the transformer magnetizing current may attain a momentary peak value up to 25 times rated full-load peak current. The inrush current is very highly damped and declines to one-tenth of its initial value in a few cycles. The peak value of the inrush current is a function of the value of the residual magnetization of the transformer core, the normal operating peak flux density and the air-core inductance of the primary coil. In addition it depends upon the instantaneous value of the line voltage at the instant at which the contactor closes and also upon the impedance of the supply line.[3] The high electromagnetic forces resulting from the peak inrush current may force the contacts apart. In this case a sudden interruption of the alternating current may then result with the effects described under "Alternating - Current Interruption." High voltages may be induced not only in the a-c windings of the transformer but also in the d-c windings. Fig. 3 shows transient voltages induced in the output of a 12-kv full-wave rectifier due to transformer inrush current.

Retarded Firing of Rectifier Due to Grid Control

In full wave and multiphase rectifier circuits, each tube fires in turn as its anode voltage becomes more positive than that of the preceding tube. The current flow is transferred from one phase to the other at this time. The rates of decay and rise of current in each phase are controlled by the commutating reactance of the transformer. During this period both the rectifier tube which has been carrying current and the one that is beginning are conducting current simultaneously, consequently the transformer windings are short-circuited. This means that the ends of the windings are held at some voltage between the normal induced values. At the end of commutation this short circuit is removed and the winding-terminal voltages then suddenly assume their proper values. The rate at which the winding that has ceased to carry current assumes its normal voltage is determined by the

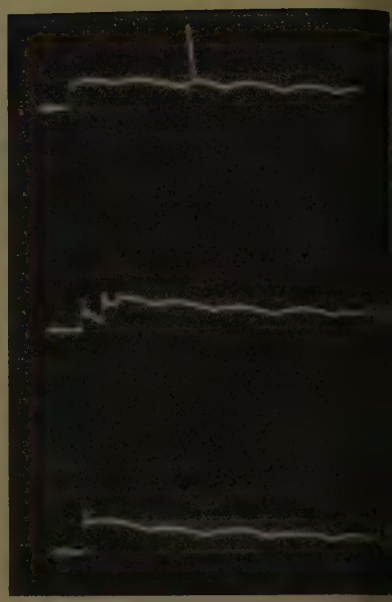

Fig. 3. Transients in rectifier output volta due to transformer inrush current. Verti scale, 12 kv per division

leakage inductance and distributed ca pacitance of that winding. If the l circuit formed by this winding has relatively high Q the voltage will ov shoot by a value that nearly equals t difference voltage that existed at t instant current ceased to flow. In ma rectifier applications grid-control tub are used to reduce the output volta As the firing angle of such a tube retarded these voltage differences beco increased in magnitude. The volta transients repeat each cycle and, the fore, produce a continual overstressing the transformer winding, or may ev cause arc backs in the rectifier tubes.

Effect of Transformer Reactance on Transient Conditions

The leakage reactance of the tra former windings is the main factor co trolling the magnitude of fault curre due to a short circuit within the d-c circ or due to a rectifier-tube arc back. Th fault currents, if allowed to exceed reas able values, will destroy the tubes a also cause damage to the transfor windings themselves as a result of sev overheating and particularly as a res of the enormous electromagnetic for acting upon the windings.

From this point of view the leaka reactance should be high, preferab about 10%. Such a high value of actance, however, would result in p regulation and from this point of vie undesirable.

Likewise, high reactance is undesira since it increases the peak voltages

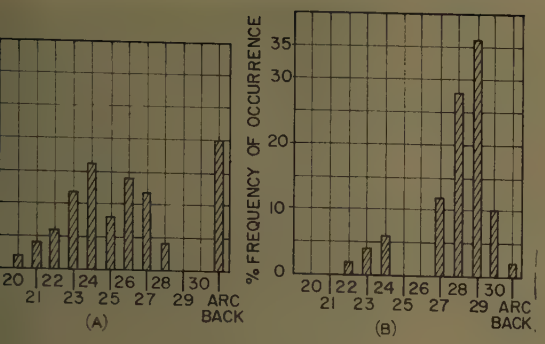

Fig. 4. Transformer terminal-to-ground voltages due to interruption of 3.5 amperes d-c in output of 12-kv 6-phase double-way rectifier. Peak kv induced in one phase

A—Transformer impedance, 3.1%

B—Transformer impedance, 4%

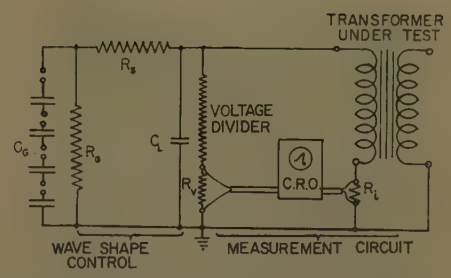

Fig. 6. Diagram of Marx circuit-impulse-test set

d at the secondary terminals as a t of current interruption in the d-c it or at the primary terminals due urrent interruption at the primary actors. The secondary overvoltages ar at the anode as excessive reverse ges and may produce an arc back of ectifier tubes.

vacuum switch was inserted in series the load supplied by a 6-phase le-way rectifier. This vacuum switch opened a large number of times and peak induced voltage between one e secondary transformer terminals ground was recorded. Fig. 4 shows relative number of occurrences of us values of peak voltages for two ent values of transformer reactance. higher value of reactance was ob- d by means of air-core inductance inserted in the primary leads of the former. The number of arc backs, ing in opening of the primary t breaker, is also recorded for each Overvoltages undoubtedly occurred time the vacuum switch was d but they did not always occur phase to which the oscilloscope was cted. From visual observation, it bvious that incipient arc backs oc- d with virtually every operation of acuum switch. The fact that com- flashover resulting in opening of imary circuit breaker occurred less ntly with the higher reactance, in of the greater frequency of higher oltages, may be attributed to the value of fault current.

selected value of transformer re- e must, therefore, be a compromise en the requirements of low regulation and limitation of fault current. The type of circuit used and the type of operation also should be considered. In applications where frequent switching with primary contactors is contemplated, the use of primary inductance coils for controlling the over-all value of transformer reactance should be considered, as these coils help to limit the peak values of primary inrush current.

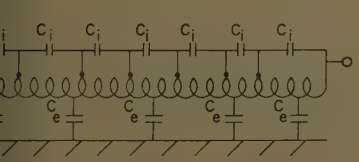

Fig. 5. Winding capacitances

C_i = internal distributed capacitance
C_e = external distributed capacitance

Impulse Waves and Voltage Distribution Within the Transformer Windings

Winding Capacitance

A transformer winding, in addition to inductance, also possesses capacitance. Fig. 5 shows a simplified representation of the winding capacitances. While they are shown here as lumped values, in actual fact they are, of course, composed of an infinite number of individual capacitances from each turn to ground (the external distributed capacitance) and from each turn to every other turn (the internal distributed capacitance). In a winding devoid of capacitance, voltage transients travel through the winding due to the inductive coupling between turns, resulting in uniform voltage distribution throughout the winding. In actual fact, such voltage transients travel through the winding at a speed dependent upon the relative values of the various capacitances. In addition, because of inductance, the waveshape of the transient is modified as it travels through the winding and oscillation will occur.[5,6] Thus it is not sufficient to know only the magnitude of the voltage transients that may occur in a given rectifier circuit in order to design a satisfactory transformer. It is also necessary to know in what way these transients will be distributed through the winding, that is, to what maximum value of voltage each individual piece of insulation (turn insulation, layer insulation, section insulation) might be subjected during these voltage transients. Both the steepness of the wavefront and the physical winding configuration affect this voltage distribution.

Impulse Testing

In the past 40 years, considerable theoretical and experimental work has been done to determine the effect of winding configuration and design upon voltage distribution. In this field of engineering the predominant cause of concern has been the abnormal voltage transients arising when lightning strikes the transmission line to which the transformer is connected. It has been determined that an impulse wave which rises to peak value in $1^1/_2$ μsecs and decays to half value in 40 μsecs is representative of the most severe lightning-surge conditions that may arise in service. This type of transient can be duplicated in the laboratory by means of the Marx circuit-impulse generator shown schematically in Fig. 6.

The operation of this circuit is briefly as follows:

The capacitors C_G are charged from a rectifier to the desired value while connected in parallel. They are then switched in series and discharged into the circuit. The voltage across the load (the transformer winding being tested) rises until the potentials across C_G and C_L are equal. This portion of the impulse is the wavefront. The steepness of the wavefront is controlled by the series resistance R_S. C_G and C_L are now in parallel and discharge through the load resistance and R_G. The rate of decay (the wavetail) is varied by adjusting R_G. Since the constants of the transformer winding also affect the impulse waveshape R_S and R_G must be adjusted for each new transformer design.

To determine the required values of R_S and R_G, a transient analyzer is used. This is a scale model of the Marx circuit in which low-voltage pulses are repeated at a 60-cycle rate. This equipment is also used to determine the voltage distribution within the transformer windings. For this latter purpose special coils need to be built with a large number of taps brought out from various parts of the winding.

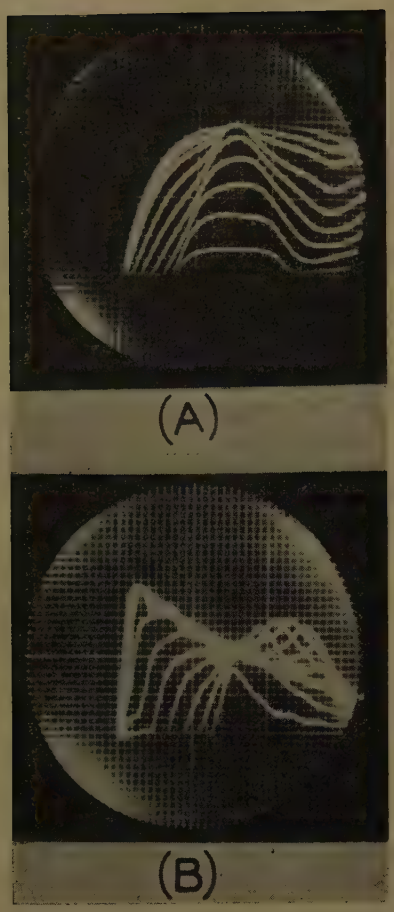

Fig. 7. Time-voltage relationships in coil

A—10x100-μsec wave impressed at terminal. Horizontal scale 1 μsec per division
B—0.6x10-μsec wave impressed at terminal. Horizontal scale 0.5 μsec per division

It has been considered that the same approach used in power transformers also be used for determining the adequacy of design of rectifier transformers. In power transformers a basic impulse insulation level (BIL) is used to determine the adequacy of the design and insulation system. Thus a transformer with a BIL of 90 kv has been tested and shown to be capable of withstanding the standard $1\frac{1}{2} \times 40$-μsec inpulse waves of a crest value of 90 kv. However, cases have occurred where rectifier transformers with d-c windings of 50-kv BIL and even 90-kv BIL have failed in rectifier circuits with a 12-kv direct-

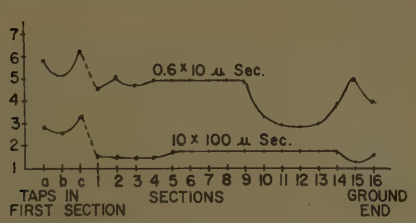

Fig. 8. Distribution of K factor within winding. As shown by taps in first section, stresses within each section may be higher than indicated

voltage output. This approach by itself is therefore demonstrated to be inadequate.

Effect of Waveshape on Voltage Distribution

The steepness of the wavefront has considerable effect upon the voltage distribution within a coil. If we assume a constant applied voltage and a constant velocity of travel of voltage through the coil due to the combined capacitive and inductive coupling between portions of the winding, the faster the rate of rise in potential at a given point and the greater will be the ratio that exists between this rate of rise and the rate of propagation. Thus, the steeper the voltage wavefront, the higher the instantaneous potential difference that arises between two portions of the winding. Figs. 7(A) and (B) illustrate this point dramatically. In these oscillograms the potentials to ground at a number of taps within a pie-wound coil due to an impulse wave impressed on one end of the winding are superimposed. In Fig. 7(A) the shape of the impulse wave is 10×100 μsecs, in Fig. 7(B) it is 0.6×10 μsecs. In each case the crest voltage is identical. The instantaneous potential existing between any two taps can be obtained by subtracting the corresponding instantaneous values from one another. An arithmetical representation of the nonuniformity of voltage may be obtained by calculating the voltage distribution factor

$$K = \frac{\text{Instantaneous volts between taps as per cent of impressed crest value}}{\text{Turns between taps as per cent of total winding}}$$

for the condition of maximum instantaneous potential appearing between any two taps. (In a low-frequency induced test $K = 1$.)

Values of K are plotted in Fig. 8 for two different impulse waves impressed on the same pie-wound coil. From this graph it is obvious that a coil of this design might pass a test in which the impressed impulse wave has a slow front, but would fail when tested with an inpulse wave of a much steeper wavefront, as portions of the insulation are so much more severely stressed by the latter test.

Winding-Voltage Stresses in a Rectifier Circuit

Induced Voltages in the Transformer Windings

Voltage transients due to sudden changes of current are induced within the

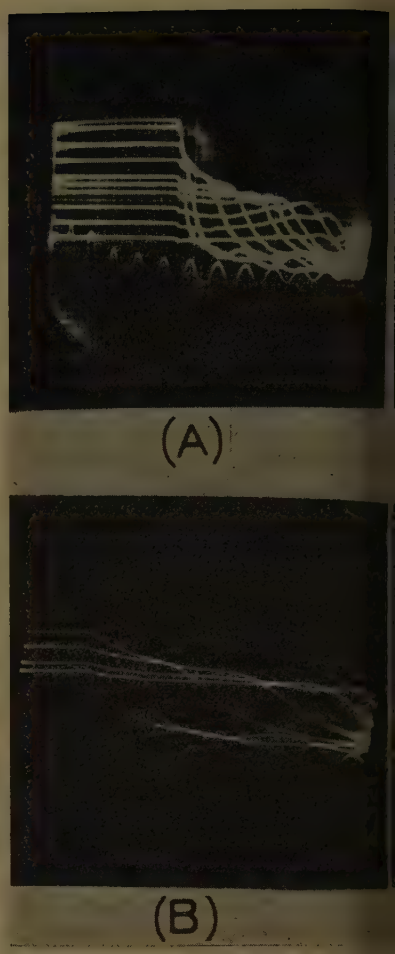

Fig. 9. Time-voltage relationships with winding during arc back

A—Horizontal scale 0.3 μsec per divisi
B—Horizontal scale 0.1 μsec per divisi

windings of the transformer (or inductor in accordance with the equation

$$e = -L_{l,s}\frac{di}{dt}$$

Due to capacitive effects oscillatio may arise of frequency

$$f = \frac{1}{2\pi\sqrt{L_{l,s}C_s}}$$

where

$L_{l,s}$ = leakage inductance referred to s ondary
C_s = distributed capacitance of seconda winding

The values of $L_{l,s}$ and C_s are such th these transients are relatively slow, w rates of rise from zero to crest of t order of at least 50 μsecs. Therefo these transients are relatively even distributed throughout the windin that is, $K \approx 1$.

The design of the transformer to wi stand these induced-voltage transie is a relatively simple matter provided maximum possible value of the indu

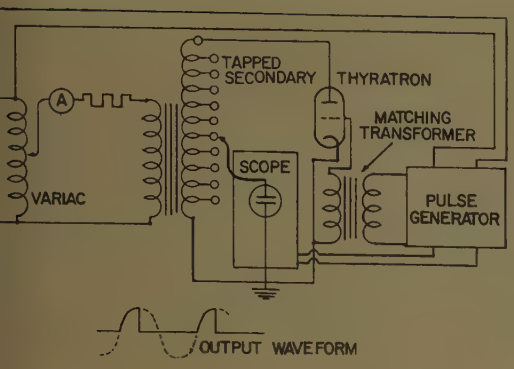

Fig. 10 (left). Circuit used to simulate arc back

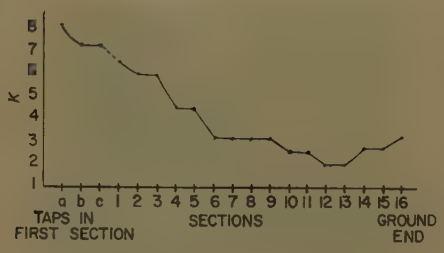

Fig. 11 (right). Distribution of K factor in 16-section coil during arc back

age can be predicted. For some es of interrupted direct current, -induced voltages at taps within coil are also shown in Fig. 2. Since voltage distribution is essentially orm the voltage stresses turn-to-turn, r-to-layer and between sections can alculated and the required insulation vided. Voltage stresses between layers best reduced by splitting the coil into rge number of sections or "pies," thus viding a large number of layers each a small number of turns. The lation, or spacing between sections, t be sufficient to withstand the voltage lients between them.

tage Stresses Due to Arc Back

hen the tube arcs back, the anode ntial suddenly becomes equal to the ode potential (neglecting tube drop). potential existing across the coil wise collapses. The rate of voltage pse at the secondary line terminal be of the order 0.1 to 0.2 μsec. n the point of view of voltage distri- on within the coil this is equivalent mpressing upon the coil an impulse e of 0.1- to 0.2-μsec front and a very tail.

gs. 9(A) and (B) show the change of ntial at a secondary terminal and ne various taps of a coil under simu- l arc-back conditions. Fig. 9(B) is tical to 9(A) except that the sweep is increased to emphasize the po- ial differences existing at the line of the coil. The induced voltages ach of the taps appear as straight because of the speed of sweep com- d to the 60-cycle induced voltage. coil is the same as that used to obtain 7. The diagram of connections his test is shown in Fig. 10. Briefly, nethod used is as follows: The trans- er primary is excited continuously a 60-cycle source. The thyratron iggered to fire at the peak of the ced voltage in the transformer sec- ry. The sweep of the oscilloscope is ted slightly earlier. A resistance e primary circuit is used to limit the short-circuit current. By means of this test circuit the arc back of a tube in a 3-phase single-way Y circuit may be duplicated.

It will be seen from Fig. 9(A) that the steepness of the wavefront is quite rapidly attenuated, but because of the low internal distributed capacitance of the pie-wound winding, several μsecs elapse before the voltage collapses in the last of the pies. The maximum voltage appearing across the first section is equal to about 36% of the total peak induced voltage across the whole coil. Fig. 11 shows the K values for this test which may be compared with Fig. 8.

In a 6-phase double-way circuit two tubes carry load current in series when operating normally. When an arc back occurs, arc-back current from the transformer must flow through the tube of the other phase which is normally conducting, thus the collapse of voltage occurs across two terminal-to-neutral phases in series. To simulate this condition a 3-phase circuit similar to that of Fig. 10 was set up. In this case the thyratron was connected between the two line terminals of two phases. The voltage-versus-time relationships at the taps is shown in Fig. 12. Voltages for all of the taps are not shown. However, inspection reveals that the voltage distribution within the coil which is connected to the anode of the arcing tube is much the same as in the previous case. The other phase is protected by the first phase since the steepness of wavefront (voltage collapse) has been considerably reduced by the time the neutral point is reached.

From the point of view of internal voltage stresses within the coil, it is seen that the most serious condition occurs during tube arc back. In turn, arc back is most likely to occur when an inverse voltage in excess of its rating is impressed upon the tube such as by an excessively high voltage being induced at the transformer terminals due to a sudden change of direct current or some other cause. Then, if the normally conducting tube, which must then carry a heavy short-circuit current, should suddenly cease to conduct, further and still higher voltages may be induced in the transformer coils and cause even greater damage to their insulation system. During the tests that were run to obtain the data of Fig. 4, simultaneous arc backs on as many as three tubes were observed.

Maximum Expected Voltages

The peak value of the terminal voltage induced in a coil has been shown to be a function of the rate of change of current and also the inductance and surge impedance of the windings. If all these factors are known the peak induced voltage can be calculated. In the higher power rectifiers the calculated values can easily reach 100 kv or more under the worst predictable conditions. At such high voltages some circuit component invariably breaks down or at least a flashover occurs at insulators or exposed terminals. Also, if the peak voltage is not limited by some device such as nonlinear resistors, lightning arresters, spark gaps, or capacitor-resistance networks, such induced voltages will generally exceed the inverse-voltage rating of the tube and cause an arc back. Therefore, in the absence of any other voltage-limiting devices, the actual arc-back voltage of the tube is the maximum peak voltage which must be considered in transformer design.

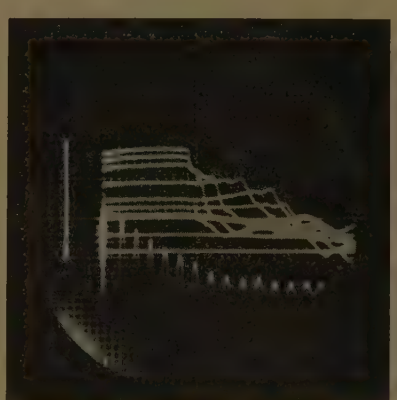

Fig. 12. Time-voltage relationships with arc back across two phases. Horizontal scale, 0.5 μsec per division

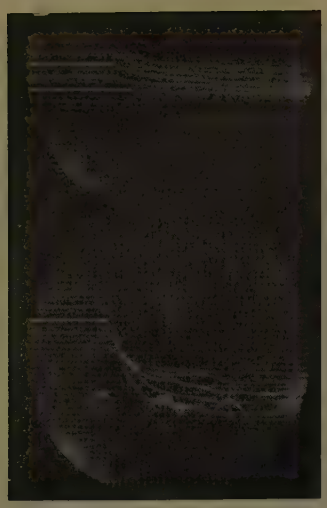

Fig. 13. Time-voltage relationships in 2-section coil during arc back. Turns spaced in first layer. Horizontal scale, 0.1 μsec per division

Unfortunately, tubes themselves are quite erratic and cannot be depended upon to arc back at any specific voltage level since this depends upon the age of the tube, the load current, and the temperature of the tube. In general, however, most high-voltage rectifier tubes should be expected to arc back at a voltage which does not exceed about twice their inverse-voltage rating. Transformer coils designed to handle induced voltages with a peak value equal to twice the inverse-voltage rating of the tube and to successfully survive the internal voltage stresses (and also mechanical stresses) resulting from arc back at such a voltage level should certainly outlast several sets of tubes.

Preventative Measures

Coil Design

The coils must be designed to withstand the previously discussed voltage stresses. Their capability to do so will be much enhanced if the extremely uneven voltage distribution shown to exist, for example, in the pie-wound coil with a large number of sections, can be improved.

The initial voltage distribution is a function of

$$\alpha = \sqrt{\frac{C_e}{C_i}}$$

where

C_e = external distributed capacitance
C_i = internal distributed capacitance. See Fig. 5

The lower the value of α, the more the voltage distribution within the coil approaches uniformity for any given waveshape. When $\alpha \approx 0$ the voltage gradient across the whole winding is essentially uniform, or $K \approx 1$ in all parts of with winding.[5,6]

From this it is seen that the internal distributed capacitance should be large compared with the external distributed capacitance. This condition is approached in a simple layer-wound coil. Fig. 13 shows the relative voltage distribution in a coil wound in two sections. This coil has the same physical dimensions and exactly the same number of turns as the 16-section coil used to obtain Figs. 8 and 11. In this case taps were brought out at the ends of the layers. Comparison between the figures reveals that the voltage distribution is, as expected, much more uniform. Fig. 14 shows the values of K throughout the winding.

However, this type of winding is not necessarily the best suited to withstand rectifier transients. Although the voltage distribution of the 2-section type is much more uniform for a given coil geometry, the actual layer-to-layer voltage stresses are higher, both under the induced condition and the arc-back condition, than in the multisection coil. An optimum design is obtained by adjusting the total number of sections so as to provide a reasonable compromise between transient-voltage distribution and normal interlayer voltage stresses.

Another approach to the voltage distribution problem is to use electrostatic shielding. External shields connected to the terminal lead in effect neutralize the external distributed capacitance of the winding and thus reduce α. Theoretically, it is possible to design a series of such shields spaced in such a manner as to obtain uniform transient-voltage distribution, but it is not practical to do so in transformers of the size under consideration.

An approach directly opposite to that of electrostatic shielding is to space the first few turns of the winding adjacent to the terminal end. This in effect decreases the capacitance which results in increased voltage stresses between spaced turns. This develops into a race between added insulation and increased voltage stresses. However, this method does provide some benefits as it reduced the steepness of the wavefront applied to other parts of the coil. This effect is seen in Fig. 14 in which the turns in the first layer were spaced apart.

Protective Devices

Since the severest voltage stresses in the coils are encountered as a result of arc back, the likelihood of this phenomenon occurring should be reduced. If induced voltages can be prevented from exceeding the rated inverse voltage rating of the tube, the probability of an arc back occurring can be substantially reduced. This improvement is also desirable from the point of view of tube life, and over-all performance of the circuit.

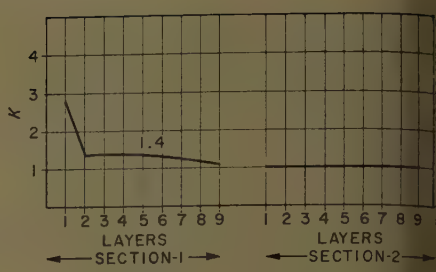

Fig. 14. Distribution of K factor in 2-section coil during arc back. Turns spaced in first layer

Spark gaps set to flashover at a predetermined value will achieve this if series resistors of proper values are used to limit the current in the arc. Such spark gaps should be sealed to prevent tampering and to reduce variations due to atmospheric conditions and surface contamination.

Nonlinear resistors such as Thyrite* are very effective in limiting overvoltage. However, in higher voltage circuits the number of such nonlinear resistors that need to be used in series becomes prohibitive in cost and space requirements.

In the higher voltage circuits, a combination of nonlinear resistors and sealed sparkgaps offer a satisfactory solution at reasonable cost. Such combinations are available in the form of standard lightning arresters used to protect distribution transformers from lightning and switching surges, for example Magnevalve* arresters.

For the higher voltage rectifiers *R-C* networks also offer a solution. However, they should be individually designed for each application and circuit to obtain the desired characteristics.

All such protective devices should be connected across each winding of the transformer with leads which are as short as possible. In delta-connected transformers and even Y-connected transformers feeding 6-phase double-way rectifiers, neither end of the transformer winding is grounded. This requires some modification of the mounting of standard lightning arresters since they are designed for normal operation with the lower terminal grounded.

* Registered trade-mark of the General Electric Company.

ting

resent standard test procedures pro- for adequate testing of major insula- between windings and winding-to- und. However, none of the existing dard test procedures for rectifier sformers provide for an adequate ing of the direct current windings to stand the kind of voltage transients ussed in this paper. Standard in- ed-voltage procedures provide for ing at twice normal rated voltage. ess protective devices are provided will definitely limit induced voltages uch a value, it is evident from the eding discussion that this value is h too low. Furthermore, a 400- e induced test gives no indication ne ability of the winding to withstand p-front or high-frequency transients ven this low a value.

he authors propose that an adequate procedure should consist of inducing direct current winding to a peak ue equal to two times the rated-peak rse-voltage rating of the tubes to be l in the circuit (the purchaser would ify this value in each case). In the t that protective equipment is to be vided, the peak value of the induced- age test could be reduced to a value al to 120% of the overvoltage cut- oint of the protective device.

rc backs at this voltage level would be ulated by a circuit similar to that vn in Fig. 10 except that cascaded rogen Thyratrons would replace the shown. The Thyratrons would be gered to fire at the peak of the induced age wave at least once every second. induced voltage test would need to t a frequency of 400 cycles per second and should be continued for 10 seconds. Failure of the windings might be detected by observing the input current on the primary side of the transformer.

An alternative method might consist of an induced test of the same value as described before, followed by a chopped-wave impulse test of crest value equal to 110% of the peak of the induced voltage, followed by a further induced-voltage test. The impulse wave would be impressed on the high-voltage (direct-current) windings of the rectifier transformer.

Conclusions

This paper has attempted to bring into proper perspective the relationship between the transformer design and the other elements of a power-rectifier circuit in which mercury-vapor-filled tubes are used as the rectifying element. To obtain satisfactory over-all performance, co-ordination is required between the manufacturer of the rectifier tubes, the transformer, and of the ultimate equipment. It is believed that many of the difficulties that arise from time to time could be avoided if the designers of each of these components and systems were better acquainted with the characteristics and requirements of each other's devices.

All too frequently, specifications for a rectifier transformer spell out nothing more than the input and output voltages and the output current ratings. From this meager information, the transformer designer is expected to design a satisfactory transformer. However, transformers of identical designs sometimes perform satisfactorily in one application but give trouble in another.

No rigorous mathematical solutions have been provided in this paper. The data given are based on actual tests and should be considered only as reference points indicating the order of magnitude of some of the phenomena that may be encountered. Many of the references go into much greater detail of particular aspects of the problem. The authors feel that much more work needs to be done in this area and specific data should be gathered, both in the field and in the laboratory, to assist the designers both of the transformers and over-all power-rectifier circuits in obtaining optimum designs.

Finally, specific test methods and values need to be established in order to give the transformer designer a specification value to use for design purposes and a method of checking the product. This will also assure the equipment manufacturer that he is obtaining the required quality. It is hoped that the procedures and values suggested here may serve as a useful starting point for the establishment of such standards.

References

1. Industrial Electronics Reference Book (book). John Wiley & Sons, Inc., New York, N. Y., 1948, p. 52 ff.

2. Rectifier Fault Currents—II, **C. C. Herskind, A. Schmidt, Jr., C. E. Rettig.** *AIEE Transactions*, vol. 68, pt. I, 1949, pp. 243–52.

3. Electronic Transformers and Circuits (book), **Reuben Lee.** John Wiley & Sons, Inc., 1947, p. 100.

4. Voltage Impulses in Rectifiers, **T. Douma.** *Philips Technical Review*, Eindhoven, Netherlands, vol 9, no. 5, 1945, pp. 135–146.

5. The Insulation of Electrical Equipment (book), **Willis Jackson.** John Wiley & Sons, Inc., 1954, pp. 259–77.

6. Transformer Engineering (book), **L. F. Blume, A. Boyajian.** John Wiley & Sons, Inc., pp. 463–81.

Discussion

ben Lee (Westinghouse Electric Corpo- n, Baltimore, Md.): The authors have ned several of the transient-voltage itions in rectifier transformers, some of rather exhaustively. With most of nformation in this paper those familiar high-voltage rectifier design will agree. w points appear to deserve further tion.

Arc back is treated as an abnormal con- n "likely to occur when an inverse ge in excess of its rating is impressed the tube." It is further stated that nduced voltage can be prevented from ding the rated inverse voltage of the the probability of an arc back can be antially reduced."

evention of arc backs is part of rectifier n and the inverse-voltage rating of the should take into account the possibility of arc back in gas-filled rectifiers. Similarly, the transformer should be so insulated that it will be the least likely circuit element to fail in the event of arc back or any voltage transient.

2. For "transformer coils designed to handle induced voltages with a peak value equal to twice the inverse-voltage rating of the tube," an induced voltage of twice normal value is recommended. But the basis for this part of the recommended test procedure is uncertain. Under average service conditions it may be adequate if backed up by some sort of short-duration test, but there may be applications such as laboratory rectifiers where this induced voltage would be unduly severe. It would be interesting to know why a general twice-normal induced voltage test is proposed.

3. The example given concerning BIL seems hardly to demonstrate the inadequacy of BIL for rectifier transformers. For 12-kv direct-voltage output, 15-kv insulation class would be used by experienced designers. In an oil-immersed transformer below 500 kva the American Standard Power Transformer Standard[1] specifies 110-kv chopped wave or 95-kv full-wave impulse test. If the transformer in question had been designed according to this standard it might not have failed.

4. Before adopting the test similar to Fig. 10, in which the surge has shorter duration than standard impulse tests, additional testing would be necessary to correlate results with known levels of insulation. Furthermore, the thyratron simulates gas-filled rectifier operation, and would not apply to high-vacuum and solid-state rectifiers. For these latter types, either the present standard BILs should be used or still other standards formulated.

Reference

1. Transformers, Regulators, and Reactors. *American Standard C57.12*, American Standards Association, New York, N. Y., 1958.

Andrew A. Halacsy (Federal Pacific Electric Company, Newark, N. J.): For better clarity I recommend the use of e_p and e_s in the equations giving the value of the induced voltage. In the usual manner, the authors stressed that the capacitance of the winding has to be considered as distributed among the parts of the winding. It would be interesting to investigate the effect of the nonuniform distribution of the leakage inductance, which is the case when the spacing of the turns within the same coil is not uniform or when the position of some primary turns relative to the secondary coil differs from that of other turns, such as those at the ends and in the axial middle of a coil.

The circuit shown in Fig. 10 is recommended to simulate an arc back. It does so except the direction of the reversed current. This is clear when Figs. 1 and 10 are compared. A reversed current, of course, will create the same voltage transient but of reversed polarity. Breakdown of insulation depends on the polarity of such steep voltage waves. To restore the simulated conditions a reversal of the connections of the secondary coil is required.

In the paragraph under "Inrush Current" it is stated that "the peak inrush current may force the contacts apart." How often was this fault of the circuit breaker observed and in what kind of breaker?

B. C. Biega and **H. W. Lord:** Mr. Lee in his first point emphasizes once more the importance of proper co-ordination between the design of the transformer, the tubes, and the over-all equipment.

The induced-voltage test of peak value equal to twice rated inverse voltage of the tube is recommended on the premise that, if no other voltage-limiting devices are included in the circuit, induced voltages of this magnitude are likely to occur before the tube arcs back. Induced voltages of such magnitude may be caused by any of the circumstances described in the paper.

The 50-kv BIL referred to in the paper is that recommended by American Standard for dry-type transformers of the 15-kv insulation class. But a 95-kv or even 110-kv standard-impulse test does not guarantee that a transformer will stand up under arc-back conditions in rectifier service where the wavefront is so much more severe.

With regard to item 4 of Mr. Lee's discussion, the proposed test procedures are intended for transformers working with mercury-vapor rectifier tubes. It is agreed that much more work needs to be done.

Dr. Halacsy's point on polarity is correct, but in this particular case relative potential with respect to the ground plane is of lesser importance than the internal momentary voltage distribution within the coil.

The forcing apart of contacts by the peak inrush current has not been physically observed. However, the transient voltages observed can hardly be explained if this is not assumed. This occurred with standard contactors used for control of a particular circuit in which the transients shown in Fig. 3 were observed.

Significance of Heat Pump Coefficient of Performance

CONSTANTINE W. BARY
FELLOW AIEE

Synopsis: This paper deals with the load aspects and economic aspects of three types of residential heat pump systems which employ supplementary heat sources. It contains illustrations of their load characteristics over a wide range of annual COP (coefficient of performance), depicts relationships of the relative costs to serve these loads from long-range and short-range considerations, and provides, as a reference, load characteristics and economic data for three comparable types of resistance heating systems with their complementary electrical cooling loads, and a band of competitive operating costs to customers using gas for heating and cooling.

THE COP of a refrigerating system is defined as the ratio of the heat absorbed at low temperature to the heat equivalent of work done. For an electric heat pump, operating on the heating cycle, it may be stated as the ratio of the total useful heat output (heat absorbed at low temperature plus the heat equivalent of work done) to the equivalent heat of electric energy input. The COP's general thermodynamic principles are well known and its theoretical and practical aspects have been covered in the technical literature.[1] Throughout this paper, and to simplify the presentation, the abbreviation COP will be used for this ratio as applying to conditions of an electric heat pump on its heating cycle, including its auxiliaries, but excluding supplementary heat sources, such as resistors or heat storage means. When prefaced by the word "annual" the term means the integrated results over a period of one year.

Over the past 10 years, the application of the heat pump to provide year-round comfort in the home has grown gradually in the United States. Much has been written on the subject including a number of papers by the author on its significance as a residential electric load, and the economic aspects thereof.[1-4] But continued research, in the light of almost universal practice among manufacturers of providing relatively large amounts of supplementary resistance heating in conjunction with air-source heat pumps, has revealed some new load and economic aspects which are believed to be of vital significance in the economics of supplying electricity to this device. These must be fully realized by all concerned if the electrical heat pump is to take its economic place as a mass-market device in providing comfort through the heating and cooling of homes, and thus fulfill the aspirations of many thoughtful men in electric utility industry for all-electric home living.

The object of this paper is to set forth the results of research on the load aspects and economic aspects of several residential heat pump systems which employ supplementary heat sources; and to show a relative comparison of the economics of the utility's cost of service supply over a wide range of annual COP. (Comparison of first cost of equipment and its maintenance expense are not included because they represent different facets of the problem and do not affect the features related in this paper.)

All data used in the paper reflect either the results of actual experience, or the careful research which the author, his colleagues,

Paper 59-20, recommended by the AIEE Domestic and Commercial Applications Committee and approved by the AIEE Technical Operations Department for presentation at the AIEE Winter General Meeting, New York, N. Y., February 1–6, 1959. Manuscript submitted September 18, 1958; made available for printing November 13, 1958.

CONSTANTINE W. BARY is with the Philadelphia Electric Company, Philadelphia, Pa.

The author acknowledges the valuable assistance and suggestions of A. Abramovitz, W. C. Astley, and J. A. Thielman, all of the Philadelphia Electric Company.

and others in the industry have conducted over many years. They reflect the fundamental concepts and well-tested techniques which have been established and used in studying the behavior of electric loads, and the costs involved in serving them.[5-7] Actual experience has proved them to be reliable guides in determining the economics of the service rendered by systems with which the author is familiar. Although the basic data used herein apply to conditions of a large metropolitan system operating in the northeastern part of the United States, and the results obtained for that particular system will undoubtedly differ in detail from those that may be derived for other systems, nevertheless, it is believed that the general character of the results contained herein is of fundamental nature and should be useful to others.

Load Characteristics

The load characteristics used in this paper have been derived painstakingly, as previously described[4] for the same size house of 55,000-Btu-per-hour heat loss as that described in reference 4, and for the same significant features of climatological characteristics. These load characteristics data are summarized in Table I for three types of heat pump systems, and for three types of resistance heating systems with their complementary electric cooling loads. Each type of heat pump employs air as a heat source or heat sink, and each is sized at 60% of design heating requirements, which is ample to meet the design cooling requirements of the climatological conditions of the area. Types *A* and *B* employ resistors as supplementary heat sources to satisfy the peak heating requirements, and type *C* employs a heat storage system for that purpose.[8] Resistors of type *A* are sized for, and the system operates under, the conventional night set-back of indoor thermostats with quick heat recovery in the morning, as now commonly practiced in homes with existing fuel-fired systems. The resistors of type *B* are sized for, and the system operates under, a fixed setting of the indoor thermostat which, perhaps, residential customers could be induced to follow with a heat pump installation. Type *C* employs a heat storage system which embodies resistors for charging. These resistors are electrically interlocked with the heat pump so as to permit their operation only during the time when the heat pump is not operating.[3,9] For purposes of this study it is assumed that changes in the annual COP of the heat pump would be reflected in the same relative degree over the entire temperature range of heat pump operation.

To provide a reference point for the load characteristics of heat pumps, Table I also contains data on the load characteristics of three comparable types of resistance heating systems with their complementary electric cooling loads. Type *D* is sized for, and operates under, the conventional night set-back of indoor thermostat with a quick heat recovery in the morning; type *E* under fixed setting of thermostat. Type *F* is sized for 60% of the design heating requirements, as is the case with the type *C* heat pump, and it employs a heat storage system to satisfy the peak heating requirements. Such storage system embodies resistors for charging, which are interlocked with the main resistance heaters so as to permit their operation only during the time when the main heaters are not in use.

Three levels of diversified demands are shown for each of the types of installations: 1. the maximum, which determines the economics of long-range considerations, and which occurs in the morning on an average day of the coldest spell in the winter; and 2. two smaller values, which determine the economics of short-range considerations and occur either in the evening of such a day or in the evening of an average day of the warmest spell in the summer.

The following important features are revealed by these data:

1. The diversified annual load factors of types *A* and *B* systems, decrease with an improvement in the annual COP but, for type *C*, the annual load factor increases with such improvement.

2. The diversified annual load factors of systems which employ heat storage are much higher than those of other systems shown.

3. The magnitudes of maximum demands and energy use of all types of heat pump systems are substantially lower than those of comparable types of resistance systems; and the spread increases with an improvement in the annual COP.

4. The coldest-spell evening diversified demands of all types of heat pumps are at the level of the maximum diversified demand of the heat pump with supplementary heat storage (type *C*). The warmest-spell evening diversified demands of all types of heat pumps are all at the same level, and of a magnitude which is about 60% of the maximum diversified demand of type *C*.

5. Under present-day levels of annual COP, the energy use by supplementary resistors is relatively small, but its kilowatt demand is high. With increasing annual COP the significance of these quantities increases. Although the energy use by supplementary heat storage is larger than by supplementary resistors, contribution to the demand of the system is zero.

6. The coldest-spell evening diversified demands of resistance type systems are substantially higher than those of corresponding heat pump systems. But their warmest-spell evening diversified demands are generally in line with the demands of heat pump systems for annual COPs in the order of 3.

Long-Range Economic Considerations

It is a well-established principle in the economics of utility service that the use of the maximum diversified demand of a large-sized electric load application, such as house heating, determines the fundamental nature of the utility's cost to serve such load, independent of any temporary effects that may be created by, or on, the load characteristics of the class of service of which the load is a part. This principle reflects thus the economics of service supply under long-range considerations. Based on load characteristics shown in Table I, and employing the maximum diversified demands, it is possible to depict the trends in the utility's added annual cost to serve the load of each of the three types of heat pump systems, with improvement in their annual COP, and of each of the three types of resistance systems. These cost trends, computed from the full-cost-to-serve relationship shown in Fig. 1 and described in reference 4, are shown in Fig. 2(A) and (B). They are computed under the assumption that the 100% datum point in Fig. 1. is at a level of two cost units per kw-hr (kilowatt-hour), the basis for which was also described in reference 4.

Total Cost

Fig. 2(A) depicts the trends in total annual costs. For a better understanding of their significance it also provides a reference band of competitive operating costs to customers, which was computed for a home with the same heating requirements as stated in this paper, using gas for heating and cooling, including electricity for auxiliaries and water, all at existing rates in the area of the system described herein.

The following important features are revealed from such long-range considerations:

1. Improvement in the annual COP of heat pumps has a pronounced effect upon making the cost to serve the load of each of the types analyzed come closer to the competitive reference band. However, only the heat pump system with supplementary heat storage approaches this reference band in the region of annual COP of 3, and drops below that band beyond that region.

2. Heat pump systems employing supple-

Table I. Illustrative Characteristics of Electric Load of Heating and Cooling an Average-Size Home

		Heat Pump Annual COP for Heating	Annual Noncoincident Maximum Demand, Kw			Annual Diversified Demand, Kw			Annual Energy Use, Kw-Hr×10³			
			Total	Heat Pump Portion	Resistors Portion	Maximum 1	Winter, 6 P.M., EST* 1	Summer, 6 P.M., EDT† 2	Total	Heat Pump Portion	Supplementary Resistors Portion 3	Annual Diversified Load Factor, Per Cent
Heat Pump Systems												
A.	With supplementary resistors; night set-back of indoor thermostat	2	18.1	6.8	11.3	12.6	6.8	4.0	18.1	15.8	2.3	16.4
		3	15.8	4.5	11.3	10.4	4.6	2.7	12.8	10.5	2.3	14.0
		4	14.7	3.4	11.3	9.3	3.4	2.0	10.2	7.9	2.3	12.5
		5	14.0	2.7	11.3	8.7	2.7	1.6	8.6	6.3	2.3	11.3
B.	With supplementary resistors; fixed setting of indoor thermostat	2	12.0	6.0	6.0	8.2	6.8	4.0	17.7	16.3	1.4	24.6
		3	10.0	4.0	6.0	6.0	4.6	2.7	12.2	10.8	1.4	23.2
		4	9.0	3.0	6.0	4.9	3.4	2.0	9.5	8.1	1.4	22.1
		5	8.4	2.4	6.0	4.2	2.7	1.6	7.9	6.5	1.4	21.5
C.	With supplementary heat storage	2	8.0	8.0		6.8	6.8	4.0	18.7	15.3	3.4	31.4
		3	5.3	5.3		4.6	4.6	2.7	13.6	10.2	3.4	33.8
		4	4.0	4.0		3.4	3.4	2.0	11.0	7.7	3.4	37.3
		5	3.2	3.2		2.7	2.7	1.6	9.5	6.1	3.4	40.2
Resistance Heating System, Including Electric Cooling (4)												
D.	With night set-back of indoor thermostat		20.9			18.0	12.2	2.9	30.6			19.4
E.	With fixed setting of indoor thermostat		16.1			13.1	22.2	2.9	30.6			26.7
F.	With supplementary heat storage		9.8			9.8	9.8	2.9	30.6			35.6

* Eastern standard time. † Eastern daylight time.

1. Maximum diversified demands and diversified demands for winter conditions are for an average day of coldest spell.
2. Diversified demands for summer conditions are for an average day of warmest spell.
3. Includes energy use for defrosting.
4. Separate cooling system reflects a 20% better efficiency than present-day cooling equipment.

mentary resistors fall far short of meeting the reference band in the present-day range of annual COP. But the type with supplementary resistors and fixed setting of indoor thermostat, reaches it in the very high region of annual COP.

3. All three types of resistance systems fall far short of meeting the reference band.

4. In the region of annual COP of 3, the difference in the cost to serve the heat pump systems with supplementary heat storage and to serve those with supplementary resistors is in the order of 70×10^2 cost units with respect to type *B*, and 350×10^2 cost units with respect to type *A*. These differences represent 17% and 52% respectively of the annual cost to serve the loads of these two types of heat pump systems.

Cost Rate per Kw-Hr

Fig. 2(B) depicts the relationships of the cost-to-serve rates per kw-hr, with changing annual COP. The following important features will be noted.

1. Only the heat pump with supplementary heat storage provides an ever-declining cost-to-serve rate per kw-hr. Heat pumps with supplementary resistors reflect the reverse phenomenon: their cost-to-serve rates per kw-hr rise appreciably with an improvement in the annual COP.

2. The cost-to-serve rates per kw-hr of resistance systems are fixed. They lie in the range between $2^1/_2$ and 4 cost units. For the system with supplementary heat storage the cost rate approaches that of the heat pump with supplementary heat storage at an annual COP of 3.

These features in the cost-to-serve rates per kw-hr should be of extreme significance to utility managements in establishing pricing policies for the supply of these loads, not only in respect to the level but, more importantly, in respect to the proper form of rates. A simple energy rate per kw-hr, for example, now generally in use on electric utility systems in the United States for service supplied to residential customers, cannot adequately meet the conditions depicted in Fig. 2(B) not only as to various types of heating systems, but also as to probable future improvements in the annual COP. To illustrate, if the price per kw-hr of such a rate is set to satisfy, say, the type *A* system at a given annual COP, it would be far too high for the types *B* and *C* at the same annual COP, and too high for any of the resistance-type systems. On the other hand, if the price per kw-hr of such a rate is set to satisfy the requirements of type *C* system at a given annual COP, it would be too low to satisfy the requirements of types *A* and *B* at that COP, and too low to satisfy the requirements of resistance types *D* and *E* systems and even of type *F*, if the rate is set for a COP region beyond $3^1/_2$. Even more significant, if a simple energy type rate were set to satisfy, say, the requirements of either type *A* or *B*, under the now existing low levels of heat pump COP, it would become inadequate in the future for an improvement in their COP.

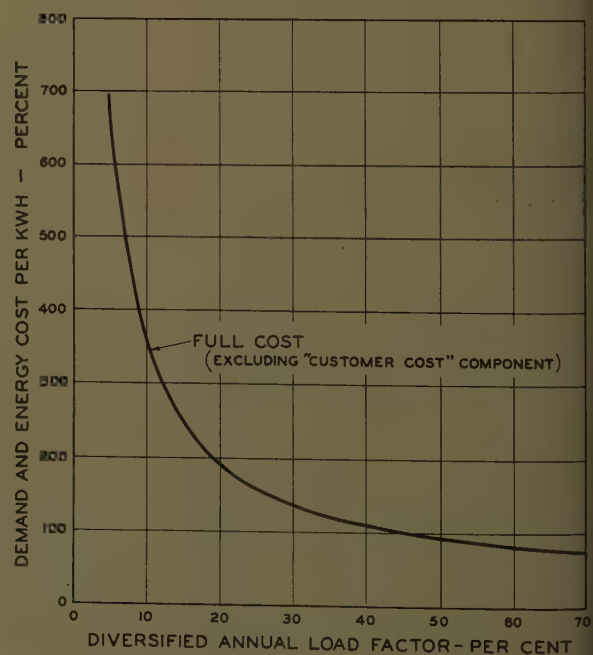

Fig. 1. Relation of demand and energy cost per kw-hr and annual diversified load factor, 100% full cost per kw-hr, at 45% annual load factor

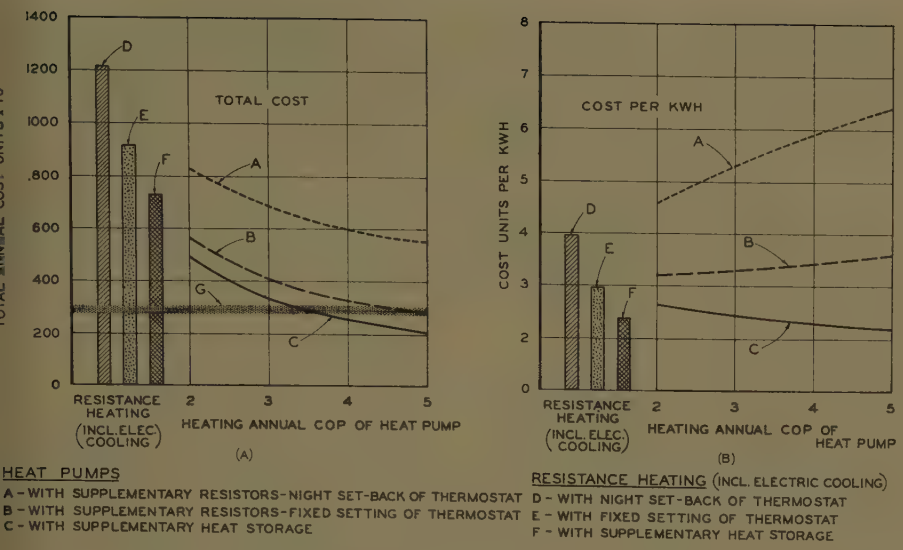

Fig. 2. Long-range considerations: trends in added annual cost to serve electricity for heating and cooling of average sized home, reflecting unlimited saturations

This is the only residential utilization device known to the author which would require an increase in the price per kw-hr with an improvement in its efficiency of performance.

Thus, it behooves those responsible for pricing policies of utility services to bear in mind these important and fundamental economic features of electric heating loads, and especially those of the heat pumps with supplementary resistors. As has been pointed out in reference 4, with the wide variation possible in the relative cost to serve various types of heat pump, resistance heating, cooling, and other loads in the residential field, together with the wide variety of operating conditions that may be encountered in the characteristics of these loads, adequate pricing for the all-electric home, equitable to various types of residential customers and to utilities, can be accomplished only through some form of "demand-energy" type of rates. It could be met reasonably well also through a form which would employ some kind of dual-dial metering of energy, or its equivalent, by applying a lower price for the kw-hr registered during certain specified hours of the day, as contrasted with a much higher price for either all, or the excess over a given base, of kw-hr registered during the remaining or peaking, hours of the day, as has been suggested in reference 10.

Short-Range Economic Considerations

Departing now from the fundamental, or long-range, considerations to those which are temporarily affected by the load characteristics of the residential class of service of which the loads of the heating systems are a part, the economic aspects of these loads, from short-range considerations, are found to differ from those which have been described for the long-range. This is due to two factors: first, as has been pointed out in reference 4, the total load of the residential class of customers, as it exists at any given time, contains peaks and valleys in relation to its morning and evening loads in the winter, and in relation to its seasonal peak patterns between summer and winter; and second, the load of heating systems with their complementary cooling possesses its own peaks and valleys and its own seasonal patterns. These characteristics of the heating and cooling loads thus can be fitted into the load patterns of the residential class. However, these favorable conditions exist only for relatively small saturation levels of these loads.[4] Thus, from such short-range considerations, the economic aspects fall into two categories: 1. those applying to conditions when the total load of the residential class peaks in the winter, and 2. those applying to conditions when that load peaks in the summer.

Since, for winter conditions, the present-day residential class peak occurs in the evening, while the maximum load of heating occurs in the morning,[11] the resulting load diversity permits the acquisition of a limited amount of the heating load at lower demand cost responsibility than applies to its morning peak. For summer peak conditions, the summer demand of a combination heating and cooling system on the average day of the warmest spell is lower than on the average day of the coldest spell in the winter.[11] The resulting load diversity here also permits the acquisition of a limited amount of this load at a lower demand cost responsibility than applies to its winter peak.

Fig. 3(A) and (B) depict the cost-to-serve relationships, under the aforementioned lower demand cost responsibilities, and show the limits of saturation which would be permissible under these short-range considerations. The cost curves were computed with the use of the load characteristics data shown in Table I and diversified demands applicable to the winter evening or to the summer evening conditions, as the case might be. In making these computations use was made

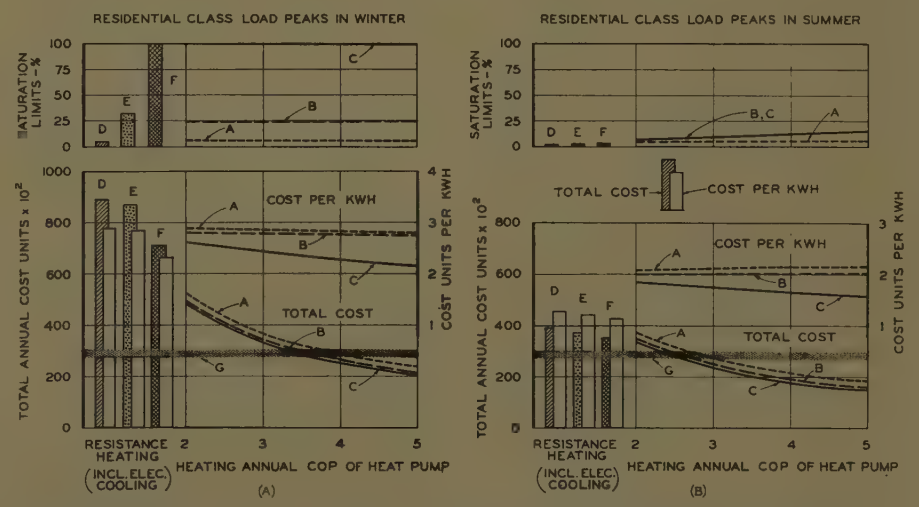

Fig. 3. Short-range considerations: trends in added annual cost to serve electricity for heating and cooling of average sized home and permissible limits of saturation

of the cost-to-serve relationship shown in Fig. 1 under the same assumptions as were used in preparing Figs. 2(A) and (B), except for the application of an additional cost factor to reflect adequately the customer demand component of the basic cost equation described in references 5 and 7. Under the lower diversified demands here employed, the cost relationship of Fig. 1 does not reflect fully this component of costs, since it is based on the maximum of such demands.

The curves for permissible saturations were developed from data of the residential class of service of the metropolitan electricity supply system previously described, for the foreseeable magnitude of margins available between the winter period evening peak and the morning load; and between the estimated summer and winter peaks a decade after the class peak were to shift to the summer period. Although different numerical results would be obtained for a set of different assumptions, those used herein are believed to be within practical possibilities. It must be noted, however, that the magnitudes of these margins do not remain fixed over a period of time because of the continuous ebb and flow in the use of electricity by customers and the constantly changing patterns of that use, as set forth in reference 12. Such margins may either increase or decrease as time goes on. Thus any computations made on the basis of foreseeable conditions possess elements of chance as to the probable future behavior of the load patterns of a whole class of customers, and therefore should be viewed in a broad sense as indicative of the relative significance in the permissible saturations of the various types of heating systems shown.

From Fig. 3(A), which depicts the economics of short-range considerations for the conditions when the load of the residential class peaks in the winter, it will be noted that:

1. For all three types of heat pump systems, the total annual cost-to-serve curves fall within a relatively narrow range, and approach the cost level of type *C*, as depicted in Fig. 2(A).

2. The cost per kw-hr curves of types *A* and *B* systems become fixed as contrasted with the increasing trends depicted for these types in Fig. 2(B). The downward trend of type *C* remains unaltered from that shown in Fig. 2(B).

3. The total annual costs to serve all three types of heat pump systems reach the competitive reference band around an annual COP of 3.

4. The total costs to serve the load of all types of resistance heating systems fall far short of the competitive reference band.

5. Except for types *C* and *F* systems, whose cost to serve are the same as in Fig. 2(A), and whose permissible saturations therefore are unlimited, for the other types, whose cost-to-serve levels have decreased from those shown in Fig. 2(A), their permissible limits of saturation become restricted to relatively low values.

From Fig. 3(B), which depicts the economics of short-range considerations for condition when the load of the residential class peaks in the summer, it will be noted that:

1. The total cost-to-serve level for all types of heat pump systems drops to about three quarters of the level depicted in Fig. 3(A) for the winter peak conditions. All of them reach the competitive reference band around annual COP of $2^1/_2$. But this is accompanied also by a restriction in the permissible limits of saturation for all systems, including type *C* whose permissible saturation was unrestricted under the winter peak conditions at the higher costs.

2. Similarly, the total cost-to-serve level for all types of resistance heating systems drops to one-half of the level depicted in Fig. 3(A), for the winter peak conditions. But even at this low level, neither of them reach the competitive reference band; and their permissible saturation limits decrease to insignificance.

Thus, from short-range considerations also, it behooves those responsible for pricing policies of utility services to realize that the lower costs to serve are feasible for electric heating systems only during the period while their load is filling valleys which exist in the hourly and seasonal patterns of the residential class load. Once these valleys are filled, additional load must bear the full and higher demand cost responsibilities. Higher saturations are permissible with heat pumps than with resistance systems, and higher saturations are permissible with heat pumps having supplementary heat storage than with supplementary resistors. Of the latter, the system using fixed thermostat setting permits higher saturation than the system with a night set-back. Therefore, while permitting temporarily lower utility rates, the short-range considerations require the same type of rate forms as were outlined herein for the long-range considerations, in order to provide incentives for discouraging the use of night set-backs of indoor thermostats and for encouraging the use of heat storage, and to provide means for an easier transition in the future to the ultimate conditions reflected by long-range considerations.

Conclusions

From the preceding analysis on the basis of long-range and short-range considerations it can be concluded that:

1. Of all the systems considered, the heat pump with supplementary heat storage provides the lowest cost-to-serve level, and at an annual COP of around 3 approaches the reference band of competitive operating costs.

2. Heat pump systems with supplementary resistors produce acceptable cost-to-serve levels at higher COP than 3, provided they are sized for, and operate under, a fixed setting of indoor thermostats. When employing night set-back of such thermostats their cost-to-serve levels become unacceptably high.

3. Improvements in the annual COP into the region of 3 and higher are essential for reducing the cost-to-serve relationship of heat pump systems toward the reference band of competitive operating costs. But for heat pumps which employ supplementary resistors such improvement will be accompanied ultimately with higher cost-to-serve rates per kw-hr than exists under the lower COPs.

4. The cost-to-serve levels of any of the resistance-type systems described fall far short of meeting the reference band of competitive operating costs. Their permissible saturation limits become insignificantly low under the short-range considerations as a possible seasonal valley-filling load.

Thus, if an all-electric home is to become a mass-market reality, there must be further intensification in research and development of the heat pump for substantial improvement in its annual COP, and the adoption of some form of supplementary heat storage, which is dependent upon a successful development of heat storage means. To provide incentives toward encouraging these requirements, and discouraging the use of supplementary resistors in conjunction with the heat pump, especially under night set-backs of indoor thermostat settings, and to facilitate meeting the economic necessities of long-range considerations, electric service to all types of house heating systems, with their complementary cooling, should be priced under some form of "demand-energy" rates, or its equivalent, because this type of rate form can be made to meet, over a wide range of load factors, the fundamental hyperbolic nature of the cost-to-serve versus load factor relationship such as is depicted in Fig. 1.

References

1. The Heat Pump—Its Significance as a Potential Residential Electric Load, Constantine Barry. *AIEE Transactions*, vol. 68, pt. I, 1949, pp. 1–8.

2. The Heat Pump Load—Good or Bad? Constantine Bary. *Refrigerating Engineering*, American Society of Refrigerating Engineers, New York, N. Y., May 1950, pp. 451–55.

3. Residential Heat Pump Experiments in Philadelphia—Suggested Possibilities for

ACTICAL APPLICATIONS, **Constantine Bary.** *EE Transactions*, vol. 71, pt. II, 1952 (Jan. 3 section), pp. 361–65.

LOAD AND ECONOMIC ASPECTS OF THE RESI-TIAL HEAT PUMP ON ELECTRIC UTILITY SYS-S, **Constantine W. Bary.** *Ibid.*, vol. 76, pt. II, y 1957, pp. 49–54.

ECONOMIC SIGNIFICANCE OF LOAD CHARACTER-ICS AS APPLIED TO MODERN ELECTRIC SERVICE, **nstantine Bary.** *Minutes*, 53rd Annual Meeting, ociation of Edison Illuminating Companies, w York, N. Y., 1937 (printed but not pub-ed).

6. LOAD-STRUCTURE OF A MODERN ELECTRIC UTILITY SYSTEM, **Constantine W. Bary.** *Proceedings*, American Power Conference, Chicago, Ill., vol. XVI, also *Electric Light and Power*, Chicago, Ill., May, 1954.

7. LOAD CHARACTERISTICS OF "SMALL LIGHT AND POWER" CUSTOMERS—THEIR ECONOMIC SIGNIFICANCE, **Constantine W. Bary.** *Electric Light and Power*, Chicago, Ill., Oct. 15, 1955.

8. REPORT ON HEAT STORAGE, **Joint AEIC-EEI Heat Pump Committee.** *Bulletin*, Edison Electric Institute, New York, N. Y., Aug. 1958, p. 261.

9. HEAT PUMP APPARATUS, **Constantine W. Bary.** *U. S. Patent no. 2,723,083*, Nov. 8, 1955.

10. *Discussion* by **Constantine Bary.** *Minutes*, 65th Annual Meeting, Association of Edison Illuminating Companies, 1949, p. 80.

11. COOLING LOAD NEEDS COMPLEMENT, **Constantine W. Bary.** *Electrical World*, New York, N. Y., May 9, 1955.

12. COINCIDENCE-FACTOR RELATIONSHIPS OF ELECTRIC-SERVICE-LOAD CHARACTERISTICS, **Constantine Bary.** *AIEE Transactions*, vol. 64, 1945, pp. 623–28.

Discussion

Grant De Remer (Consulting Engineer, arien, Conn.): This paper is vitally portant in showing the marked distinction tween short-range and long-range con-lerations. Throughout the history of ctrical utility operation the industry has ffered the penalty involved in supplying ak power at midwinter. Until recently, e peak usually occurred on the Saturday ght before Christmas.

I have examined load curves of large ilities covering the past 40 years, many which show that because of this fact, om one quarter to one third of the total ant and distribution system investment s been involved in the production of ly about 1% of the annual output. The vious high fixed charges resulting from is condition have always been a challenge the electrical engineering profession.

Now, however, with the coming of sum-er air conditioning and large irrigation mping, particularly in the western states, me utilities are experiencing maximum nual peaks in the summer. It is these nditions which Mr. Bary so clearly sets rth in this paper.

Until the time in the not distant future nen the new peak from summer air condi-oning exceeds the winter peak in a system, e cost and rate factors involved take on e characteristics of his short-range anal-is. As the long-range period approaches, r. Bary brings out clearly the importance storage, especially heat storage, in con-ction with the use of the heat pump. The ssibilities in this direction are very great, pecially when they are considered in njunction with solar heat sources.

The vital feature needed here is the dis-very of a practical, low-cost heat storage edium, preferably one that is applicable short-hour, high-temperature, daily off-ak storage, sufficient to carry a residence er the off-peak hours, as is done with ctric water heaters, plus a longer-hour, w-temperature heat storage in the 40-60-degree Fahrenheit range.

The magnitude of this latter storage ll be determined by the extreme weather nditions in the latitudes concerned. ajor attention, therefore, should be given research organizations into the possi-lities of these types of heat storage. ne thinking in this direction is compre-nded by Mr. Bary's reference to "new proaches," as a radical breakthrough ems to be needed at this point.

P. Herrington (John B. Pierce Founda-on, Inc., New Haven, Conn.): Mr. Bary's analyses serve to reinforce certain earlier conclusions on short-range effects and to extend information on long-range effects. Of the many features that may be deduced from his data, the following items probably need wider appreciation among groups concerned with heat pump design and manufacture rather than utility operation:

1. The summer margin which may be filled with a seasonal load such as cooling is an area which, when filled, changes the economic status of the cooling load from one of partial cost to a full-cost basis. In view of the hyperbolic relation between diversified annual load factor and demand-and-energy cost per kw-hr, the full-cost basis above the marginal area exceeds the partial cost per kw-hr by a factor as large as seven at low diversified annual loads. This is in accord with the established principle that cost-to-serve on large loads such as house heating must be considered with respect to maximum diversified demand as well as with respect to short-term effects on the load characteristics of a specified class of service.

2. Since the competitive aspects of sales of heating as contrasted with cooling service are markedly different for electric systems, it is important to know the effect of annual heat pump system COP on this factor. The data indicate that although improvement in COP has a favorable effect on cost-to-serve, it is only the heat pump system with supplementary heat storage that approaches competitive status with an annual COP of 3.

3. A further fact which characterizes the heat pump with supplementary heat storage as contrasted with supplemental resistance heat is that systems with heat storage provide a steady decrease in cost-to-serve in contrast to the increasing costs of resistance heat supplement.

4. Improvement in cost-to-serve factors with heat pump systems are noted for the condition of fixed as opposed to night set-back thermostat operation, design factors being assumed adequate for this operation. Consideration of this understandable conclusion ought to be influenced by two factors: 1. the common impression of the fuel savings achieved by night thermostat set-back is probably greater than is actually the case, and 2. the night reduction in thermostat level achieves cooler sleeping quarters, without drastic ventilation, a performance feature valued by many.

5. Mr. Bary's highly informed study is probably widely applicable, his northeastern metropolitan system being reasonably typical of future demand. Generalization of his equations and data on costs, general system operating characteristics, and specific equipment characteristics, which are currently to some degree dimensionally distinct, might present a formidable problem but would be in line with the recent extension in the feasibility of practical computation, and would provide a valuable guide for policy in electric systems differently situated.

D. W. Locklin and **J. A. Eibling** (Battelle Memorial Institute, Columbus, Ohio): Electric-heating specialists generally recognize that night set-back of the thermostat is undesirable with electric space-heating systems. However, it is doubtful that there is always appreciation of the magnitude of the penalty inflicted by night set-back if extended to high saturation. The paper forcibly shows the need to discourage night set-back of the thermostat.

Another highly revealing point demonstrated by the analysis is that the annual diversified load factor decreases appreciably with improvement in COP when supplementary resistance heating without heat storage is used. Thus, with the present practice of using supplementary resistance heating, further improvements in heat-pump performance made by manufacturers can actually result in higher average power cost per kw-hr if such systems are installed in substantial saturation. Conversely, it is particularly interesting to learn of the great extent to which supplementary heat storage would reduce the demand factor of the electric rate structure. This attests to the desirability of having as soon as possible a reliable, low-cost storage system for residential application.

Recently, an exploratory study of heat storage as applied to residential heat pumps was conducted at Batelle for the Joint Association of Edison Illuminating Companies–Edison Electric Institute Heat Pump Committee. This study revealed that the development of compact and reliable heat storage is feasible with the use of high-temperature storage media charged by resistance heaters. In application, the high-temperature storage would be charged during periods controlled by a time clock or demand switch, in such a way as to provide desirable load characteristics. The utilization of the heat of fusion of certain salt hydrates has received widespread attention for lower temperature storage, but their usage is faced with difficulties, mainly associated with erratic crystallization behavior, yet to be overcome.

From Mr. Bary's analysis, the development of practical and economical heat storage systems is seen to be an extremely imporant factor in the broadening of the electric-space-heating market. As a corol-

lary to this, an incentive such as a lower power rate must be offered to purchasers of residential heat pumps to encourage their investing in supplementary heat storage in preference to supplementary resistance heating. Careful analyses such as this are an important adjunct toward defining the direction of research and development.

Constantine W. Bary: I am grateful to the discussers for their emphasis on one or more of the aspects contained in the paper for the achievement of the all-electric home as a mass-market reality. Their thoughts should aid in bringing about better realization of the concerted actions needed in the fields of the following:

1. Intensive research and development for the use of economically acceptable supplementary electrical heat storage means, to minimize the cost to serve the electrical load of an all-electric home.

2. Continued research and development for substantial improvements in the COP of the electrical heat pump, to bring about costs of heating with electricity closer to the competitive reference band.

3. Establishment of demand-energy rates for such applications to insure the relative adequacy of electricity prices over a wide range of conditions, and to provide self-acting economic incentives for encouraging the use of supplementary heat storage and for discouraging the use of night set-back of indoor thermostats.

All three of these actions are required at the utilization level of electric systems operations. Mr. De Remer mentions th challenges presented by short-duratio system peaks. I foresee that, in the long range aspects, and for high degree of satura tion of all-electric homes, such condition will continue to present challenges. There fore, actions will be required also at th supply level of electric systems' operations As pointed out in reference 4, this coul take the form of the relatively new idea t inject periodically into the growing capacit requirements of a supply system a certai amount of (now considered unconventional low first-cost peak-shaving generating equip ment such as the package type, unattende diesel engine or gas-turbine plants for de centralized operation throughout the dis tribution system at times of peaks and fo reserves.

Signal Stabilization of a Control System

R. OLDENBURGER
MEMBER AIEE

C. C. LIU
NONMEMBER AIEE

FEEDBACK loops, in states of self-oscillation, can often be stabilized by the introduction of an appropriate signal. In this paper a theory is developed to explain this phenomenon. The theory is applied to a system which is linear except for a limiter. Experimental results for the system showing the removal of the hunt by a stabilizing signal are given in a previous paper.[1]

For nonlinear elements with the output a function of the input a gain concept is defined so that these nonlinear elements may be replaced by simple amplifiers with this type of gain. Describing functions are used to relate sinusoidal stabilizing signals to the corresponding inputs and outputs of the limiter. This relation is described by the points of intersection of two families of curves with the frequency and amplitude of the stabilizing signal as parameters. From these curves the equivalent gain of the limiter is readily obtained, given the constants of the system and the stabilizing signal. The characteristic roots of the system are then chosen to give good transient response. Because of the general availability of 60- or 400-cycle-per-second electric power, signal stabilization can often be easily introduced in industrial applications.

Stabilization

Automatic control systems are often stabilized by the use of a properly chosen linear band of operation about equilibrium. Thus control systems that are otherwise nonlinear have been stabilized with the aid of a linear band in the sense that when the errors in the controlled variable and its derivatives are small enough, the system behaves like a linear system whose characteristic roots are satisfactory. Stability here is achieved by nonlinear means.

The phenomenon of this paper was discovered experimentally by one of the authors during frequency response runs on a hydroelectric system simulated on an analog computer.[1] The stabilization dealt with here depends on the introduction of an appropriate signal which increases or decreases the effective open-loop gain of the system in the neighborhood of equilibrium, without materially affecting the gain for large deviations from equilibrium. It is assumed, as is usually the case, that the self-oscillations of the system in the absence of the stabilizing signal are bounded. It is also assumed that the hunt is not completely wild, but that a moderate reduction in open-loop gain will remove the hunt. The stabilizing signal may then leave the response to large disturbances relatively unaffected while at the same time removing the hunt. Signal stabilization is analogous to, but not identical with, the insertion of an additional amplifier or attenuator into the given loop. Because of the genera availability of 60-cycle-per-second elec tric power, the introduction of signa stabilization is often a simple matter This paper is devoted to a method o analysis for computing stabilizing signals

MacColl showed that the introductio of a sinusoidal signal at the input to a on-off servomechanism yields a syste that behaves like a linear one for smal inputs superimposed on this signal.[2] This differs from the illustrative example of the present paper in that the syste of this paper is already linear in the neighborhood of equilibrium, whereas the system of MacColl is not.

Minorsky treated the use of a signa to excite or quench the hunt (self-oscilla tion) of a physical system described by a second-order differential equation in the variable $x(t)$, for time t, where the co efficient of the "damping" term in dx/dt is an even polynomial in x.[3] The sta bilization of Minorsky depends on proper ties of asymptotic solutions of the differ ential equation. The stabilization tech nique of this paper does not depend on these properties.

System With Bounding Element

In every problem involving a hydrauli servomotor the speed of the servomoto piston is bounded. In Fig. 1 the syste to be controlled is shown in one block

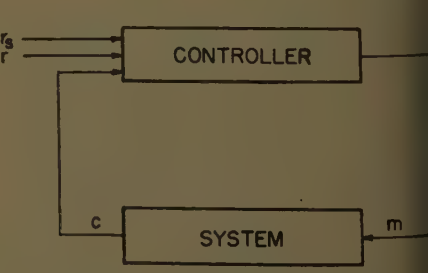

Fig. 1. System to be controlled

Paper 59-219, recommended by the AIEE Feedback Control Systems Committee and approved by the AIEE Technical Operations Department for presentation at the AIEE Winter General Meeting, New York, N. Y., February 1–6, 1959. Manuscript submitted October 20, 1958; made available for printing December 10, 1958.

R. Oldenburger is with Purdue University, Lafayette, Ind., and C. C. Liu is with the Taylor Instrument Company, Rochester, N. Y.

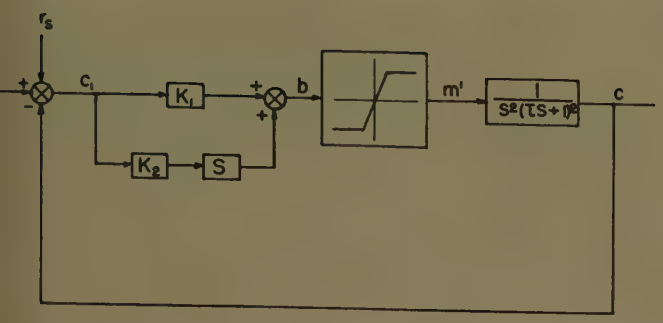

Fig. 2 (left). Nonlinear control system

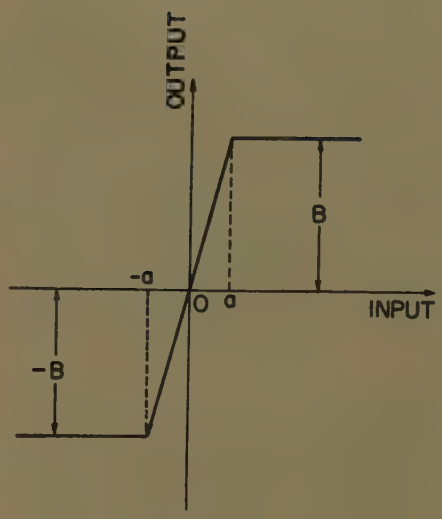

Fig. 3 (right). Characteristic of a bounded element

ıe variable m is the controlling variable, ch as the throttle on a gasoline engine. the controller is a governor, m can be ken to be servomotor piston position. ıe output of the controlled system is de- ted by c. For a governor-engine system, s engine rpm (revolutions per minute). ıe input to the controller is $r-c+r_s$, ıere r is the reference value of the con- olled variable (speed setting in the se of a governor-engine system), and r_s the value of the extra input signal used stabilize the system. Stabilization th r_s will be called "signal stabiliza- on." This signal need not be intro- ıced at the same point as the reference but for simplicity this will be assumed re.

The theory of signal stabilization will developed in this paper in connection th a controlled system possessing the ansfer function

$$\frac{1}{(\tau s+1)^2}$$

eceded by a limiter as shown in Fig. 2. ıe limiter follows a proportional plus rivative controller with gains K_1 and K_2 the proportional and derivative chan- ls respectively.

quivalent Gain of Nonlinear Element

Let the input and output to a nonlinear ment be denoted by x_1 and x_2 respec- ely, and assume that

$$x_2=f(x_1) \tag{1}$$

a function $f(x_1)$, whence the nonlinear ment is time independent. Let S^* ote a periodic stabilizing signal with erage value equal to zero. It is as- ned that when S^* is the entire input the nonlinear element, in which event $=S^*$, the average of the output of the ment is zero. A constant second input nponent K_b is added to the stabilizing nal S^* to yield an input $x_1=S^*+K_b$. t the average of the corresponding out- t of the nonlinear element be de- ed by A_v. The equivalent gain g_b of the nonlinear element is defined by the following:

$$g_b=\lim_{K_b\to 0}\frac{A_v}{K_b} \tag{2}$$

The equivalent gain is thus the limit of the average value of the output divided by the average value of the input as the average value of the input goes to zero.

For sinusoidal stabilizing signals S^* and odd functions $f(x)$ [$f(x_1)$ is odd when $f(-x_1)=-f(x_1)$] the limit process of equation 2 can be carried out. Such functions describe many of the commonly occurring nonlinearities such as limiting and dead band with the elements otherwise proportional.

The input-output characteristic of a limiter is shown in Fig. 3. The relation between the input x_1 and the output x_2 of the limiter is given for constants a and B by

$$\begin{aligned} x_2&=\frac{B}{a}x_1, && -a<x_1<a\\ x_2&=B, && x_1>a \\ x_2&=-B, && x_1<-a \end{aligned} \tag{3}$$

Let the input to the limiter be the sinusoidal wave given by

$$x_1=K_b+B_1\sin\omega t \tag{4}$$

for the positive K_b. Let

$$B_1>a+K_b \tag{5}$$

so that the input x_1 reaches both corners of the characteristic curve of the limiter. As proved in Appendix I, the equivalent gain g_b for the limiter is given by

$$g_b=\frac{B}{a}\frac{1}{\pi}\left[2\left(\frac{a}{B_1}\right)+\frac{1}{3}\left(\frac{a}{B_1}\right)^3\right] \tag{6}$$

A curve for equation 6 is plotted in Fig. 4 for the case where $a=0.2$ and $B=10$.

If a sinusoidal stabilizing signal r_s is introduced into a feedback loop with a nonlinear element, the resulting input to this element will not in general be sinusoidal. In this event, as in describing function theory, the fundamental component of the periodic wave is employed.

System Stability

The limiter in the feedback loop of Fig. 2 is replaced by a simple amplifier with the gain g_b of equation 6. The characteristic equation of the system is given by

$$\tau^2x^4+2\tau x^3+x^2+K_2g_bx+K_1g_b=0 \tag{7}$$

By Routh's stability criterion this equation is stable if and only if

$$g_b<\left(\frac{2}{K_2}-\frac{4K_1}{K_2^2}\right) \tag{8}$$

In view of the inequality of equation 8, if the equivalent gain is high enough, the loop will experience sustained oscillations. The radian frequency ω_n for sustained oscillations is given by

$$\omega_n=\frac{1}{\tau}\sqrt{1-2\tau\frac{K_1}{K_2}} \tag{9}$$

From K_1, K_2, and τ the equation

$$g_b=\left(\frac{2}{\tau K_2}-\frac{4K_1}{K_2^2}\right)$$

yields the critical value of g_b for such

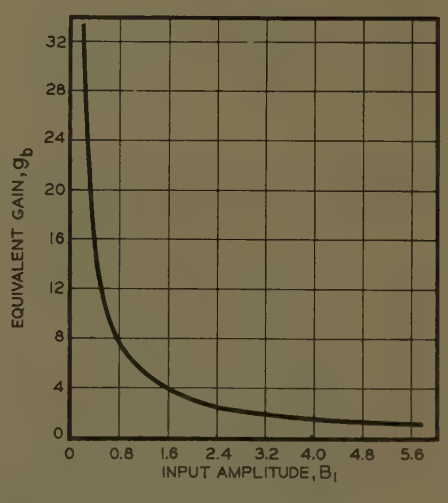

Fig. 4. Equivalent gain of bounded element

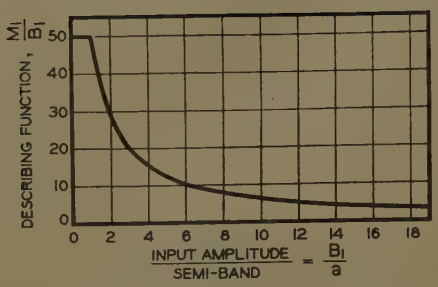

Fig. 5. Describing function of bounded element

oscillations. The amplitude of the sinusoidal stabilizing signal S^* at the limiter input is determined from equation 6, or a plot of this equation as in Fig. 4.

Describing Function

The stabilizing signal r_s that will yield the desired stabilizing signal at the input to the limiter of Fig. 2 will now be established with the aid of describing functions.

Let x_1, for

$$x_1 = B_1 \sin \omega t \tag{10}$$

be the input to the limiter, and

$$M_1 \sin \omega t \tag{11}$$

the fundamental component of the output x_2 of the limiter. The describing function[4] of the limiter is M_1/B_1, where

$$\frac{M_1}{B_1} = \frac{B}{a}\frac{2}{\pi}\left[\sin^{-1}\left(\frac{a}{B_1}\right) + \left(\frac{a}{B_1}\right)\times \sqrt{1-\left(\frac{a}{B_1}\right)^2}\right] \tag{12}$$

A plot of formula 12 is given in Fig. 5.

Let the stabilizing signal r_s be given by

$$r_s = R_s \sin \omega t \tag{13}$$

for the amplitude R_s of r_s. A modified plot of the describing function for the case where $a=0.2$, $B=10$ is shown in Fig. 6. For what is to follow the plot of M_1/R_s versus B_1/R_s is more convenient than a plot of M_1/B_1 versus B_1/a.

Frequency Response

A relation between M_1/R_s and B_1/R_s was obtained in the preceding section from the characteristics of the limiter element only with the aid of frequency response. A second relation between these quantities can be obtained from the characteristics of the rest of the loop.

The stabilizing signal r_s may be put in the complex form

$$R_s \epsilon^{j\omega t}$$

for $j=\sqrt{-1}$. Suppose that the input r to the loop is zero, and that the loop is stable when r_s is introduced. The complex forms of the fundamental components of the input and output of the limiter are taken to be

$$B_1 \epsilon^{j(\omega t+\theta)}, \quad M_1 \epsilon^{j(\omega t+\theta)}$$

respectively, for a phase angle θ. The complex form C of the fundamental component of the output c of the loop is given by

$$C = -M_1 H_1 \epsilon^{j(\omega t+\theta-2\alpha)} \tag{14}$$

where

$$\alpha = \tan^{-1} \omega\tau$$

$$H_1 = \frac{1}{\omega^2(\omega^2\tau^2+1)}$$

The complex form C_1 of the fundamental component of the controller input c_1 is given by

$$C_1 = [R_s + M_1 H_1 \epsilon^{j(\theta-2\alpha)}]\epsilon^{j\omega t} \tag{15}$$

In Appendix II, the complex form of the limiter input is equated to C_1 multiplied by the controller transfer function, and the result manipulated to yield the equation

$$\frac{B_1}{R_s} = H_2\left\{\frac{M_1 H_1}{R_s}\cos(2\alpha-\beta) \pm \sqrt{1+\left[\frac{M_1 H_1}{R_s}\sin(2\alpha-\beta)\right]^2}\right\} \tag{16}$$

For given system constants, the parameters H_1, H_2, α, and β are fixed. With R_s also given equation 16 yields a relation between B_1 and M_1.

The two relations between B_1 and M_1 determine these quantities when the stabilizing signal and the loop constants are given. The dependence of the stabilizing signal S^* at the limiter input on the system stabilizing signal r_s is now determined.

Relation Between Stabilizing Signals

In Fig. 7 a family of curves relating M_1/R_s and B_1/R_s is given with R_s as the parameter. These curves depict equation 12. On this same figure is plotted a family of curves satisfying equation 16 with ω as the parameter.

A point of intersection of a curve of one family with a curve of the other determines the amplitude of B_1, as well as M_1

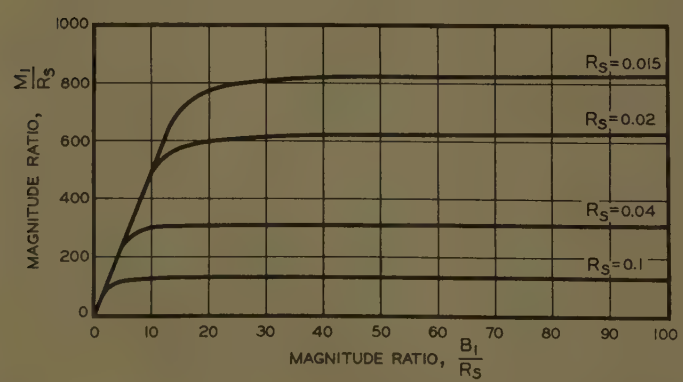

Fig. 6 (below). Modified describing function of bounded element

Fig. 7 (right). Diagram for obtaining B_1, for a given R_s and ω

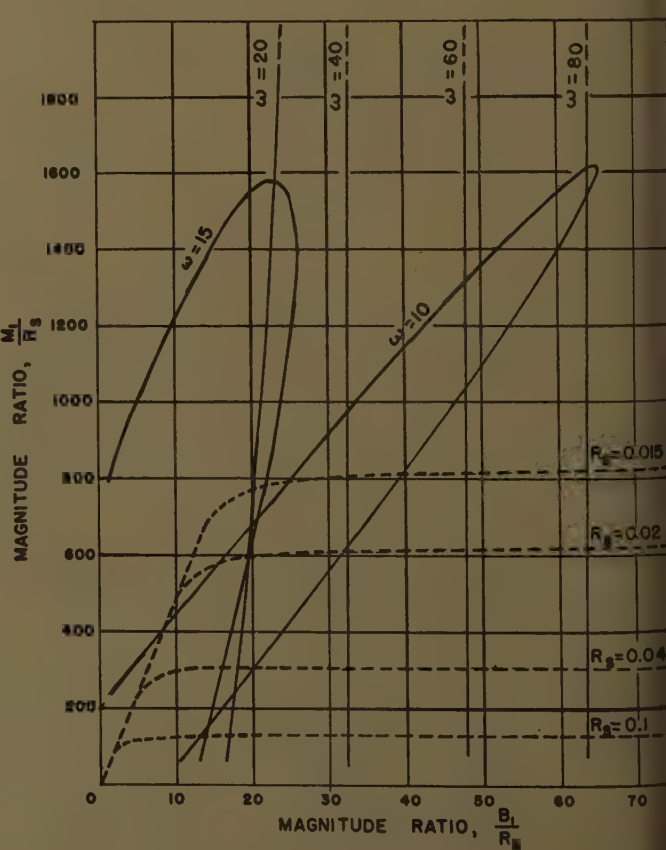

or $\omega>15$ there is only one such intersection point. In this case the amplitude of B_1, and hence M_1 is uniquely determined from the figure. With B_1 determined the equivalent gain g_b can be computed from equation 6. This may in turn be substituted into the inequality of equation 8 to determine system stability. The values of g_b must be restricted to an appropriate range so that the transient response will be satisfactory.

If the dominant roots of the system characteristic equation 7 are of the form $-P\pm jQ$, $0\leq P\leq Q\leq 2P$, the transient response is good, provided that P is large enough. Given P, and if Q dominates $2P$, the system response is too oscillatory, whereas if P dominates Q, the deviations in the output are excessive.

Numerical Case

Experimental results showing the removal of a hunt by the introduction of a stabilizing signal are given in a previous paper[1] for the system of Fig. 2 with

$K_1=1$
$K_2=0.8$
$a=10$
$K_b=0.2$
$B=0.1$

The characteristic equation for this system is given by

$$x^3+20x^2+100x+80g_bx+100g_b=0 \tag{17}$$

For system stability it is necessary that

$$g_b<18.75 \tag{18}$$

The gain 50 of the limiter for zero input is higher than this limit. Therefore in physical tests on the system, the loop went into self-oscillation. Equation 9 gives the frequency of the hunt, which is

$\omega=8.66$ radians per second

From the characteristic equation 17, the inequaly 16, and certain other considerations, it can be proved, as shown in Appendix III, that the values of equivalent gain which yield good transient response are in the range

$$3<g_b<4 \tag{19}$$

This explains the experimental run of Figs. 5 and 6 in the previous paper.[1] The range of the values of the amplitude B_1 of the fundamental component of the input to the limiter corresponding to the inequalities 19 is

$$5.6<B_1<3.9 \tag{20}$$

Appendix I. Equivalent Gain for the Limiter

Let the input x_1 to the limiter of Fig. 3 be given by

$$x_1=K_b+B_1\sin\omega t \tag{4}$$

where

$$B_1>a+K_b \tag{5}$$

The average value A_v of the output x_2 corresponding to this input x_1 is then

$$\begin{aligned}A_v=&\frac{1}{2\pi}\int_0^{\lambda_1}\frac{B}{a}(K_b+B_1\sin\omega t)d\omega t+\\&\int_{\lambda_1}^{\pi-\lambda_1}Bd\omega t+\int_{\pi-\lambda_1}^{\pi+\lambda_2}\frac{B}{a}(K_b+B_1\times\\&\sin\omega t)d\omega t+\int_{\pi+\lambda_2}^{2\pi-\lambda_2}-Bd\omega t+\\&\int_{2\pi-\lambda_2}^{2\pi}\frac{B}{a}(K_b+B_1\sin\omega t)d\omega t\\=&\frac{B}{\pi}\left[\frac{K_b}{a}(\lambda_1+\lambda_2)+\right.\\&\left.\frac{B_1}{a}(\cos\lambda_2-\cos\lambda_1)+(\lambda_2-\lambda_1)\right]\end{aligned} \tag{21}$$

where

$$\lambda_1=\sin^{-1}\left(\frac{a-K_b}{B_1}\right)$$

$$\lambda_2=\sin^{-1}\left(\frac{a+K_b}{B_1}\right)$$

The quantities λ_1 and λ_2 may be expanded into a power series in $(a-K_b)/B_1$, and $(a+K_b)/B_1$ respectively. Assume that $B_1>>K_b$ (B_1 dominates K_b), $B_1>a+K_b$, and that the fifth or higher power terms in the series expansion can be neglected. It follows that

$$\lambda_1=\sin^{-1}\left(\frac{a-K_b}{B_1}\right)\cong\frac{a-K_b}{B_1}+\frac{1}{6}\left(\frac{a-K_b}{B_1}\right)^3 \tag{22}$$

$$\lambda_2=\sin^{-1}\left(\frac{a+K_b}{B_1}\right)\cong\frac{a+K_b}{B_1}+\frac{1}{6}\left(\frac{a+K_b}{B_1}\right)^3 \tag{23}$$

$$\cos\lambda_1=1-\frac{a^2-2aK_b}{2B_1^2}-\frac{(a^2-2aK_b)^2}{8B_1^4} \tag{24}$$

$$\cos\lambda_2=1-\frac{a^2+2aK_b}{2B_1^2}-\frac{(a^2+2aK_b)^2}{8B_1^4} \tag{25}$$

Substituting λ_1, λ_2, $\cos\lambda_1$, $\cos\lambda_2$, from these equations into equation 21, and dividing both sides by the average value K_b of the input, one obtains

$$g_b=\lim_{K_b\to 0}\frac{A_v}{K_b}=\frac{B}{a}\frac{1}{\pi}\left[2\left(\frac{a}{B_1}\right)+\frac{1}{3}\left(\frac{a}{B_1}\right)^3\right] \tag{26}$$

Appendix II. Frequency Response

The transfer function of the controller is given by

$$K_1+j\omega K_2$$

Multiplying the complex form C_1 of the controller input, given in equation 15, by this transfer function and equating this to the complex form of the limiter input, one has

$$\begin{aligned}B_1\epsilon^{j(\omega t+\theta)}=&(K_1+j\omega K_2)\times\\&[R_s+M_1H_1\epsilon^{j(\theta-2\alpha)}]\epsilon^{j\omega t}\end{aligned} \tag{27}$$

whence

$$B_1\epsilon^{j\theta}=H_2[R_s\epsilon^{j\beta}+M_1H_1\epsilon^{j(\theta+\beta-2\alpha)}] \tag{28}$$

for

$$\beta=\tan^{-1}\omega\frac{K_2}{K_1}$$

$$H_2=\sqrt{K_1^2+\omega^2K_2^2}$$

Multiplying both sides of equation 28 by $\epsilon^{-j\theta}$, one obtains

$$\begin{aligned}B_1=&H_2[R_s\epsilon^{j(\beta-\theta)}+M_1H_1\epsilon^{j(\beta-2\alpha)}]\\=&H_2\{[R_s\cos(\beta-\theta)+M_1H_1\\&\cos(\beta-2\alpha)]+j[R_s\sin(\beta-\theta)+\\&M_1H_1\sin(\beta-2\alpha)]\}\end{aligned} \tag{29}$$

Since B_1 must be real, the imaginary part of equation 29 must be zero, whence

$$\sin(\beta-\theta)=\frac{M_1H_1}{R_s}\sin(2\alpha-\beta) \tag{30}$$

and

$$\cos(\beta-\theta)=\pm\sqrt{1-\left[\frac{M_1H_1}{R_s}\sin(2\alpha-\beta)\right]^2} \tag{31}$$

Substituting for $\cos(\beta-\theta)$ from equation 31 into equation 29, one obtains equation 16.

Appendix III. Equivalent Gain for Good Transient Response

To determine how the roots of equation 17 are affected by the equivalent gain g_b, the following right to left synthetic division is performed,[5] where it is assumed that $g_b=2$.

1	20	100	$80g_b$	$100g_b$	1, 20,	100
		g_b	$20g_b$			
		100	$60g_b$		$0.6g_b$,	g_b
	$0.6g_b$	$12g_b$				
1	20	100				

This division shows that the roots of equation 17 are approximately equal to the roots of the equation

$$x^2+20x+100=0 \tag{32}$$

and the equation

$$x^2+0.6g_bx+g_b=0 \tag{33}$$

The roots of equations 32 and 33 are

$$-10,\ -10,\ -0.3g_b\pm j\sqrt{g_b} \tag{34}$$

for practical purposes. If $g_b<1.25$ the imaginary part of the complex roots is at

least three times the real part. The roots are then too oscillatory.

For $g_b=1.6$ the roots are -13, -5.84, $-0.59\pm1.33j$; whereas for $g_b=4$ they are -14, -2.2, $-1.75\pm3.2j$. For $g_b>4$ the roots are more oscillatory and less satisfactory. For good transients the gain g_b should therefore be in the range $-1.6<g_b<4.0$.

References

1. Signal Stabilization of a Control System, Rufus Oldenburger. *ASME Transactions*, American Society of Mechanical Engineers, New York, N. Y., vol. 79, no. 8, 1957, pp. 1869–72.

2. Fundamental Theory of Servomechanisms (book), LeRoy A. MacColl. D. Van Nostrand Company, Inc., Princeton, N. J., 1945, pp. 78–87.

3. On Asynchronous Action, N. Minorsky. *Journal*, Franklin Institute, Philadelphia, Pa., vol. 259, no. 3, 1955, pp. 209–19.

4. Frequency Response (book), Rufus Oldenburger. American Society of Mechanical Engineers; also Macmillan Company, New York, N. Y., 1956, p. 242.

5. Algebraic Approach to Design of Automatic Controls, Rufus Oldenburger. *ASME Transactions*, American Society of Mechanical Engineers, vol. 80, no. 2, 1958, pp. 433–43.

Discussion

Takashi Nakada (Purdue University, Lafayette, Ind.): The authors state that signal stabilization is analogous to, but differs from, the insertion of an amplifier or attenuator into the feedback loop. The difference may readily be seen by considering a loop with a dead zone nonlinear element. Such a dead zone yields a zero gain open loop. Insertion of an amplifier or attenuator ahead of this nonlinear element will not change the zero open loop gain. However, a properly chosen stabilizing signal will change the open-loop gain to a value different from zero.

R. Oldenburger and C. C. Liu: The example cited by Prof. Nakada emphasizes a difference between the technique of signal stabilization and that of inserting an amplifier into the feedback loop. When the open-loop gain of the unstabilized system is different from zero the results due to the insertion of a stabilizing signal are closer to those achieved with an amplifier or attenuator. The performance of a stable system can be altered within limits by the use of the "stabilizing" signal, i.e., by the introduction of an extra signal, as is done when the gain of an amplifier in the loop is changed. The paper shows how the extra signal can be determined by calculation. Replacing the nonlinear element by an amplifier (or attenuator) makes it possible to compute by conventional methods the gain this amplifier must have to yield desired performance. This is then the equivalent gain to be obtained for the nonlinear element. From the relation between the extra signal and the equivalent gain of the nonlinear element one can determine the signal that will yield the correct equivalent gain. The approach is valid for systems with multiple nonlinearities.

A Study of Nonlinear Systems With Random Inputs

KUEI CHUANG
NONMEMBER AIEE

LOUIS F. KAZDA
MEMBER AIEE

IT IS THE PURPOSE of this paper to present the results of investigating the probability distribution of the response of a nonlinear system when it is subjected to a Gaussian random input. The mathematical theory of a Markoff random process is used; the associated Fokker-Planck equation for a generalized continuous nonlinear system is presented. The justification for assuming the error response of a nonlinear control system as being a Markoff process is discussed.

The theoretical result of this investigation for the stationary case is obtained in a closed form. It was verified by an experimental method which used an automatic electronic counting device to record the percentage of total observation time that a random signal exceeded a certain preset voltage level. The agreement between the theoretical calculations and the experimental measurements lies within the limits of experimental accuracy.

From the results of this investigation the following conclusions may be drawn:

1. The probability density function of the error of a second-order nonlinear system is an exponential function of the form $\exp[-A\int K(\epsilon)d\epsilon]$, where $K(\epsilon)$ describes the behavior of the nonlinear element.

2. If $K(\epsilon)$ is approximately linear, then the probability density function of item one reduces to a Gaussian function of ϵ.

Paper 59-147, recommended by the AIEE Feedback Control Systems Committee and approved by the AIEE Technical Operations Department for presentation at the AIEE Winter General Meeting, New York, N. Y., February 1–6, 1959. Manuscript submitted November 5, 1958; made available for printing December 22, 1958.

Kuei Chuang and Louis F. Kazda are with the University of Michigan, Ann Arbor, Mich.

This work contains part of the results of a thesis submitted by Kuei Chuang in partial fulfillment of the requirements for the degree of Doctor of Philosophy at the University of Michigan.

The response of a nonlinear system to a random input usually cannot be obtained with the use of the phase space or the describing function methods of analysis, since these methods are applicable to only a nonlinear system which contains only prescribed functions for its input. On the other hand, when a system contains a random input, this input can be characterized only by a set of statistical properties. To overcome this difficulty, Booton first introduced a linearization technique based upon the assumption that the probability distribution of the response of a nonlinear closed-loop system containing a zero memory nonlinearity, when excited by a Gaussian random input, is approximately Gaussian.[1] This statistical linearization method has been checked experimentally and the results agree with the theoretical calculations within the limits of experimental measurement.

This paper determines the theoretical probability distributions of Booton's type of nonlinear system when some special conditions are imposed on the random input function. It simultaneously explains, therefore, the validity of Booton's assumption under these special conditions.

I. Statistical Idea From Phase Space Point of View

It is well known by most engineers that the response of any dynamical system can be represented by a point in phase space. For a second-order system the phase space reduces to a phase plane. In this plane a point represents the position and the velocity of the dynamical system at a certain instant of time. With increasing time the representative point, which is continuously moving in this plane, describes a phase trajectory. Its path is analogous to the stream line of flow in hydrodynamics, and it represents the history of the dynamical system. If the input to the system is a random function of time which has a wide uniform power spectrum, the representative point of the system, when described in the phase space, undergoes a random motion. This random motion, if observed on an oscilloscope, reminds one

e Brownian movement of a particle on e surface of liquid. It is this analogy at led the authors to consider a Markoff ndom process technique for this motion. is interesting to point out that the alogy between the phase space flow d the nonlinear differential equation s first considered by Kaplan.[2] The esent idea of the random motion of a presentative point in phase space uld be considered as an extension the ideas of phase space flow. A oment's reflection would have revealed at both of these ideas could have been rived from Boltzmann's equation.[3]

Conditions Imposed on Random Input Functions and Effect of Feedback

To apply the Markoff random process chnique to a dynamical system, some nditions must be imposed on the ndom input $F(t)$, as follows:

$$F(t)>_{avg}=0 \tag{1}$$

$$F(t)F(t+\tau)>_{avg}=2D\delta(\tau) \tag{2}$$

$$)=\text{Gaussian distributed random function} \tag{3}$$

ndition 2 implies that the input func- n $F(t)$ has a white spectrum.

By imposing conditions 1 and 2 on the ndom input function, one might assume at the Markoff random process tech- que is not useful in analyzing a feed- ck control system. This impression based upon the fact that the power ctrum of the random input to a dback control system usually is limited a region of extremely low frequency, ile condition 2 requires the random ut to have a white power spectrum. wever, in the following discussion it is wn that this impression is not a e one. In reality the feedback action the system creates an effective input, ich is a linear combination of the true ndom input and its higher-order deriva- es, rather than a true random input.

Consider, for example, the first-order vomechanism which contains an inte- tor and a nonlinear element $K(\epsilon)$ in forward path. The following two ations define the dynamic behavior he system:

$$\theta_i-\theta_0 \tag{4}$$

$$=K(\epsilon) \tag{5}$$

ere θ_0, θ_i, and ϵ are respectively the put, input, and error. Substitution equation 4 into equation 5 results in an equation relating the error ϵ and input θ_i:

$$\frac{d\epsilon}{dt}+K(\epsilon)=\frac{d\theta_i}{dt}=F(t) \tag{6}$$

The random function $F(t)$ is called an effective random input and is assumed to have the properties prescribed by equations 1, 2, and 3. Since $F(t)$ is a linear function of the true random input $\theta_i(t)$, which is a Gaussian random function, it follows immediately that conditions 1 and 3 are satisfied by $F(t)$. According to power spectrum analysis, the power spectrum $\phi_F(\omega)$ of the effective random input $F(t)$ and the power spectrum $\phi_{\theta i}(\omega)$ of the true random input $\theta_i(t)$ are related by

$$\phi_F(\omega)=|j\omega|^2\phi_{\theta_i}(\omega) \tag{7}$$

If the power spectrum $\phi_{\theta_i}(\omega)$ is of the following form:

$$\phi_{\theta_i}(\omega)=\frac{D}{(\omega^2+\alpha^2)(\omega^2+\beta^2)} \tag{8}$$

where α, β, and D are constants. Then, from equation 7 the power spectrum $\phi_F(\omega)$ of the effective random input $F(t)$ will have the following form:

$$\phi_F(\omega)=\frac{\omega^2D}{(\omega^2+\alpha^2)(\omega^2+\beta^2)} \tag{9}$$

If in the frequency range of interest the value of the constant α^2 in equation 9 is very much smaller than ω^2, and if the value of the constant β^2 is very much larger than ω^2, the power spectrum $\phi_F(\omega)$ can be approximated by the following:

For $\omega^2<\alpha^2$

$$\phi_F(\omega)\cong\frac{D\omega^2}{\alpha^2\beta^2} \tag{10A}$$

For $\alpha^2<\omega^2<\beta^2$

$$\phi_F(\omega)\cong\frac{D}{\beta^2} \tag{10B}$$

For $\omega^2>\beta^2$

$$\phi_F(\omega)\cong\frac{D}{\omega^2} \tag{10C}$$

In Fig. 1 will be found the power spectra $\phi_{\theta_i}(\omega)$ and $\phi_F(\omega)$ as function of ω.

Inspection of Fig. 1 reveals the power spectrum of the effective random input $F(t)$ to be almost flat over the frequency range $\alpha<\omega<\beta$. If the frequency range $\alpha<\omega<\beta$ is much larger than the system bandwidth and if, in addition, the value α is very small, the power spectrum $\phi_F(\omega)$ of the effective random input may be considered as a white spectrum. (In an actual case, if a power spectrum is uniform over a frequency range which is greater than the frequency range of the system, the power spectrum may be considered as a white spectrum.) Under these conditions the effective random input has approximately the properties described by equation 2. The Markoff random process technique can be applied therefore to the first-order system provided the random input θ_i has the power spectrum $\phi_{\theta_i}(\omega)$ of the form described by equation 9.

In general, if the error of a servomechanism or of a feedback system can be described by the following equation:

$$\sum_{n=0}^{N}a_n\frac{d^n\epsilon}{dt^n}+K(\epsilon)=\sum_{n=0}^{N}a_n\frac{d^n\theta_i}{dt^n} \tag{11}$$

Since a_n's are constants, as previously defined, the right-hand side of equation 11 can be lumped together to form an effective input function $F(t)$ which is given by

$$F(t)=\sum_{n=0}^{N}a_n\frac{d^n\theta_i}{dt^n} \tag{12}$$

Accordingly, the power spectrum $\phi_F(\omega)$ of the effective input $F(t)$ and the power spectrum $\phi_{\theta_i}(\omega)$ of the true input $\theta_{i(t)}$ are related as follows:

$$\phi_F(\omega)=\left|\sum_{n=0}^{N}(j\omega)^na_n\right|^2\phi_{\theta_i}(\omega) \tag{13}$$

By properly choosing the form of the power spectrum $\phi_{\theta_i}(\omega)$, it is always possible to obtain a power spectrum

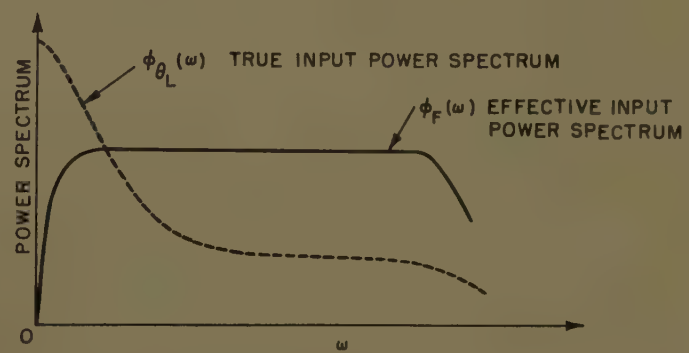

Fig. 1. Power spectrum of true and effective inputs

$\phi_F(\omega)$ which is approximately a white spectrum from a physical point of view.

The block diagram representation of equation 11 can be given in two equivalent forms: as a closed-loop representation, as shown in Fig. 2(A), and as an open-loop representation as in (B).

From Fig. 2(B) it is readily seen that the effective input to the system is essentially white noise provided that the input power spectrum is restricted to a special form determined by equation 13. Because of the power spectrum's changing property in a feedback system, it is possible to use Markoff random process technique to analyze several commonly encountered nonlinear servomechanisms.

III. Markoff Random Process and Fokker-Planck Equation

A discrete Markoff process can be interpreted as a process in which the occurrence of an event depends only on the occurrence of an event immediately preceding it. For a continuous case it is usually defined in terms of its conditional probability density function by an important relation given by equation 14, which is known as the Chapmann-Kolmogoroff equation:

$$f(t_2;\ y_1,y_2,\ldots y_n|S;\ \xi_1,\xi_2,\ldots\xi_n) = \int f(t_1;\ x_1,x_2,\ldots x_n|S;\ \xi_1,\xi_2,\ldots\xi_n) f(t_2;\ y_1,y_2,\ldots y_n|t_1; x_1,x_2,\ldots x_n)dx_1,dx_2\ldots dx_n \quad (14)$$

The function $f(t_1;\ x_1,\ x_2\ldots x_n|\ S;\ \xi_1,\ \xi_2,\ldots\xi_n)$ stands for the probability density function which states mathematically that at time t_1 the random variables are at $x_1,\ x_2,\ldots x_n$ on the assumption that at time S they were at $\xi_1, \xi_2, \ldots \xi_n$. For simplification in writing, vector notation is often used; equation 14 when written in vector from becomes

$$f(t_2;\ \mathbf{y}|S;\ \xi) = \int f(t_1;\ \mathbf{x}|S;\ \xi) f(t_2;\ \mathbf{y}|t_1;\ \mathbf{x})\mathbf{dx} \quad (15)$$

Based upon some conditions imposed on the conditional moments of those random variables, equation 15 can be reduced to a linear partial differential equation know as Fokker-Planck equation:[4]

$$\frac{\partial f}{\partial t} = -\sum_{i=1}^{N}\frac{\partial}{\partial_{y_i}}[\beta_i f] + \frac{1}{2}\sum_{i,j}^{N}\frac{\partial}{\partial_{y_i}}\frac{\partial}{\partial_{y_j}}[\beta_{ij} f] \quad (16)$$

where

$$\beta_i = \lim_{\Delta t\to 0}\frac{1}{\Delta t}\int(\Delta y_i) f(t+\Delta t;\ \mathbf{y}+\Delta\mathbf{y}|\mathbf{t};\mathbf{y})d(\Delta\mathbf{y})$$

$$\beta_{ij} = \lim_{\Delta t\to 0}\frac{1}{\Delta t}\int(\Delta y_i)(\Delta y_j) f(t+\Delta t;\ \mathbf{y}+\Delta\mathbf{y}|\mathbf{t}:\ \mathbf{y})d(\Delta\mathbf{y})$$

$$\beta_{i,j,k}\ldots 1 = 0$$

for any β whose subscripts have three or more letters.

IV. Second-Order Nonlinear Servo System and Its Relation to Fokker-Planck Equation

The dynamic behavior of a second-order servo system may be described by the second-order differential equation

$$\frac{d^2\theta_0}{dt} + a\frac{d\theta_0}{dt} + b\theta_0 = K(\epsilon) \quad (17)$$

where $K(\epsilon)$ is a function ϵ, a and b are constant, and θ_i and θ_0 are as previously defined.

By substituting $\epsilon = \theta_i - \theta_0$, equation 17 can be written as

$$\frac{d^2\epsilon}{dt^2} + a\frac{d\epsilon}{dt} + b\epsilon + K(\epsilon) = \frac{d^2\theta_i}{dt^2} + a\frac{d\theta_i}{dt} + b\theta_i \quad (18)$$

If the right side of equation 18 is written as a single function $F(t)$, the equation will reduce to

$$\frac{d^2\epsilon}{dt^2} + a\frac{d\epsilon}{dt} + b\epsilon + K(\epsilon) = F(t) \quad (19)$$

Since the function $F(t)$ is a linear combination of a Gaussian input function θ_i, it follows that $F(t)$ is a Gaussian random function. Furthermore by proper choice of the power spectrum of θ_i as shown in section II, $F(t)$ can be approximately treated as Gaussian white noise, and under this condition the Markoff random process technique will apply.

Now let $d\epsilon/dt = y_1$, $\epsilon = y_2$; then equation 19 becomes two first-order simultaneous differential equations in phase space $y_1 - y_2$:

$$\frac{dy_1}{dt} + ay_1 + by_2 + K(y_2) = F(t) \quad (20A)$$

$$\frac{dy_2}{dt} = y_1 \quad (20B)$$

Let t be increased to $t + \Delta t$ where Δt is very small compared with the response time of the system, but is not necessarily small compared with the function $F(t)$. Putting the two simultaneous equations 20(A) and 20(B) into the incremental form yields

$$\Delta y_1 + ay_1\Delta t + [by_2 + K(y_2)]\Delta t = \int_t^{t+\Delta t} F(t)dt \quad (21A)$$

$$\Delta y_2 = y_1\Delta t \quad (21B)$$

where $\int_t^{t+\Delta t} F(t)dt$ indicates that $F(t)$, in this small time interval Δt, is a rapidly changing function of time. By using equations 21(A) and (B), it is possible to calculate the functions β_i, $\beta_{i,j}$, β_{ijk}, ... $\beta_{ij\ldots m}$ of the Fokker-Planck equation given in section IV.

For the case of the second-order servomechanism expressed by equation 19 the Fokker-Planck equation has the following form:

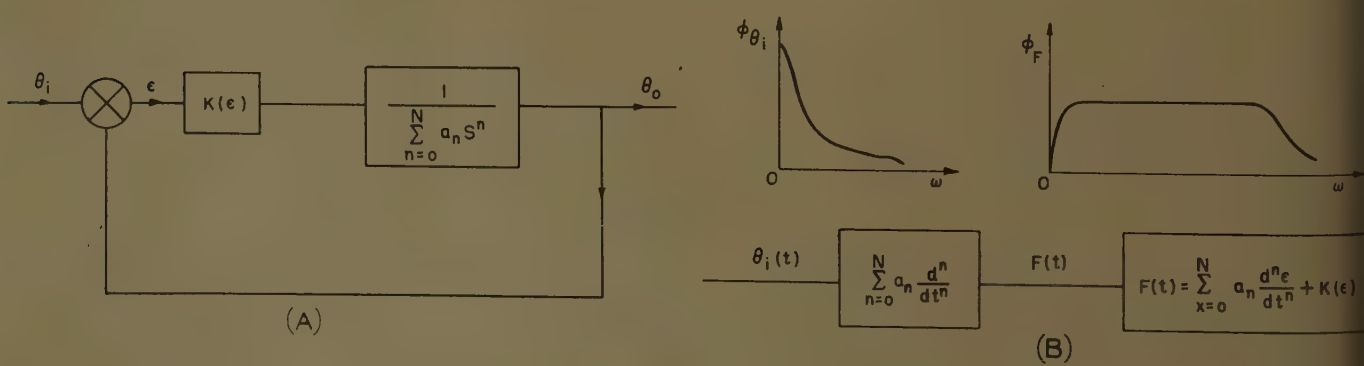

Fig. 2. Representations of nth order nonlinear servomechanism

A—Closed-loop
B—Open-loop

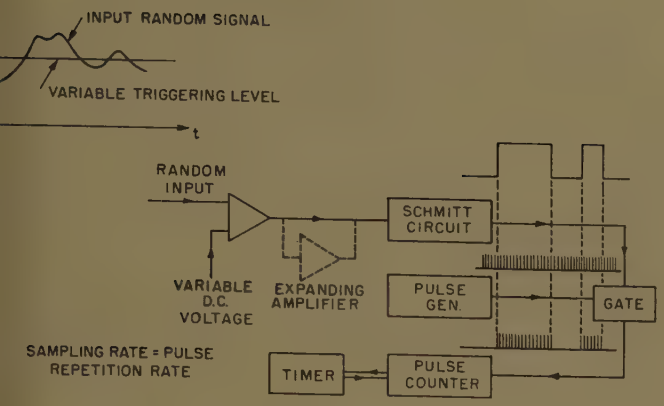

Fig. 3. Functional diagram of amplitude distribution analyzer

$$= -\frac{\partial}{\partial y_2}(y_1 f) + \frac{\partial}{\partial y_1}[[ay_1 + by_2 + K(y_2)]f] + D\frac{\partial^2 f}{\partial y_1^2} \quad (22)$$

ere the assumption is used that $<F(t)F(t+\tau)>_{avg} = 2D\delta(\tau)$ where $\delta(\tau)$ is a delta nction and D a constant.

The solution of equation 22 gives the nditional probability density function the nonlinear servo system. This solu-on, in general, is a function of y_1, y_2, t d initial conditions y_{10}, y_{20}, t_0. How-er, as $t \to \infty$ the solution becomes in-pendent of y_{10}, y_{20} and t_0. This is what e would expect, since any random variable after a long time interval becomes independent of its initial conditions. Consequently, as $t \to \infty$, the conditional probability function becomes a first probability function.[5]

When the first probability density function is desired, it can be found from the steady-state solution or by letting $\partial f/\partial t = 0$ in equation 22. The Fokker-Planck equation 22 reduces in this case to the following form:

$$0 = -\frac{\partial}{\partial y_2}(y_1 f) + \frac{\partial}{\partial y_1}\{[ay_1 + by_2 + K(y_2)]f\} + D\frac{\partial^2 f}{\partial y_1^2} \quad (23)$$

The additional conditions that the stationary solution must satisfy are:

1. $f(y_2, y_1, t = \infty) \to 0$ as $|y_1| \to \infty$ or as $|y_2| \to \infty$ or both $|y_1|$ and $|y_2| \to \infty$.
2. $f(y_2, y_1, t = \infty)$ should always be a positive function.
3. $\int_{-\infty}^{+\infty}\int_{-\infty}^{+\infty} f(y_2, y_1, t = \infty)\,dy_1 dy_2 = 1$

If a stationary solution is assumed of the form $f[my_1^2 + n\int[by_2 + K(y_2)]dy_2]$, and these three conditions are used, it can be shown that

$$f(y_2, y_1\, t = \infty) = A \exp\left\{\frac{-a}{2D}y_1^2 - \frac{a}{D}\int[by_2 + K(y_2)]dy_2\right\} \quad (24)$$

where A is determined by the normalized condition 3.

The steady-state solution or first probability density function in phase-space is the most general type of solution obtainable from a second-order system which has an arbitrary zero memory nonlinearity in its forward path, when the system has been subjected to a Gaussian random input. From this solution it is readily seen that in spite of a nonlinearity in this type of second-order system, the rate of the response of the

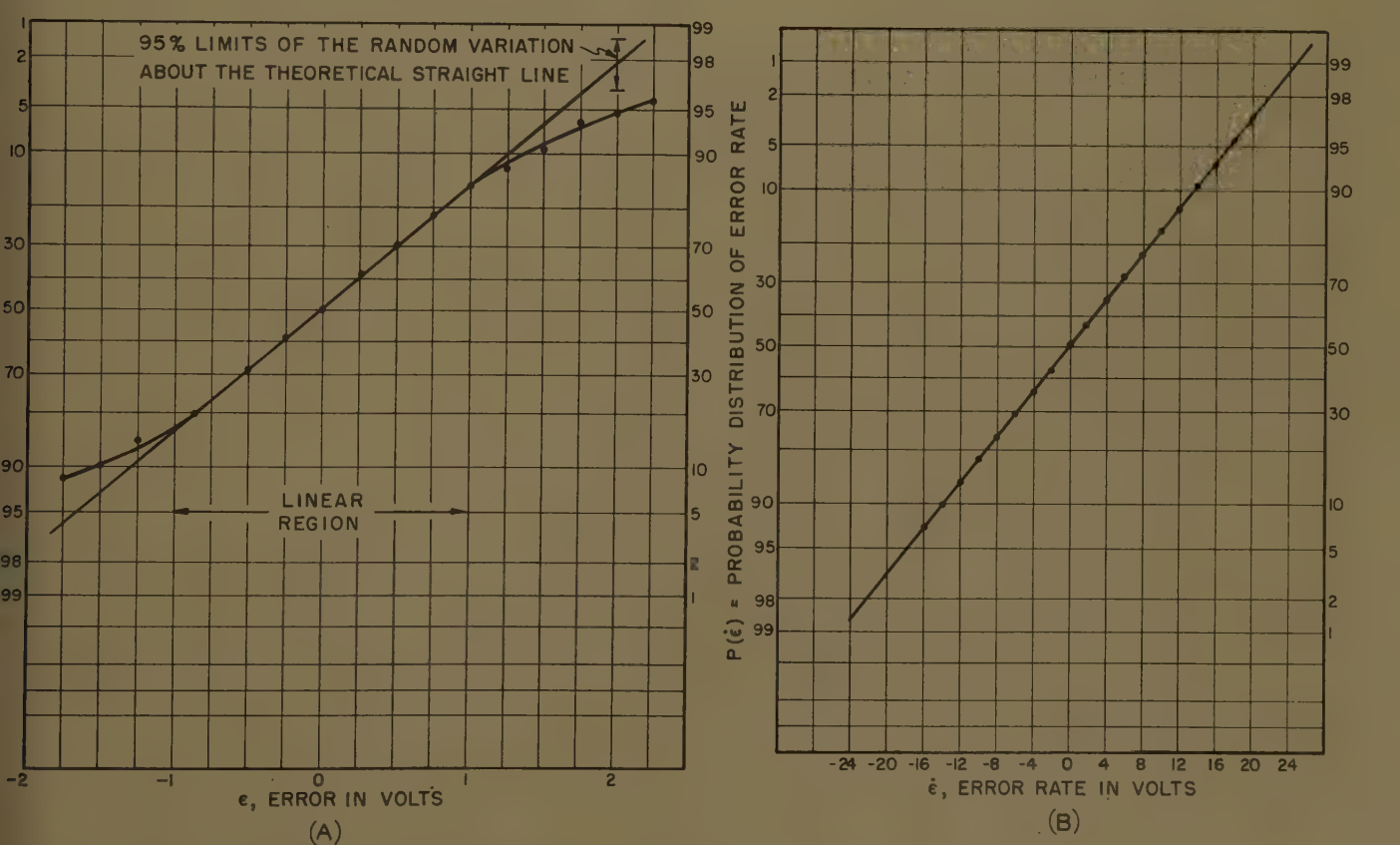

Fig. 4. Probability distribution of second-order servomechanism with saturation

A—Error
B—Error rate

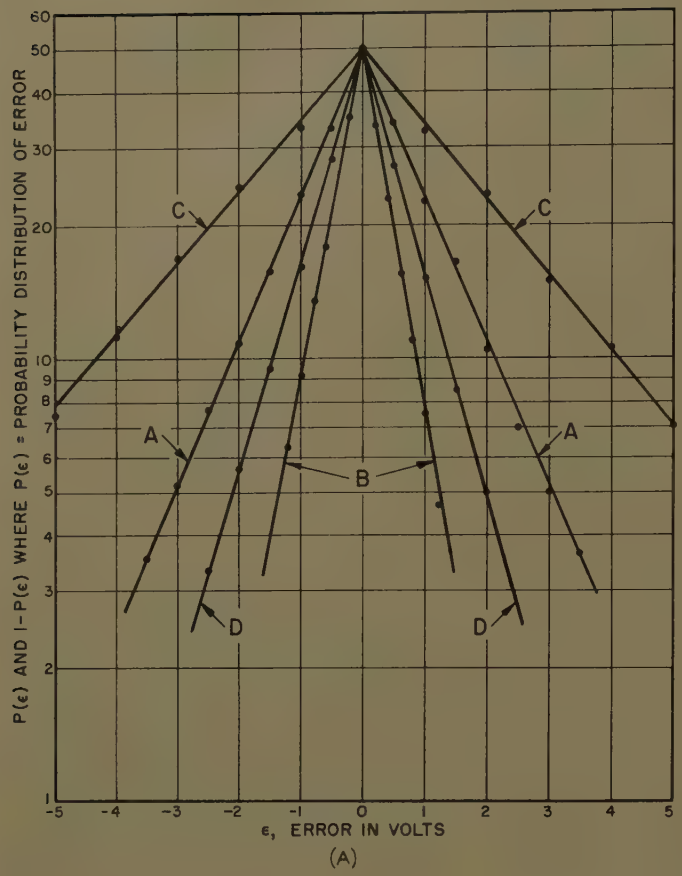

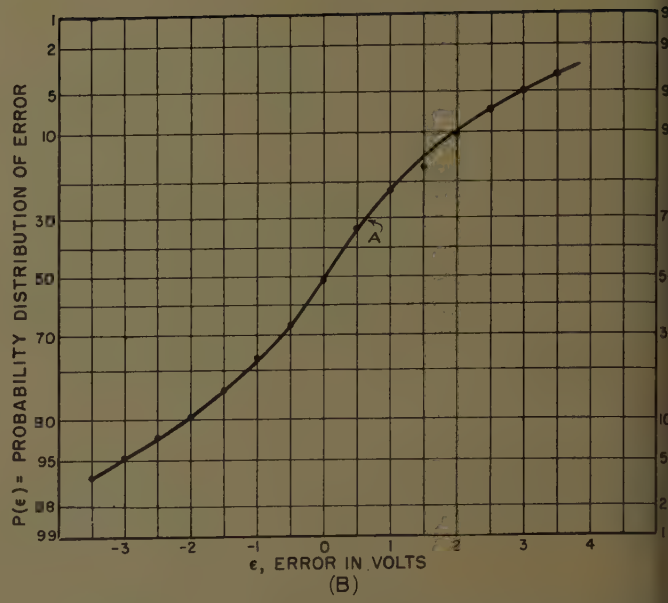

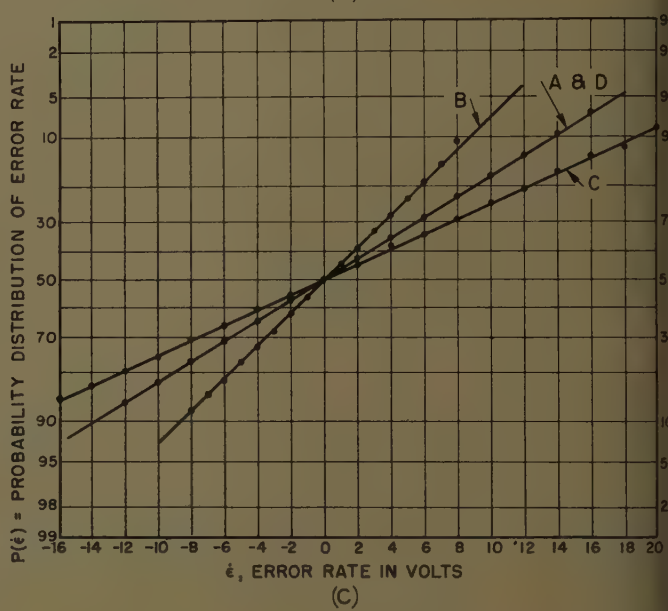

Fig. 5. Error probability distributions of second-order relay servomechanism. B —Plotted on Gaussian paper

system y_1 still retains the Gaussian property. However, the response y_2 itself is changed to a random process that is of a non-Gaussian type.

For the case in which the nonlinear function $K(y_2)$ is approximately linear in the region around y_2, such as the case of saturated amplifier approximated by $K(y_2)=\tanh(cy_2)$, the first probability function $f(y_2,y_1,t=\infty)$ may almost be considered as approximating a Gaussian probability density function. This may be seen from the expression

$$f(y_2,y_1,t=\infty)=A\exp\left(\frac{-a^2}{2D}y_1^2\right)\times\exp\left[\frac{-a}{D}\int\tanh(cy_2)dy_2\right]$$

$$=A\exp\left[\frac{-a^2}{2D}Y_1^2\right]\times\exp\left[\frac{-a}{D}\ln\cosh(cy_2)\right]$$

when $|cy_2|<1$ $\ln\cosh(cy_2)\approx(cy_2)^2$ then

$$f(y_2,y_1,t=\infty)=A\exp\left[\frac{-a^2}{2D}y_1^2\right]\exp\left[\frac{-a}{D}(cy_2)^2\right]$$

which is evidently the same as a Gaussian probability density function.

V. Higher-Order System

The technique applied to a class of second-order systems in section IV can be extended to higher-order systems. However, in the case of higher-order systems, only under very special conditions could the steady-state solution be obtained by the authors. To be specific, only in those systems that can be decomposed into the following form can the steady-state solution of the Fokker-Planck equation be obtained:

$$\frac{dx_i^2}{dt^2}+a_i\frac{dx_i}{dt}+K_i(x_i)+\sum_{j=1}^{N}g_{ij}(x_j)=F_i(t),\quad i=1,2,\ldots,N \qquad (25)$$

where a_i's are constants, $g_{ij}(x_j)$ and $g_{ji}(x_j)$ are of the same functional form, and $F_i(t)$'s are Gaussian white noise. The first probability density function usuall has the following form:

$$f=A\exp\left[\sum_{i=1}^{N}b_iV_i^2+\sum_{i=1}^{N}C_i\int K_i(x_i)dx_i+\sum_{i=1}^{N}d_i\sum_{j=1}^{N}\int g_{ij}(x_j)dx_j\right.$$

where $V_i=dx_i/dt$ and b_i's, C_i's, and d_i are constants. The constant A is th normalization factor.

It should be pointed out that when higher-order system is decomposed into system of equations 25, it is no longer the form of equation 11:

$$\sum_{n=0}^{N}a_n\frac{d^n\theta_0}{dt^n}+K(\epsilon)=\sum_{n=0}^{N}a_n\frac{d^n\theta_i}{dt^n} \qquad (1$$

Consequently, the argument used section III is no longer valid, because this case one cannot write the effecti

ɔut $F(t)$ as a linear combination of the ıe input θ_i. However, if the input is n-Gaussian distributed and the over-all ect of the nonlinear combination of the ıe input θ_i still gives an effective input t), which is Gaussian distributed and s white spectrum, then it is possible to tain the first probability density func-n of this system.

. Computer Study

To verify the result of the analysis esented in the previous sections, an alog computer study was made on a cond-order nonlinear servomechanism. fore the results of the computer study e discussed, the measuring equipment or e single-channel amplitude distribution alyzer will be described. The func-nal diagram of the analyzer is given in g. 3. This analyzer measures the ɔbability distribution function $P(x)$ of random variable x, the relation be-een the probability distribution func-n $P(x)$ and the probability density ıction $f(x)$ which is of the form:

$$x)=\int_{-\infty}^{x} f(x)dx \qquad (26)$$

The resolution of the analyzer was ecked against a known function of time ch as a triangular wave. It may be own the probability distribution func-n $P(x)$ versus the amplitude x of the angular wave theoretically is a straight e. Excellent agreement was found tween the theoretical straight line and e experimental points. The noise gen-tor used was constructed in the Servo-chanism Laboratory, had a flat spec-m from approximately 1/37.5 to 25 les per second and was Gaussian-tributed.

The equation of the second-order vomechanisms under study is of the m

$$+\beta\frac{d\epsilon}{dt}+K(\epsilon)=\frac{d^2\theta_i}{dt^2}+\beta\frac{d\theta_i}{dt}=F(t) \qquad (27)$$

e two different kinds of function $K(\epsilon)$ d are as follows: For the case of the urated amplifier:

$$)=\left\{\begin{array}{l}100,\ \epsilon>1\\ 100\epsilon,|\epsilon|<1\\ -100,\ \epsilon<1\end{array}\right\}\text{ and }\beta=10 \qquad (28)$$

the case of the relay amplifier:

$$)=\left\{\begin{array}{l}K=100,\epsilon>0\\ -K=-100,\epsilon<0\end{array}\right\}\beta=20 \qquad (29)$$

n the case of equation 28 the measure-nts were intended to show the depar-e of the distribution of the error ϵ n normality in the nonlinear region; therefore, under these conditions only, is the test of normality of the error important. To confirm the belief that the departure from normality was not due to statistical fluctuation of the data, a confidence interval test was performed. The results of the experimental data, which were plotted on normal probability papers, are given in Fig. 4(A) and (B). In the second case, a detailed study was made because of the nonlinearity occurring for small values of error as well as for large. It presents, therefore, a severe test of the validity of the analysis given in previous sections.

For equation 27 with $K(\epsilon)$ and β as given in equation 29, the first probability density function $f(\epsilon,\dot{\epsilon})$, according to equation 23, is of the form

$$f(\dot{\epsilon},\epsilon)=A\ \exp\left(\frac{-\beta}{2D}\dot{\epsilon}^2+\frac{K\beta}{D}\epsilon\right)\text{ for }\epsilon<0 \qquad (30A)$$

$$=A\ \exp\left(\frac{-\beta}{2D}\dot{\epsilon}^2-\frac{K\beta}{D}\epsilon\right)\text{ for }\epsilon>0 \qquad (30B)$$

where A is a constant. By using the normalization condition $\int_{-\infty}^{+\infty}\int_{-\infty}^{+\infty}f(\dot{\epsilon},\epsilon)d\dot{\epsilon}\,d\epsilon=1$, it is possible to determine the constant A. The first probability of ϵ alone is determined from the relation:

$$f(\epsilon)=\int_{-\infty}^{+\infty}f(\dot{\epsilon},\epsilon)d\dot{\epsilon}$$

$$=\frac{K}{2D}\exp\left[\frac{K\beta}{D}\epsilon\right]\text{ for }\epsilon<0 \qquad (31A)$$

$$=\frac{K}{2D}\exp\left[\frac{-K\beta}{D}\epsilon\right]\text{ for }\epsilon>0 \qquad (31B)$$

The probability distribution function $P(\epsilon)$, defined in the following, is related to the probability density function $f(\epsilon)$ by the following relations:

$$P(\epsilon)=\int_{-\infty}^{\epsilon}f(t)dt=\frac{1}{2}\exp\left[\frac{K\beta}{D}\epsilon\right]\text{ for }\epsilon<0 \qquad (32A)$$

$$P(\epsilon)=1-\frac{1}{2}\exp\left[\frac{-K\beta}{D}\epsilon\right]\text{ for }\epsilon>0 \qquad (32B)$$

Since the functions $P(\epsilon)$ and $1-P(\epsilon)$ are equal to some exponential functions of ϵ, it is evident that the graph of the data plotted on semilogarithmic paper should be a straight line. Furthermore, if $\epsilon=-D/\beta K$ is substituted in equation 32(A), $P(\epsilon)$ is found to equal 0.1834. Based upon this fact, by finding the point on the graph of $P(\epsilon)$ versus ϵ at which the function $P(\epsilon)$ is equal to 18.34%, it is possible to determine the value of ϵ which corresponds to the quantity $D/\beta K$. The results of the experimental data, plotted on semilogarithmic paper and on normal probability paper, are given in Fig. 5(A), (B), and (C). The effects of the parameters on the probability distribution were checked by comparing the change with an arbitrarily chosen standard system. The theoretical calculation and the measured data are listed in Table I, and the results were amazingly close.

Table I. Theoretical Calculation and Measured Data

Curve	Changed Parameter	Theoretical Calculation	Measured Data	Remarks
B	$D_N=\frac{1}{1.5^2}D_S$	$\frac{D_S}{D_N}=2.25$	$\frac{D_S}{D_N}=2.22$	D_N = changed effective input power spectrum
C	$\beta_N=\frac{1}{2}\beta_S$	$\frac{\beta_S}{\beta_N}=2.0$	$\frac{\beta_S}{\beta_N}=2.0$	β_N = changed damping
D	$K_N=1.5K_S$	$\frac{K_S}{K_N}=0.666$	$\frac{K_S}{K_N}=0.690$	K_N = changed force
A	Standard system			D_S = effective input power spectrum; β_S = damping; K_S = restarting force

Summary Conclusions

The purpose of this paper is to present a method of determining the first probability density function of a nonlinear system subjected to a Gaussian random input. The Markoff random process technique used. The results from the computer study agree with the theoretical calculations within the limits of experimental error. Although this study is limited to a Gaussian input with some definite power spectrum, this analysis can be applied to a large class of nonlinear systems.

References

1. The Analysis of Nonlinear Control Systems With Random Input, R. C. Booton, Jr. *Proceedings, Symposium on Nonlinear Circuit Analysis*, Polytechnic Institute, Brooklyn, N. Y., vol. 2, 1953, p. 369.

2. Some Methods for Analysis of the Flow in Phase-Space, W. Kaplan. *Proceedings, Symposium on Nonlinear Circuit Analysis, Ibid.*, p. 99.

3. M. C. Wang. *Ph.D. Thesis*, University of Michigan, Ann Arbor, Mich.

4. M. C. Wang, G. E. Uhlenbeck. *Reviews of Modern Physics*, New York, N. Y., vol. 17, no. 2 and no. 3, 1945, pp. 323–42.

5. Analytische Methoden der Wahrscheinlichkeitsrechnung, A. N. Kolmogoroff. *Mathematische Annaler*, Berlin, Germany, vol. 104, 1931, p. 436.

Elements of Reactor-Controlled Reversible Induction-Motor Drives

WERNER LEONHARD
ASSOCIATE MEMBER AIEE

THE PROBLEM of controlling continuously the speed of induction motors is as old as the motor itself. Numerous schemes have been developed and successfully applied since the end of the last century. Most of them are relatively efficient but require auxiliary machines. Some are inherently critical in manufacture and operation. As a result, when efficient and continuous speed control over a wide range is necessary, the adjustable-voltage d-c drive is still the most frequent choice.

In a number of applications in the low- and medium-power field, high efficiency is not of primary concern so that speed adjustment under load suffices. This is true for many intermittent drives encountered in material handling processes, overhead cranes, and the like. If induction motors are to be used, they could have secondary resistor control for motoring, and for braking overhauling load, their stators could be excited by direct current, be unsymmetrically connected, or a load brake could be added. Such drives are inefficient except at full speed, but they are simple and inexpensive. Naturally, the quality of control, i.e., the shape of the speed-torque curves obtainable, is very limited.

More recently, techniques, common with small quarter-phase servomotors, have been successfully employed for reversible intermittent drives at ratings beyond 100 kw. Typical examples are crane hoist, bridge, and trolley drives, and, at lower power, rudder control of ships or electrode control of arc furnaces.[1–6] The circuits employ static components, such as saturable reactors and magnetic amplifiers, to control the primary voltages of high-slip induction motors, usually in dependence of the motor speed. Motoring and braking torques for both directions of rotation are available without the use of reversing contactors. The speed-torque curves resemble those of Ward-Leonard drives with smooth speed control extending down to about 1% of synchronous speed. Satisfactory dynamic response and relative stability can be accomplished. Since the efficiency is low at reduced speed, as with secondary-resistor control, the application is normally restricted to intermittent slow-speed duty. The advantages of standard induction motors in conjunction with static-control apparatus are evident since the combination assures high reliability and long-life expectancy.

The historic, but apparently isolated, example of a nonreversing reactor-controlled induction-motor drive was developed by Alexanderson[7] to trim the speed of a 200-kw high-frequency alternator in his transoceanic radio-communication system.

The intent of this paper is to discuss and compare several alternative reactor circuits for reversible-motor control on the basis of their open-loop properties. No effort is made to describe an over-all speed-control system.

Principle of Operation

Symmetrical Control

The two solid curves in Fig. 1 represent the speed-torque curves of a polyphase wound-rotor motor with fixed secondary resistance, when the motor is fed with rated symmetrical line voltages, V_{mo}, of alternative sequence. Each curve consists of three branches, describing oversynchronous regenerative braking, undersynchronous motoring, and counter-torque braking operation. When varying the secondary resistance R_2, the curves are compressed or expanded in the vertical direction, since the slip at which a particular torque, for example pull-out torque, occurs is proportional to R_2. When the motor voltages, V_m, are reduced symmetrically, the curves can also be compressed in the horizontal direction by the approximate factor $(V_m/V_{mo})^2$, thus covering the area between the solid lines and the ordinate axis. Curve *a* in Fig. 1 is an example for $V_m/V_{mo}=0.5$. The reactor-control circuits, to be discussed, are primarily voltage-control schemes, but a variation of the secondary resistance is usually needed when a wide speed range is required. Motor efficiency varies proportionally with the motor speed, when the primary copper, iron, and friction losses are neglected:

$$\eta \leqq n/n_0 \qquad (1)$$

This simplification is justified at high slip, where most of the losses occur in the rotor circuit. With wound-rotor motors the rotor losses present no serious cooling problem due to their mostly being generated outside the motor. Induction motors with eddy-current-type rotors, which would dispose of the slip rings and secondary-resistor control, would require forced cooling except for very light slow-speed duty.

In Fig. 2 a static scheme for voltage control and sequence inversion is drawn.[8] The figure shows a 3-phase motor connected with its primary terminals into a network of six statically adjustable reactors. If their admittances are varied such that either

$$g_{min} \leqq g_1 \leqq g_{max} \qquad g_2 = g_{min} \approx 0 \qquad (2)$$

or

$$g_{min} \leqq g_2 \leqq g_{max} \qquad g_1 = g_{min} \approx 0 \qquad (3)$$

holds, the motor is supplied with adjustable voltages of alternative sequence. The two reactors connected to line terminal *3* may be combined to a single unit.

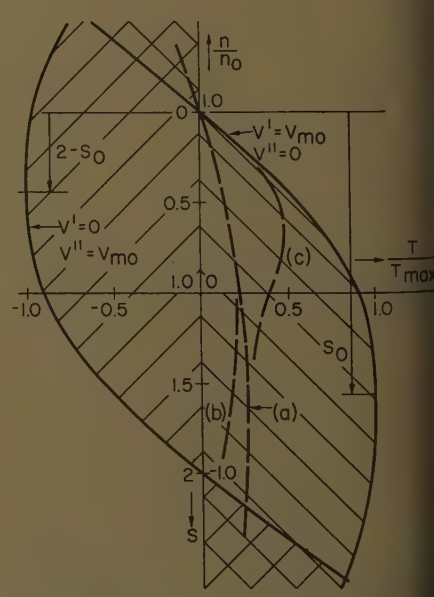

Fig. 1. Speed-torque curves of wound-rotor induction motor

Paper 58-1176, recommended by the AIEE Industrial Control Committee and approved by the AIEE Technical Operations Department for presentation at the AIEE Fall General Meeting, Pittsburgh, Pa., October 26–31, 1958; and re-presented at the Winter General Meeting, New York, N. Y., February 1–6, 1959. Manuscript submitted May 26, 1958; made available for printing July 31, 1958.

WERNER LEONHARD, formerly with Westinghouse Electric Corporation, Pittsburgh, Pa., is now in Stuttgart, Germany.

The contributions of B. H. Beattie of the New Products Engineering Department, Westinghouse Electric Corporation, are gratefully acknowledged. The author wishes also to thank H. A. Zollinger for presenting the paper at the AIEE Winter General Meeting.

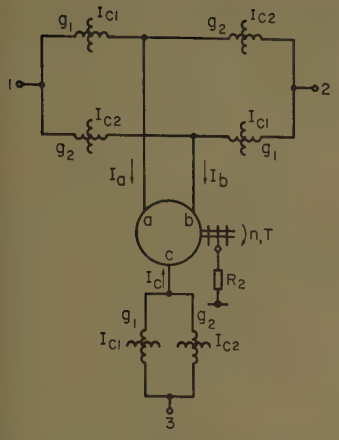

g. 2. Wound-rotor motor with static voltage control

The speed-torque curves for any given ternal-reactance setting will differ from ose obtained with adjustable-voltage ntrol. The reason is that the speed-pendent motor impedances interact ith the fixed external reactances in ch a manner that the motor voltages d hence the torque are reduced as the ip is increased. Fig. 1 demonstrates is effect where curve *a* for constant otor voltage is now transformed into rve *b* for constant external reactances.

The reactors in Fig. 2 usually have the rm of d-c controlled saturable reactors self-saturating magnetic amplifiers doubler connection. Both circuits oduce harmonics and both have non-ear average voltage-current character-ics. The first complication is neglected, t the second may be qualitatively scussed. Figs. 3(A) and (B) depict the ealized output characteristics of a turable reactor and a self-saturating agnetic amplifier. The "low-imped-ce" output of the self-saturating plifier will make the motor character-ic for constant amplifier-control current proach those obtained with straight ltage control (*a* in Fig. 1). In turn, e saturable reactors with their high cremental impedance in the operating gion will distort greatly the motor aracteristics. At speeds close to nchronism, the motor impedance is gh; correspondingly, most of the line ltage appears across the motor, while e reactors, operating in their initial low-pedance region, absorb little voltage. nce the torque approaches that ob-ned with full motor voltage. When the increases, the motor impedance comes lower and the currents rise. a certain value of the motor current, termined by the reactor control current the reactor voltages increase sharply. a result, the motor voltage decreases and the torque falls off rapidly (Fig. 1, curve *c*). This effect may introduce considerable negative slope ($\partial T/\partial s$) at speeds where the original motor characteristic still has definite positive slope. The distortion is most undesirable since it may cause unstable motor operation with constant-torque loads. Although the motor can be safely stabilized by a speed-feedback loop, its design is more difficult. The system then becomes a case of "conditional stability."

The preceding discussion and other aspects, such as reactor size, power gain, and response time, favor the self-saturating amplifiers, but the fact that they introduce rectifiers with relatively low short-time overload capacity into the power circuit limits their application. All the following discussions will deal with the saturable-reactor approach.

Asymmetrical Control

Symmetrical operation is increasingly desirable at higher power ratings where the effect of asymmetrical load on the supply must be considered. On the other hand, past experience has shown that a limited unbalance is not objectionable with high-slip motors of small and medium ratings. Since the size and the cost of the control equipment for reversible drives can be reduced when tolerating asymmetry in the motor supply, these circuits have gained some importance in practice. The restriction to high-slip motors is very important, since with low slip, such as normal National Electrical Manufacturers' Association *B* squirrel-cage motors, the customary dislike of asymmetry in the supply is fully justified. There, already a slight asymmetry, which hardly produces a control effect on the motor characteristics in the usual speed range, increases the motor currents by a substantial amount.[10,11]

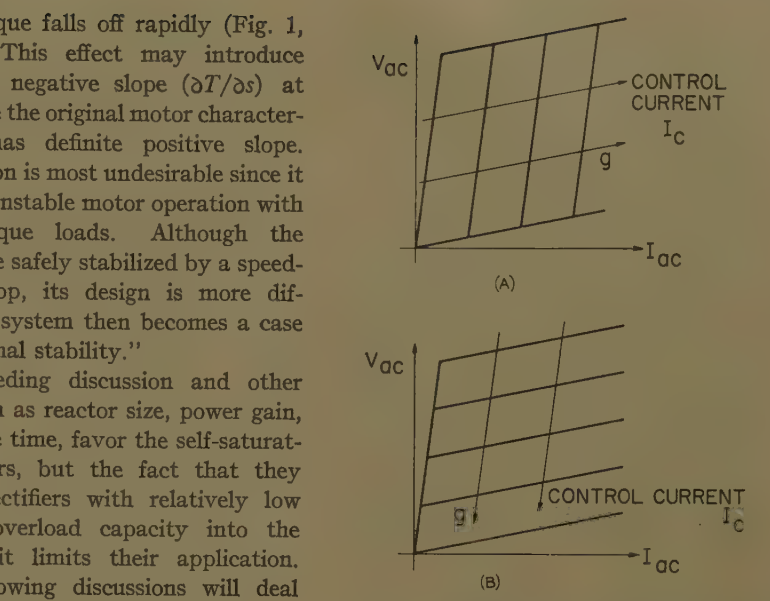

Fig. 3. Voltage-current characteristics of control components

A—Saturable reactors
B—Self-saturating magnetic amplifier

When voltage and current components, $\mathbf{V}'$, $\mathbf{I}'$ and $\mathbf{V}''$, $\mathbf{I}''$ of positive and negative sequences are simultaneously allowed at the motor terminals, the speed-torque area of Fig. 1 may be covered with a multitude of combinations between $\mathbf{V}'$, $\mathbf{V}''$, and R_2. (A zero sequence component cannot exist in the terminal voltages and currents of a symmetrically wound motor when the neutral of its star-connected stator winding is isolated or when its delta-connected stator winding is not altered.) The degree of freedom is illustrated by the fact that the starting torque of an induction motor with a given secondary resistance is proportional to the area enclosed by the vector diagram of the three sinusoidal stator voltages, independent of the shape of the vector diagram.[12] In practice, however, the

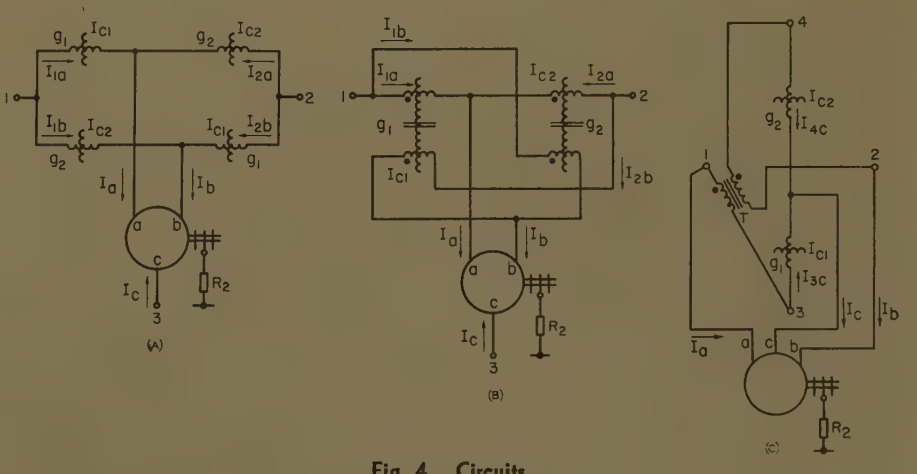

Fig. 4. Circuits

A—4-reactor circuit B—2-saturable transformer circuit C—2-reactor circuit

best possible electrical symmetry is always the aim, even with unsymmetrical circuits, because the simultaneous presence of voltage and current components of both sequences may reduce the efficiency far below the limit indicated by equation 1.

Fig. 4(A) shows the 4-reactor circuit, a simplification of the 6-reactor circuit.[13] Complete control of the motor currents is still possible, since for $g_1=g_2=g_{min}$, no motor phase can carry any appreciable current. The circuit in Fig. 4(B) is obtained by combining the two pairs of reactors in Fig. 4(A) into two "d-c saturable transformers" having the adjustable magnetizing admittances g_1 and g_2.[14] This reduces the eight cores to four larger ones. The control effect is not as good as before, because for $g_1=g_2=g_{min}$, the motor operates on single phase. The same is true for the 2-reactor circuit of Fig. 4(C) which has been frequently applied for crane controls.[2,4] Two terminals of the motor (*a*,*b*) are directly connected to two lines (*1*,*2*). The third motor terminal, *c*, can, by static control of the reactors g_1 and g_2, be positioned between the line (*3*) and the transformer terminal (*4*). Thus, the motor voltages can be made to approach symmetry with positive or negative sequence.

Approximate Analysis of Several Circuits

The circuits described in the preceding section are highly nonlinear and an exact analysis would meet with considerable difficulties. Since our present concern is not an accurate design calculation, but rather a quick comparison of the four circuits on the basis of equal assumptions, a simplified analysis will suffice.

Assumptions

Motor. The single-phase equivalent circuit of an induction motor is shown in Fig. 5(A). V_1 is a line-to-neutral voltage and I_1 the pertinent motor current. The primary-winding resistance, saturation, and iron and friction losses are neglected; X_{L1} and X_m are the primary-leakage reactance and the magnetizing reactance at line frequency; X_{L2}' and R_2' are the reflected secondary-leakage reactance and total rotor resistance per phase. The slip of the rotor against the positive-sequence field is *s*.

The total leakage factor is defined as

$$\sigma=1-X_m^2/(X_m+X_{L1})(X_m+X_{L2}') \qquad (4)$$

the pull-out slip is

$$s_0=R_2'/\sigma(X_m+X_{L2}') \qquad (5)$$

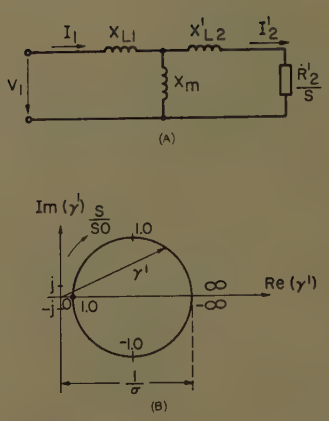

Fig. 5. Induction motor

A—Equivalent circuit
B—Normalized primary admittance

and the motor admittance at no load, $s=0$, is

$$g_{m0}=1/j(X_m+X_{L1}) \qquad (6)$$

With these definitions, the normalized single-phase motor admittance, g_m', may be written as

$$\gamma'=\frac{g_m'}{g_{m0}}=\frac{1+j\frac{1}{\sigma}\frac{s}{s_0}}{1+j\frac{s}{s_0}} \qquad (7)$$

Equation 7 is the well-known circular diagram for the primary admittance of the induction motor; Fig. 5(B). It is completely determined by the relative slip s/s_0 and the leakage factor σ, which is normally around 0.10.

With the foregoing simplifications, the torque T is proportional to the input power of the motor. Assuming a standard overload capacity $T_{max}=2.75\ T_r$, the torque may be expressed in terms of the rated torque T_r:

$$\frac{T}{T_r}=\left(\frac{V_m}{V_{m0}}\right)^2\frac{2T_{max}/T_r}{s/s_0+s_0/s}=\left(\frac{V_m}{V_{m0}}\right)^2\frac{5.5}{s/s_0+s_0/s} \qquad (8)$$

The rated motor admittance, g_{mr}, is of some interest and is derived from equation 7. By inserting $V_m=V_{m0}$ and $T=T_r$ into equation 8, one finds the rated relative slip $s_r/s_0=0.19$. With $\sigma=0.10$, equation 7 results in

$$g_{mr}/g_{m0}=2.10e^{j51\text{ degrees}} \qquad (9)$$

This indicates a motor with a no-load current $I_0=0.48\ I_r$ and a rated power factor $\cos\varphi_r=0.78$. Both are reasonable practical values.

When the motor voltages are asymmetrical, it is necessary to distinguish between the motor admittances g_m' and g_m'' for positive- and negative-sequence voltages, respectively. From equation 7 is found

$$\gamma''=\frac{g_m''}{g_{m0}}=\frac{1+j\frac{1}{\sigma}\frac{2-s}{s_0}}{1+j\frac{2-s}{s_0}} \qquad (10)$$

The resulting torque is obtained by superposition:

$$\frac{T}{T_r}=\left(\frac{V'}{V_{m0}}\right)^2\frac{5.5}{\frac{s}{s_0}+\frac{s_0}{s}}-\left(\frac{V''}{V_{m0}}\right)^2\frac{5.5}{\frac{2-s}{s_0}+\frac{s_0}{2-s}} \qquad (11)$$

where V' and V'' must be computed from the network to which the motor is connected.

Reactors. For ease of analysis, the nonlinear saturable reactors are replaced by linear reactors, having the reactive admittances g_1 and g_2 adjustable between the limits g_{min} and g_{max}. $g_{1,2}$ are normalized with the no-load admittance g_{m0} of the motor

$$\gamma_1=g_1/g_{m0} \qquad \gamma_2=g_2/g_{m0} \qquad (12)$$

In practice, γ is variable by a factor of approximately 200.

It is realized that due to the excessively nonlinear-reactor characteristics, the systems could not be described properly if one were to assume the existence of a unique relation $\gamma(I_c)$ between the reactor admittance γ and the control current I_c. Therefore, $\gamma_{1,2}$ are used as the primary parameters.

Six-Reactor Circuit, Fig. 2

The complete symmetry provided by the conditions 2 and 3 makes the analysis very simple. With equation 2 and $g_{min}=0$, the voltage between two motor terminals, for example *a* and *b*, is, with equations 7 and 12:

$$\mathbf{V}_{ab}/\mathbf{V}_{12}=\gamma_1/(\gamma_1+\gamma') \qquad (13A)$$

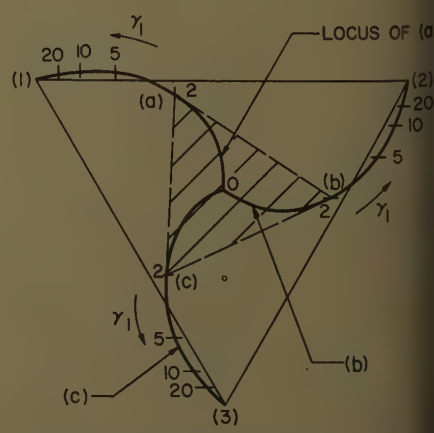

Fig. 6. Voltage diagram of 6-reactor circu

condition 3 is realized instead, the me voltage becomes

$$_{ab}/V_{12} = -\gamma_2/(\gamma_2+\gamma'') \qquad (13B)$$

By inserting equation 7 or 10, the otor voltages may be calculated in ependence of $\gamma_{1,2}$, s/s_0 and σ. Fig. 6 ows the vector diagram of the voltages Fig. 2 with the assumptions $\sigma=0.1$, $s_0=0.25$ (for example $s_0=4$, $s=1$, andstill) and $\gamma_2=0$. The three curves e the loci for the motor voltages as γ_1 varied. If the other reactors are cited instead, equation 3, a will tend its travel towards 2 and b toward while c remains on the path between eutral and 3.

The speed-torque characteristics for osen values of γ, σ, and s_0 may be mputed, for example, by inserting uation 13(A) with equation 7 into 8. he curves are very steep, similar to rve b in Fig. 1. Since they are not entical with the curves for constant actor control current due to the non-earity of the reactors, they are not nsidered now. Of much greater interest, pecially for the asymmetrical circuits, the function relating the motor currents ith torque and speed, since excessive otor heating is a frequent argument gainst reactor control. Fortunately, the nlinearity of the reactor characteristics of little consequence for the current-rque relation.

For the 6-reactor circuit, the motor rrents are derived simply by assuming mmetrical voltage control (equations -9). The resulting curves in Fig. 7 ow the motor current for $\sigma=0.10$ and veral values of relative slip s/s_0. he end point of each curve corresponds full motor voltage, i.e., $\gamma_1=\infty$ or $=\infty$. At no load, the current is zero

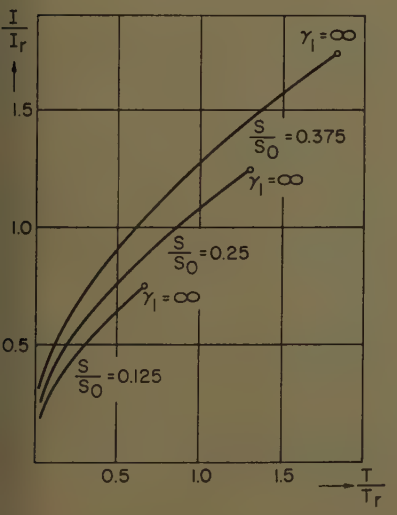

. 7. Motor currents of 6-reactor circuit, symmetrical voltage control

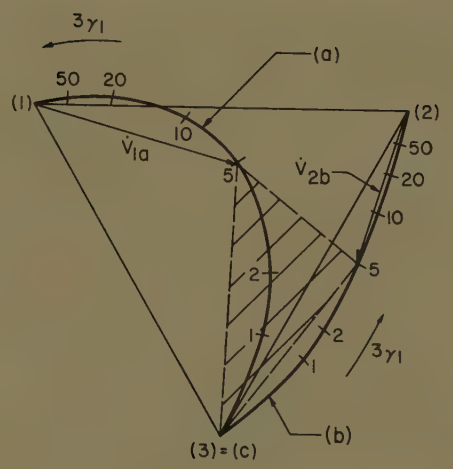

Fig. 8. Voltage diagram of 4-reactor circuit

regardless of speed, because of zero motor voltage.

In practice, the following should be noted. Symmetrical voltage control in accordance with the conditions 2 or 3, causes the torque at a given speed, to increase with the square of the motor voltage. Hence, the torque gain $\partial T/\partial\gamma$ for s=constant at light load is much lower than at full load. When the motor is controlled by a speed-feedback loop, this effects a substantial variation of the loop gain, causing the system to respond quite differently at various operating points. To overcome this, the control characteristics of g_1 and g_2 can be made overlapping such that, at low torque, both channels are partially conductive. This results in circulating currents between lines *1* and *2* and in higher motor currents, but also results in a leveling effect for the torque gain. When the motor delivers load torque of either direction, one set of reactors is driven into and remains at cut-off, while the other begins to control the motor voltages in the usual symmetrical manner. Thus, the deliberately introduced asymmetry raises the current at low load, but in the higher torque region the curves of Fig. 7 remain valid.

It has been pointed out that symmetrical control produces the best efficiency for a given set of parameters s_0, σ, s, and T; therefore, the degree of approximation of the symmetrical conditions is a good criterion for the asymmetrical circuits to be discussed now.

Four-Reactor Circuit, Fig. 4(A)

Due to the asymmetry of this circuit, voltages of both sequences are simultaneously present at the motor terminals. This is true even when following equations 2 or 3 with $g_{min}=0$.

The circuit will be analyzed, with the assumption of finite g_1 and g_2. With $\alpha=e^{-j2\pi/3}$ we define the line voltages:

$$\mathbf{V}_{12}=V_0 \qquad \mathbf{V}_{23}=\alpha V_0 \qquad \mathbf{V}_{31}=\alpha^2 V_0 \qquad (14)$$

the symmetrical components $\mathbf{V}'$ and $\mathbf{V}''$ of the motor voltages:

$$\mathbf{V}_{ab}=\mathbf{V}'+\mathbf{V}'' \qquad \mathbf{V}_{bc}=\alpha\mathbf{V}'+\alpha^2\mathbf{V}'' \qquad \mathbf{V}_{ca}=\alpha^2\mathbf{V}'+\alpha\mathbf{V}'' \qquad (15)$$

and the symmetrical components of the motor currents:

$$\mathbf{I}_c=\mathbf{I}'+\mathbf{I}'' \qquad \mathbf{I}_a=\alpha\mathbf{I}'+\alpha^2\mathbf{I}'' \qquad \mathbf{I}_b=\alpha^2\mathbf{I}'+\alpha\mathbf{I}'' \qquad (16)$$

Equations 14, 15, and 16 contain redundancies.

$\mathbf{I}'$ and $\mathbf{I}''$ are determined by $\mathbf{V}'$ and $\mathbf{V}''$ and the motor admittances g_m' and g_m'':

$$\mathbf{I}'=\frac{j}{\sqrt{3}}\,g_m'\mathbf{V}' \qquad (17)$$

$$\mathbf{I}''=-\frac{j}{\sqrt{3}}\,g_m''\mathbf{V}'' \qquad (18)$$

An inspection of Fig. 4(A) results in the following set of equations:

$$\mathbf{V}_{ab}=V_0+\frac{1}{g_1}(\mathbf{I}_{2b}-\mathbf{I}_{1a}) \qquad (19)$$

$$\mathbf{V}_{bc}=\alpha V_0-\frac{1}{g_1}\,\mathbf{I}_{2b} \qquad (20)$$

$$V_0=\frac{1}{g_1}\mathbf{I}_{1a}-\frac{1}{g_2}\,\mathbf{I}_{2a} \qquad (21)$$

$$V_0=\frac{1}{g_2}\mathbf{I}_{1b}-\frac{1}{g_1}\,\mathbf{I}_{2b} \qquad (22)$$

$$\mathbf{I}_a=\mathbf{I}_{1a}+\mathbf{I}_{2a} \qquad (23)$$

$$\mathbf{I}_b=\mathbf{I}_{1b}+\mathbf{I}_{2b} \qquad (24)$$

Equations 14–24 are solved for $\mathbf{V}'$ and $\mathbf{V}''$. With the abbreviations (equations 7, 10, 12), is found:

$$\frac{\mathbf{V}'}{V_0}=\frac{3\gamma_1(\gamma_1+\gamma_2)+\gamma''(2\gamma_1+\gamma_2)}{(\gamma_1+\gamma_2)[3(\gamma_1+\gamma_2)+2(\gamma'+\gamma'')]+\gamma'\gamma''} \qquad (25)$$

$$\frac{\mathbf{V}''}{V_0}=-\frac{3\gamma_2(\gamma_1+\gamma_2)+\gamma'(\gamma_1+2\gamma_2)}{(\gamma_1+\gamma_2)[3(\gamma_1+\gamma_2)+2(\gamma'+\gamma'')]+\gamma'\gamma''} \qquad (26)$$

As must be expected, the following symmetry conditions hold: for $\gamma_1\longleftrightarrow\gamma_2$ and $\gamma'\longleftrightarrow\gamma''$, i.e., $s\longleftrightarrow(2-s)$, one finds: $V'\longleftrightarrow V''$ or with equation 11: $T\longleftrightarrow -T$. This confirms that equivalent operating conditions exist at any two points in the $T-n$ plane (Fig. 1), symmetrical to the origin. Equal external admittances $\gamma_1=\gamma_2$ and $\gamma'=\gamma''$, i.e., standstill, result in $\mathbf{V}'=-\mathbf{V}''$, or with equation 15: $V_{ab}=0$, $\mathbf{V}_{bc}=-\mathbf{V}_{ca}$. This indicates that the motor then operates on single-phase and, with equation 11, develops no starting torque. $\gamma_1=\gamma_2=0$ corresponds to com-

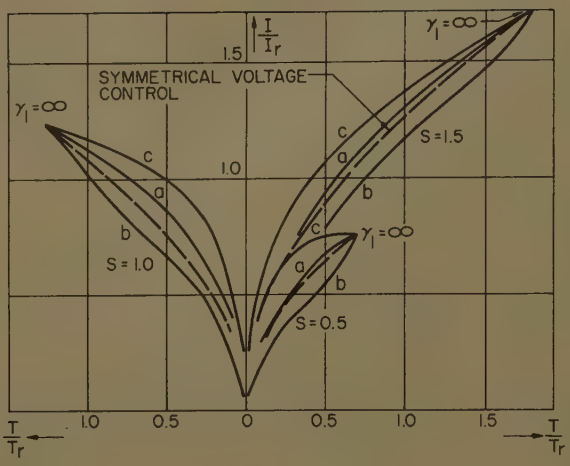

Fig. 9 (left). Motor currents of 4-reactor circuit

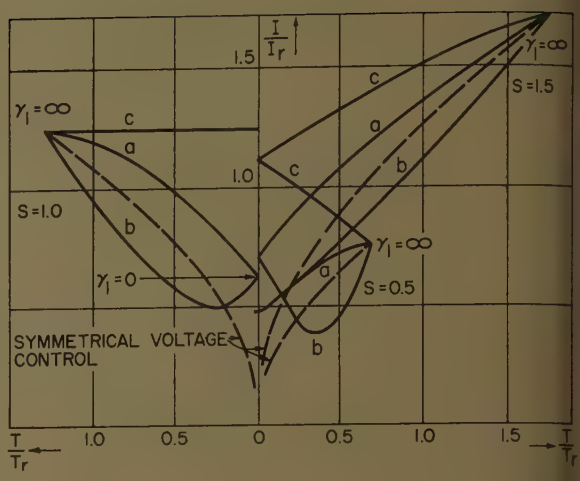

Fig. 11 (right). Motor currents of 2-saturable-transformer circuit

plete cutoff; motor voltages and torque are zero. It is recognized that due to the simultaneous occurrence of γ' and γ'' in equations 25 and 26, the specification of the relative slip s/s_0 is no longer sufficient. Both s and s_0 have to be prescribed.

Figure 8 shows the voltage diagram of the 4-reactor circuit for the following parameters: $\sigma=0.10$, $s_0=4$, $s=1$, $\gamma_2=0$ (i.e., exclusive reactor control, condition 2). When γ_1 is increased from zero, the potentials of the motor terminals *a* and *b* follow the loci towards the potentials of line terminals *1* and *2*. When g_1 is rendered nonconducting and g_2 conductive instead, the loci are interchanged, *a* is then traveling towards *2* and *b* towards *1*. Naturally, the loci are the same only if the motor is at standstill. As noted from Fig. 8, the motor voltages are definitely asymmetrical, but symmetrical conditions are approached at low and at high torque. Since the diagram is drawn for standstill, the shaded area in Fig. 8 is proportional to the starting torque. The preceding remarks with regard to uniform torque gain apply here also. Some overlap of the reactor-control characteristics is desirable to produce consistent response of the speed-feedback loop.

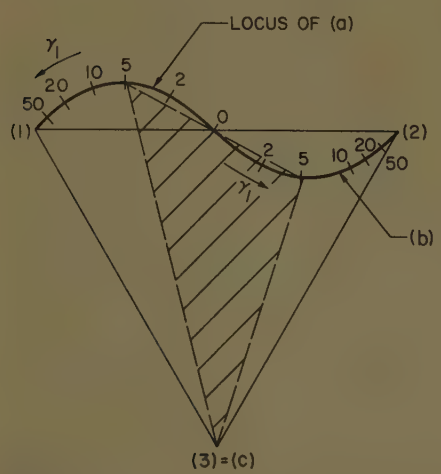

Fig. 10. Voltage diagram of 2-saturable transformer circuit

The motor current-torque function as computed from equations 7, 10, 11, 16–18, and 25–26, is again of special interest. The currents are plotted in Fig. 9 for $\sigma=0.10$, $s_0=4$, $\gamma_2=0$ and $s=0.5$, 1.0, and 1.5. For better visibility, the curves for $s=1.0$ are drawn to the left. A comparison of the currents with those obtained with symmetrical voltage control suggests that the omission of the two reactors in the third motor phase does not greatly affect the motor losses and heating. As seen later, it does allow a substantial saving in components.

Two D-C Saturable-Transformer Circuit, Fig. 4(B)

This circuit is analyzed using the same assumptions as before and equations 14–18. The normalized magnetizing admittances of the saturable transformers are γ_1 and γ_2. Their leakage reactances are neglected. The solutions for $\mathbf{V}'$ and $\mathbf{V}''$ of the network equations are

$$\mathbf{V}'/V_0=(\gamma_1+\gamma'')/(\gamma_1+\gamma_2+\gamma'+\gamma'') \quad (27)$$

$$\mathbf{V}''/V_0=-(\gamma_2+\gamma')/(\gamma_1+\gamma_2+\gamma'+\gamma'') \quad (28)$$

It is recognized that for $\gamma_1=\gamma_2=0$, i.e., no d-c excitation on either transformer, the ratio of the positive- and negative-sequence voltages equals the ratio of the two motor impedances, a characteristic of single-phase operation. Under this condition, the motor will have the well-known z-shaped speed-torque characteristic producing motoring torque in the speed range

$$|n/n_0|<\sqrt{1-(s_0\sigma)^2}$$

The single-phase torque is small for higher values of s_0. For example, $\sigma=0.10$, $s_0=4$ result in a pull-out torque of 0.16 T_r. Consequently, the negative slope $\partial T/\partial s$ in the low-speed region, introduced by single-phase operation with $\gamma_1=\gamma_2=0$, is not too disturbing.

Fig. 10 shows the vector diagram of the voltages in Fig. 4(B), again with the values $\sigma=0.1$, $s_0=4$, $s=1$, $\gamma_2=0$, and $0\leqq\gamma_1<\infty$. The diagram is drawn for standstill, hence the shaded area is proportional to the starting torque. For $\gamma_1=0$, $0\leqq\gamma_2<\infty$, the two loci for the voltages of terminals *a* and *b* are again interchanged. Due to the single-phase excitation, torque becomes immediately available when one of the control currents rises. Therefore, this circuit does not show the low gain at no load, observed with the previous circuits for exclusive reactor control (conditions 2 or 3). However, the asymmetry of the motor voltages is appreciable.

In Fig. 11, the calculated motor current-torque curves are plotted for several speeds, in comparison to those with symmetrical voltage control (values are $\sigma=0.1$, $\gamma_2=0$, $s_0=4$). The curves for $s=1$ are again drawn to the left. The no-load currents are now markedly increased. Note that at stand-by ($s=1$, $T=0$), the motor currents can no longer be "interrupted" by controlling the transformers, but that a contactor operation is necessary.

Two-Reactor Circuit, Fig. 4(C)

With the isolation transformer T_r a fourth supply phase is established. Accordingly, equations 14 are supplemented by

$$\mathbf{V}_{24}=\alpha^2 V_0 \quad (14A)$$

Equations 15–18 remain unaltered. Solving the network equations leads to

$$\frac{\mathbf{V}'}{V_0}=\frac{3\gamma_1+\gamma''}{3(\gamma_1+\gamma_2)+\gamma'+\gamma''} \quad (29)$$

and

$$\frac{\mathbf{V}''}{V_0}=\frac{3\gamma_2+\gamma'}{3(\gamma_1+\gamma_2)+\gamma'+\gamma''} \quad (30)$$

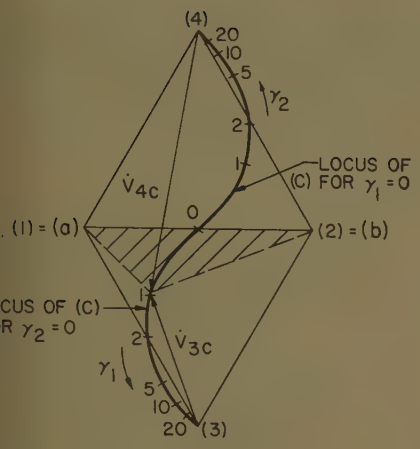

Fig. 12 (left). Voltage diagram of 2-reactor circuit

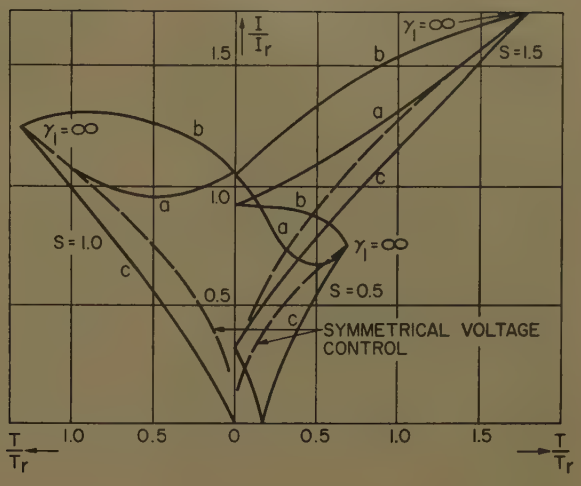

Fig. 13 (right). Motor currents of 2-reactor circuit

comparison of equations 29 and 30 th 27 and 28 reveals that, except for e insignificant variation $\gamma_{1,2} \rightarrow 3\gamma_{1,2}$, ly the sign of $\mathbf{V}''$ is changed. This dicates that the same open-loop speed-rque characteristics are obtained with th circuits. The single-phase operation of course, much more conspicuous now, th two motor terminals directly con-cted to the line.

Fig. 12 represents the voltage diagram the circuit in Fig. 4(C), assuming the evious parameters. For $\gamma_2=0$, $0 \leqq \gamma_1 <$, potential c is moving toward 3. hen the other reactor is excited, c proaches 4. Again, because of the ngle-phase excitation, the torque rises mediately as one reactor is excited. is apparent that the operation of this rcuit resembles most nearly, of all the hemes compared, the type of control at is common with small quarter-phase rvo-motors.

In Fig. 13, the current-torque curves e plotted. They differ from those in g. 11 due to the different sign in uations 28 and 30. The high single-ase current at no load is again character-istic. Since only one motor current can be cut off by reactor control, a line contactor operation is necessary for stand-by. The single-phase current for $\gamma_1=\gamma_2=0$, $a=1$ may be computed as follows:

$$\frac{I_{a,b}}{I_r} = \frac{\sqrt{3}}{2} \frac{g_{m0}}{g_{mr}} \sqrt{\frac{1+\frac{1}{\sigma^2}\frac{1}{s_0^2}}{1+\frac{1}{s_0^2}}} \approx \frac{\sqrt{3}}{2} \frac{g_{m0}}{g_{mr}} \frac{2}{\sigma s_0} \tag{31}$$

The approximation is valid for $s_0 \gg 1$. The ratio g_{m0}/g_{mr} of no load to rated-motor admittance is obtained from equations 7 and 8.

Discussion

Selection of s_0

Before the four circuits are compared on the basis of the calculated motor currents, the reactor sizes, and the control-power requirements, a brief remark on the selection of the secondary resistance (s_0) is appropriate. Since the correct resistance depends on the required speed range and torque, the conditions for a typical crane drive may serve as an example: the motor speed should be variable in ten steps between $s=0$ and $s \approx 2.1$ with the limits corresponding to full-speed hoisting and lowering respectively. Between the steps, that is, mainly around standstill, $0.8 < s < 1.2$, the speed should be continuously variable. The required torque is essentially unidirectional. $T=1.20\,T_r$ is often specified for hoisting (at $s>0.1-0.15$) and $T=T_r$ for lowering speeds. A breakaway torque $1.5\,T_r$ is desirable. Reverse torque is needed during transients and in order to overcome friction, when lowering light loads.

It is evident that the speed range is too large to work with a fixed value of secondary resistance. No compromise could be struck between the contradictory requirements for sufficient motor torque when hoisting at high speed, and for acceptable motor currents and sufficient torque when lowering heavy load. Therefore, the secondary resistance must be varied in accordance with the motor speed or the speed-setting device, for example, the master switch. This complication could be avoided when using a motor with a suitable eddy-current-type rotor.

A typical set of values for the secondary resistance, expressed in terms of pull-out slip s_0 for symmetrical motor operation, is listed in Table I. It is seen that four different values for the secondary resistance are desirable. Note that for high-speed lowering, the motor is operated with negative-sequence voltages. If the hook is loaded, the motor will regenerate.

Motor Currents

As an example of the motor currents to be encountered with the different control circuits, we select from the calculated current-torque curves, drawn in Figs. 7, 9, 11, and 13, those for $s_0=4$, $s=1.5$. A

ble I. Pertinent Values of Slip and Pull-Out Slip; Symmetrical Operation for Typical Crane Drive ($s=0$: Full-Speed Hoisting)

.....	0–0.2	0.3–0.6	0.6–1.2	1.2–2.0	2.0–2.1
.....	0.4–0.5	1.0–1.2	2.2–2.5	3.5–4	0.4–0.5

Table II. Comparison of Four Reactor Circuits; $\sigma=0.10$, $s_0=4$, $s=1.5$

	6-Reactor Circuit (a)	4-Reactor Circuit (b)	2-Saturable-Transformer Circuit (c)	2-Reactor Circuit (d)
Equivalent Symmetrical Motor Current				
0	0	0	0.82 I_r	0.82 I_r
0.5 T_r	0.91 I_r	0.94 I_r	1.08	1.08
T_r	1.27	1.28	1.34	1.34
Rating Factor of Main Control Components				
	3.80	3.00	2.66	2.96
Relative-Control Power				
	1.0	0.73	0.44	0.46

comparison with Table I shows that this corresponds to a practical operating condition for a crane drive. The three motor currents at a given torque are combined to an equivalent symmetrical motor current, which would result in the same copper and secondary resistance losses. Table II contains these equivalent currents referred to rated current for the four circuits. Since the equivalent motor current depends only on the magnitude of the positive- and negative-sequence current components, identical results are obtained with circuit *c* and *d*, even though the motor currents themselves are different. The relatively high no-load currents of circuits *c* and *d* reflect the large asymmetry, but as pointed out earlier, the no-load currents of circuits *a* and *b* will also rise in practice, due to overlapping reactor control. At full torque, the circuits are almost equivalent, since each approaches symmetrical conditions. This is similarly true for other suitable combinations of s and s_0 (Table I).

Rating of Control Components

As an indication of the size and cost of the major control components, a rating factor

$$f_R = \frac{\frac{1}{2}\sum V_n I_n}{\sqrt{3}\, V_{m0} I_{mr}} \qquad (32)$$

is defined relating the 2-winding transformer capacity of the saturable reactors and the isolation transformer, at the given duty cycle, to the nominal primary motor kva. The load and control windings of the saturable reactors are assumed to have equal rating. In the case of the two saturable transformers, the control windings are determined by the vectorial sum of both alternating load currents. In systems where the two reactor channels have different duty cycles, for example in hoist drives, the UP and DOWN channels may be designed for different ratings; for simplicity, it is assumed that the two channels in each circuit are equal. This is frequently so in practice. Using as a base $\sigma = 0.10$, equation 2 or 3, and the parameters $s_0 = 4$, $s = 1.5$, $T = T_r$, the rating factors of Table II were computed.

Reactor-Control Power

An important point of comparison is the amount of control power required to excite the reactors in each circuit since it affects the rating of the control source. Frequently a 2-channel magnetic amplifier or, for larger drives, a rotary exciter is used.

Since, with the different circuits, the total control power is supplied to one, two, or three reactors of different ratings P_L, the control power P_c, i.e., the losses in the reactor-control winding, must be known as a function of the reactor size. Design data for commercially available reactors indicate that the following empirical relation holds:

$$P_{c1}/P_{c2} = (P_{L1}/P_{L2})^x \qquad (33)$$

with $x \approx 0.5$ for $3 < P_L < 50$ kva, and $x \approx 1.0$ for $60 < P_L < 200$ kva.

In the preceding section, the reactor ratings, P_L, were determined with $\sigma = 0.10$, $s_0 = 4$, $s = 1.5$, $T = T_r$. It is assumed that all reactors fall in the lower power range. For convenience, the control power computed for each circuit is referred to that for the 6-reactor circuit. If the relative amounts of forcing are assumed to be the same in all four circuits, the results, listed in Table II, are representative for ratings of the control sources required. Table II shows a substantial saving in control power with the last two circuits. This is to be expected because they have only one reactor in operation at a time.

Results

The rating factors, control power requirements, and consequently the costs, appear to favor the 2-saturable transformer and the 2-reactor circuit. A distinct disadvantage of these schemes, however, is the fact that the single-phase motor current cannot be reduced by reactor control. This is of special importance on crane drives having frequent stand-by periods. Also, the asymmetry of the motor voltages and currents is relatively large at low load.

The 6- and 4-reactor circuits appear more favorable in these respects. By properly biasing the magnetic control amplifiers, all motor currents can be reduced to the reactor magnetizing current, i.e., below 0.1 I_r. Thus, the motor may be kept on the line for stand-by periods whose lengths are not limited by thermal considerations. This eliminates frequent in-rush currents and voltage surges with their detrimental effects on the motor life. When comparing the 6-reactor with the 4-reactor circuit, one notes that the electrical symmetry is obtained at considerable cost. Therefore, in cases where complete symmetry is not mandatory, the 4-reactor circuit should be a good compromise.

A final argument for the 6- and 4-reactor circuits lies in the fact that they are adaptable for faster responding and more accurate drives, due to the fact that they can better accommodate saturable reactors with series-connected load windings. By paralleling the pertinent reactor-control windings and inserting a common forcing resistor in each channel, the following will be obtained:

1. Due to the proper phase relation between the induced even-harmonic voltages, harmonic currents circulate unimpeded through the parallel connected control windings. (This statement is exact only for the 6-reactor circuit where the even harmonics in the three reactor-control windings of each channel form symmetrical 3-phase voltage and current systems. With the 4-reactor circuit, it is an approximation, Fig. 8, but the circuit was found to operate very satisfactorily. The same principle was used by Alexanderson[7] in his quarter-phase motor-control scheme.) This results in lower distortion of the motor voltages.
2. The reactors do not depend on even harmonic currents flowing through the control source where they could interact with a magnetic amplifier.
3. By forcing, the reactor-response times can be effectively reduced. This is of paramount importance for obtaining fast, accurate, and stable speed-control loops.

The 2-reactor and the 2-transformer schemes have only one reactor conducting at one time. When employing series-type reactors, appreciable harmonics would appear at the motor terminals and in the control circuit having detrimental effects on the motor and a magnetic preamplifier. On the other hand, parallel-type reactors with their slow response impose serious limitations on the performance of a control system.

Comparison Tests

General

In support of the analysis, a number of laboratory tests were undertaken. A few of the results will be shown.

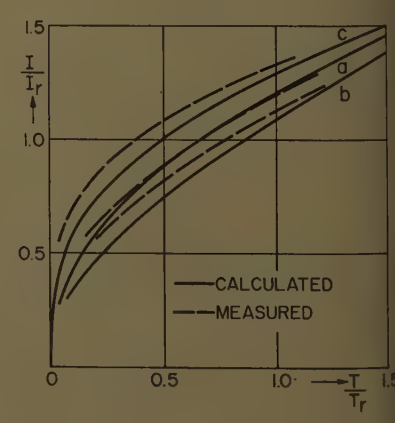

Fig. 14. Motor currents versus torque for 4-reactor circuit

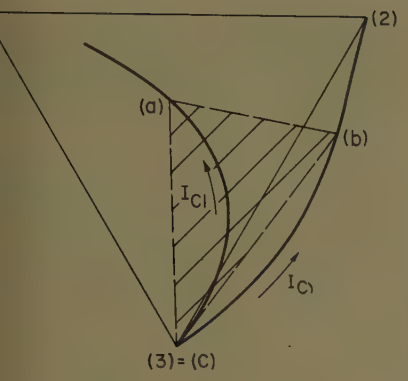

15. Measured voltage diagram of 4-reactor circuit

$\sigma = 0.11$
$I_{c2} = 0$
$s_0 = 3.6$
$s = 1.0$

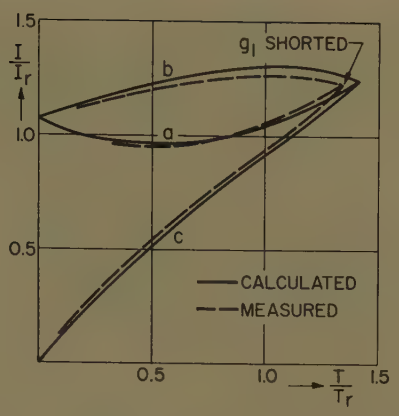

Fig. 16. Motor currents of 2-reactor circuit

$\sigma = 0.11$
$\gamma_2 = 0$
$s_0 = 3.6$
$s = 1.0$

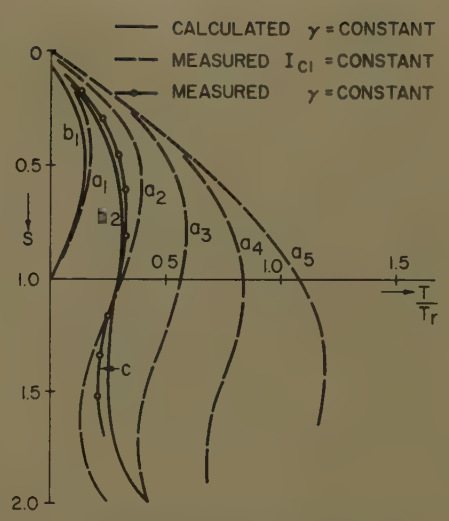

Fig. 17. Open-loop speed-torque characteristics of 2-reactor circuit

$\sigma = 0.11$
$\gamma_2 = 0$
$s_0 = 3.6$

he standard wound-rotor motor used the tests had the following specifica-s: 15 horsepower; 1,150 rpm; 220 s, 42.6 amperes primary; 240 volts, 5 amperes secondary, cos $\varphi_r = 0.79$, oad current 19.5 amperes; maximum ue 190 foot-pounds; rated torque 69 -pounds.

rom measurements with symmetrical age, a leakage factor $\sigma = 0.10-0.11$ deduced.

he 4- and the 2-reactor circuits were ed; accordingly, two types of re-rs were needed:

actor circuit.
-c: 220 volts, 40 amperes
-c: main winding, N_0, 4.35 ohms, 5.5 amperes
two auxiliary windings, 0.25 N_0, 1.30 ohms, 5.5 amperes

actor circuit.
-c: 380 volts, 40 amperes
-c: main winding, N_0, 5.2 ohms, 5.5 amperes
two auxiliary windings, 0.25 N_0, 1.4 ohms, 5.5 amperes

he single-phase transformer for the actor circuit was designed for 220 s, 40 amperes, primary and secondary. ratings correspond to intermittent y (10%). All reactors were of the llel type; those for the 4-reactor uit were later rewound for series ation.

T With the 4-Reactor Circuit

s an example, the three motor currents sured with $s_0 = 3.6$, $s = 1.5$, are com-d with the results of the calculation ig. 14. The measurement was taken one pair of reactors unexcited, i.e., at minimum admittance. Consider-the crude approximations in the se of the analysis, the agreement is Some of the discrepancies may be explained as follows: For the calculation, it was assumed that the two conducting reactors have equal admittances, whereas in practice, they have equal control currents. If the reactor voltages differ (as seen from Fig. 8, V_{1a}, V_{2b}), the admittances will also be different. As a qualitative description, it can be stated that the constant-current branches of the reactor characteristics tend to equalize the currents in the two controlled motor phases. This is clearly seen from Fig. 14 (I_a, I_b).

Fig. 15 is the measured voltage diagram for standstill. A comparison with Fig. 8 indicates that the analysis describes the system properly.

Two-Reactor Circuit

In Fig. 16, calculated and measured motor currents are compared. The agreement is better than before because now the admittance of a single reactor is the only implicit parameter. This reduces the effect of the nonlinear-reactor characteristics.

Fig. 17 shows some open-loop speed-torque curves, measured for constant reactor control current ($a_1 - a_5$). With both reactors set at minimum admittance, a_1 corresponds to single-phase operation. The curves b_1 and b_2 are calculated using the admittance parameters b_1: $\gamma_1 = \gamma_2 = 0$, b_2: $\gamma_1 = 2/3$, $\gamma_2 = 0$. While b_1 is in reasonable agreement with a_1, b_2 deviates considerably from curve a_2 for constant-control current. The distortion is due to the nonlinearity of the reactors as previously discussed. This explanation is supported by curve c, which was measured with constant-reactor admittance ($\gamma_1 \approx 2/3$. The curve was obtained by varying suitably the reactor control current during the test.

Conclusions

This paper presents a discussion and a simplified analysis of several reversible reactor-control schemes for intermittent induction-motor drives. The principles of the control operations are explained and numerical data are derived suitable for a comparison of the different circuits. Test results indicate that the theory, despite its simplicity, offers an adequate description of the major phenomena.

The evaluation suggests that the 4-reactor control circuit is most desirable for medium-power applications because it combines acceptable electrical symmetry with good operational characteristics (reduced line contactor duty, lack of frequent in-rush currents, fast response). At the same time, it offers a cost compromise between the simpler reactor-control schemes with their high electrical asymmetry and the fully symmetrical but more expensive 5- or 6-reactor control circuits.

The discussion is restricted to the open-loop characteristics and does not include the speed-feedback loop necessary to impart to the reactor-controlled induction motor the properties of an adjustable speed drive. Development is directed toward the more extensive use of motors with simple eddy-current rotors. By eliminating the secondary resistor control, an important step could be made towards an all static induction-motor control.

References

1. Variable-Unbalanced-Voltage Control, W. R. Wickerham. *AIEE Transactions*, vol. 64, 1945, pp. 98–102.

2. Load-O-Matic A-C Crane Hoist Control, W. R. Wickerham. *Westinghouse Engineer*, Pittsburgh, Pa., Mar. 1952, pp. 56–61.

3. Ein neue Elektrodenregelung mit Magnetverstärkern, Wilhelm Kafka. *Stahl und Eisen*, Düsseldorf, Germany, 1956, pp. 381–90.

4. A-C Crane Control with Load-O-Matic, H. A. Zollinger. *Westinghouse Engineer*, Mar. 1957, pp. 54–57.

5. Speed Control of Induction Motors Using Saturable Reactors, P. L. Alger, Y. H. Ku. *AIEE Transactions*, vol. 75, pt. III, 1956 (Feb. 1957 section), pp. 1335–41.

6. Der durch Magnetverstarker gestcuete Asynchronmotor, W. Kafka, W. Doell. *Elektrotechnische Zeitschrift*, Wuppertal-Elberfeld, Germany, vol. 78, 1957, pp. 884–90.

7. Transoceanic Radio Communications, E. F. W. Alexanderson. *AIEE Transactions*, vol. 38, pt. II, Oct. 1919, pp. 1269–85; also *General Electric Review*, Schenectady, N. Y., vol. XXIII, no. 10, 1920, pp. 794–804.

8. Motor Control Apparatus, W. C. Carl, E. C. Rhyne, Jr. *Patent Case no. 28,056, Serial no. 521076*, Westinghouse Electric Corporation, East Pittsburgh, Pa., 1955.

9. An Electrical Servo-Mechanism With Speed Regulation, O. I. Aven, E. D. Demidenko, S. M. Domanitsky, E. K. Krug. *Avtomatika i Telemekhanika*, Moscow, USSR, vol. XVII, no. 3, 1956.

10. Unbalanced Voltage and Wound-Rotor Motors, R. F. Woll. *Westinghouse Engineer*, Ma 1944.

11. Operation of 3-Phase Induction Motor on Unbalanced Voltages, J. E. Williams. *AIE Transactions*, vol. 73, pt. III-A, Apr. 1954, p 125–33.

12. Anwendung der Methode der sy metrischen Komponenten auf unsymmetrisch Ständerschaltungen von Drehstromasyn chronmotoren, Heinz Jordan. *Archiv für Ele trotechnik*, Berlin, Germany, vol. 30, 1936, pp. 81 18.

13. Alternating Current Hoist Contro W. R. Wickerham. *U.S. Patent 2,440,319*, Apr. 2 1948.

14. *U.S. Patent*, W. R. Wickerham.

Discussion

H. Gleixner (General Electric Company, Schenectady, N. Y.): Mr. Leonhard's paper is very interesting. It describes four distinct types of reactor-controlled motor drives and it presents their advantages and disadvantages. The author suggests the 4-reactor control circuit as best from an overall viewpoint considering cost as well as performance. However, this scheme does introduce a good deal of current unbalance. As the author points out, unsymmetrical circuits cause extra motor heating and have other disadvantages.

I should like to offer for consideration a circuit that has recently been announced by the General Electric Company and has been described by L. R. Foote.[1] This circuit uses two saturable reactors and one saturable transformer. The power circuit is shown in Fig. 18. For positive torque, reactors *SX1* and *SX2* are saturated. The transformer secondary (*SXT-S*) is connected so that its output voltage is 180 degrees out of phase with its primary voltage (*SXT-P*). The motor terminals *T1*, *T2*, and *T3* are effectively connected to lines *L2*, *L1*, and *L3* respectively. For negative torque, reactor *SX2* and the transformer *SXT* are saturated. Motor terminals *T1*, *T2*, and *T3* are effectively connected to lines *L1*, *L2*, and *L3*. Intermediate values of torque are obtained by varying the amount of saturation.

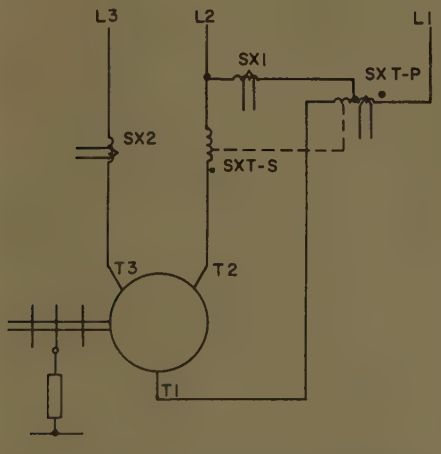

Fig. 18. Reactor-controlled reversible induction-motor drive

SX1, SX2 = saturable reactors
SXT = saturable transformer

Reactor *SX2* is used to provide the desired symmetry. The transformer primary is an autotransformer which provides compensation for the voltage drop in reactor *SX1*.

Using comparison Table II of Mr. Leonhard's paper, for the same secondary resistance values, the circuit just described should have equivalent symmetrical current values between those listed for 6-reactor and 4-reactor circuits. With reactors *SX1* and *SX2* saturated, the only unbalance is caused by the small voltage drop across the reactor *SX2*. The voltage drop across *SX1* is compensated for by the autotransformer action of the transformer. In the negative direction, a slight unbalance may occur due to some difference in impedance of the transformer and the reactor *SX2*. Nearly balanced currents are maintained throughout the entire speed range. At no time does single phasing occur.

Using a reactor-rating method which takes into account the motor current at full load, minimum slip and the maximum voltage drop across the primary control components, it is my belief that this new circuit requires considerably less main-control components rating than the 6-reactor circuit and slightly less than the 2-reactor circuit. It follows that the control-power requirements should also be less for this new circuit.

I concur with the author in that a limited unbalance is permissible for high-slip motors, particularly for wound-rotor motors with high secondary resistance. However, any unbalance causes extra motor heating, particularly in the low-slip range of operation. Therefore, the fact that the new circuit just described maintains nearly balanced currents for the full range of operation is a marked advantage.

A decrease in torque gain at light load is noted by Mr. Leonhard in paragraph 4 under "Six-Reactor Circuit, Fig. 2" in the section "Approximate Analysis of Several Circuits" describing the completely balanced 6-reactor circuit. His method of compensating for this effect is to overlap the conductance of the reversing reactors. In the case of a crane drive, it may be more desirable to retain the variation in gain in favor of the reduced line current with reduced motor and reactor heating. Further, if a stepless reference is provided for the regulator, the desired light-load speed can be obtained by manipulation of the master switch.

Under the subject of "Reactor-Control Power," the author indicates a rotary exciter for the control source of larger drives. It would be interesting to know at wha horsepower Mr. Leonhard recommend changing over from magnetic amplifiers t rotating exciters.

Reference

1. Adjustable Speed Control of A-C Motors L. R. Foote. *AIEE CP59-84* (available on re quest).

Werner Leonhard: Mr. Gleixner present a very interesting reactor-control scheme fo reversible induction-motor drives. How ever, some of his statements may warrant closer examination.

In order to compare his circuit with thos discussed in the paper (Table II), we refe to the same set of parameters: $\sigma=0.1$ $s_0=4$, $s=1.5$, $T=T_r$. For simplicity, w assume first that the circuit provide perfect symmetry of the motor voltages an currents ($I_m=1.27\,I_r$). Also, we neglect th extension of winding *SXT-P* beyond th connection with *SX1*. Thus, the ratin factor of the major control components computed as: $f_R=3.05$, which is slightl higher than the corresponding figure of th 4-reactor circuit. *SX1* and *SXT* accoun for the main portion of f_R. *SX1* ha approximately the size of one reactor in th 2-reactor scheme (it carries the difference o two motor currents), while *SXT* is simila in size to one of the transformers in the saturable transformer circuit covered in th paper.

When estimating the relative magnitud of the required control power, one find again with the assumptions on which Tabl II is based, the following figures: *SX* 0.48; *SX2:* 0.28; *SXT:* 0.46. For pos tive torque (*SX1* and *SX2* saturated), th total relative control power amounts t 0.76, and for negative torque, the figure i 0.74. These values are again very close t those of the 4-reactor circuit. When thre separate amplifiers are employed for excitin the three reactors, a slight advantage i total amplifier rating but probably not i cost, is realized in that the control source fo *SX2* does not need to be duplicated. Whe instead *SX2* is alternatively excited fro one of two control amplifiers, their pow rating is directly comparable to the amplifie rating needed with the 4-reactor circuit.

The new circuit is claimed to yield bett symmetry than the 4-reactor circuit. U doubtedly, measurements are given reference 1 of Mr. Gleixner's discussion substantiate this claim. In the meanwhil I submit some considerations which lead m to believe that Mr. Gleixner's statemen

arding symmetry may be somewhat op-istic. Consider first the case where *SXT* *SX2* are excited. *SX2* is inserted in motor phase while the two others con- reactances of the two transformer load dings. If they were independent re-ances as Mr. Gleixner assumes, it would n indeed that nearly perfect symmetry ld be achieved. However, since the dings are in close proximity, linking the e cores, there will be a certain amount of tual coupling. As can be deduced from . 10, any coupling between *SXT-P* and *T-S* will cause asymmetry of the motor ages. When *SXT* is fully saturated, degree of coupling between the load dings may be small but is certainly not ligible. For partial excitation of *SXT* *SX2*, considerable coupling and hence mmetry of the motor voltages must be ected.

imilar conditions exist when *SX1* and *2* are excited. The transformer *SXT*, whose primary voltage depends on the voltage across *SX1*, will cause asymmetry. Again, this will be particularly pronounced for partial excitation.

It would be interesting to know how the problem of controlling the reactors and the transformer from the control amplifiers has been solved. As pointed out in the paper, proportional control of an individual saturable reactor from a magnetic amplifier may require that the reactor be of the slow-responding-parallel type or that the harmonics in the control winding of the series-type reactor be by some means kept away from the rectifiers of the magnetic amplifier. With the proposed circuit, this will present some problems since the two reactors and the transformer are all of different ratings and do not permit convenient interconnections of the control windings as is possible with the 4-reactor circuit. There, the control windings of pairs of four equal-series-type reactors can be paralleled forming low-impedance circulating paths for the larger harmonics.

It may not have been made sufficiently clear in the paper that the overlap of the conductance regions of the reversing reactors is an optional measure. If, in a certain case, the increase of the motor currents prohibits an overlap, it may be omitted. In that case, the speed-control loop will show in the low-torque region a sluggish response and increased regulation. Otherwise, there are no detrimental effects.

The question as to when rotating exciters may become advantageous as control sources for the reactors is difficult to answer. It depends, of course, on the availability of the larger amplifiers and the relative cost. The fact that one rotating exciter would replace both amplifier channels is worth mentioning. If drives of this type with a rating of several hundred horsepower are ever designed, it seems that rotating exciters should certainly be considered.

The Linear Least Squares Synthesis of Multivariable Control Systems

R. C. AMARA
NONMEMBER AIEE

A MULTIVARIABLE system is characterized by a multiplicity of uts and outputs. In the following, it be assumed that such systems can described by linear, time-in variant, ut-output relations over the whole ge of operation or over the restricted ge of interest. Thus, let

$$\begin{vmatrix} r_1 \\ r_2 \\ \cdot \\ \cdot \\ \cdot \\ r_p \end{vmatrix} \quad C = \begin{vmatrix} c_1 \\ c_2 \\ \cdot \\ \cdot \\ \cdot \\ c_q \end{vmatrix} \quad A = \begin{vmatrix} a_{11}a_{12} \cdots a_{1p} \\ \cdot \quad\quad \cdot \\ \cdot \quad\quad \cdot \\ \cdot \quad\quad \cdot \\ \cdot \quad\quad \cdot \\ a_{q1} \cdots \cdots a_{qp} \end{vmatrix} \tag{1}$$

n, the system input-output relation y be expressed compactly as

$$AR \tag{2}$$

ere R, C, and A are input, output, and nsfer-function matrices respectively; Fig. 1. It is seen that a multivariable em derives each output by a simul-eous operation on all its inputs. thermore, it is apparent that the s of multivariable systems includes the mon single-variable system as a ial case.

umerous practical examples of multi-able control systems can be cited. of the first to receive attention as such the turbojet engine. In this case, there are two principal inputs, namely, rate of fuel flow and exhaust nozzle area, and the two outputs, engine speed and engine temperature. Adjustment of either input affects both quantities simultaneously. A steel-rolling mill represents an example of a system with many more variables. Here the input variables can be such quantities as steel input gage, rolling speed, distance between rollers, and roller torque, while the output quantities may be steel output gage and steel tension between rolling stands. Other examples are provided by any number of manufacturing and chemical processes in which the control of each output quantity depends on the precise control of several input variables.

The general objective to be achieved by a multivariable control system may be stated simply as follows: to operate on the input variables in such a way that the output variables behave as closely as possible in a desired or prescribed manner. As in single-variable systems, feedback may or may not be used for this purpose. In addition, as in the single-variable case, a multivariable system may be assumed to operate entirely with continuous signals, entirely with discrete signals, or with combinations of both. In this connection, it may be noted that one of the principal reasons for the rapid growth in interest in multivariable systems may be traced to the possibility of using discrete elements, or digital computers, to perform the required control function.

The primary purpose of this paper is to describe a practical synthesis procedure for multivariable control systems subject to stationary stochastic inputs. Although the analysis deals only with a consideration of the continuous signal case, an extension of the method to hybrid (continuous-discrete) and discrete signal systems way be readily made.

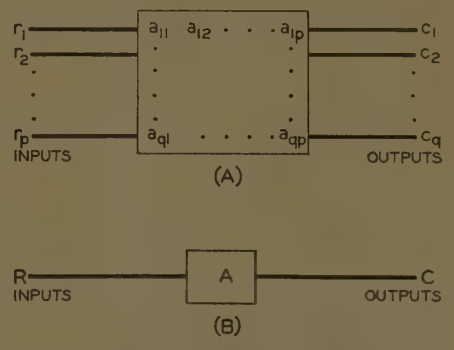

Fig. 1. Representations of linear multivariable system

Paper 59-214, recommended by the AIEE Feedback Control Systems Committee and approved by the AIEE Technical Operations Department for presentation at the AIEE Winter General Meeting, New York, N. Y., February 1–6, 1959. Manuscript submitted August 27, 1958; made available for printing December 19, 1958.

R. C. AMARA is with the Stanford Research Institute, Menlo Park, Calif.

Appreciation is expressed for the continuous encouragement and advice given by Prof. G. F. Franklin of Stanford University under whose supervision this study was undertaken. Acknowledgement is also made of the stimulating guidance provided by Dr. T. H. Meisling of Stanford Research Institute.

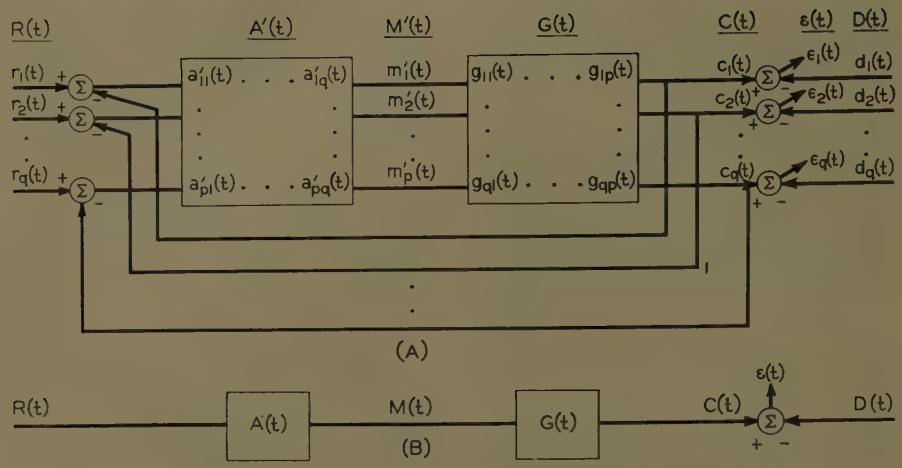

Fig. 2. Feedback and cascade representations of the general control problem

Basic System Equations

The principal properties of the systems to be considered and the criterion which is to be used as a measure of performance are stated in the following:

1. All signals are members of stationary, random, continuous processes with power spectra expressible as rational functions. In any practical problem, the usual procedure is to approximate all power spectra by rational functions in order to obtain transfer functions in useful form.

2. The fixed plant matrices as well as the operator matrices to be synthesized are linear, continuous, time-invariant, and stable; they may be represented by transfer function matrices whose elements are expressible as rational functions of complex frequency.

3. The criterion of system performance is the minimization of the sum of the mean-square errors between the set of actual outputs and a set of ideal or desired outputs. This has the merit both of lending itself to analytical treatment and of being applicable to many real problems.

The foregoing conditions or assumptions are essentially direct analogs of those normally applying to the equivalent single-variable case.

Fig. 2(A) shows the basic multivariable control system; as may be seen, direct negative feedback from output to input is considered an integral part of the system. In the figure the plant matrix G is $q\times p$ and the compensating matrix A' is $p\times q$; also, the signals R, M', C, D, and ε are $p\times 1$ or $q\times 1$ column matrices as required. Instead of working directly with the feedback configuration shown, it is more convenient to replace it by an equivalent cascade combination of matrices as indicated in Fig. 2(B). The relationship between the matrices A' and A is readily derived to be

$$A'=A(I-GA)^{-1} \tag{3}$$

Furthermore, it can be shown that no design freedom is lost in replacing one configuration by the other provided that G is stable, as assumed.

From Fig. 2(B) the total mean-square error $\overline{\varepsilon_T^2(t)}$ for a plant with p inputs and q outputs is

$$\overline{\varepsilon_T^2(t)}=\sum_{h=1}^{q}\overline{c_h^2(t)}-\overline{2c_h(t)d_h(t)}+\overline{d_h^2(t)} \tag{4}$$

where the c_h and d_h are the actual and desired outputs respectively. A direct expansion of equation 4 in terms of the elements of matrix A, the elements of matrix G, and suitably defined correlation functions yields

$$\begin{aligned}\overline{\varepsilon_T^2(t)}=\sum_{h=1}^{q}\Bigg[&\sum_{i,k=1}^{p}\sum_{j,l=1}^{q}\int_{-\infty}^{\infty}d\alpha g_{hi}(\alpha)\times\int_{-\infty}^{\infty}d\beta g_{hk}(\beta)\int_{-\infty}^{\infty}d\sigma a_{ij}(\sigma)\times\\&\int_{-\infty}^{\infty}d\rho a_{kl}(\rho)\phi_{r_jr_l}(\sigma+\alpha-\rho-\beta)-\\&2\sum_{i=1}^{p}\sum_{j=1}^{q}\int_{-\infty}^{\infty}d\alpha g_{hi}(\alpha)\int_{-\infty}^{\infty}d\sigma a_{ij}(\sigma)\phi_{r_jd_h}(\sigma+\alpha)+\phi_{d_hd_h}(0)\Bigg]\end{aligned} \tag{5}$$

where the correlation function $\phi_{xy}(\tau)$ is defined in the usual way as

$$\phi_{xy}(\tau)=\lim_{T\to\infty}\frac{1}{2T}\int_{-T}^{T}dt\,x(t)y(t+\tau)=\overline{x(t)y(t+\tau)} \tag{6}$$

Now, a minimization of equation 5 may be performed with respect to the a_{ij} or a_{kl} by a standard variational procedure. The result is that

$$\begin{aligned}&\sum_{h=1}^{q}\sum_{k=1}^{p}\sum_{l=1}^{q}\int_{-\infty}^{\infty}d\alpha g_{hi}(\alpha)\int_{-\infty}^{\infty}d\beta g_{hk}(\beta)\times\\&\qquad\int_{-\infty}^{\infty}d\rho a_{kl}(\rho)\phi_{r_jr_l}(\sigma+\alpha-\rho-\beta)-\\&\qquad\sum_{h=1}^{q}\int_{-\infty}^{\infty}d\alpha g_{hi}(\alpha)\phi_{r_jd_h}(\sigma+\alpha)=0;\ \sigma\gtrless 0\end{aligned}$$

$$\begin{aligned}i&=1,2,\dots p\\j&=1,2,\dots q\end{aligned} \tag{7}$$

are the qp minimizing equations which must be satisfied. When the a_{kl} satisfy equation 7, the minimum realizable error $\overline{\varepsilon_T^2(t)}_{\min}$ is achieved. An expression for evaluating it may be obtained by noting that equation 5 reduces to

$$\begin{aligned}\overline{\varepsilon_T^2(t)}_{\min}=\sum_{h=1}^{q}\sum_{i=1}^{p}\sum_{j=1}^{q}\Big[&\phi_{d_hd_h}(0)-\\&\int_{-\infty}^{\infty}d\alpha g_{hi}(\alpha)\int_{-\infty}^{\infty}d\sigma a_{ij}(\sigma)\phi_{r_jd_h}(\sigma+\alpha)\Big]\end{aligned}$$

when equation 7 is satisfied.

The frequency domain versions of equations 7 and 8 are most useful in obtaining numerical solutions. Equation 7 may be considered a function of a designated $f_{ji}(\sigma)$; when a Fourier transformation is made, the result is

$$\begin{aligned}f_{ji}(s)=&\sum_{h=1}^{q}\sum_{k=1}^{p}\sum_{l=1}^{q}g_{hi}(-s)g_{hk}(s)a_{kl}(s)\times\\&\phi_{r_jr_l}(s)-\sum_{h=1}^{q}g_{hi}(-s)\phi_{r_jd_h}(s)\\&\qquad\begin{aligned}i&=1,2,\dots p\\j&=1,2,\dots q\end{aligned}\end{aligned}$$

where $s\triangleq j\omega$, and $f_{ji}(s)$ has no poles in the left half of the s-plane. Since the factors of the terms within the summations are expressible as rational functions of s, a partial fraction expansion with respect to left-half s-plane poles must equate to zero.

Therefore

$$\left[\sum_{h=1}^{q}\sum_{k=1}^{p}\sum_{l=1}^{q}g_{hi}(-s)g_{hk}(s)a_{kl}(s)\phi_{r_jr_l}(s)\right]^{+}=\left[\sum_{h=1}^{q}g_{hi}(-s)\phi_{r_jd_h}(s)\right]^{+}$$

where $[\dots]^+$ indicates the expansion in terms of left-half s-plane poles only. Now, by using matrix notation the expression may be simplified even further. Let Φ_{rr} be the $q\times q$ matrix of elements $\phi_{r_jr_l}(s)$, Φ_{rd} be the $q\times q$ matrix of elements $\phi_{r_jd_h}(s)$, G be the $q\times p$ matrix of elements $g_{hk}(s)$, and A be the $p\times q$ matrix of elements $a_{kl}(s)$.

Equation 10 becomes

$$[\Phi_{rr}A^TG^T\bar{G}]^+=[\Phi_{rd}\bar{G}]^+$$

where, for any matrix $X(s)$, $X(-s)$ is written as $\bar{X}$, and X^T is the transpose of X. Next, equation 8 may be written in its transformed version as

$$\overline{\varepsilon_T^2(t)}_{\min}=\sum_{h=1}^{q}\sum_{i=1}^{p}\sum_{j=1}^{q}\frac{1}{2\pi j}\int_{-j\infty}^{j\infty}\times$$

$$[\phi_{d_hd_h}(s)-g_{hi}(-s)a_{ij}(-s)\phi_{r_jd_h}(s)]ds$$

Now, letting Φ_{dd} be the $q\times q$ matrix of elements $\phi_{d_ud_v}(s)$ and using the oth

rices as defined previously yields

$$t)_{\min}=\frac{1}{2\pi j}\int_{-j\infty}^{j\infty} tr\{\Phi_{dd}-\bar{G}\bar{A}\Phi_{rd}\}ds \quad (13)$$

re $tr\{\ldots\}$ denotes the trace of a rix.

thod of Solution: Free-Configuration Control Problem

When the plant matrix G becomes the ntity matrix, equation 11 reduces to form in which the plant imposes no rictions on the $\overline{\varepsilon_T{}^2}(t)_{\min}$ which may be ained. This is sometimes referred to a "free-configuration" design; for case equation 11 reduces to

$$[A^T]^+=[\Phi_{rd}]^+ \quad (14)$$

t will be shown that the method of ution which is applied to this simpler cial case can also be used in the most eral control case. Accordingly, equa- 14 will be used as the basis for eloping the method.

Explicit solutions for matrix A^T or A y be obtained from equation 14 when trix Φ_{rr} satisfies prescribed conditions. example, when Φ_{rr} is diagonal, the hods of spectrum factorization devel- d by Wiener for the single-variable e may be applied to yield.

$$=(\Phi_{rr}{}^+)^{-1}[\Phi_{rd}(\Phi_{rr}{}^-)^{-1}]^+ \quad (15)$$

n equation 13, $\Phi_{rr}=\Phi_{rr}{}^+\Phi_{rr}{}^-$, where elements of $\Phi_{rr}{}^+$ have all their poles zeros in the left-half s-plane and elements of $\Phi_{rr}{}^-$ have all their poles zeros in the right-half s-plane. en Φ_{rr} is not diagonal, matrix trans- nation methods may still be applicable obtain explicit solutions. However, the most general form of Φ_{rr} no method nown for obtaining explicit solutions matrix A. For this case, an implicit hod has been developed.

The basis for the method stems from principal observations: 1. rational -power and cross-power spectra result a transfer function matrix A whose nents are also rational functions, and he number of independent equations e satisfied as a result of the partial tion expansions of equation 14 grows e rapidly than the number of available nowns unless the poles of each element matrix A are initially assumed to be itical with those of all other elements the matrix. Equipped with these ervations, the method of solution may readily derived.

For the kth row of A, equation 14 may written in the form

$$\begin{aligned}
&[a_{k1}(s)\phi_{r_1r_1}(s)]^+ + [a_{k2}(s)\phi_{r_1r_2}(s)]^+ + \ldots \\
&\qquad [a_{kq}(s)\phi_{r_1r_q}(s)]^+ = [\phi_{r_1d_k}(s)]^+ \\
&\qquad\qquad \vdots \qquad\qquad\qquad \vdots \\
&[a_{k1}(s)\phi_{r_qr_1}(s)]^+ + [a_{k2}(s)\phi_{r_qr_2}(s)]^+ + \ldots \\
&\qquad [a_{kq}(s)\phi_{r_qr_q}(s)]^+ = [\phi_{r_qd_k}(s)]^+
\end{aligned} \quad (16)$$

If the $a_{k1}, a_{k2}, \ldots a_{kq}$ have identical poles and, in the most general case, none of these correspond to the left-half s-plane poles of the $\phi_{r_jr_l}(s)$ or $\phi_{r_jd_k}(s)$, it follows that for n such poles $-\alpha_u (u=1,2,\ldots n)$

$$\begin{aligned}
&(s+\alpha_u)a_{k1}(s)\phi_{r_1r_1}(s)\big|_{s=-\alpha_u} + \\
&\qquad (s+\alpha_u)a_{k2}(s)\phi_{r_1r_2}(s)\big|_{s=-\alpha_u} + \ldots \\
&\qquad\qquad (s+\alpha_u)a_{kq}(s)\phi_{r_1r_q}(s)\big|_{s=-\alpha_u}=0 \\
&\qquad\qquad\qquad \vdots \qquad\qquad\qquad \vdots \\
&(s+\alpha_u)a_{k1}(s)\phi_{r_qr_1}(s)\big|_{s=-\alpha_u} + \\
&\qquad (s+\alpha_u)a_{k2}(s)\phi_{r_qr_2}(s)\big|_{s=-\alpha_u} + \ldots \\
&\qquad\qquad (s+\alpha_u)a_{kq}(s)\phi_{r_qr_q}(s)\big|_{s=-\alpha_u}=0
\end{aligned} \quad (17)$$

It is at once apparent from the form of the equations that the matrix $\Phi_{rr}(-\alpha_u)$ can be considered the coefficient matrix of the residues of the $a_{kl}(s)$ at each pole $s=-\alpha_u$. If a nontrivial solution is to exist for the foregoing set of homogeneous equations, then the determinant of the coefficient matrix must be zero, or

$$|\Phi_{rr}(-\alpha_u)|=0 \quad (18)$$

Since Φ_{rr} is Hermitian, equation 18 will always be an even equation in the unknowns α_u. This in turn assures that exactly half of its roots will have positive real parts; these represent poles in the left-half s-plane as required. Since Φ_{rr} is positive semidefinite as well as Hermitian, this applies even when some of the roots of equation 18 are purely imaginary; otherwise, if such roots did not occur in pairs, there would be a shift of sign along the imaginary axis, which would violate the condition of positive semidefiniteness. Thus, a division can always be made to separate the roots into two groups, one on each side of the imaginary axis. In this way, the $\alpha_1,\alpha_2,\ldots\alpha_n$ poles of the $a_{kl}(s)$ are determined, where $2n$ is the order of the determinant of Φ_{rr}.

In a manner which is somewhat analogous to that of the solution of differential equations, the foregoing poles may be considered to correspond to the natural or "force-free" poles of the system. To these poles must now be added the left-half s-plane poles of the $\phi_{r_jd_k}(s)$ (acting as forcing terms) which do not already appear as poles of the $\phi_{r_jr_l}(s)$. This completes the determination of all the poles of the $a_{kl}(s)$.

As a final step, the number of independent equations which result from the partial fraction expansions may now be determined. The number of such equations determines the number of unknowns that are available as coefficients for the assumed numerator polynomials in s of the various $a_{kl}(s)$. The distribution of these coefficients among the various $a_{kl}(s)$ can readily be determined by inspection of the power spectra of the inputs. Now, by equating residues of all poles on each side of the group of equations represented by equation 16, a set of linear algebraic equations in the unknowns results for which a solution uniquely determines the coefficients of the numerator polynomials of the $a_{kl}(s)$, or the location of the zeros. In this manner the elements of A are completely determined.

Since the preceding derivation is based on the most general form of solution, any number of special cases within this formulation are also included. For example, if the partial fraction expansions result in powers of s degrees or higher, it can be shown that the preceding method is still valid. Or if any of the natural poles of the $a_{kl}(s)$ correspond to left-half s-plane poles of the $\phi_{r_jd_k}(s)$, the solution proceeds in exactly the same manner. Similarly, it is also now apparent that the natural poles of the $a_{kl}(s)$ cannot, in general, be identical to those of any individual $\phi_{r_jr_l}(s)$; this is because the poles of the $a_{kl}(s)$ represent zeros of the determinant of Φ_{rr}, whereas the poles of the $\phi_{r_jr_l}(s)$ represent poles of the same determinant.

In recapitulation, the principal steps of the implicit method of solution are listed as follows:

1. The determinant of Φ_{rr} is set equal to zero; the left-half s-plane roots of this even polynomial in s (or α_u) determine the nat ural poles of all $a_{kl}(s)$.

2. The left-half s-plane poles of the $\phi_{r_jd_k}(s)$ not appearing in the $\phi_{r_jr_l}(s)$ are added to the poles determined in the foregoing.

3. A partial fraction expansion is made and the number of independent equations is counted. This determines the total number of polynomial coefficients for the numerators of the $a_{kl}(s)$.

4. The residues for each pole on both sides of the equations are equated and the resulting set of linear algebraic equations is solved. This completely specifies all $a_{kl}(s)$.

Adaptation of Method of Solution to General Control Problem

The implicit method of solution clearly depends on the existence of a Hermitian coefficient matrix for the elements of the unknown matrix. It will now be shown that such an "effective coefficient matrix" always does exist for the most general case as represented by equation 11. For this purpose it is more suitable to transpose both sides of equation 11 to give

$$[\Phi_{gg}{}^{T}A\Phi_{rr}{}^{T}]^{+}=[\bar{G}^{T}\Phi_{rd}{}^{T}]^{+} \tag{19}$$

where the matrix Φ_{gg} has been defined by $\Phi_{gg}=G^{T}\bar{G}$. Both $\Phi_{gg}{}^{T}$ and $\Phi_{rr}{}^{T}$ are, of course, still Hermitian. If $\Phi_{gg}{}^{T}$ alone operated on A, the columns of A would have $\Phi_{gg}{}^{T}$ as their coefficient matrix; similarly, if $\Phi_{rr}{}^{T}$ alone operated on A, Φ_{rr} would be the coefficient matrix for the rows of A. Therefore it is clear that both matrices operating on A simultaneously produce a composite coefficient matrix which operates on both the rows and columns of A. The nature of this matrix will now be examined.

Let A, $\Phi_{rr}{}^{T}$ and $\Phi_{gg}{}^{T}$ be represented by

$$A=\begin{Vmatrix}\rho_1{}^{A}(s)\\ \rho_2{}^{A}(s)\\ \vdots\\ \rho_p{}^{A}(s)\end{Vmatrix},\quad \Phi_{rr}{}^{T}=[\rho_1{}^{rr}(s)\rho_2{}^{rr}(s)\ldots\rho_q{}^{rr}(s)],$$

$$\Phi_{gg}{}^{T}=\begin{Vmatrix}\phi_{g_1g_1}(s)\phi_{g_2g_1}(s)\ldots\phi_{g_pg_1}(s)\\ \vdots\qquad\qquad\vdots\\ \phi_{g_1g_p}(s)\ldots\ldots\ldots\phi_{g_pg_p}(s)\end{Vmatrix} \tag{20}$$

where $\rho_k{}^{A}(s)$ is the kth row vector of A, $\rho_j{}^{rr}(s)$ is jth row vector of Φ_{rr}, and $\phi_{g_ug_v}(s)$ is the element in the uth row and vth column of Φ_{gg}. Therefore

$$A\Phi_{rr}{}^{T}=\begin{Vmatrix}(\rho_1{}^{A}\times\rho_1{}^{rr})(\rho_1{}^{A}\times\rho_2{}^{rr})\ldots(\rho_1{}^{A}\times\rho_q{}^{rr})\\ \vdots\qquad\qquad\qquad\vdots\\ (\rho_p{}^{A}\times\rho_1{}^{rr})\ldots\ldots\ldots(\rho_p{}^{A}\times\rho_q{}^{rr})\end{Vmatrix} \tag{21}$$

An examination of each row of this new matrix shows that Φ_{rr} is the coefficient matrix for each row of A. Now, the complete product is written as

$$\Phi_{gg}{}^{T}A\Phi_{rr}{}^{T}=\begin{Vmatrix}\phi_{g_1g_1}\phi_{g_2g_1}\ldots\ldots\phi_{g_pg_1}\\ \vdots\qquad\qquad\vdots\\ \phi_{g_1g_p}\ldots\ldots\ldots\phi_{g_pg_p}\end{Vmatrix}\begin{Vmatrix}(\rho_1{}^{A}\times\rho_1{}^{rr})(\rho_1{}^{A}\times\rho_2{}^{rr})\ldots(\rho_1{}^{A}\times\rho_q{}^{rr})\\ \vdots\qquad\qquad\qquad\vdots\\ (\rho_p{}^{A}\times\rho_1{}^{rr})\ldots\ldots\ldots(\rho_p{}^{A}\times\rho_q{}^{rr})\end{Vmatrix} \tag{22}$$

It is possible to deduce sufficient information about the structure of the new matrix without completely performing the foregoing operation. Each element of the resulting matrix contains all rows of A and therefore all elements of A. If a matrix composed of the rows of A taken sequentially is considered, a $pq\times1$ vector can be formed for which an effective coefficient matrix exists. To form such a coefficient matrix, each element of the matrix of equation 22 is considered a row in a new $pq\times pq$ matrix; furthermore, each row in this new matrix is arranged in the same sequence as the corresponding element from which it was generated by standard matrix operations.

When the rows of the new matrix are examined, it is at once apparent that the

$$\Phi_{gg}=G^{T}\bar{G}=\begin{bmatrix}\phi_{g_1g_1}(s)\ \phi_{g_1g_2}(s)\ldots\phi_{g_1g_p}(s)\\ \vdots\qquad\qquad\vdots\\ \phi_{g_pg_1}(s)\ \ldots\ \phi_{g_pg_p}(s)\end{bmatrix};\ \Phi_{rr}=\begin{bmatrix}\phi_{r_1r_1}(s)\ \phi_{r_1r_2}(s)\ldots\phi_{r_1r_q}(s)\\ \vdots\qquad\qquad\vdots\\ \phi_{r_qr_1}(s)\ \ldots\ \phi_{r_qr_q}(s)\end{bmatrix}$$

$$\hat{\phi}_{g_ug_v}=\overbrace{\begin{bmatrix}\phi_{g_ug_v}(s)\ \phi_{g_ug_v}(s)\ldots\phi_{g_ug_v}(s)\\ \vdots\qquad\qquad\vdots\\ \phi_{g_ug_v}(s)\ \ldots\ \phi_{g_ug_v}(s)\end{bmatrix}}^{q}\Big\}q\qquad\begin{matrix}u=1,2,\ldots p\\ v=1,2,\ldots p\end{matrix}$$

$$\mathring{\Phi}_{gg}=\begin{bmatrix}\hat{\phi}_{g_1g_1}\ \hat{\phi}_{g_2g_1}\ldots\hat{\phi}_{g_pg_1}\\ \vdots\qquad\qquad\vdots\\ \hat{\phi}_{g_1g_p}\ \ldots\ \hat{\phi}_{g_pg_p}\end{bmatrix};\ \mathring{\Phi}_{rr}=\overbrace{\begin{bmatrix}\Phi_{rr}\ \Phi_{rr}\ldots\Phi_{rr}\\ \vdots\qquad\qquad\vdots\\ \Phi_{rr}\ \ldots\ \Phi_{rr}\end{bmatrix}}^{p}\Big\}p$$

$$K=\left\{\mathring{\Phi}_{gg}\diamond\mathring{\Phi}_{rr}\right\}=\begin{bmatrix}\left\{\hat{\phi}_{g_1g_1}\diamond\Phi_{rr}\right\}\ \left\{\hat{\phi}_{g_2g_1}\diamond\Phi_{rr}\right\}\ldots\left\{\hat{\phi}_{g_pg_1}\diamond\Phi_{rr}\right\}\\ \vdots\qquad\qquad\qquad\vdots\\ \left\{\hat{\phi}_{g_1g_p}\diamond\Phi_{rr}\right\}\ \ldots\ \left\{\hat{\phi}_{g_pg_p}\diamond\Phi_{rr}\right\}\end{bmatrix}$$

Fig. 3. Generation of effective coefficient matrix K for control problem

vth set of q rows incorporates the factor $\phi_{g_1g_v}(s)$ in its first q columns, $\phi_{g_2g_v}(s)$ in its second set of q columns, and the factor $\phi_{g_pg_v}(s)$ in the pth set of q columns. Thus in the new matrix each element of $\Phi_{gg}{}^{T}$ exerts an influence in a $q\times q$ submatrix corresponding to its original position in $\Phi_{gg}{}^{T}$. Now, if a $pq\times pq$ matrix is constructed in which each of its submatrices consists of a $q\times q$ matrix of identical elements of $\Phi_{gg}{}^{T}$, the first portion of the effective coefficient matrix would be thus formed. It is easily verified by inspection that such a matrix, $\mathring{\Phi}_{gg}$ is always Hermitian; see Fig. 3. To determine the contribution of Φ_{rr} to the coefficient matrix, it is seen that performing the operations indicated by equation 22 involves sequencing from column to column as each element is generated. Since each such element is a row of the new matrix, each q successive rows of this matrix contain the q rows of Φ_{rr} in sequence. Thus, in the new matrix, designated $\mathring{\Phi}_{rr}$ Φ_{rr}, appears intact as a $q\times q$ matrix repeated $p\times p$ times. That this second portion of the effective coefficient matrix is also Hermitian can also be easily verified by inspection; see Fig. 3. The composite matrix may thus now be constructed by an operation of matrix superposition. This operation is defined as follows: Two matrices X and Y of the same dimensions are superposed by multiplying corresponding elements of each matrix to obtain the corresponding element of the new matrix, $W=(X\diamondsuit Y)$. In Fig. 3 the resulting matrix is the $pq\times pq$ coefficient matrix K; it is also Hermitian since it is clear that superposition preserves the Hermitian property of the superposed matrices.

To preserve the form of equation 19 it is also necessary to construct new matrices for the right side of the equation. When this is done by a process similar to that just described, the reduction process is complete. Equation 11 thus may be rewritten as

$$[K\tilde{A}]^{+}=[\tilde{\Phi}_{rd}]^{+} \tag{23}$$

where K is the $pq\times pq$ coefficient matrix defined in the foregoing, and where $\tilde{A}$ and $\tilde{\Phi}_{rd}$ are the $pq\times1$ matrices formed by arranging sequentially by rows the elements of A and $\bar{G}^{T}\Phi_{rd}{}^{T}$, respectively. In this form the matrix K plays the same role in the solution for all the elements of A as Φ_{rr} does in the filter or free-configuration solution for each row of A. Accordingly, the implicit method of solution can be applied directly to equation

It should be emphasized that it is necessary to perform formally the uction to equation 23 in order to ob- a solution to the multivariable con- problem. For any specific problem, irect expansion of equation 11 into its nponent equations automatically yields coefficient matrix K.

strative Example

To demonstrate the implicit method solution one of the simplest 2-input–utput free configuration examples will examined. Since it has been shown t the most general control problem always be reduced to this equivalent m, the method may equally well be plied to more complex configurations. e system is shown diagrammatically in . 4. Each of the two inputs (r_j) is nposed of a message (m_j) corrupted white noise (n_j). The noises are correlated with each other and with h message, while the message at the ond input is specified to be the deriva- e of the message at the first input. is desired to extract the best m_1 a mean-square sense) by operating on nd r_2 simultaneously. The given data y be summarized as follows:

$$\phi_{r_1}(s)=\phi_{m_1m_1}(s)+\phi_{n_1n_1}(s)$$
$$=\frac{3}{4-s^2}+1=\frac{7-s^2}{4-s^2}$$

$$\phi_{r_2}(s)=\phi_{m_2m_2}(s)+\phi_{n_2n_2}(s)$$
$$=-\frac{3s^2}{4-s^2}+1=\frac{4-4s^2}{4-s^2}$$

$$\phi_{r_1r_2}(s)=\phi_{m_1m_2}(s)=\frac{3s}{4-s^2}$$

$$\phi_{m_jd_1}(s) \qquad (24)$$

In the first step of the solution pro- lure the determinant of the matrix is set equal to zero as follows:

$$\frac{1}{(4-s^2)^2}\begin{vmatrix}7-s^2 & +3s\\ -3s & 4-4s^2\end{vmatrix}=0 \qquad (25)$$

Two "natural" system poles are pro- ed, one at $s=-2$ and the other at

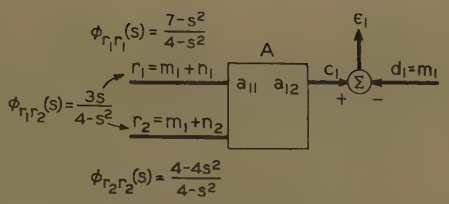

Fig. 4. Block diagram of illustrative example

$s=-1.32$. However, the pole at $s=-2$ is cancelled out by a corresponding zero thus leaving a single natural pole at $s=-1.32$. Now, since the left-half s-plane poles of the $\phi_{r_jd_1}(s)$ also appear in the $\phi_{r_jr_l}(s)$, no additional poles are present in the $a_{kl}(s)$. The form of the $a_{kl}(s)$ is thus

$$a_{11}(s)=\frac{p_{11}(s)}{s+1.32}$$

$$a_{12}(s)=\frac{p_{12}(s)}{s+1.32} \qquad (26)$$

where the $p_{kl}(s)$ are undetermined polynomials in s.

A partial fraction expansion of the elements of the matrices of equation 11 may now be made. This indicates that the number of independent equations to be satisfied is two; therefore, it follows that $p_{11}(s)=x_{0_{11}}$ and $p_{12}(s)=x_{0_{12}}$ are simple gain constants. The two independent equations which result from equating residues are

$$5.25x_{0_{11}}-3.96x_{0_{12}}=0$$
$$3x_{0_{11}}-6x_{0_{12}}=2.04 \qquad (27)$$

from which

$$x_{0_{11}}=0.411;\ x_{0_{12}}=0.545 \qquad (28)$$

and

$$a_{11}(s)=\frac{0.411}{s+1.32},\ a_{12}(s)=\frac{0.545}{s+1.32} \qquad (29)$$

Now, using equation 13 and substituting appropriately, the $\epsilon_1^2(t)_{\min}$ is computed to be 0.41.

A relative measure of this performance may be obtained by examining the best single-variable solutions for this example. If the best m_1 is extracted from r_1 alone, the use of equation 15 yields

$$a_{11}(s)=\frac{0.65}{s+2.65} \qquad (30)$$

with a resulting

$$\overline{\epsilon_1^2(t)}_{\min}=0.65$$

Similarly, if the best m_1 is extracted from r_2 alone, the results are

$$a_{12}(s)=\frac{0.5}{s+1} \qquad (31)$$

and

$$\overline{\epsilon_1^2(t)}_{\min}=0.50$$

Thus, the $\overline{\epsilon_1^2(t)}_{\min}$ of 0.41 for the multivariable solution compares favorably with the value of 0.50 which may be obtained by the best single-variable operation. As expected, the cost of this improvement is in the form of a more complex over-all transfer function.

References

1. General Algebraic Method Applied to Control Analysis of Complex Engine Types, A. S. Boksenbom, R. Hood. *Technical Report 980*, Lewis Flight Propulsion Laboratory, National Advisory Committee for Aeronautics, Cleveland, Ohio, 1950.

2. A Theory of Multidimensional Servo Systems, M. Golomb, E. Usdin. *Journal*, Franklin Institute, Philadelphia, Pa., vol. 253, no. 1, Jan. 1952, pp. 29–57.

3. The Synthesis of Multipole Control Systems, H. Freeman. *Technical Report T-15/B*, Electronics Research Laboratories, Columbia University, New York, N. Y., Apr. 1956.

4. The Application of Matrix Methods to Multi-Variable Control Systems, R. J. Kavanagh. *Journal*, Franklin Institute, vol. 262, no. 5, Nov. 1956, pp. 349–67.

5. The Theory of Multivariate Stochastic Processes, N. Wiener, P. Masani. *Acta Mathematica*, Stockholm, Sweden, vol. 98, 1957.

6. The Use of Canonical Expansions of Random Functions in Determining an Optimum Linear System, V. S. Pugachev. *Automation and Remote Control*, Moscow, USSR.

7. Design of Multivariable Optimum Filters, J. H. Westcott. *Transactions*, American Society of Mechanical Engineers, New York, N. Y., vol. 80, no. 2, Feb. 1958, pp. 463–67.

8. The Linear Least Squares Synthesis of Continuous and Sampled Data Multivariable Systems, R. C. Amara. *Technical Report no. 40*, Stanford Electronics Laboratories, Stanford, Calif., July 1958.

Discussion

Freeman (Massachusetts Institute of chnology, Cambridge, Mass.): Dr. ara extends Wiener's theory of optimum r design to linear multivariable systems. e resultant matrix solution of the modi- Wiener-Hopf equation represents a th-while addition to our understanding nultivariable systems, and the author is e congratulated on his efforts.

t is believed that a somewhat too restrictive point of view is taken when it is implied that the fixed plant matrix must be the identity matrix before the solution can reduce to that for a free configuration. Actually, the free-configuration solution will apply (at least in principle) for any plant matrix, provided the following three conditions are satisfied: 1. the inverse of the plant matrix exists, 2. the elements of the plant matrix have all their poles in the left-half s-plane, and 3. the zeros of the plant determinant lie in the left-half s-plane.[1]

The author states that he expects his technique to provide a practical synthesis procedure for multivariable control systems. The application of the optimization techniques based on the mean-square error criterion to control system synthesis has always been criticized for its supposed academic naïvete in ignoring the kernel of the control problem. The real objective of a control system is to obtain a specific, desired output behavior, precisely related to the inputs, in spite of the ever-present nonlinearities, time variations, and general

disturbances. For this reason also a practical control system without feedback is unthinkable, feedback being the necessary mechanism to remove the effects of whatever nonlinearities, time variations, or disturbances are inherently in the system. This is quite different from the problem of filter design, where feedback is not required per se. The author, instead of dealing with multivariable control systems, is actually describing what should be called a multivariable filter, and, indeed, his example also points this out.

This is not to imply that the application of the mean-square error criterion to a multivariable system is without merit; it is, however, only the first step to a possible practical synthesis procedure. The method would gain considerably in value if the optimization is made subject to the constraints that the mean-square values of the signals which are subject to saturation be held well within their linear range. This concept was introduced by Newton[2] for single-variable systems. Its extension to multivariable systems modifies equation 11 to the following form:

$$[\Phi_{rr}A^T(G^T\bar{G}+LG_s{}^T\bar{G}_s)]_+ =(\Phi_{rd}\bar{G})_+$$

where G_s = saturating signal transfer matrix, and L = diagonal Lagrangian multiplier matrix, and all other symbols are as used by the author.

Solution of this equation (i.e., finding the matrix A which satisfies it) will give a system transfer matrix which is optimum in the sense that it will have the minimum mean-square error consistent with the constraint that the probability of saturation be low. It is believed that some such procedure is absolutely necessary in the case of multivariable systems to give the optimization technique based on the mean-square error some practical significance.

It can also be pointed out that it is a relatively simple matter to extend the synthesis procedure described by the author to the case of deterministic signals (steps, ramps, etc.). This requires merely the use of the integral-square error rather than the mean-square error, with corresponding changes in the definitions of the power density spectra.

References

1. Stability and Physical Realizability Considerations in the Synthesis of Multipole Control Systems, Herbert Freeman. *AIEE Transactions*, vol. 77, pt. II, March 1958, pp. 1–5.

2. Compensation of Feedback-Control Systems Subject to Saturation, George C. Newton, Jr. *Journal*, Franklin Institute, Philadelphia, Pa., vol. 254, no. 4 and 5, Oct. and Nov. 1952, pp. 281–96, 391–413.

R. J. Kavanagh (University of Toronto, Toronto, Ont., Canada): The author approaches the problem of the synthesis of multivariable control systems incorporating feedback by designing an equivalent cascade system which may then be transformed into the corresponding feedback system. The process of transforming to the desired feedback system would appear to the writer to give rise to two difficulties in certain cases.

In the first place, while equation 3 is a valid relationship between A and A', there is no guarantee that A' is necessarily physically realizable. The criterion for realizability may be seen to be that the zeros of the determinant of $(I-GA)$ must be in the left half of the s-plane (disregarding any possible cancellations with right-half plane zeros of A).

The second difficulty arises in connection with the free configuration control problem. This problem occurs when the plant transfer matrix G becomes the identity matrix. If G is the identity matrix, this implies that either $p=q$ or that G is a $p\times p$ matrix. If $p=q$, there is no problem other than that of realizability since the cascade system is readily converted to a feedback system. However, if G is a $p\times p$ matrix and $p\neq q$, the problem is not solvable in terms of a feedback system since the number of outputs of G and the number of inputs to A' (and to A) must be equal. Hence it is the writer's belief that the procedure for the free-configuration case, while valid for any cascade system, is only valid for feedback systems when $p=q$.

R. C. Amara (Stanford Research Institute, Menlo Park, Calif.): Dr. Freeman is entirely correct in pointing out that the free-configuration solution may be applied whe the three conditions he enumerates for th plant matrix are satisfied. The author di not intend to imply that the form of equa tion 14 results only when G is the identit matrix. The particular cases in whic equation 11 is reducible to the form of equa tion 14 are discussed elsewhere (see referenc 8 of the paper).

The extension of the synthesis procedur to optimization subject to constraints o the mean-square values of plant inpu saturation signals is indeed commendable The possibility and desirability of includin such a constraint in the procedure for th multivariable case has been previously suggested in reference 8 of the paper. How ever, the statement that the synthesis procedure described deals only with multivariable filters is not believed to be correct Feedback is included as an integral part o the control systems considered. The particular multivariable filter example which is used as an illustration was chosen primarily for its simplicity. The application of the method to the solution of multivariable control examples is included in reference 8 of the paper.

It may also be noted that, in addition t the extension of the procedure to deterministic signals as indicated by Dr. Freeman, it is also a relatively simple matter t adapt the method to synthesis for minimization of the sum of the weighted-output mean-square or integral-square errors.

Dr. Kavanagh properly indicates that the solution of equation 3 does not guarantee the physical realizability of matrix A' When the zeros of the determinant $(I-GA$ do not all lie in the left half of the s-plane, a $q\times q$ matrix B may be inserted in the feedback loop. This will introduce sufficient freedom to satisfy the condition that all the zeros of the determinant $(I-BGA)$ be in the left-half s-plane. A similar procedure is used in single-variable systems.

Finally, as indicated previously, the free-configuration case as represented by equation 14 may be applied whenever the three conditions stated by Dr. Freeman are satisfied. Since G^{-1} must exist, then p must equal q for this case. When p is not equal to q, the problem is solvable as in the general control case.

ffect of Closed-Loop Transfer Function ole and Zero Locations on the Transient Response of Linear Control Systems

OLLE I. ELGERD
MEMBER AIEE

WILLIAM C. STEPHENS
NONMEMBER AIEE

HE ROOT LOCUS methods have in recent years gained a widespread ularity among control engineers en- ed in the work of both analysis and thesis. The reason for this is rather ious; the root locus techniques give system designer more information the kind in which he is interested en analyzing a given system; when is synthesizing a control network, se techniques permit him to build the ired characteristics into the system a much more direct fashion than did old frequency response techniques. e basis for this statement is that in large majority of control systems, transient, not the frequency, response f overshadowing importance.

To understand better the aim of this per, it will be necessary to review efly the basic idea of the root locus thods as described in the literature[1-4] he reference list is by no means plete but contains a representative ction of the most popular techniques.) the purpose of demonstration, a ple 1-loop system having a forward p transference $G(s)$ and a feedback p transference $H(s)$ is chosen for the cussion.

The transient response of this system n input signal $r(t)$ can be written

$$= \mathcal{L}^{-1}\left(R(s)\,\frac{G(s)}{1+G(s)H(s)}\right) \qquad (1)$$

$$= \mathcal{L}^{-1}[R(s)\times K(s)] \qquad (2)$$

n the second expression is introduced closed-loop transference

$$K(s)=\frac{G(s)}{1+G(s)H(s)}$$

If attention is limited to true follow-up systems of lumped type, i.e., systems with zero position error for a step input, then it is possible, as is easily verified by means of the "final value theorem," to put $K(s)$ in the following form:

$$K(s)=\frac{\prod_{i=1}^{n}(-P_i)}{\prod_{i=1}^{m}(-Z_i)}\,\frac{\prod_{\mu=1}^{m}(s-Z_\mu)}{\prod_{\nu=1}^{n}(s-P_\nu)} \qquad (3)$$

The $Z\mu$'s are the closed-loop (and at the same time open-loop) zeros and P_ν's the closed-loop (but not the open-loop) poles.

By choosing as a test signal a unit step input, equation 2 will give after application of Heaviside's expansion theorem

$$c(t)=1+\sum_{\nu=1}^{n}A_\nu\epsilon^{P_\nu t} \qquad (4)$$

The amplitudes A_ν can be calculated from

$$A_\nu=\frac{1}{P_\nu}\,\frac{\prod_{i=1}^{n}(-P_i)}{\prod_{i=1}^{m}(-Z_i)}\,\frac{\prod_{i=1}^{m}(P_\nu-Z_i)}{\prod_{i=1}^{\nu-1}(P_\nu-P_i)\prod_{i=\nu+1}^{n}(P_\nu-P_i)} \qquad (5)$$

The closed-loop poles and zeros may be either real or conjugate complex but for any stable, physically realizable system they will contain negative real parts. It is also clear from equation 4 that all terms appearing under the summation symbol represent the transient part of the time response. These terms are either monotonously decaying (in the case where the corresponding poles are real) or oscillatorily decaying (should any poles appear as conjugate complex). Note that the zeros will affect only the magnitude of the amplitudes.

Equations 4 and 5 reveal one very important fact: The time response (once the input is known) is uniquely determined by the location of the closed-loop poles and zeros in the s-plane. All root locus techniques are primarily based on this very fact. The designer manipulates the circuit parameters either in the forward or feedback path in such a manner that the closed-loop zeros and poles will form an s-plane configuration corresponding to the particular response desired. Unfortunately, this is easier to say than do.

There are three main hurdles that the designer must overcome:

1. He must find the numerical values of the poles and zeros of the open-loop transfer functions. Often he may be able to work under the assumption of noninteraction between the different blocks of the system. In such a case the problem of finding these poles and zeros is quite simple.

2. Using semigraphical techniques, he will investigate how the closed-loop poles and zeros travel throughout the s-plane when system parameters are subject to changes. This part of the over-all problem has been lucidly treated in the literature. Some more or less complex devices, for example, the Spirule, have been designed to help out with this task.

3. The most difficult problem is the translation of the pole-zero configuration into time response. Principally, this is an easy task. After having made a parameter adjustment and after having located the new positions of the closed-loop poles and zeros, one simply utilizes the two equations, 4 and 5. One should remember, however, that to get full information in the real time domain it is necessary to calculate the output for a sequence of time values. It is also worth remembering that if the result is not satisfactory the same procedure has to be repeated once or several times depending upon how fast the result converges toward an acceptable response.

Obviously, a digital computer is a very helpful aid, but from a financial point of view it is seldom feasible to employ such a device. To perform the necessary computations with a slide rule or with a desk calculator is in most cases extremely time consuming. This particular disadvantage of the root locus methods has quite possibly caused many a control system engineer to take a reserved attitude toward these techniques.

Objectives

The material presented in this paper is intended to be of help for the designer who utilizes the root locus techniques in his work. The bulk of the information is given in the form of graphs which are intended to serve as a table for the designer. By means of these graphs he will be able to correlate immediately the connection between pole-zero configura-

er 59-197, recommended by the AIEE Feed- Control Systems Committee and approved by AIEE Technical Operations Department for ntation at the AIEE Winter General Meeting, York, N. Y., February 1-6, 1959. Manu- t submitted October 27, 1958; made available rinting December 3, 1958.

E. I. ELGERD is with the University of Florida, esville, Fla., and WILLIAM C. STEPHENS is with U. S. Army Combat Surveillance Agency, Ar- on, Va.

paper reports the results from an investigation rmed at the University of Florida Electrical artment.

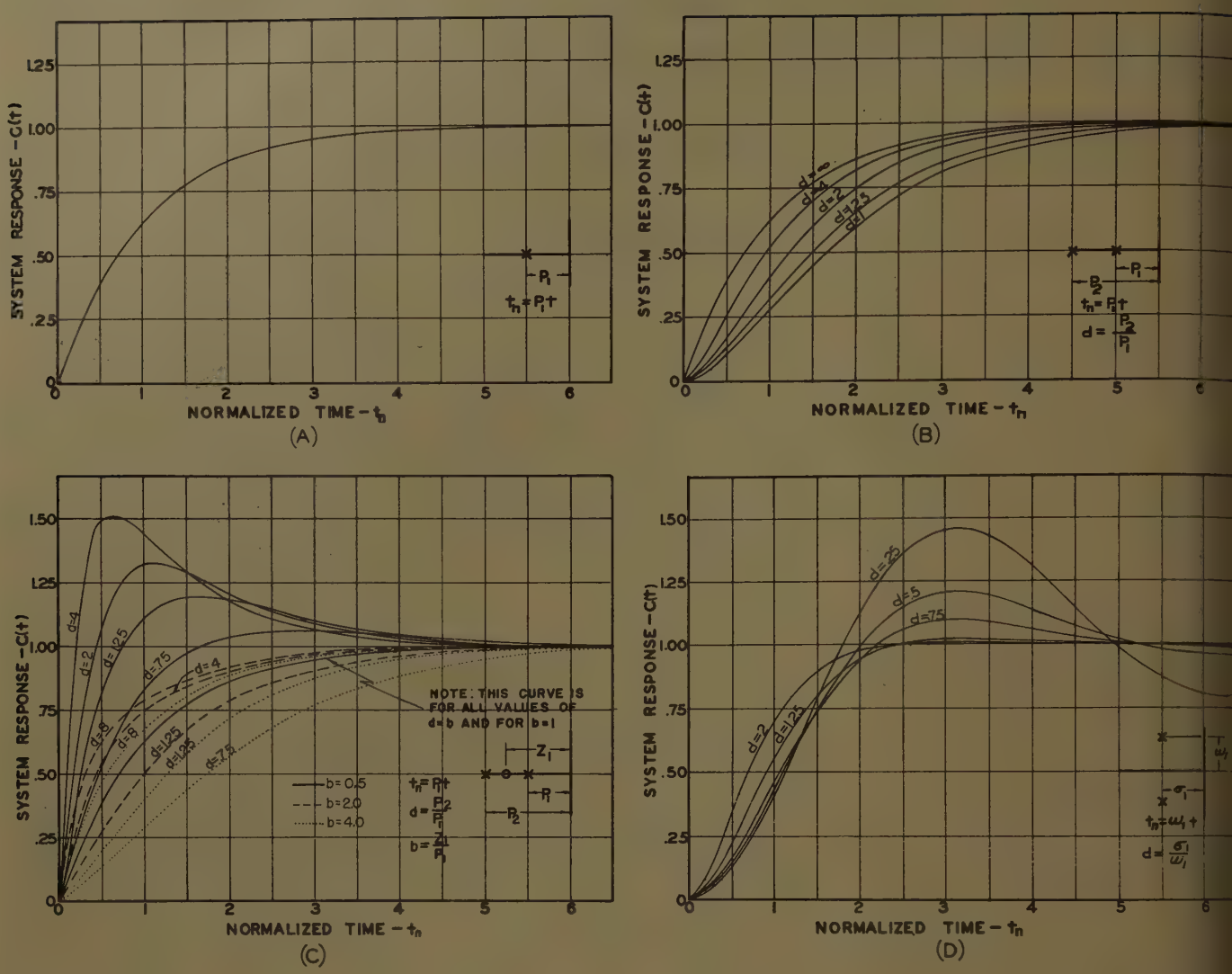

Fig. 1. Responses to a step input of systems of varying characteristics

A—Having one negative real closed-loop pole only
B—Having two negative real closed-loop poles
C—Having two closed-loop poles and one zero; all real and negative
D—Having two conjugate complex poles

tion and real-time response. They serve, in other words, in a similar way, as does a table of Laplace transforms; from such a table one finds the real-time response associated with a particular function in the complex *s*-domain.

A Laplace transform table will always be characterized by a certain degree of incompleteness. To make it complete it would be necessary to include an infinite number of transform pairs. It is appreciated however, that even a limited Laplace transform table is extremely helpful because it will contain the types of functions most frequently encountered.

The same general statements apply to the graphs in this paper. It would seem at first glance to be a prodigious task to try to investigate and tabulate every possible pole-zero configuration, of which there exists an infinite number. How this difficulty has been circumvented will be shown later; first, the earlier work done in this general area will be briefly surveyed.

Review of Previously Published Work

No attempt has been made to include here the many papers concerned with obtaining the transient response from a knowledge of the frequency response because this is, as already stated, not the objective of this paper. Only those treatises will be mentioned where a direct relationship is established between system transfer function pole and zero locations and time response. Not very much information is available in the technical literature.

One of the most fundamental pole-zero configurations is the one consisting of two conjugate complex poles. It is natural that this case first appeared in the literature. In 1947, James, Nichols, and Phillips[6] presented a series of graphs showing the unit-step-function response for such a system. Truxal, in 1955, added a negative real zero to the conjugate complex pole pair and calculated some data for this configuration.

Mulligan had already in 1948 in his doctorate dissertation[7] made an extensive study of the connection between the

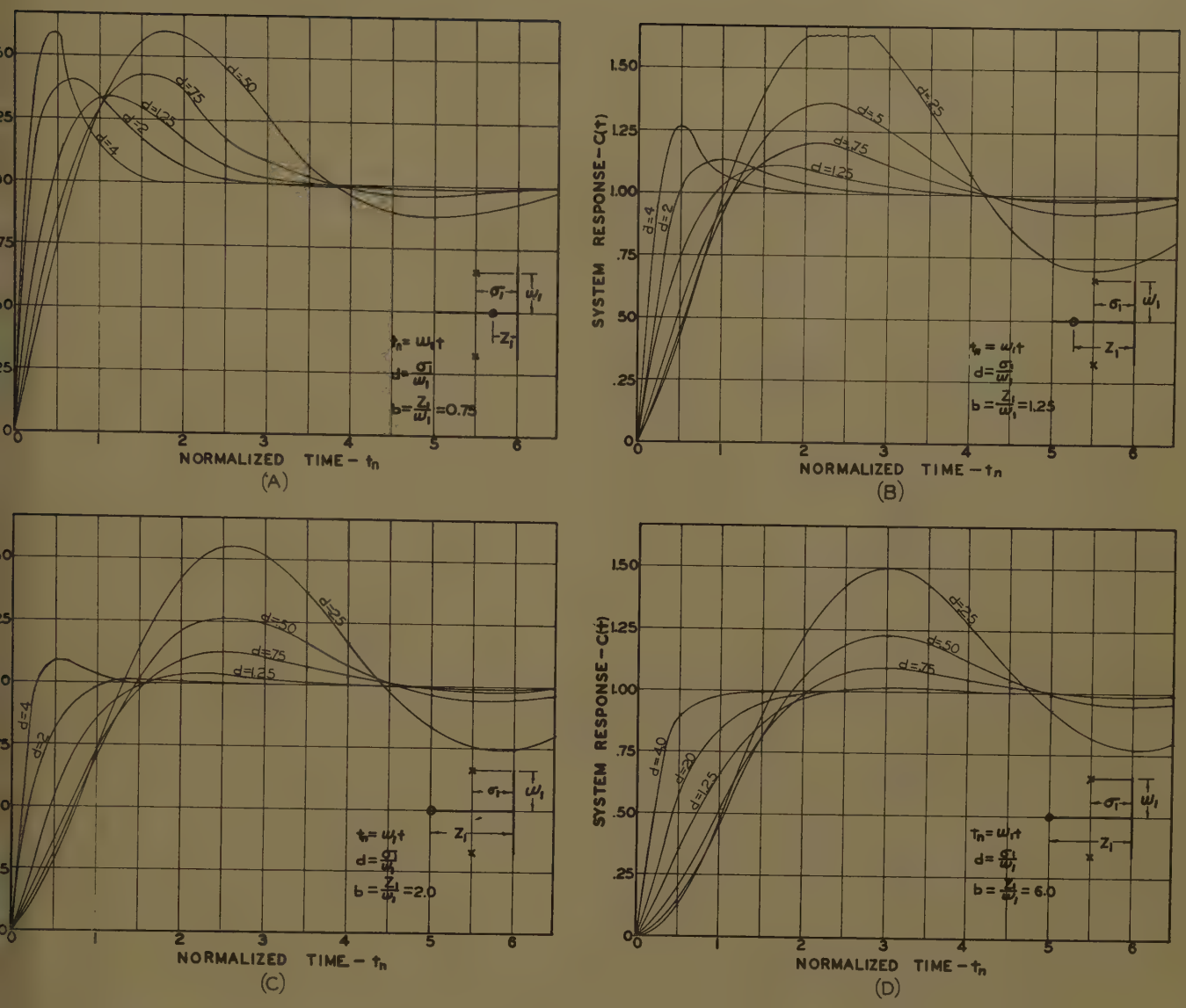

Fig. 2. Responses to step input for system having two closed-loop conjugate complex poles and one negative real zero

and zero locations and the maxima minima of the transient response. was particularly interested in the onse of multistage, nonfeedback am- ers, but because of his general oach, his results have had some ication also in the control field.

manian in 1955 in his doctorate rtation[8] extended the work of Mul- to include a method of finding that e of time at which the response es the final value line. Elgerd duced on a very limited scale the of the present paper into the field ampled-data systems in a paper[9] aring in July 1958. An attempt was e to classify sampled-data systems on basis of the closed-loop pole and zero gurations.

recent paper by Huang[10] takes up iscussion the sensitivity of the system response of the pole locations. In particular, he co-ordinates the constancy of response of a closed-loop system by a definition of the sensitivity of a closed-loop pole as the percentage variation of this pole for a given percentage variation of one of the open-loop parameters.

Fundamental Pole-Zero Configurations

One of the main problems in this investigation has been to extract from the infinite number of pole-zero configurations the ones that have a practical significance. When, after a careful sampling procedure, these fundamental cases have been selected, there remains the problem of bringing to a minimum the number of independent graphs needed to cover each case adequately. This task of system classification is greatly simplified due to a fundamental characteristic feature of linear systems, namely, the predominance of certain poles and zeros. A study of equation 5 will reveal that those amplitudes A_ν that are associated with poles P_ν, located comparatively far away from the origin in the s-plane, will be of relatively small magnitude. Not only do these transient terms in equation 4 have small magnitudes but they will also die out very fast. One might, therefore, without losing much accuracy, obtain the response of a specific system by considering only the poles and zeros located closest to the origin. It is difficult to give a general rule of thumb as to where to put the limit. Truxal[11] mentions a criterion sometimes used in design.

The following configurations have been

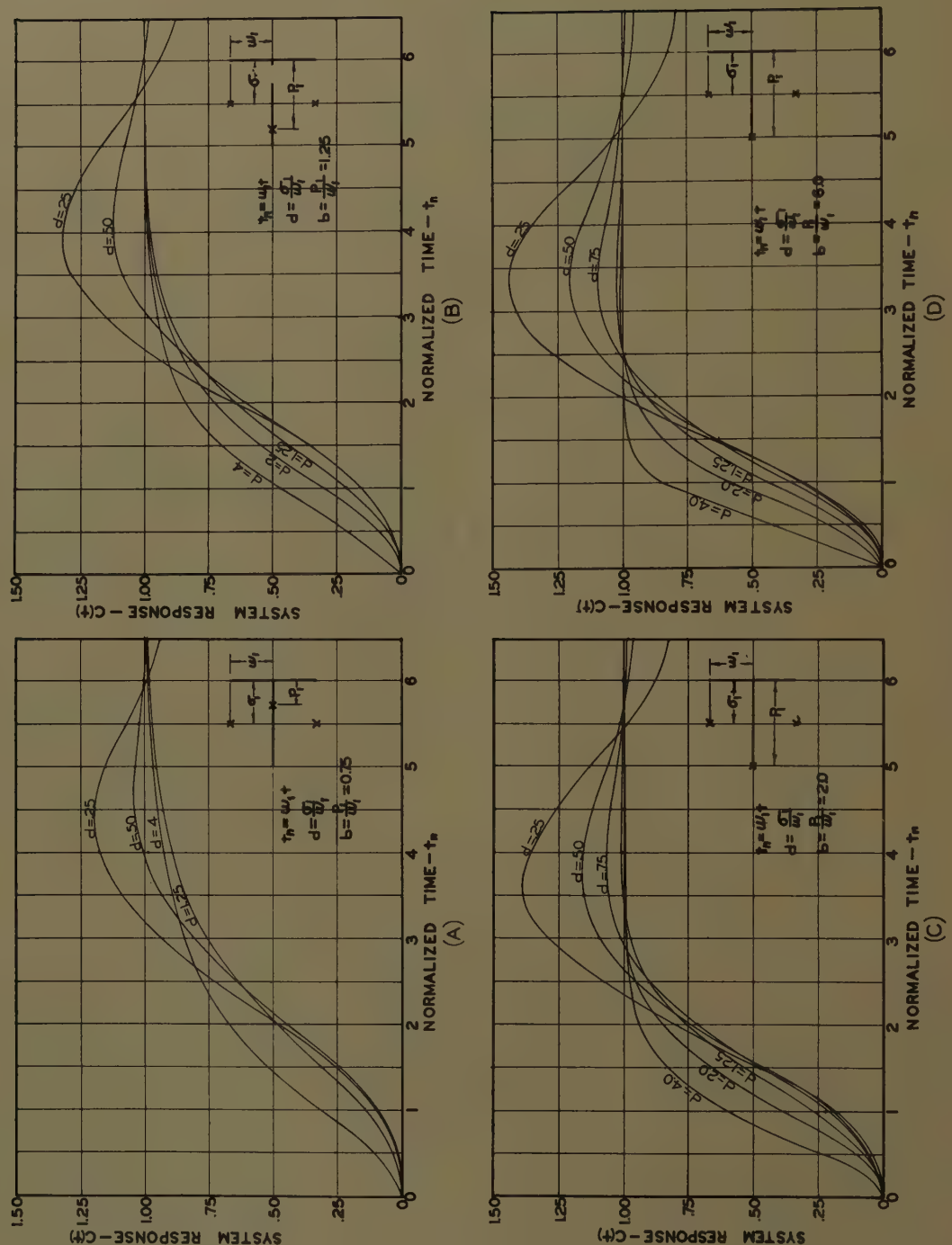

Fig. 3. Responses to step input for system having three closed-loop poles: two conjugate complex and one real

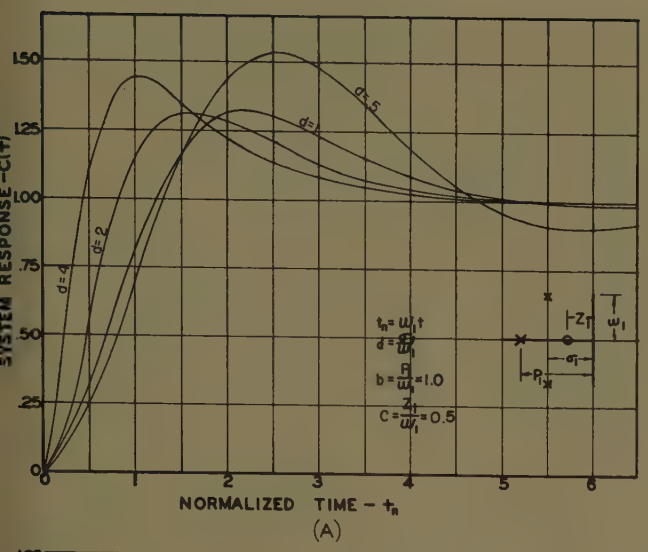

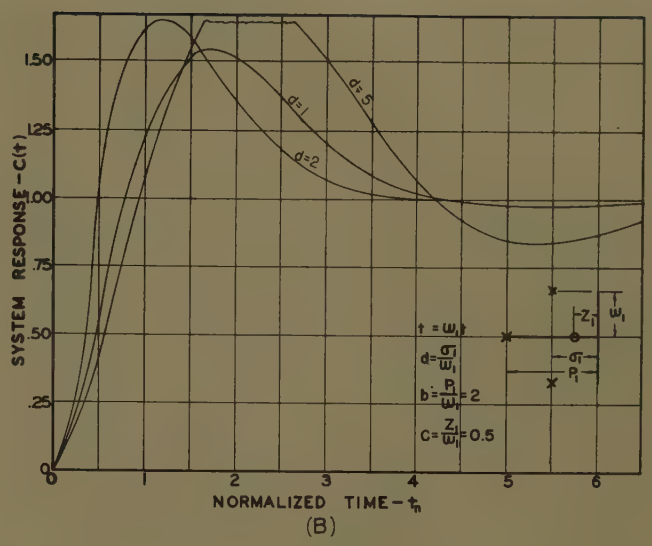

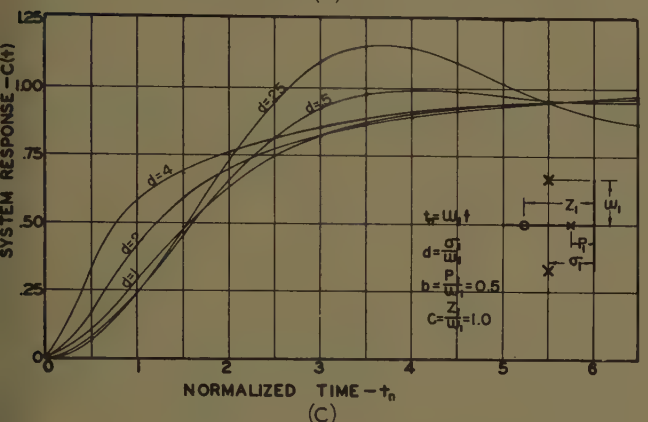

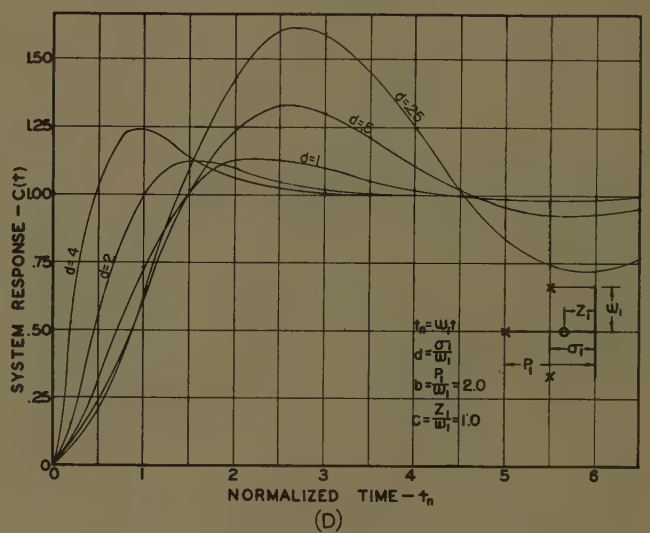

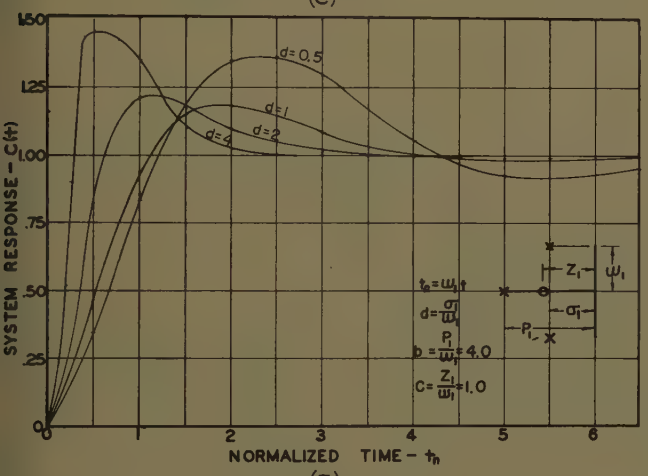

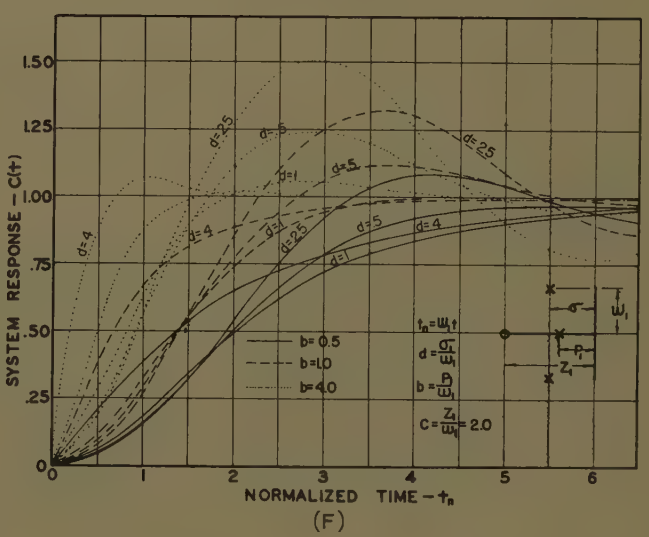

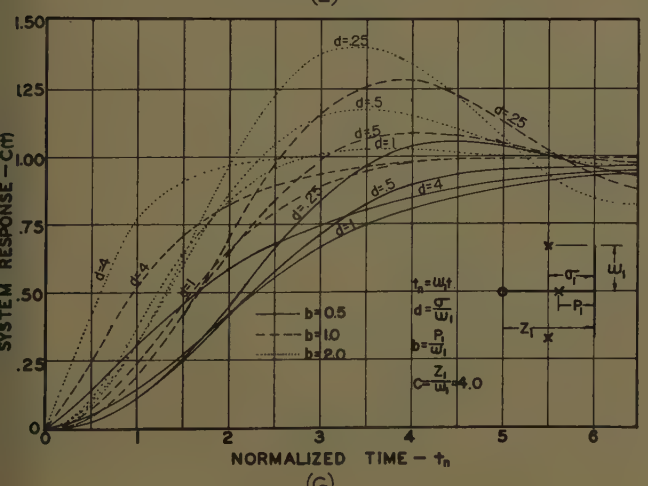

Fig. 4. Responses to step input for system having three closed-loop poles, two conjugate complex and one real, plus one zero

studied and the results are shown in the graphs indicated:

Case *A:* One negative real pole; see Fig. 1(A).

Case *B:* Two negative real poles; see Fig. 1(B).

Case *C:* Two negative real poles, one negative real zero; see Fig. 1(C).

Case *D:* Two conjugate complex poles; see Fig. 1(D).

Case *E:* Two conjugate complex poles, one negative real zero; see Fig. 2.

Case *F:* Two conjugate complex and one negative real pole; see Fig. 3.

Case *G:* Two conjugate complex and one negative real pole, one negative real zero; see Fig. 4.

Case *H:* Two conjugate complex and one negative real pole, two conjugate complex zeros; see Fig. 5.

Case *I:* Two pairs of conjugate complex poles; see Fig. 6.

The numerical work on which all graphs are based was performed on an International Business Machines Corporation digital computer, type *650*. For the purpose of fast identification, the particular pole-zero configuration with which each set of curves is associated is shown in the lower right corner of each figure where, also, all parameters are defined.

Rules for Reading the Charts

All charts are based on a normalized time variable. This has obviously been done to make them applicable to any system independent of speed of response. This normalizing procedure is based on the well-known equation

$$\mathcal{L}\left[f\left(\frac{t}{a}\right)\right]=a\mathcal{L}[f(t)] \qquad (6)$$

or, expressed in words: If the pole-zero configuration in the s-plane is shrunk uniformly in the ratio of a to 1, the corresponding time function is stretched in the ratio of 1 to a. If a is chosen larger than unity, this evidently means that the time response has been slowed down. The normalized time variable t_n is defined in each separate case, as shown in the charts.

The usage of the charts will be demonstrated with the following example: The response of a particular control system is dominated by a closed-loop conjugate pole pair located at $-10 \pm j40$ in the s-plane.

This system is quite undamped and it is desired to reduce the overshoot by introducing another pole located somewhere along the negative real axis. Assuming that the position of the original pole pair will be unchanged, the new response will be compared with the o one.

From Fig. 1(D) the following is fou for the original system:

Overshoot: 45%

Rise time (defined as the time at which t system passes final value): 1.8 seconds

(This value for the rise time is in no malized units. Actual rise time will 1.80/40 = 0.045 seconds.)

Figs. 3(A) through (D) give immedia information about overshoot and ri time for different positions of the re pole. Table I is obtained by inspection.

The closer to the origin the pole placed the less overshoot is obtained, bu at the same time one loses speed response. From data such as that Table I, it is possible to make an accep able compromise or perhaps find that different pole-zero configuration mus be chosen to meet specifications.

Summary

The material presented is intended t be of help to the system designer wh designs in terms of transference po and zero locations. The main obstacle i this type of design approach is to interpr the pole-zero configuration in terms time response. A system classification o

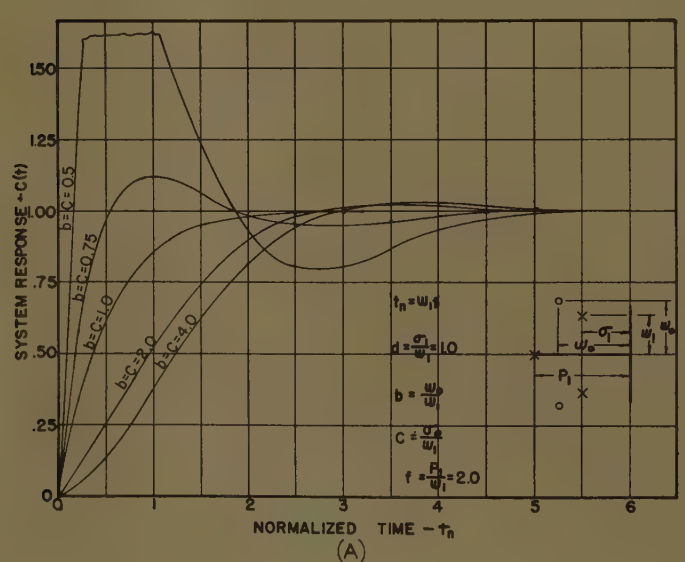

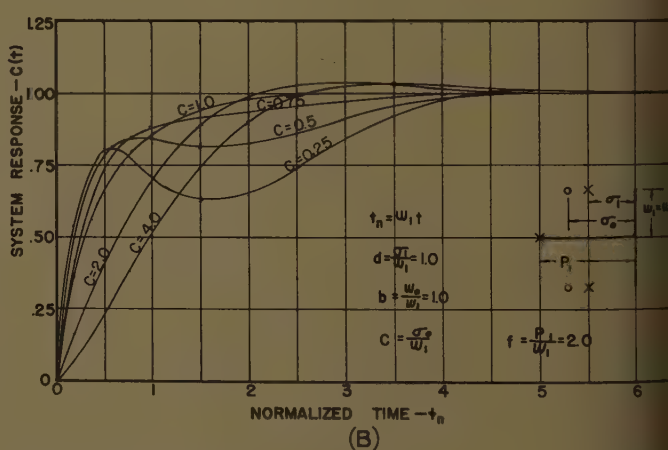

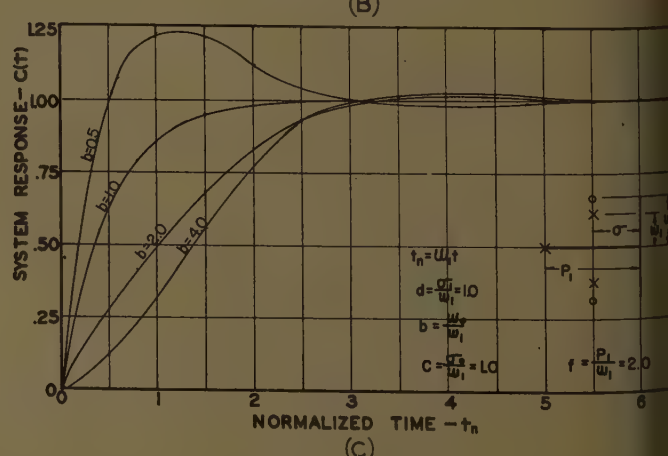

Fig. 5. Responses to step input for system having three closed-loop poles, two conjugate complex and one real, plus two conjugate complex zeros

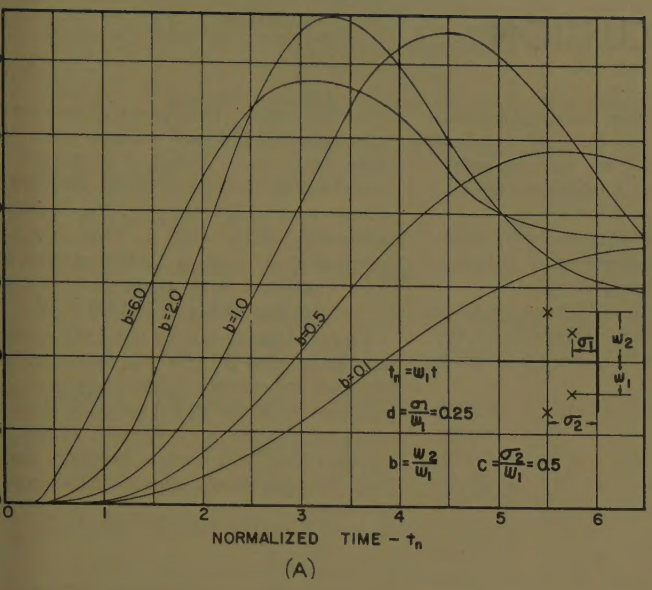

(A)

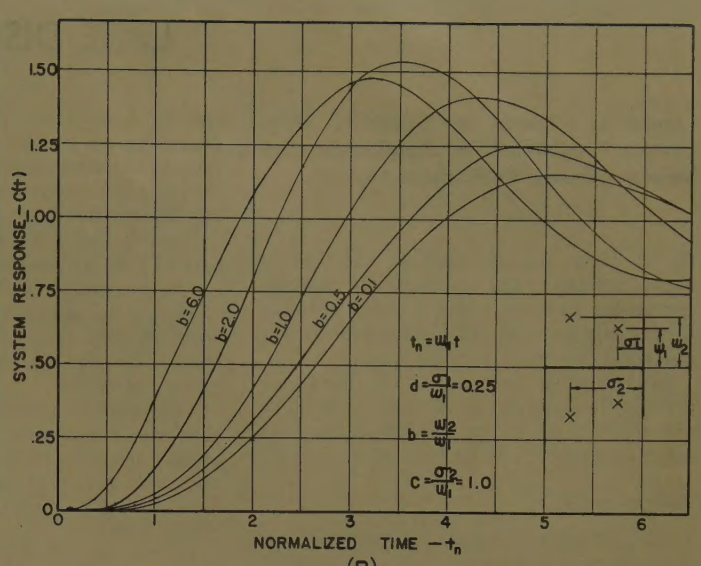

(B)

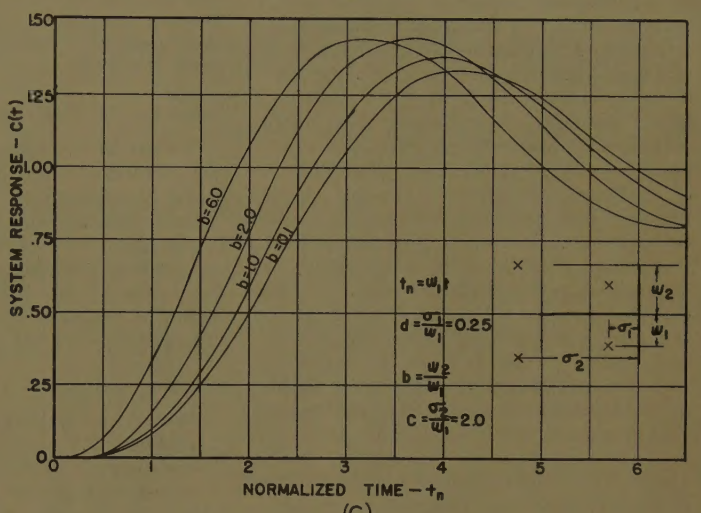

(C)

6. Responses to step input for system having one pair of ugated complex closed-loop poles and one pair of zeros

e I. Overshoot and Rise Time for Real Pole Variation

le ion	Overshoot, Per Cent	Rise Time Seconds
0	19	3.2
0	32	2.65
0	39	2.35
40	44	2.0

basis of pole-zero configuration has attempted; for each fundamental of system the time response has then calculated and plotted versus a ıalized time variable.

ıenclature

amplitudes defined in equation 4 and calculable from equation 5
=time response of system
=Laplace transform of $c(t)$
=open-loop transference
=feedback loop transference
=closed-loop transference
poles of $K(s)$; $\nu=1,2,\ldots n$
=system input
=Laplace transform of $r(t)$
ormalized time variable, defined for each case in the graphs
zeros of $K(s)$; $\mu=1,2,\ldots m$

Some parameters, a, b, c,... are used in connection with the graphs where they also have been defined in each case.

References

1. Control System Dynamics (book), **W. R. Evans.** McGraw-Hill Book Company, Inc., New York, N. Y.

2. Control System Synthesis (book), **L. G. Truxal.** McGraw-Hill Book Company, Inc., 1955.

3. Integrated s-Plane Synthesis Using 2-Way Root Locus, **John Zaborszky.** *AIEE Transactions*, (Jan. 1957 section), pp. 797–801.

4. Root Locus in Feedback System Synthesis, **John A. Aseltine.** *Proceedings*, Institute of Radio Engineers, New York, N. Y., Mar. 1956, p. 402.

5. Theory of Servomechanisms (book), **H. M. James, N. B. Nichols, R. S. Phillips.** McGraw-Hill Book Company, Inc., 1947, p. 143.

6. **Truxal,** op. cit., pp. 40–41.

7. The Effect of Pole and Zero Locations on the Transient Response of Linear Dynamic Systems, **L. H. Mulligan, Jr.** *Proceedings*, Institute of Radio Engineers, vol. 37, May 1949, pp. 516–29.

8. Further Effects of the Pole and Zero Locations on the Step Response of Fixed Linear Systems, **Armen H. Zemanian.** *AIEE Transactions*, vol. 74, pt. II, March 1955, pp. 52–55.

9. An Analog Computer Study of the Transient Behaviour and Stability Characteristics of Serial-Type Digital Data Systems, **Olle I. Elgerd.** *Ibid.*, vol. 77, pt. I, July, 1958, pp. 358–366.

10. The Sensitivity of the Poles of Linear Closed-Loop Systems, **R. Y. Huang.** *Ibid.*, pt. II, Sept. 1958, pp. 182–87.

11. **Truxal,** op. cit., p. 43.

Closure to "Trends in Automatic Hoist Controls," published in Applications and Industry, January 1959, pages 609–18.

G. L. Tiley and **E. Zucker:** Mr. Ivy's comments are to the point and his remarks concerning the design of a hoisting installation should have the full support of everyone concerned with running a mine.

Mr. Eastcott has been good enough to comment in detail on several aspects of our paper. We appreciate his effort very much and have the following to say in reply.

Regulators

Mr. Eastcott has stressed the need for accurate acceleration control. We are of the opinion that an accurate form of deceleration control is much more important. Variation of acceleration away from a level is acceptable within quite a wide range, and is determined largely by psychological factors. On a skip hoist, acceleration under current-limit control will give the maximum possible production for all conditions of loading. The speed of run-out of the inductor will determine the maximum acceleration rate in case of a downgoing load.

A hoist, on the other hand, must be decelerated and brought to rest in a very definite distance. Variation in deceleration rate will result in either the conveyance creeping too far, or overtraveling. It is for this reason that the hoist should be decelerated under a speed-control signal that is a function of the distance from the final stopping position. The drive should always have maximum torque available to meet such a speed program.

We are in full agreement with Mr. Eastcott on the desirability of using a rate feedback for stabilizing, especially on a current-limit control where a double-rate feedback is most effective.

The use of a tachogenerator voltage or a generator voltage feedback is largely a matter of convenience. Both can be made to give accurate speed control. In the former case, some complications arise in suiciding at standstill. In the latter case, different values of current-resistance compensation have to be used for creep and full speed.

Program Devices

The use of simple limit switches, in place of the advance selector, does not necessarily result in simplification of the control circuits. If maximum production is required, even on a single-level single-skip hoist, two sets of limit switches are needed (one for hoisting and one for lowering) because: 1. acceleration away from a level can be more rapid than deceleration approaching it; and 2. the time lags, etc., of the electric circuits work to decrease speed during acceleration and to increase it during deceleration.

The advance selector automatically takes care of this, as the speed reference inductor can be run out at any desired speed.

The use of an inductor instead of limit switches eliminates many contacts in the control circuits, as well as giving stepless control of speed.

The advance selector circuitry is such that the speed cam switch inductor exercises overriding control of acceleration and deceleration at all points in the shaft, even during manual operation of an automatic hoist.

In the case of emergency, the advance selector can be cut out of circuit by reconnecting two wires, to replace the speed cam switch inductor signal by a constant maximum speed signal.

Brake Test Equipment

We are in full agreement with Mr. Eastcott regarding the relative usefulness of the distance - measuring device. Mechanical counters are available that will satisfactorily count up to 25 pulses a second. This corresponds to one pulse per foot at 1,500 feet per minute. At higher speeds, the circuitry is arranged to count one pulse per 2 feet of rope travel.

Brake Design and Performance

We are not quite sure what is meant by Mr. Eastcott's statement that the brake shoes store 4% of the impact energy during a rapid, unregulated, emergency application. We assume it to mean that, on a weight-applied brake, the dead weight stores 96% of the impact energy. Under these circumstances, the elimination of the dead weights would allow the application time to be speeded up by a factor of $\sqrt{24}$ or 4.9.

About the minimum application time that can be achieved without excessive overshoot by a weight-applied brake is 2 seconds. Therefore we would not expect that an air-applied caliper-type brake, adjusted to normal operating clearances, can be applied in better than 0.4 second without excessive overshoot. If an application time of 0.2 second is required, the inertia would have to be reduced to 1%.

We have conducted many tests on brake disks under all conditions of operation and are convinced that disks will prove far more satisfactory brake paths than the old ones from both the mechanical and thermal points of view.

We have witnessed acceptance tests on six hoists equipped with air-applied Microspot caliper brakes, and the brake application time under emergency conditions ha been between 0.8 and 1.2 seconds. Whe these tests were taken, the brakes we operating at normal running clearances.

Fig. 1 of this closure is a speed–tim recording, taken with a Visicorder, of a emergency stop on a 14-foot double-dru hoist equipped with these brakes. Cha speed was 0.2 inch per second.

The overspeed cam of the Lilly controlle was advanced to trip the hoist at abou 800 feet per minute. The control circuitr was such that the signal to apply the brak was given at the same instant as the sign to open the loop circuit breaker, and th loop breaker took about 0.1 second t open.

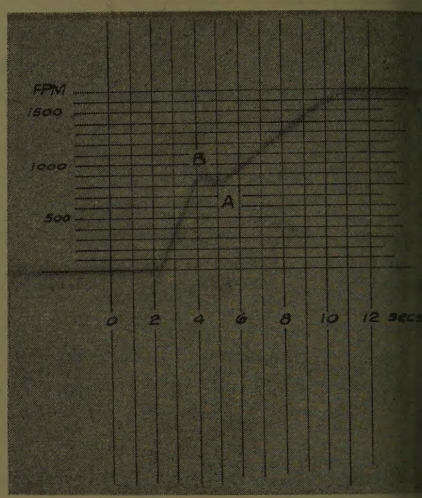

Fig. 1. Visicorder speed–time recording air-operated caliper brakes on 14-foot doubl drum hoist

At *A*, the hoist started to speed u signifying that the loop breaker had opene Speed increased due to the out-of-balan rope torque until *B*, where the brak started to apply. Dead time was about 0 second, i.e., the actual brake applicati time was about 0.9 second. The differen between the times we observed and t times recorded by Mr. Eastcott, probab can be accounted for by the clearance nece sary in practice between the shoes and t brake drum. This clearance prevents t brakes binding when the drum heats u and mine operating personnel keep it safe values.

In conclusion, we are in full agreeme with Mr. Eastcott on the desirability priming to reduce impact shock loads on t brake mechanism.

Power Apparatus and Systems—April 1959

Conference Paper Open for Discussion

The conference paper listed below has been accepted for AIEE Transactions and is now open for written discussion until June 26. Duplicate double-spaced typewritten copies of each discussion should be sent to Edward C. Day, Assistant Secretary for Technical Papers, American Institute of Electrical Engineers, 33 West 39th Street, New York 18, N. Y., on or before June 26.

Preprints may be purchased at 40¢ each to members; 80¢ each to nonmembers if accompanied by remittance or coupons. Please order by number and send remittance to:

AIEE Order Department
33 West 39th Street
New York 18, N. Y.

59-256 Three-Phase Induction Heating Coils.....Rose

AIEE PUBLICATIONS

	Member Prices	Nonmember Prices
Electrical Engineering		
Official monthly publication containing articles of broad interest, technical papers, and three news sections: Institute Activities, Current Interest, and Electrical Engineering Education. Automatically sent to all members and enrolled students in consideration of payment of dues.		annually $12* per year
* Subscription price and $1.00 extra for foreign postage both payable in advance in New York exchange.		Single copies $1.50
Bimonthly Publications		
Containing all officially approved technical papers collated with discussion (if any) in three broad fields of subject matter as follows:	annually	annually
Communication and Electronics	$5.00†	$8.00‡
Applications and Industry	$5.00†	$8.00‡
Power Apparatus and Systems	$5.00†	$8.00‡
† Members may receive one subscription to any one of the bimonthlies for $2.50. The balance of the $5.00 subscription price shown above will be paid by application of one's annual dues for the year of the subscription. (Members may not reduce the amount of their dues payment by reason of nonsubscription.) Additional subscriptions will be at the $5.00 rate shown above.		
‡ Subscription price and 50 cents extra for foreign postage both payable in advance in New York exchange.		
Single copies may be obtained when available.	$1.50 each	$1.50 each
AIEE Transactions		
An annual volume in three parts containing all officially approved technical papers with discussions corresponding to six issues of the bimonthly publication of the same name bound in cloth with a stiff cover.	annually	annually
Part I Communication and Electronics	$4.00	$ 8.00**
Part II Applications and Industry	$4.00	$ 8.00**
Part III Power Apparatus and Systems	$4.00	$ 8.00**
Annual combination subscription to all three parts (beginning with vol. 77 for 1958).	$10.00	$15.00***
Annual combination subscription to any two parts.		$12.00***
** Subscription price and 75 cents for foreign postage both payable in advance in New York exchange.		
*** Subscription price and $1.00 extra for foreign postage both payable in advance in New York exchange.		
Electrical Engineering and Transactions		
An annual combination subscription to both publications (effective August 1, 1958).		$24.00§
§ Subscription price and $2.00 extra for foreign postage both payable in advance in New York exchange.		
AIEE Standards		
Listing of Standards, test codes, and reports with prices furnished on request.		
Special Publications		
Committee reports on special subjects, bibliographies, surveys, and papers and discussions of some specialized technical conferences, as announced in ELECTRICAL ENGINEERING.		

Discount 25% of above nonmember prices to college and public libraries. Publishers and subscription agencies 15% of above nonmember prices. For available discounts on Standards and special publications, obtain price lists from Order Department at Headquarters. Send all orders to:

Order Department
American Institute of Electrical Engineers
33 West 39th Street, New York 18, N. Y.